

**SYNTHESIS AND EVALUATION OF NOVEL NON-ENZYMATIC
SOLID-PHASE NANOCOMPOSITES FOR HYDROGEN PEROXIDE
SENSORS**

FARNAZ LORESTANI

**FACULTY OF SCIENCE
UNIVERSITY OF MALAYA
KUALA LUMPUR**

2015

**SYNTHESIS AND EVALUATION OF NOVEL
NON-ENZYMATIC SOLID-PHASE NANOCOMPOSITES FOR
HYDROGEN PEROXIDE SENSORS**

FARNAZ LORESTANI

**THESIS SUBMITTED IN FULFILMENT OF THE
REQUIREMENTS FOR THE DEGREE OF DOCTOR OF
PHILOSOPHY**

**FACULTY OF SCIENCE
UNIVERSITY OF MALAYA
KUALA LUMPUR**

2015

UNIVERSITI MALAYA

ORIGINAL LITERARY WORK DECLARATION

Name of Candidate: Farnaz Lorestani

Registration/Matric No.: SHC120016

Name of Degree: Doctor of Philosophy (Ph.D.)

Title of Project Paper/Research Report/Dissertation/Thesis ("this Work"):

SYNTHESIS AND EVALUATION OF NOVEL NON-ENZYMATIC SOLID-PHASE NANOCOMPOSITES FOR HYDROGEN PEROXIDE SENSORS

Field of Study: Analytical chemistry-Electrochemistry

I do solemnly and sincerely declare that:

- (1) I am the sole author/writer of this Work;
- (2) This Work is original;
- (3) Any use of any work in which copyright exists was done by way of fair dealing and for permitted purposes and any excerpt or extract from, or reference to or reproduction of any copyright work has been disclosed expressly and sufficiently and the title of the work and its authorship have been acknowledged in this Work;
- (4) I do not have any actual knowledge or ought I reasonably to know that the making of this Work constitutes an infringement of any copyright work;
- (5) I hereby assign all and every rights in the copyright to this Work to the University of Malaya ("UM"), who henceforth shall be owner of the copyright in this Work and that any reproduction or use in any form or by any means whatsoever is prohibited without the written consent of UM having been the first had and obtained;
- (6) I am fully aware that if in the course of making this Work I have infringed any copyright whether intentionally or otherwise, I may be subject to legal action or any other action as may be determined by UM.

Candidate's Signature

Date:

Subscribed and solemnly declared before,

Witness's signature

Date:

Name:

Designation: Department of Chemistry,
Faculty of Science, University of Malaya, Kuala Lumpur, 50603, Malaysia
Tel./Fax: +60379675160/ +60 379674193.

ABSTRACT

Glassy carbon electrode (GCE) was modified with six novel solid-phase nanocomposites as substrate for non-enzymatic hydrogen peroxide (H_2O_2) sensor have been utilized in this study. This work was conducted to study the effect of different novel solid-phase nanocomposites with different morphologies toward H_2O_2 , and also evaluate and enhance the performance of modified glassy electrodes with the prepared nanocomposites as hydrogen peroxide sensor. The first four composites were based on polyaniline as the polymer matrix. Silver nanoparticles-polyaniline nanotubes (AgNPs-PANINTs(A)) composite prepared via one-step modified free chemical template method and AgNO_3 was used as the source of Ag nanoparticles (AgNPs). By reducing the temperature of the reaction, the nanotube morphology changed to rod shape and silver nanoparticle-polyaniline nanorods (AgNPs-PANINRs) composite is obtained. The AgNPs-PANINRs composite exhibited better electrochemical performance toward H_2O_2 detection with limit of detection (LOD) of $0.13 \mu\text{M}$ as compared to AgNPs-PANINTs(A) composite, due to higher surface area and content of AgNPs. The source of silver changed to $\text{Ag}(\text{NH}_3)_2\text{OH}$ instead of AgNO_3 in nanotube morphology of nanocomposite to get better distribution of AgNPs. The performance of the obtained composite (AgNPs-PANINTs(B)) with LOD of $0.6 \mu\text{M}$ significantly improved as compared to the nanotube composite prepared with AgNO_3 as a source of silver. The combination of two different methods in synthesizing of the forth nanocomposite was conducted to obtain a better performance of materials for sensing H_2O_2 . Silver nanoparticle-reduced graphene oxide-polyaniline nanofibers (AgNPs-PANINFs-rGO) were synthesized using two-step method. PANINFs were prepared in the presence of sulfuric acid applying vertical sonochemical method. AgNPs-rGO, which was prepared separately by hydrothermal method, was dropped on the surface of GCE followed by PANINFs to fabricate the

modified electrode. The modified electrode was prepared by dropping the obtained AgNPs-rGO and PANINFs on the glassy carbon electrode (GCE). The prepared modified electrode shows LOD of 0.117 μM . This composite indicated smaller LOD as compared to AgNPs-PANINTs(B) and AgNPs-PANINRs composites due to the presence of rGO. The two last composites are carbon-based composites. Silver nanoparticles-reduced graphene oxide-carbon nanotubes (AgNPs-MWCNT-rGO) were prepared using two different methods which are hydrothermal (AgNPs-MWCNT-rGO(H)) and electrochemical (AgNPs-MWCNT-rGO(E)). These methods provided the notable advantage of a single-step reaction without employing any toxic solvent or reducing agent by providing a novel green synthetic route to produce the AgNPs-MWCNT-rGO.

The hydrothermal AgNPs-MWCNT-rGO(H) composite exhibited a LOD around 0.9 μM . Finally, the electrodeposited AgNPs-MWCNT-rGO(E) composite displayed LOD of 1.4 μM that is less than hydrothermal composite. All the synthesized nanocomposites were characterized by using X-ray Diffraction, Field Emission Scanning Electron Microscopy, Transmission Electron Microscopy and Atomic Force Microscopy meanwhile the reactivity of the prepared composites towards H_2O_2 were analyzed using cyclic voltammetry and chronoamperometry. All the nanocomposites modified electrodes exhibited excellent electrocatalytic activity for the reduction of H_2O_2 with a fast amperometric response time less than 3 s. Among all six prepared nanocomposites, AgNPs-PANINFs-rGO composite is the best solid-phase nanocomposites system for H_2O_2 detection with LOD = 0.117 μM .

ABSTRAK

Elektrod karbon berkaca (GCE) yang diubahsuai dengan menggunakan enam novel nanokomposit fasa pepejal sebagai substrat untuk penderia tanpa enzim hidrogen peroksida telah digunakan dalam kajian ini. Kerja-kerja ini dijalankan untuk mengkaji kesan novel nanokomposit fasa pepejal yang berbeza dengan morfologi berbeza terhadap H_2O_2 , dan juga menilai dan meningkatkan prestasi diubahsuai elektrod berkaca dengan nanokomposit bersedia sebagai sensor hidrogen peroksida. Empat komposit pertama adalah berdasarkan polianilina sebagai matrik polimer. Komposit tiub-nano nanopartikel-polianilina (AgNPs-PANINTs(A)) perak disediakan melalui kaedah templet pengubahsuaian bebas bahan kimia satu langkah dan $AgNO_3$ telah digunakan sebagai sumber Ag nanopartikel (AgNPs). Dengan mengurangkan suhu tindak balas, morfologi tiub-nano bertukar kepada bentuk rod dan komposit nanorod nanopartikel-polianilina perak (AgNPs-PANINRs) diperolehi. Komposit AgNPs-PANINRs menunjukkan prestasi elektrokimia yang lebih baik terhadap pengesanan H_2O_2 berbanding komposit AgNPs-PANINTs(A) dengan had pengesanan (LOD) $0.13 \mu M$, disebabkan oleh luas permukaan yang lebih tinggi dan kandungan AgNPs. Sumber perak ditukar kepada $Ag(NH_3)_2OH$ berbanding $AgNO_3$ untuk mendapatkan taburan AgNPs yang lebih baik di dalam morfologi tiub nano nanokomposit. Prestasi komposit yang diperolehi bertambah baik dengan ketara berbanding komposit tiub nano AgNPs-PANINTs(B) yang disediakan dengan $AgNO_3$ sebagai sumber perak dengan LOD $0.6 \mu M$. Gabungan dua kaedah yang berbeza didalam nanokomposit seterusnya telah dijalankan untuk mendapatkan prestasi bahan yang lebih baik untuk pengesanan H_2O_2 . Nanopartikel-penurun grafin oksida-polianilina nanofiber perak (AgNPs-PANINFs-rGO) telah disintesis menggunakan kaedah dua langkah. PANINFs telah sediakan menggunakan kaedah sonokimia menegak dengan kehadiran asid sulfurik. AgNPs-rGO yang telah disediakan secara berasingan, telah dititiskan dipermukaan GCE diikuti oleh PANINFs untuk febrikasi elektrod yang

diubahsuai. Elektrod yang diubahsuai telah disediakan dengan menitiskan AgNPs-rGO dan PANINFs pada permukaan elektrod karbon berkaca (GCE). Elektrod tersebut menunjukkan LOD 0.117 μM . Komposit ini menunjukkan LOD lebih kecil berbanding komposit AgNPs-PANINTs(B) dan AgNPs-PANINRs dengan kehadiran rGO. Dua komposit terakhir adalah komposit berasaskan karbon. Tiub-nano nanopartikel-penurunan grafin karbon-oksida perak (AgNPs-MWCNT-rGO(H)) telah disediakan dengan menggunakan dua kaedah berbeza iaitu hidroterma dan elektrokimia AgNPs-MWCNT-rGO(E). Kaedah ini telah memberikan kelebihan tindakbalas satu langkah tanpa menggunakan pelarut toksik atau agen penurunan dengan menyediakan cara penyediaan laluan novel sintetik hijau untuk menghasilkan AgNPs-MWCNT-rGO.

Komposit hidroterma AgNPs-MWCNT-rGO(H) mempamerkan LOD sekitar 0.9 μM . Akhir sekali, komposit electrodeposit AgNPs-MWCNT-rGO(E) menunjukkan pengurangan beberapakali ganda LOD iaitu 1.4 μM berbanding komposit hidroterma. Kesemua nanokomposit yang telah sintesis dicirikan dengan menggunakan pembelauan sinar-X, mikroskopi elektron imbasan pancaran medan, *Transmission Electron Microscopy* dan *Atomic Force Microscopy*. Manakala kereaktifan komposit yang dihasilkan terhadap H_2O_2 telah di analisis dengan menggunakan voltametri kitaran dan *chronoamperometry*. Antara kesemua enam nanokomposit yang telah disediakan, komposit AgNPs-PANINFs-rGO adalah fasa pepejal sistem nanokomposit terbaik untuk mengesan H_2O_2 dengan LOD = 0.117 μM .

*All that I am or ever hope to be, I owe to
my angel mother*

University of Malaya

ACKNOWLEDGMENTS

PhD is a rewarding journey full of wonderful experiences that is not possible without support and encouragement of many people. Now since my journey is near to the end, I would like to take the opportunity to express my sincere thanks to all amazing people who helped me along the way.

First and foremost, I offer my profoundest gratitude to my supervisors, Professor Yatimah Alias and Dr. Ninie Suhana Abdul Manan, who awarded me the opportunity to pursue my studies in their group. I would like to thank them for continuous guidance, support and encouragement throughout all rough and enjoyable moments of my PhD endeavor.

I would also like to express special thanks to my lab mates and collaborators in the University of Malaya for their helpfulness and friendship throughout.

I wish acknowledge High Impact Research Grant UM-MOE UM.C/625/1/HIR/MOE/F00004-21001 from the Ministry of Education Malaysia, and PG135-2012B from the University of Malaya for granting scholarships and travel supports enable me to do the research in this thesis and attend international conferences.

I would like to give heartfelt thanks to my parents, my sister and my brother for endless help, supports, and love.

Lastly and most importantly, I thank my precious husband Pooya for standing beside me, for his endurance supports and unwavering love that will always be in my heart. These few words are not enough to express my deepest appreciation for efforts he has done during the past years.

Farnaz Lorestani

May, 2015

TABLE OF CONTENTS

CHAPTER1:	INTRODUCTION.....	1
1.1	GENERAL INFORMATION.....	1
1.2	OBJECTIVES OF STUDY	3
1.3	ORGANIZATION OF THIS DISSERTATION	3
CHAPTER2:	LITERATURE REVIEW.....	4
2.1	HYDROGEN PEROXIDE ELECTROCATALYSIS MATERIALS	4
2.1.1	Conductive polymers base nanocomposites materials.....	5
2.1.2	Nobel metal base nanocomposite materials	8
2.1.3	Graphene base nanocomposite materials	11
2.1.3.1.	Chemical reduction of graphene oxide.....	14
2.1.3.2.	Hydrothermal reduction of graphene oxide	15
2.1.3.3.	Electrochemical reduction of graphene oxide.....	15
2.1.4	Carbon nanotube (CNT).....	16
2.1.5	Carbon nanotube base nanocomposites materials.....	16
2.1.6	Nanocomposite of graphene, carbon nanotube and noble metals for detecting of H ₂ O ₂	17
2.2	METHODS TO FABRICATE NANOCOMPOSITES MATERIALS	18
2.2.1	Chemical preparation of nanocomposites materials.....	19
2.2.2	Hydrothermal preparation of nanocomposites materials	20
2.2.3	Electrochemical preparation of nanocomposites materials.....	21
2.3	SENSOR TECHNIQUES FOR HYDROGEN PEROXIDE DETECTION	22
2.3.1	Titration methods	22
2.3.2	Spectrophotometric methods.....	22
2.3.3	Fluorescence methods	23

2.3.4	Chemiluminescence methods.....	24
2.3.5	Electrochemical methods	25
2.3.5.1.	Amperometric sensors.....	26
2.3.5.2.	Potentiometric sensors.....	27
2.3.5.3.	Conductometric sensors	28
CHAPTER3: EXPERIMENTAL PROCEDURES.....		30
3.1	INTRODUCTION	30
3.2	CHEMICALS	31
3.3	SYNTHESIS AND CHARACTERIZATIONS	32
3.3.1	Preparation of PANI.....	32
3.3.1.1.	Synthesis of polyaniline by bath sonochemical method	32
3.3.2	Preparation of PANI nanofibers (PANINFs) via vertical sonication method.	33
3.3.3	Preparation of silver nanoparticles.....	33
3.3.4	Preparation of silver ammonia solution	33
3.3.5	Preparation of graphene oxide (GO).....	34
3.3.6	Functionalization of MWCNT by carboxylic groups (MWCNT-COOH).....	35
3.3.7	Synthesis of nanocomposites and electrode preparation.....	36
3.3.7.1.	Preparation of Silver- Polyaniline nanotubes composites [AgNPs-PANINT(A)]	36
3.3.7.2.	Preparation of H ₂ O ₂ modified electrode of (AgNPs-PANINTs/GCE)	36
3.3.7.3.	Preparation of silver nanoparticles-polyaniline nanorods composite (AgNPs-PANINRs);.....	37
3.3.7.4.	Preparation of H ₂ O ₂ modified glassy carbon electrodes of AgNPs-PANINRs composite (AgNPs-PANINRs/GCE)	37
3.3.7.5.	Preparation of Silver nanoparticle-reduce graphene oxide (AgNPs-rGO) composite	37

3.3.7.6.	Preparation of H ₂ O ₂ Modified glassy carbon electrode of Silver nanoparticles-reduced graphene oxide-polyaniline nanofiber composite (AgNPs- PANINFs-rGO/GCE)	38
3.3.8	Synthesis of silver nanoparticle- multi walled carbon nanotube-reduced-graphene nanocomposite (AgNPs-MWCNT-rGO) by hydrothermal method [AgNPs-MWCNT-rGO(H)]	40
3.3.8.1.	Synthesis of silver nanoparticle-multi walled carbon nanotube (AgNPs-MWCNT) by stirring method.....	40
3.3.8.2.	Synthesis of silver nanoparticle-multi walled carbon nanotube- graphene nanocomposite (AgNPs-MWCNT-GO) by stirring method	41
3.3.8.3.	Preparation of H ₂ O ₂ modified of AgNPs-MWCNT-GO/ GCE	41
3.3.8.4.	Preparation of H ₂ O ₂ modified electrode of AgNPs-MWCNT-rGO/GCE electrode	42
3.3.8.5.	Silver nanoparticle-multi walled carbon nanotube-reduced-graphene oxide-composite (AgNPs-MWCNT-rGO) by electrodeposition synthesis method [AgNPs-MWCNT-rGO(E)]	42
3.3.9	Characterization	43
3.4	INSTRUMENTATION	44
3.4.1	Electrodeposition and electrochemical study of modified electrodes.....	44
3.4.2	Field Emission Scanning Electron Microscope (FESEM) and Energy Dispersive X-Ray (EDX)	46
3.4.3	X-Ray Diffraction (XRD)	47
3.4.4	Transmission Electron Microscopy (TEM)	49
CHAPTER4: RESULTS AND DISCUSSION.....		52
4.1	Silver-polyaniline nanotube composite [AgNPs-PANINTs(A)]	52
4.1.1	Morphology analysis of AgNPs-PANINTs(A) composite	52
4.1.2	XRD analysis, EDX and FT-IR spectroscopy characterization of AgNPs-PANINTs(A) composite.....	54
4.1.3	Electrochemical characterization of AgNPs-PANINTs(A) composite.....	57
4.1.3.1.	Cyclic voltammogram (CV) of the modified AgNPs-PANINTs(A)/GCE to hydrogen peroxide.....	57

4.1.3.2.	Amperometric response of the modified electrode (AgNPs-PANINTs(A)/GCE) to hydrogen peroxide	59
4.2	Silver-polyaniline nanorods composite [AgNPs-PANINRs]	60
4.2.1	Morphology analysis of AgNPs-PANINRs composite.....	61
4.2.2	Electrochemical characterization of AgNPs-PANINRs composite	67
4.2.2.1.	Cyclic voltammogram (CV) of the modified electrode (AgNPs-PANINRs/GCE) to hydrogen peroxide.....	70
4.2.2.2.	Amperometric response of the modified AgNPs-PANINRs/GCE electrode to hydrogen peroxide.....	73
4.3	Silver-polyaniline nanotube composite [AgNPs-PANINTs(B)] using silver ammonia complex $\text{Ag}(\text{NH}_3)_2\text{OH}$	77
4.3.1	Morphology analysis of AgNPs-PANINTs(B) composite.....	77
4.3.2	XRD analysis, EDX and FT-IR spectroscopy characterization of AgNPs-PANINTs(B) composite.....	79
4.3.3	Electrochemical characterization of modified AgNPs-PANINTs(B)/GCE....	81
4.3.3.1.	Cyclic voltammogram (CV) of the modified electrode (AgNPs-PANINTs(B)/GCE) to hydrogen peroxide.....	83
4.3.3.2.	Amperometric response of the modified electrode (AgNPs-PANINTs(B)/GCE) to hydrogen peroxide.....	86
4.4	Polyaniline nanofibers-silver nanoparticles decorated reduced graphene oxide nanocomposites [AgNPs-PANINFs-rGO]	90
4.4.1	Morphology analysis of bulk PANI by bath sonication.....	90
4.4.2	Morphology analysis of PANINFs.....	90
4.4.3	Morphology analysis of rGO.....	94
4.4.4	Morphology analysis of AgNPs-rGO.....	95
4.4.5	XRD analysis, EDX and FT-IR spectroscopy characterization of AgNPs-PANINFs-rGO composite.....	97
4.4.6	Electrochemical characterization of AgNPs-PANINFs-rGO composite	101
4.4.6.1.	Cyclic voltammogram (CV) of the modified electrode (AgNPs-PANINFs-rGO /GCE) to hydrogen peroxide	101

4.4.6.2.	Amperometric response of the modified electrode (AgNPs-PANINFs-rGO /GCE) to hydrogen peroxide	103
4.4.7	Repeatability, reproducibility and stability	104
4.5	Carbon base composites for hydrogen peroxide sensing.....	108
4.5.1	Silver nanoparticle- carbon nanotube reduced-graphene oxide composite by hydrothermal method [AgNPs-MWCNT-rGO(H)]	108
4.5.1.1.	Morphology analysis of AgNPs-MWCNT-rGO(H)	108
4.5.2	XRD analysis, EDX and FT-IR spectroscopy characterization of AgNPs-MWCNT-rGO(H) composite	111
4.5.2.1.	Electrochemical characterization of AgNPs-MWCNT-rGO(H) composite .	114
4.5.2.2.	Cyclic voltammogram (CV) of the modified electrode (AgNPs-MWCNT-rGO(H)/GCE) to hydrogen peroxide.....	116
4.5.2.3.	Amperometric detection of hydrogen peroxide at modified AgNPs-MWCNT-rGO(H)/GCE	120
4.5.3	Electrodeposited silver nanoparticle-reduced-graphene oxide-carbon nanotube nanocomposites [AgNPs-MWCNT-rGO(E)].....	124
4.5.4	XRD analysis, EDX and FT-IR spectroscopy characterization of AgNPs-MWCNT-rGO(E) composite.....	126
4.5.4.1.	Morphology analysis of AgNPs-MWCNT-rGO(E).....	129
4.5.4.2.	Cyclic voltammogram (CV) of the modified AgNPs-MWCNT-rGO(E)/GCE to hydrogen peroxide.....	131
4.5.4.3.	Amperometric detection of H ₂ O ₂ at modified AgNPs-MWCNT-rGO(E)/GCE electrode	135
CHAPTER5: CONCLUSION.....		138
5.1	Recommendation for Future Work	141
1.	Alloy nanocomposites	141
2.	Functionalization of rGO	141

REFERENCES 142

Honors and Awards..... 161

Publications 162

University of Malaya

LIST OF FIGURES

Figure 2.1 Three oxidation states for PANI.....	7
Figure 2.2 Graphene oxide structure.....	13
Figure 2.3 Preparation process of graphene.....	14
Figure 3.1 Methodology chart of this dissertation.....	31
Figure 3.2 graphene oxide suspension.....	34
Figure 3.3 Graphene oxide.....	35
Figure 3.4 Set up of Autolab PGSTAT-302N.....	45
Figure 3.5 A photograph of FESEM with EDX set-up.....	47
Figure 3.6 Basic features of a typical XRD experiment as well as the Siemens D5000 set-up.....	49
Figure 3.7 photograph of the TEM microscope unit.....	50
Figure 4.1. FESEM images of AgNPs-PANINTs(A) composite.....	54
Figure 4.2 EDX results of AgNPs-PANINTs(A) composite.....	55
Figure 4.3 XRD pattern of AgNPs-PANINTs(A) composite.....	55
Figure 4.4. FT-IR of (a) PANINTs (b) AgNPs-PANINTs(A) composite.....	56
Figure 4.5 CVs of (a) bare GCE, (b) PANINTs/GCE, (c) AgNPs/GCE, (d) AgNPs-PANINTs(A)/GCE in 0.2 M phosphate buffer solution (Na_2HPO_4 and NaH_2PO_4) pH 6.5 in the presence of 1.0 mM H_2O_2 using 20 m Vs^{-1} scan rate.....	58
Figure 4.6 A: Steady-state response of AgNPs-PANINRs/GCE to successive injections of H_2O_2 in 0.2 M phosphate buffer solution (Na_2HPO_4 and NaH_2PO_4) pH 6.5 with an applied potential -0.35 V B: the steady-state current vs. H_2O_2 concentration.....	60
Figure 4.7. FESEM images of AgNPs-PANINRs composite by using 0.01 g AgNO_3 (a), AgNPs-PANINRs composite by using 0.03 g AgNO_3 (b), AgNPs-PANINRs composite by using 0.05 g AgNO_3 (c), AgNPs-PANINTs(A) composite by using 0.01 g AgNO_3 and PANINRs (e) ,(f) and (g) Normal and backscatter FESEM images of AgNPs-PANINRs composite by using 0.03 g AgNO_3	

respectively,(h) size distribution diagram of the polyaniline nanorods of AgNPs-PANINRs composite by using 0.03 g AgNO ₃	63
Figure 4.8. TEM image of (a) AgNPs-PANINTs(A) composite (b), AgNPs-PANINRs composite by using 0.03 g AgNO ₃ and (C) size distribution diagrams of AgNPs-PANINRs.....	64
Figure 4.9 EDX result of AgNPs-PANINRs composite	65
Figure 4.10. XRD pattern of (a) pure PANI (b) AgNPs-PANINRs composite	66
Figure 4.11. FT-IR of (a) pure PANI (b) AgNPs-PANINRs composite.....	67
Figure 4.12. Nyquist plots of (a) bare electrode, (b) PANI, (c) AgNPs-PANINTs(A) and (d) AgNPs-PANINRs	68
Figure 4.13 A: Bode plots of (a) bare electrode, (b) PANI, (c) AgNPs-PANINTs(A) and (d) AgNPs-PANINRs. B: EIS Bode log f vs. θ plots at Nyquist plots of (a) bare electrode, (b) PANI, (c) AgNPs-PANINTs(A) and (d) AgNPs-PANINRs.....	69
Figure 4.14. Effect of the applied potential on the current response of AgNPs-PANINRs/GCE to 1.0 mM H ₂ O ₂ in 0.2 M phosphate buffer solution (Na ₂ HPO ₄ and NaH ₂ PO ₄) pH 6.5	70
Figure 4.15.A CVs of (a) bare GCE, (b) PANINRs/GCE, (c) AgNPs/GCE, (d) AgNPs-PANINRs/GCE in 0.2 M phosphate buffer solution (Na ₂ HPO ₄ and NaH ₂ PO ₄) pH 6.5 in the presence of 1.0 mM H ₂ O ₂ using 20 mVs ⁻¹ scan rate and Fig. 8.B CVs of AgNPs-PANINRs/GCE in 0.2 M phosphate buffer solution (Na ₂ HPO ₄ and NaH ₂ PO ₄) pH 6.5 in the presence of 1.0 mM H ₂ O ₂ using 20 mVs ⁻¹ scan rate without H ₂ O ₂ (a) and with H ₂ O ₂ (b).	72
Figure 4.16. Steady-state response of AgNPs-PANINRs/GCE to successive injections of H ₂ O ₂ in 0.2 M phosphate buffer solution (Na ₂ HPO ₄ and NaH ₂ PO ₄) pH 6.5 with an applied potential -0.35 V (b). calibration curves of low and (c) high concentrations of H ₂ O ₂ steady-state response of AgNPs-PANINRs/GCE..	74
Figure 4.17 Amperometric response of AgNPs-PANINRs/GCE electrode upon the successive addition of 1.0 mM H ₂ O ₂ , 1.0 mM H ₂ O ₂ , glucose, glycine, ethanol, ascorbic acid, 1.0 mM H ₂ O ₂ and again 1.0 mM H ₂ O ₂ into 0.2 M phosphate buffer solution (pH 6.5) with an applied potential - 0.35 V under a stirring condition.....	75
Figure 4.18. FESEM images and size distribution diagram of AgNPs-PANINTs(B) composite prepared by using the solution with PANI to Ag(NH ₃) ₂ OH (0.04 M) volume ratios of 12 (a and b), 6 (c and d), and 3 (e and f) and using the solution with PANINTs to AgNO ₃ (0.04 M) volume ratio of 12(g and h)...	78
Figure 4.19 A: EDX results of AgNPs-PANINTs(B) composite. B: XRD pattern of AgNPs-PANINTs(B) composite.	79

Figure 4.20. FT-IR of (a) PANINTs (b) AgNPs-PANINTs(B) composite.....	81
Figure 4.21 Effect of the applied potential on the current response of 1.0 mM H ₂ O ₂ on the AgNPs-PANINTs(B)/GCE electrode in 0.2 M PBS (pH 6.5).....	82
Figure 4.22 Effect of the pH of PBS on the current response of 1.0 mM H ₂ O ₂ on the AgNPs-PANINTs(B)/GCE electrode.	82
Figure 4.23 A: CVs of (a) bare GCE, (b) PANINT/GCE, (c) Ag/GCE, (d) AgNPs/PANINTs-2/GCE and B: CVs of Modified AgNPs-PANINTs(B) nanocomposite using different volume ratios of Ag(NH ₃) ₂ OH (0.04 M) of 12, 6, and 3, respectively (b–c), and AgNPs-PANINTs(B)/GCE prepared by using AgNO ₃ (0.04 M) volume ratio of 12 (d) in 0.2 M phosphate buffer solution (Na ₂ HPO ₄ and NaH ₂ PO ₄) pH 6.5 in the presence of 1.0 mM H ₂ O ₂ using 20 mVs ⁻¹ scan rate.	84
Figure 4.24 Nyquist diagrams of (a) GCE, (b) PANINT/GCE and (c) AgNPs-PANINTs(B)-2/GCE in 0.1 M KCl solution containing 1.0 mM Fe(CN) ₆ ^{3-/4-} (1:1).....	86
Figure 4.25. Steady-state response of AgNPs-PANINTs(B)/GCE to successive injections of H ₂ O ₂ in 0.2 M phosphate buffer solution (Na ₂ HPO ₄ and NaH ₂ PO ₄) pH 6.5 with an applied potential -0.35 V. The inset is the corresponding calibration curve.	88
Figure 4.26 Amperometric response of AgNPs-PANINTs(B)/GCE electrode upon the successive addition of 1.0 mM H ₂ O ₂ , glucose, glycine and ascorbic acid into 0.2M phosphate buffer solution (pH 6.5) with an applied potential -0.35 V under a stirring condition.....	88
Figure 4.27 FESEM images of PANI synthesized with different ultrasonic irradiation time; (a) 2 min, (b) 3 min, (c) 4 min, (d) 5 min.	91
Figure 4.28 FESEM images of PANINFs synthesized with different ultrasonic irradiation time; (a) 2 min, (b) 3 min, (c) 4 min, (d) 5 min.	92
Figure 4.29 From left to right FESEM and TEM images of PANINFs-2.....	93
Figure 4.30 (A) UV Vis spectra of (a) PANINFs-5min, (b) PANINFs-4min, (c) PANINFs-3min (d) PANINFs-2min. (B)Photo image of PANINFs after different sonication times	94
Figure 4.31 FESEM and TEM images of rGO.....	94
Figure 4.32 the 3D AFM images of rGO	95
Figure 4.33 TEM images and size distribution diagram of AgNPs -rGO composite prepared by using the solution with GO to Ag(NH ₃) ₂ OH (0.04 M) volume ratios of 12 (a and b), 6 (c and d), and 3 (e and f) and using the solution with a GO to AgNO ₃ (0.04 M) volume ratio of 12 (g and h).	96

Figure 4.34 FT-IR spectra for (a)GO,(b)AgNPs-rGO,(c)AgNPs-PANINFs-2-rGO-2 ...	99
Figure 4.35 (a) XRD pattern of (a) AgNPs-PANINFs-rGO-2, (b) GO and (c) AgNPs-rGO-2 and (b) EDX spectra of AgNPs-PANINFs-rGO-2.....	100
Figure 4.36 The current response affected by applied potential in the presence of 1.0 mM H ₂ O ₂ on the AgNPs-rGO coated GCE in 0.1 M phosphate buffer solution (pH 6.5); (b) CVs of different modified electrodes: (a) AgNPs-rGO-1/GCE, (b) AgNPs-rGO-2/GCE, (c) AgNPs-rGO-3/GCE and (d) AgNPs-rGO-4/GCE in 0.1 M PBS (pH 6.5) with adding 1.0 mM H ₂ O ₂ . (c) CVs of AgNPs-rGO-2/GCE in 0.1 M PBS (pH 6.5) in the presence of 1.0 mM H ₂ O ₂ at different applied potential at scan rate of 50 mVs ⁻¹ . (d) Cyclic voltammograms of (a) AgNPs-PANINFs-2-rGO-2/GCE, (b) AgNPs-PANINFs-3-rGO-2/GCE and (AgNPs-PANINFs-4-rGO-2/GCE in the presence of 1.0 mM H ₂ O ₂ in phosphate buffer solution (pH 6.5) at scan rate of 50 mV s ⁻¹	103
Figure 4.37 A: optimized the AgNPs-rGO volume ratio to detect H ₂ O ₂ , B: optimized the AgNPs-rGO volume ratio to detect H ₂ O ₂	105
Figure 4.38 Long-term stability of the AgNPs-PANINFs-2-rGO-2 studied in 2 weeks	106
Figure 4.39 TEM images of MWCNT without Ag (a) and the AgNPs-MWCNT with MWCNT(1.0mg.mL ⁻¹) to Ag(NH ₃) ₂ OH(0.04 M) volume ratios of 6(b)..	109
Figure 4.40 FESEM images and size distribution diagram of AgNPs-MWCNT-rGO(H)composite prepared by using the solution with MWCNT/GO (3:1, v/v) to Ag(NH ₃) ₂ OH (0.04 M) volume ratios of 12 (a and b), 6 (c and d), and 3 (e and f) and using the solution with a MWCNT-GO (3:1, v/v) to AgNO ₃ (0.04 M) volume ratio of 12 (g and h).	110
Figure 4.41 XRD patterns of MWCNT (a), GO (b) rGO (c) and AgNPs-MWCNT-rGO(H) composite (d).....	111
Figure 4.42 FTIR spectra of GO (a), rGO (b) MWCNT (c) and AgNPs-MWCNT-rGO(H) composite (d)	113
Figure 4.43 Nyquist Plots of: (1) bare GCE, (2) GO, (3)CNT, (4) AgNPs-MWCNT-GO and (5) AgNPs-MWCNT-rGO(H) and their equivalents circuits in 1.0 mM Fe(CN) ₆ ^{3-/4-} (1:1) solution with 0.1 M KCL supporting electrolyte.	115
Figure 4.44 CVs of various electrodes in 0.2 M PBS (pH 6.5) in the presence of 1.0 mM H ₂ O ₂ : bare GCE (a), MWCNT/GCE (b), GO/GCE (c), Ag nanoparticles/GCE (d), AgNPs-MWCNT/GCE (e) and AgNPs-MWCNT-GO/GCE(f) and AgNPs-MWCNT-rGO(H)/GCE (d).....	116
Figure 4.45 Effect of the applied potential on the current response of 1.0 mM H ₂ O ₂ on the AgNPs-MWCNT-rGO(H)/GCE electrode in 0.2 M PBS (pH 6.5).	118

Figure 4.46 Effect of the pH of PBS on the current response of 1.0 mM H ₂ O ₂ on the AgNPs-MWCNT-rGO(H)/GCE electrode.	118
Figure 4.47 CVs of various electrodes in 0.2 M PBS (pH 6.5) in the presence of 1.0 mM H ₂ O ₂ : bare GCE (a), AgNPs-MWCNT-rGO(H)/GCE prepared by using different volume ratios of MWCNT-GO (3:1, v/v) to Ag(NH ₃) ₂ OH (0.04 M) of 12, 6, and 3, respectively (b–d), and AgNPs-MWCNT-rGO(H)/GCE prepared by using the solution with MWCNT-GO (3:1, v/v) to AgNO ₃ (0.04 M) volume ratio of 12 (e).	119
Figure 4.48 Steady-state response of the AgNPs-MWCNT-rGO(H)/GCE electrode to consecutive injection of H ₂ O ₂ into the stirred 0.2 M PBS(pH 6.5) with an applied potential of 0.35V(a) the corresponding calibration curve(b).	121
Figure 4.49 Amperometric response of AgNPs-MWCNT-rGO(H)/GCE electrode upon the successive addition of 1.0 mM H ₂ O ₂ , glucose, glycine, ethanol and ascorbic acid into 0.2 M phosphate buffer solution (pH 6.5) with an applied potential -0.35 V under a stirring condition.....	122
Figure 4.50 A: Cyclic Voltammogram of AgNPs-MWCNT-rGO(E)-1(a), AgNPs-MWCNT-rGO(E)-2 (b), AgNPs-MWCNT-rGO(E)-3 (c), AgNPs-MWCNT-rGO(E)-4 (d) B: Cyclic voltammogram of AgNPs-MWCNT-rGO(E)-5 (a), AgNPs-MWCNT-rGO(E)-6 (b), AgNPs-MWCNT-rGO(E)-3 (c).....	125
Figure 4.51 XRD patterns of MWCNT (a), MWCNT-COOH (b), GO (c), rGO (d) and AgNPs-MWCNT-rGO(E) nanocomposite (e).....	127
Figure 4.52 FTIR spectra for MWCNT(a), MWCNT-COOH(b), GO(c), rGO(d) and AgNPs-MWCNT-rGO(E) nanocomposites(e).	129
Figure 4.53 FESEM images and size distribution diagram of AgNPs-MWCNT-rGO(E) composite prepared by using the solution with MWCNT-COOH and GO (1.0 mg/mL) ratio of 1:1 v/v to Ag(NH ₃) ₂ OH (0.04 M) volume ratios of 3 (a and b), 6 (c and d), and 12 (e and f), 24 (g and h) and using the solution with MWCNT-COOH and GO (1.0 mg/mL) ratio of 1:1 v/v to AgNO ₃ (0.04 M) volume ratio of 12 (i and j).....	130
Figure 4.54 CVs of various electrodes in 0.2M PBS (pH 6.5) while there is 1.0 mM H ₂ O ₂ : bare GCE(a), AgNPs-MWCNT-rGO(E)/GCE obtained by MWCNT-COOH and GO (1.0 mg/mL) ratio of 1:1 v/v and Ag(NH ₃) ₂ OH (0.04 M) with different volume ratios of 3, 6,12 and 24 (b–e), respectively, and B: CVs of various electrodes in 0.2M PBS (pH 6.5) while there is 1.0 mM H ₂ O ₂ of MWCNT-COOH and GO (1.0 mg/ml) ratio of 1:1 v/v and AgNO ₃ (0.04 M) with a volume ratio of 12 , MWCNT and GO (1.0 mg/ml) ratio of 1:1 v/v and Ag(NH ₃) ₂ OH (0.04 M) with a volume ratio of 12 and MWCNT-COOH and GO (1.0 mg/ml) ratio of 1:1 v/v and Ag(NH ₃) ₂ OH (0.04 M) volume ratios 12 (a-c) respectively.....	132
Figure 4.55 Nyquist Plots of: (1) bare GCE, (2) GO, (3) CNT, (4) AgNPs-MWCNT-GO and (5) AgNPs-MWCNT-rGO(H) hydrothermal (6) electrodeposited	

AgNPs-MWCNT-rGO(E) and their equivalents circuits in 1.0 mM $\text{Fe}(\text{CN})_6^{3-/4-}$ (1:1) solution with 0.1 M KCL supporting electrolyte..... 134

Figure 4.56 A: Steady-state response of the AgNPs-MWCNT-rGO(E)-3/GCE electrode to consecutive H_2O_2 injection into the stirred 0.2 M PBS (pH 6.5) with an applied potential of -0.35 V. B: Low concentration corresponding calibration curve. C: high concentration corresponding calibration curve. D: Amperometric response of AgNPs-MWCNT-rGO(E)-3/GCE electrode upon the successive addition of 1.0 mM H_2O_2 , glucose, glycine, ethanol and ascorbic acid into 0.2M phosphate buffer solution (pH 6.5) with an applied potential -0.35 V under a stirring condition..... 136

University of Malaya

LIST OF TABLES

Table 2.1 Examples of composite materials as hydrogen peroxide sensors	5
Table 3.1 Preparation methods of novel solid-phase nanocomposites.....	30
Table 4.1 EDX data of AgNPs-PANINTs(A) composite	54
Table 4.2. EDX data of AgNPs-PANINRs composite.....	65
Table 4.3 Comparison the LOD value from previous reports and this work with different methods	76
Table 4.4 EDX data of AgNPs-PANINTs(B) composite.....	80
Table 4.5 EIS parameters achieved by equivalent circuits of bare electrode, PANINT and AgNPs-PANINT(B)-2/GCE in 0.1 M KCl solution containing 1.0 mM Fe(CN) ₆ ^{3-/4-} (1:1).	87
Table 4.6. Comparison of the LOD value of the previous reports and this work from different methods.....	89
Table 4.7. Comparison between LOD and linear range of different nonenzymatic H ₂ O ₂ sensors	107
Table 4.8 Comparison the LOD value of the previous reports and this work from different methods	123
Table 4.9 A Comparison of this work with the other works in the literature regarding the performance of the H ₂ O ₂ measure.....	137
Table 5.1 Comparison of result on modified electrode with solid phase nanocompositebased as non-enzymatic H ₂ O ₂ sensor.....	140

LIST OF SYMBOLES AND ABBREVIATIONS

AFM	Atomic force microscopy
Ag/AgCl	Silver chloride saturated Electrode
[Ag(NH ₃) ₂ OH]	Silver-ammonia Complex
AgNO ₃	Silver nitrate
AgNPs	Silver nanoparticles
AgNPs/GCE	Modified glassy carbon electrode with Silver nanoparticles
AgNPs-PANINTs	Silver-Polyaniline nanotubes composites
AgNPs-PANINRs	Silver-Polyaniline nanotubes composites
AgNPs-PANINFs	Silver-Polyaniline nanofibers composites
AgNPs-PANINTs/GCE	Modified glassy carbon electrode with Silver-Polyaniline nanotubes composites
AgNPs-PANINRs/GCE	Modified glassy carbon electrode with Silver-Polyaniline nanorods composites
AgNPs-PANINFs/GCE	Modified glassy carbon electrode with Silver-Polyaniline nanofibers composites
AgNPs-rGO	Silver nanoparticle-reduce graphene oxide
AgNPs-MWCNT	silver nanoparticle-multi walled carbon nanotube
AgNPs-MWCNT-GO	silver nanoparticle-multi walled carbon nanotube- graphene nanocomposite
AgNPs-MWCNT-GO/ GCE	Modified glassy carbon electrode with silver nanoparticle-multi walled carbon nanotube- graphene nanocomposite
AgNPs-MWCNT-rGO	silver nanoparticle- multi walled carbon nanotube-reduced-graphene nanocomposite
APS	Ammonium PerSulfate
CA	Chronoamperometry
Ce[SO ₄] ₂	ceric sulfate
CV	Cyclic Voltammetry
DIW	De Ionized Water
EDX	Energy Dispersive X-ray
EIS	Electrochemical Impedance Spectroscopy
F	Faraday constant
FESEM	Field Emission Scanning Electron Microscopy
fMWCNT	Functionaled Multi-Walls Carbon NanoTubes
FT-IR	Fourier transform infrared spectroscopy
GCE	Glass Carbon Electrode
GO	Graphene Oxide
GO-MWCNT	Graphene Oxide- Multi-Walls Carbon NanoTubes Nanocomposite
GO-MWCNT/GCE	Modified glassy carbon electrode with Graphene Oxide- Multi-Walls Carbon NanoTubes Nanocomposite
GR/CNTs/CS	graphene/carbon nanotubes/chitosan
H ₂ SO ₄	Sulphuric acid
H ₃ PO ₄	phosphoric acid
HCl	Hydrochloric acid
NH ₃	Ammonia
HNa ₂ O ₄ P.2H ₂ O	Sodium phosphate dibasic dihydrate
H ₂ NaO ₄ P	Sodium phosphate monobasic
HNO ₃	Nitric acid

ITO	Indium Tin Oxide
KCl	Potassium Chloride
KMnO ₄	potassium permanganate
LOD	Limit Of Detection
LOQ	Limit Of Qualification
MnO ₂	Manganese dioxide
Mn ₂ O ₇	di manganese heptoxide
MWCNT	Multi-Walls Carbon NanoTubes
MWCNT/GCE	Modified glassy carbon electrode with Multi-walls carbon nanotubes
MWCNT-COOH	Functionalization of MWCNT by carboxylic groups
MWCNT-COOH/GCE	Modified glassy carbon electrode with Functionalization of MWCNT by carboxylic groups
NaBH ₄	Sodium borohydride
PANI	Polyaniline
PANI/GCE	Modified glassy carbon electrode with Polyaniline
PANINTs	Polyaniline nanotubers
PANINTs/GCE	Modified glassy carbon electrode with Polyaniline nanotubers
PANINRs	Polyaniline nanorods
PANINRs/GCE	Modified glassy carbon electrode with Polyaniline nanorods
PANINFs	Polyaniline nanofibers
PANINFs/GCE	Modified glassy carbon electrode with Polyaniline nanofibers
PBS	Phosphate Buffer Solution
PEM	Polymer electrolyte membranes
PPY	polypyrrole
PSD	position-sensitive detector
Pt	Platinum Electrode
PVP	poly(vinylpyrrolidone)
rGO	Reduced Graphene Oxide
rGO/GCE	Modified glassy carbon electrode with
rGO-MWCNT	Reduced Graphene Oxide- Multi-Walls Carbon NanoTubes Nanocomposite
rGO-MWCNT/GCE	Modified glassy carbon electrode with Reduced Graphene Oxide- Multi-Walls Carbon NanoTubes Nanocomposite
RE	Reference Electrode
ROS	Reactive Oxygen Species
RT	Room Temperature (25 °c)
S/N	Signal per Noise
TEM	Transmission Electron Microscopy
UV-vis	Ultraviolet-visible spectroscopy
XRD	X-ray Diffraction

A	Electrode Area
a_{Red}	Reductant chemical activity
a_{Ox}	Oxidant chemical activity
b	slope of the calibration curve
C	capacitance
d	the spacing of the crystal layers (path difference)
D	Diffusion Coefficient
E	Cell potential
E°	standard cell potential
F	Faraday's Constant
n	number of electrons transferred per mole
R_s	cell resistance
R_{dif}	Diffusion Resistance of Electroactive Species
s	Solubility
T	Temperature
t	Time
ν	Scan Rate
z	number of moles of electrons transferred in the cell reaction
ρ	Density
λ	the wavelength of the x-ray
θ	the incident angle (the angle between incident ray and the scatter plane)
χ^2	chi-squared
Z_w	diffusion impedance

CHAPTER 1: INTRODUCTION

1.1 GENERAL INFORMATION

Hydrogen peroxide (H_2O_2) has shown to be a highly important compound applied as an intermediate in many industrial processes as well as biological systems for several years. This has made it highly relevant in the environmental, clinical and pharmaceutical industries and related areas of research (Miao et al., 2001; Newman & Turner, 2005). The importance of H_2O_2 is due to its unique oxidizing properties. Hydroxyl radicals formed during the decomposition of H_2O_2 are used as oxidizing agents in the degradation of organic pollutants from water such as the azo dye compounds used in the textile industry, which are toxic to aquatic life and carcinogenic to humans (Wu et al., 2007). H_2O_2 and its derivatives can also be employed as powerful oxidizing agents in synthesis of many organic compounds (Norouzi et al., 2010).

Moreover, the decomposition of H_2O_2 plays a very important role in manufacturing of industrial water electrolyzers, secondary metal-air batteries and fuel cells (Ricci et al., 2005). Besides various industrial applications, H_2O_2 can also be problematic; its excessive concentration as an industrial product affects the environment (Welch et al., 2005). Polymer electrolyte membranes (PEM) used in fuel cells may be degraded by the chemical attack of hydroxyl free radicals generated from H_2O_2 (Arya, Datta, & Malhotra, 2008). Regarding medical applications, H_2O_2 is a major reactive oxygen species (ROS) in living organisms and plays a central role in causing several life-threatening human diseases. H_2O_2 is the most valuable marker for oxidative stress, which,

is related to aging and severe human diseases such as cancer, cardiovascular disorders, Alzheimer neurodegenerative diseases (Arya et al., 2008; Falcon & Carbonio, 1992; Li & Gu, 2006). Many enzymatic reactions also create H_2O_2 as a product so its concentration may be used as an indicator of the progress of the reaction. Due to these wide and varied applications, its determination represents an important analytical issue.

The electrochemical enzymatic sensors have been extensively used in determination of H_2O_2 due to their high sensitivity and good selectivity. Horseradish peroxidase and hemoglobin enzymes have been mostly used for preparation of modified enzymatic electrodes for amperometric determination of H_2O_2 (Zhang, Mao, & Cai, 2000). The inevitable disadvantage of such modified electrodes was chemical and thermal instability, which is determined part of the nature of the enzymes. This disadvantage has diverted the recent studies to direct detection of H_2O_2 by using enzymeless electrodes. Accordingly, studying on the materials applied in direct detection of H_2O_2 can develop new generation of enzymeless sensors.

In the present research, synthesis of solid-phase nanocomposites and detailed analysis of non-enzymatic H_2O_2 detection methods are carried out, with particular emphasis on electrochemical techniques. Moreover, the most significant materials and catalytic mechanisms in the literature to date are discussed, along with the main applications of non-enzymatic H_2O_2 detection.

1.2 OBJECTIVES OF STUDY

- To synthesis different novel solid-phase nanocomposites with different morphologies for application in electrochemical sensor
- To fabricate the hydrogen peroxide sensor based on synthesized novel solid-phase nanocomposites
- To evaluate and enhance the performance of modified glassy electrodes with novel solid-phase nanocomposite as hydrogen peroxide sensor

1.3 ORGANIZATION OF THIS DISSERTATION

Chapter 1 of these thesis introduces the background and importance of study and objectives. Chapter 2 presents literature review and relevant research associated with the problem addressed in this study. Chapter 3 presents the methodology and procedures used for synthesis and characterization. Chapter 4 demonstrates the results and discussion and finally Chapter 5 provides the conclusion of the research findings, implications for practice, and some recommendations for future research.

CHAPTER 2: LITERATURE REVIEW

1.4 HYDROGEN PEROXIDE ELECTROCATALYSIS MATERIALS

The main purpose of a sensor recognition system is to provide the sensor with a high level of selectivity for analyte measurement. Apart from the inherent catalytic characteristics of a material towards the analyte, its selectivity is improved by choosing a suitable electrical potential and introducing of a catalytic reaction step, through the addition of selective membranes or by further modifications. This section will review the most important materials with particular interest in the analytical parameters of the sensing devices fabricated from them.

Nanocomposites are the composites in which at least one of the phases shows dimensions in the nanometer range ($1.0 \text{ nm} = 10^{-9} \text{ m}$). Solid-phase nanocomposite materials are the materials made from two or more constituent materials with significantly different physical or chemical properties, that when combined, produce a material with characteristics different from the individual components. Various materials can be used to prepare nanocomposites depending on the achieved physical or chemical properties of the nanocomposite (Camargo, Satyanarayana, & Wypych, 2009). Table 2.1 shows some examples of composite materials with limit of detection (LOD) as hydrogen peroxide sensors.

Table 2.1 Examples of composite materials as hydrogen peroxide sensors

Composite materials as hydrogen peroxide sensor	LOD (μM)	References
AgNPs-PPYCs	0.9	(Qin et al., 2011)
AgCl-PANI	0.28	(Porchelvi, Sudarvizhi, & Pandian, 2013)
AgNPs-CNT	1.6	(Shi et al., 2011)
PANI-PdNPs	2.6	(Ivanov, Tsakova, & Bund, 2013)
Pt-MWCNTs-PANI	2.0	(Zhong et al., 2012)
RGO-Ag/GCE	1.6	(Moradi Golsheikh et al., 2013b)
AgNPs-MWCNT/Au	0.5	(Lu, Chang, et al., 2011)

1.4.1 Conductive polymers base nanocomposites materials

In recent years, considerable attention has been paid to conductive polymers due to their unique properties and their applications in several fields, such as chemical sensors, capacitors and anti-corrosion coatings (Kleiner & Matthiesen, 1989; Raghavendra et al., 2003; Wessling, 1998). The synthesis and production of nanoscale conducting polymers has become more popular because they are promising materials for the fabrication of sensors (Aussawasathien, J.H. Dong, & Dai, 2005a; Hua et al., 2011; Kan et al., 2012; Kirchner et al., 2012; Mahmoudian et al., 2012; Ndangili et al., 2010). Furthermore, conductive polymers like polypyrrole (PPY) and polyaniline (PANI) have received huge interest in the last few years and have been used in various applications as sensor and biosensors due to their polymer chain structure, high conductivity, environmental stability

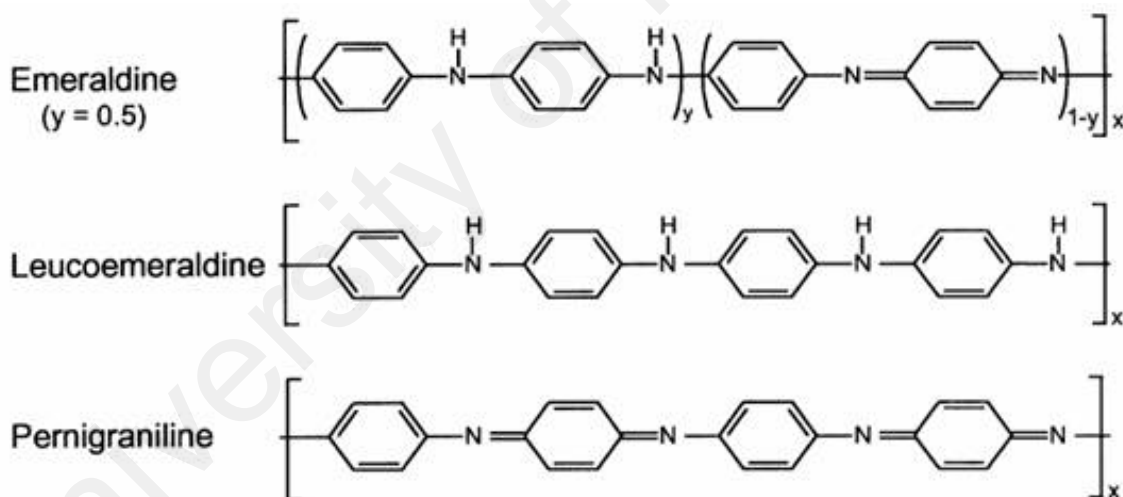
and low cost (Shahnavaz et al., 2014). One dimensional (1D) nanomaterials like nanowires (Kleiner & Matthiesen, 1989), nanofibers (Aussawasathien, Dong, & Dai, 2005b; Hua et al., 2011), nanotubes (Han et al., 2013; Poorahong et al., 2012), and nanorods (Wessling, 1998) have attracted a lot of attention in chemistry because of their particular size and morphologies. The properties of conducting polymers nanomaterials properties depend on their shape, size and dimension. In particular, a variety of materials with nanoscale size and consequently high surface area have been widely used for sensors and biosensors (Zhang et al., 2012).

It should be noted that the shape and stability of the polymers could vary depending on the synthetic procedures, such as shaking and stirring which disrupt the agglomeration of them during the polymerization. One dimensional morphology can be prepared from electrochemical and chemical methods such as template synthesis (Anilkumar & Jayakannan, 2009), nanofiber seeding (Zhang, Goux, & Manohar, 2004) and also interfacial polymerization electrospinning (Song & Choi, 2013). In addition, the preparation of these polymers via interfacial polymerization without a template with magnetic stirring and ultrasonic cleaning, with drop-wise addition of the oxidant for a long times (2 h) has also been carried out (Jing et al., 2007). Sonochemical synthesis is one of the synthesis methods, which includes three steps: formation, growth and collapse of the bubbles. It is based on the propagation of acoustic vibrations that causes the production of cavitation bubbles of high-density acoustic energy in a liquid. In the ultrasonic dispersion procedure, symmetric violations of the cavitation bubbles in the interfaces causes the bubbles to collapse. When the solution is exposed to ultrasonic irradiation, the bubbles in the solution can be eliminated by using its acoustic fields. It is also utilized to introduce shock waves in the solution and gain fast impact of liquid to the surface of the particles. Sonochemical method has been proven to be a useful technique

to obtain materials with smaller size and higher surface (Baranchikov, Ivanov, & Tretyakov, 2007).

Among conjugated polymers, Polyaniline (PANI) is considered as a good conductive polymer due to possessing doping of neutral and unoxidized form, which involves electron and proton transfer. Figure 2.1 shows three oxidation states for PANI which can be explained as following:

1. Leucoemeraldine, it is the fully reduced form (all amine nitrogens)
2. Emeraldine, it is the fully oxidized form (all imine nitrogens)
3. Pernigraniline, it is an amine/imine ratio of ~ 0.5 (Chiang & MacDiarmid, 1986; MacDiarmid et al., 1987).



4. Figure 2.1 Three oxidation states for PANI

Electronically conducting emeraldine can be obtained from the electronically insulating leucoemeraldine by standard chemical or electrochemical oxidation, which are similar to other conjugated polymers. With the increase of oxidation, a fully oxidized pernigraniline can be obtained.

In addition, it is notable that except Leucoemeraldine these various oxidation states are pH sensitive and can be switched between doped salt and nondoped base forms. Among all forms of PANI, only the emeraldine salt form is conducting. Protonic acid doping occurs by proton addition to the polymer chain rather than by partial oxidation or reduction of the polymer π -system.

The number of electrons associated with the polymer backbone does not change during the protonation while porotation caused an increase in conductivity up to 9–10 times, reaching saturation in *ca* 1.0 M HCl (Chiang & MacDiarmid, 1986; MacDiarmid et al., 1987). The process is reversed when the protonated polymer is treated with aqueous alkali. In the doped form, conducting polymers typically possess positive charges (polarons or bipolarons) along their polymer chains, whose charge is balanced by the incorporation of anions.

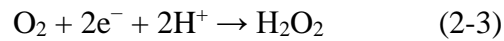
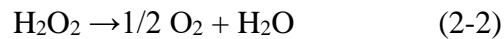
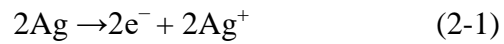
1.4.2 Nobel metal base nanocomposite materials

For incorporating metal nanoparticles into the polymeric matrix several techniques have been reported in the literature (Bein & Stucky, 1996; Li et al., 2015; Salabat et al., 2015; Soliman et al., 2015; Wang et al., 2015). Such combinations require blending or mixing the components with the polymer in solution or in melt form. However, conducting polymers are not fusible and are generally insoluble in common solvents. Therefore, synthesis techniques should be developed to incorporate inorganic components into the conducting polymer. There are two main kinds of nanosized composites of conducting polymers with metals: metal-core nanoparticles are covered with a conducting polymer shell and metal nanoparticles are embedded into a conducting polymer matrix. Metal core nanoparticles covered with a conducting polymer shell are usually prepared by the chemical or electrochemical polymerization of a thin, nanometer-

sized layer of a conducting polymer onto colloid metal particles. There are various techniques for the deposition of nanometer-sized conducting polymer layers onto different substrates, including nanosized substrates (Malinauskas, et.al 2001) Metal nanoparticles embedded into a conducting polymer matrix can be easily obtained by the chemical reduction of metal ions from their salt solution at the conducting polymer/solution interface. Many conducting polymers, when present in their reduced form, have sufficiently high reducing power with respect to some metal ions. Thus, these metal ions have a relatively high positive redox potential, for example, gold, silver, platinum, and copper, can be reduced at a layer of conducting polymer. Composites with metal-core nanoparticles covered with a polymer shell can also be prepared by chemical or electrochemical polymerization of a thin, nanometer-sized layer of polymer onto colloidal metal particles. Silver has proved to be an excellent material for the direct electroanalytical detection of H_2O_2 . (Chang et al., 2011; Fan et al., 2013; Liu, Tian, et al., 2011b; Liao, et al., 2011; Raoof et al., 2012; Song et al., 2011; Welch et al., 2005; Zhao et al., 2009). Lian et al. reported the enhanced characteristics of Ag electrode towards H_2O_2 reduction after it was roughened by electrochemical oxidation reduction cycles (ORC) in a KCl solution (Lian et al., 2009). The improvement in the catalytic activity of the roughened electrode was ascribed to the small Ag nanoparticles produced from the electrodeposition of Ag^+ during the oxidation-reduction process. A LOD of $6.0 \mu\text{M}$, a response time of 2 s and a reproducibility of 4.6% (RSD, n=10) were the analytical parameters of the sensor obtained at an applied potential of approx. -0.35 V (vs. Ag/AgCl). Zhao et al. synthesized 'flowerlike' silver microspheres, which were used to fabricate a H_2O_2 sensor by immobilization on a glassy carbon electrode (Zhao et al., 2009). Silver structures were obtained by reduction of AgNO_3 in the presence of ascorbic acid as reductant and poly vinyl pyrrolidone (PVP) as the stabilizer. The sensor exhibited

a LOD of 1.20 μM (estimated at $S/N = 3$), a response time of 3.50 s and a relative standard deviation less than 5% when the electrode was measured at approx. -0.55 V in PBS pH 7.0. Recently, Tajabadi et al. fabricated an organic-metal hybrid film based on nitrogen-doped graphene-silver nanodendrites (Ag-NG) on an indium tin oxide (ITO) electrode using a simple electrophoretic and electrochemical sequential deposition approach (Tajabadi et al., 2014). The microwave-assisted method was utilized for the synthesis of nitrogen-doped graphene. The Ag-NG-modified ITO electrode exhibited superior electrocatalytic activity toward hydrogen peroxide (H_2O_2) reduction, with a wide linear detection range of 100 μM to 80 mM ($R^2 = 0.9989$) and a detection limit of 0.26 μM with a signal-to-noise ratio of 3. The composites of noble metal nanoparticles and conducting polymers have been used as electrochemical sensors, greatly expanding the application of polymers. However, many studies have demonstrated that composite of conducting polymers and noble metal nanoparticles showed more promising results for the detection of H_2O_2 (Luo et al., 2011; Stejskal; Tian et al., 2011). These results are described to the presence of noble metal nanoparticles in the polymer. Nevertheless, it should be noted that the catalytic activity of electrodes modified with the mentioned composite is affected not only by the type of noble metal particles and polymer but also by the morphology of both materials (Luo et al., 2011; Zhong et al., 2013a). It is therefore an interesting area of research and a challenge to develop high-performance sensors based on polymer nanocomposites with specific morphologies and noble metal nanoparticles for detecting H_2O_2 .

In the presence of AgNPs, the H_2O_2 reduction becomes more irreversible because of providing electron (2-1) to reduce O_2 which has produced by H_2O_2 reduction (2-2) and cause preparing more H_2O_2 (2-3), which leads to preparing more H_2O_2 caused reducing more H_2O_2 (Honda, Koder, & Kita, 1986):



1.4.3 Graphene base nanocomposite materials

Graphene is another material, which is widely used as a sensor. Graphene, which is a single layer sheet of sp^2 -hybridized carbon atoms, has caught the attention of researchers as an extraordinary material that can provide a platform for the preparation of nanocomposite materials. Graphene has incredible chemical and physical properties as below:

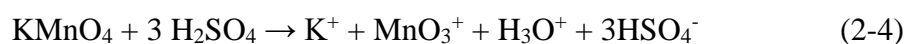
- (i) Graphene is great conductor; electrons are able to flow through graphene more easily than through even copper. The electrons travel through the graphene sheet as if they carry no mass, as fast as just one hundredth that of the speed of light.
- (ii) Graphene is a perfect thermal conductor. Its thermal conductivity was recently measured at room temperature and it is much higher than the value observed in all the other carbon structures as carbon nanotubes, graphite and diamond ($> 5000 \text{ W/m/K}$). It was found that graphene is harder than diamond and about 300 times harder than steel.
- (iii) Optical properties: Despite being the thinnest material ever made and due to its unique electronic properties, graphene absorbs as high as 2.3% of light, that passes through it and it has the "rainbow effect".

- (iv) Finally regarding the chemical properties, the most important one is that graphene can be functionalized by several chemical groups (for instances OH⁻ and F⁻) forming graphene oxide and fluorinated graphene.

These specific properties have wide potential applications in advanced technologies such as nanoelectronics, sensors, capacitors and composites (Huang et al., 2012; Liu et al., 2010; Zhou, et al. 2009).

The structure and properties of graphite oxide depend on particular synthesis method and the degree of oxidation (Dreyer et al., 2010). Graphene oxide structure is shown in Figure 2.2.

Graphene oxide can be prepared in several ways. It was first prepared by Oxford chemist Benjamin C. Brodie in 1859, through the reaction between graphite flake and a mixture of potassium chlorate and fuming nitric acid (Brodie, 1859). In 1957, Hummer and Offeman developed a safer, quicker, and efficient process, using a mixture of sulphuric acid (H₂SO₄), phosphoric acid (H₃PO₄), and potassium permanganate (KMnO₄) and achieved the similar level of oxidation (Hummers et al., 1958). Potassium permanganate in the presence of sulphuric acid as a strong acid generates di manganese heptoxide (Mn₂O₇) as in equations (2-4)-(2-5).



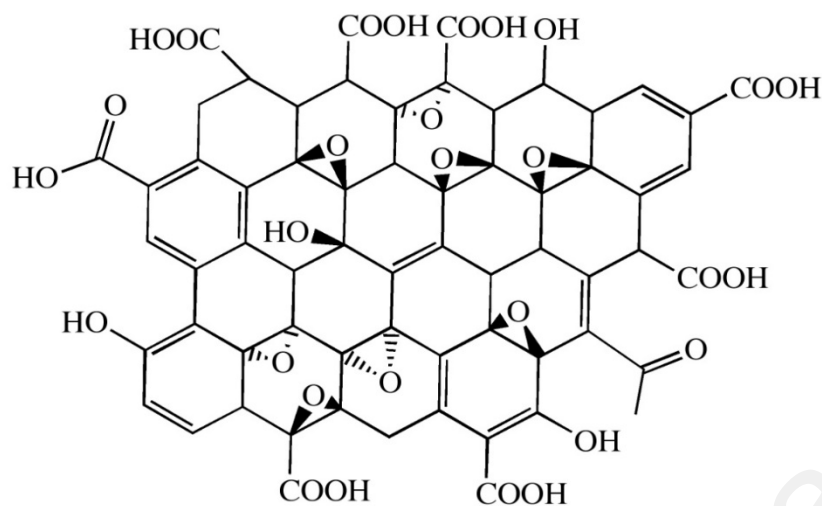


Figure 2.2 Graphene oxide structure

Improved method for GO preparation has many advantages such as simple protocol, higher yield, equivalent conductivity upon reduction for preparation in large scale and no toxic gas progression during preparation. In 2009, a mixture of H_2SO_4 and $KMnO_4$ has been used to cut open carbon nanotubes lengthwise, resulting in microscopic flat ribbons of graphene, a few atoms wide, with the edges "capped" by oxygen atoms ($=O$) or hydroxyl groups ($-OH$) (Kosynkin et al., 2009). Many methods have been reported for production of graphene, such as exfoliation (Han, Dong, & Xu, 2011), chemical methods (Grayfer et al., 2011), chemical vapor deposition (CVD) (Park et al., 2008) and electrochemical methods (Zeng et al., 2011). The most common preparation method of graphene oxide is exfoliation by using strong oxidant agents (Figure 2.3). The GO that was prepared from graphite flakes can be dispersed in water and can be used for preparation of graphene thin films because it's hydrophilicity (Yu et al., 2010). Moreover, also the size of dispersed graphene flakes exfoliated can be selected by controlled centrifugation (Khan et al., 2011).

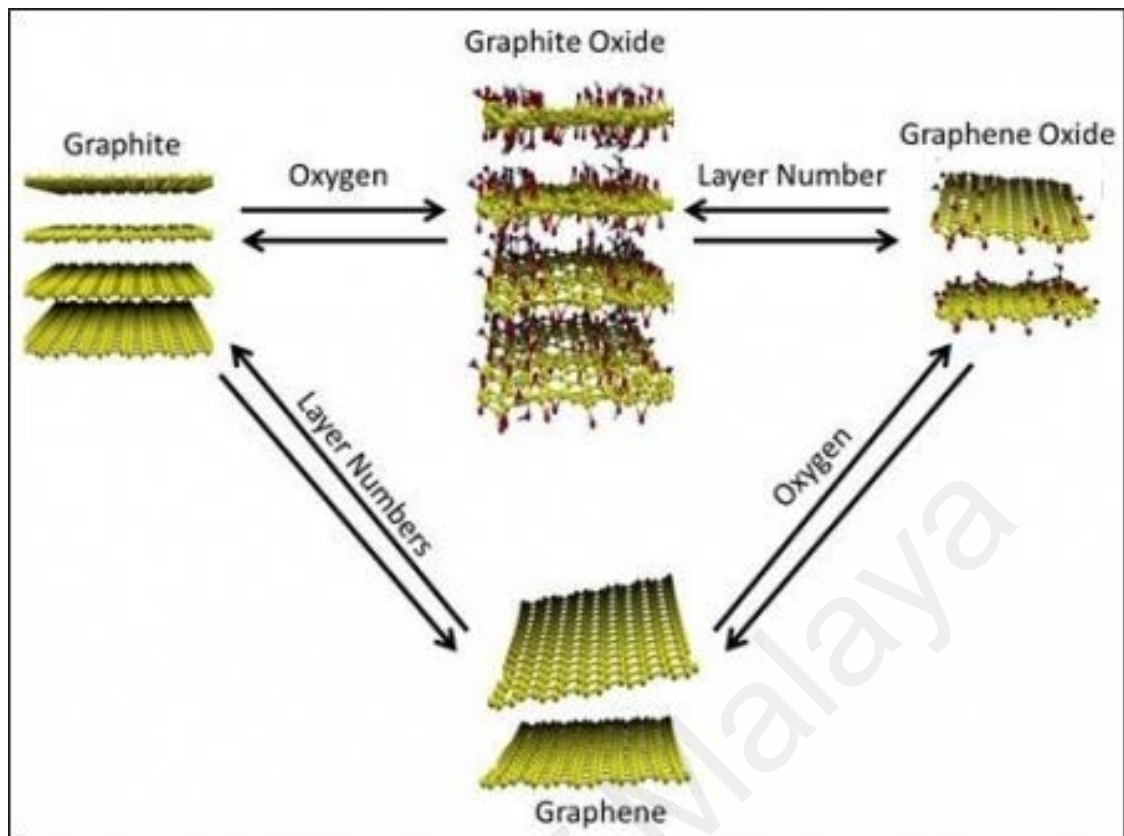


Figure 2.3 Preparation process of graphene

Nowadays, reduced graphene oxide sheets have been prepared by reduction of graphene oxide (GO) with a variety of techniques, such as chemical, vapor deposition, electrochemical reduction and hydrothermal methods (Guermoune et al., 2011; Novoselov et al., 2004; Schniepp et al., 2006; Stankovich et al., 2007).

1.4.3.1 Chemical reduction of graphene oxide

Modified graphene preparation method was developed using sulphuric acid H_2SO_4 , phosphoric acid H_3PO_4 , and potassium permanganate KMnO_4 . Adding phosphoric acid H_3PO_4 in this reaction leads in preparation improved graphene oxide. This improved method has many advantages such as simple protocol, higher yield,

equivalent conductivity upon reduction for preparation in large scale and no toxic gas progression during preparation.

The chemicals reduction of GO are usually time-consuming and contain toxic and dangerous chemicals. Thus, it is desirable to use a low-cost, facile and affective approach for preparing soluble reduced graphene oxide (rGO) sheets in high quantities. For these reasons, thermal and electrochemical reductions of graphene oxide have the privilege of being simple, fast and environmentally friendly approaches.

1.4.3.2 Hydrothermal reduction of graphene oxide

GO can be slowly reduced by heat treatment in a process named thermal annealing reduction. In the initial stages of graphene research, rapid heating was usually used to exfoliate graphite oxide and achieve graphene (Pei .et.al 2012). Furthermore, the thermal reduction of graphene oxide has the privilege of being a simple, fast and environmentally friendly approach. For example, Wang et al. proposed a mild and effective thermal strategy to prepare high-quality graphene at a low temperature of 300 °C in only 5 min under an ambient atmosphere (Wang et al., 2012). Moreover, using one step hydrothermal method, Xu et al. successfully prepared a self-assembled high performance graphene hydro gel (SGH) which is electrically conductive, mechanically strong, and thermally stable and also exhibits a high specific capacitance (Xu et al., 2010).

1.4.3.3 Electrochemical reduction of graphene oxide

Electrochemical reduction of GO has attracted huge attention, due to its green and rapid process and its controllable film thickness. Recently it has been reported that reduced-graphene oxide (rGO) could be prepared trough one-step electrodeposition (Liu et al., 2011). Clearly, one-step electrodeposition procedure has several explicit

advantages such as being faster and simpler, having no toxic solvent, which is naturally able to control the deposited film thickness as compared to two-step electrodeposition method (Chen et al., 2011; Gao et al., 2012; Wu et al., 2011).

1.4.4 Carbon nanotube (CNT)

Another excellent material, namely carbon nanotubes and graphene, has been widely used in nonenzymatic sensors due to their large surface area, high chemical stability, and excellent electrical conductivity (Jin et al., 2012; Konwer, Guha, & Dolui, 2013; Liang et al., 2013; Nie et al., 2011; Yin et al., 2013). Therefore, there are growing numbers of peer reviewed studies focusing on the preparation of nanostructured sensors-based modified carbon electrodes (GCE) using carbon nanotubes (MWCNT) (Fang et al., 2012; Gooding, 2005; Merkoçi et al., 2005; Nasab et al., 2013; Rivas et al., 2007; Wang, 2005; Wang, Musameh, & Lin, 2003) as an electrochemical biosensor in general, and H₂O₂ biosensor in particular.

1.4.5 Carbon nanotube base nanocomposites materials

Another excellent material, namely carbon nanotubes and graphene, have been widely used in non-enzymatic sensors due to their large surface area, high chemical stability, and excellent electrical conductivity (Jin et al., 2012; Konwer, Guha, & Dolui, 2013; Liang et al., 2013; Nie et al., 2011; Yin et al., 2013). Therefore, growing numbers of peer reviewed studies focused on the preparation of nanostructured sensors based modified carbon electrodes (GCE) using multi-walls carbon nanotubes (MWCNT) (Fang et al., 2012; Gooding, 2005; Merkoçi et al., 2005; Nasab et al., 2013; Rivas et al., 2007; Wang, 2005; Wang, Musameh, & Lin, 2003) as an electrochemical biosensor in general, and H₂O₂ biosensor in particular.

Most carbon materials for electrochemical purposes have surface oxygen groups such as carboxylic, carboxyl, phenolic and aldehyde as well as other groups. Oxygen functional groups can increase the carbon surface hydrophilicity in aqueous solutions. So the functional MWCNTs with carboxylic, carboxyl, phenolic, aldehyde and other groups could improve the chemical and electrochemical properties of them. Meanwhile, when the carbon is used as the anode, the stability of the carbon increased with the oxygen content, while it decreased when used as cathode (Nakamura, Nakanishi, & Yamamoto, 1996).

1.4.6 Nanocomposite of graphene, carbon nanotube and noble metals for detecting of H₂O₂

GO sheets have a high edge density (ρ_L) but in three-dimensional (3D) arrangement, the absence of edge density is observed. On the other hand, MWCNT has 3D network with high surface area, but lower surface charge density. The 3D network of GO–MWCNT nanocomposite could efficiently high surface area of MWCNT with high charge density of GO to prepare dramatically high edge density per unit nominal area. Hence, high edge density shows superior performance for GO–MWCNT nanocomposite as compared to GO or MWCNT individually (Lorestani et al., 2014). The noncovalent rGO-MWCNT composite could be used as good conductive carbon nanomaterials with an excellent catalytic effect for electrochemical research.

Wei et al. have reported preparation of hydrogen peroxide (H₂O₂) sensor via two-step method by convenient electrodeposition of Ni(OH)₂ nanoparticles on graphene–MWCNT film on modified glass carbon electrode (GCE) (Gao et al., 2014). Bose et al. has fabricated an amperometric biosensor based on cytochrome c (Cyt c) immobilized graphene oxide–multiwall carbon nanotube (GO–MWCNT) composite chemically and

dropped it on a nano Au modified glassy carbon electrode for detection of H₂O₂ (Dinesh et al., 2014). Based on previous studies decoration of graphene or carbon nanotubes with metal nanoparticles could enhance the electrochemical properties of the composite compared to using each constituent individually. Moreover, recently, graphene, or MWCNT composites with Ag, Pt, and Au nanoparticles have been used for detecting H₂O₂ (Feng et al., 2011; X. Liu et al., 2013b; Rajabzade et al., 2012; Wang & Yun, 2013; Yu et al., 2013). Among these materials, silver nanoparticles (AgNPs) demonstrated excellent catalytic activity for H₂O₂ reduction (Welch et al., 2005). The performance of a hydrogen peroxide sensor could be affected by the shape, size, and dispersion of AgNPs on the electrodes (Chen et al., 2011). Therefore, the composite matrix plays an important role in gaining a high dispersion of AgNPs, as well as its respective size and shape. For example, Yang et al. and also Compton's group discussed the chemical and physical methods that have been employed to fabricate AgNPs-MWCNT composites (Wildgoose, Banks, & Compton, 2006; Yang et al., 2008). Other reported methods to produce AgNPs-MWCNT composite are templates, chemical reagents, and irradiations (Bale et al., 2007; Lin et al., 2009), electrodeposition method, (Tsai et al., 2009) and synthesis by functionalization of MWCNT without the addition of any chemical (reducing agent) or exposure to irradiation. The AgNPs were reduced onto the MWCNT surface and resulted in the excellent dispersion of AgNPs in the AgNPs-MWCNT composite which also displayed superior performance in sensing H₂O₂ at high sensitivity levels (Li et al., 2013; Zhao et al., 2009).

1.5 METHODS TO FABRICATE NANOCOMPOSITES MATERIALS

One dimensional (1D) nanomaterials like nanowires (Kleiner & Matthiesen, 1989), nanofibers (Aussawasathien et al., 2005b; Hua et al., 2011), nanotubes (Han et al.,

2013; Poorahong et al., 2012) and nanorods (Wessling, 1998) have attracted huge attention in chemistry because of their particular sizes and morphologies. The nanomaterial properties depend on their shape, size and dimension. In particular, these kind of nanoscale-sized materials, which possess high surface area materials have been widely used for sensors and biosensors (Ghadimi et al., 2013; S. Zhang et al., 2012). There are several methods to fabricate different morphologies of nanocomposites materials.

1.5.1 Chemical preparation of nanocomposites materials

In the past decade, conducting nanostructures have become a rapidly growing field of research, because they display new properties related to their nanoscale size and have greatly improved the performance of devices (Ma et al., 2010). For example conducting polymer nanostructures can be synthesized by several approaches, such as well-controlled solution synthesis (Chiou & Epstein, 2005; Huang & Kaner, 2004b), soft-template methods (Wan, 2008), hard-template methods (LJ Pan et al., 2007; Yang et al., 2005), and electrospinning technology (Lijia Pan et al., 2010; Yu, Fridrikh, & Rutledge, 2004).

Each method of 1D nanostructures synthesis has its specific merits and inevitable weaknesses. The template-directed synthesis is generally acceptable to provide a simple, high throughput, and cost-effective procedure that allows the complex topology of a template to be duplicated in single step. The major advantage is that both the dimensions and compositions of nanowires and nanotubes can be easily controlled by varying experimental conditions. The main limits of the template-directed synthesis are the following.

Removal of the template through a post-synthesis process may cause damage to the nanowire and nanotube products. In addition, most nanowires synthesized using template-directed methods are polycrystalline in structure, an unwanted feature that may limit their use in device fabrication and fundamental studies (Gu et al., 2014; Huang & Kaner, 2004a; Wang, & Xia, 2003; LJ Pan et al., 2007). Moreover, the use of a template limits the quantity of structures that can be produced in each run of synthesis. To solve this major limitation, research studies will have to focus on template-free methods and control the morphology by controlling the physical condition of the synthesis method like reaction temperature or acidic condition (Ding et al., 2008; Huang & Lin, 2009).

1.5.2 Hydrothermal preparation of nanocomposites materials

Hydrothermal synthesis includes various techniques of crystallizing substances from high-temperature aqueous solutions at high vapor pressures. For example, graphene based composites which, need to be reduced could be synthesized by hydrothermal method. Although the reduction of GO could be accomplished using reductants like hydrazine, hydroquinone and NaBH_4 . The processes are usually time-consuming and contain toxic and dangerous reductants. Thus, it is desirable to use a low-cost, facile and effective approach for preparing soluble rGO sheets in high quantity. For these reasons, thermal reduction of graphene oxide has the privilege of being a simple, fast and environmentally friendly approach (Long, et al. 2010).

Graphene's excellent characteristics such as high electrical conductivity, excellent chemical tolerance and high surface to volume ratio make it an attractive matrix for composites. Graphene and multi-walled carbon nanotube (GO-MWCNT) has been proven to be a good material combination for preparing nanocomposites (Kim, Hwang, & Kim, 2014). Previous studies have shown that GO-MWCNT nanocomposite resulted

in large electrochemical surface area and fast electron transfer for sensor applications (Chen et al., 2012; Woo et al., 2012).

1.5.3 Electrochemical preparation of nanocomposites materials

Electrochemical synthesis represents a highly efficient method for the fabrication of nanostructured energy materials, such as nanorods, nanowires, nanotubes, nanosheets, dendritic nanostructures, and composite nanostructures, which can be easily fabricated, with advantages of low cost, low synthetic temperature, high purity, simplicity, and environmental friendliness.

Different kinds of graphene-based hybrids have been fabricated to elevate electrochemical sensing platforms. An approach to build a high-performance graphene-based sensing composite in a rapid, simple, controllable and green way has become a key subject. Until now, graphene-based materials have been normally prepared from chemical reductions of graphene oxide (GO) and then dropped onto an electrode surface (Pumera et al., 2010). These kinds of preparation methods involved some limitations such as lack of film thickness control and toxic chemicals and the point that they are not so producible (Dreyer et al., 2010). Recently, GO electrochemical reduction has attracted much attention due to its green, rapid process as well as controllable film thickness. It has been reported that the rGO could be prepared through a one-step electrodeposition (Liu et al., 2011). GO also contains hydrophilic oxygen groups and multiple aromatic parts that could assist in obtaining a GO-MWCNT complex with strong π - π stacking interaction (Li et al., 2012; Lu et al., 2011). Yan et al. have reported a one-step electrodeposition graphene/carbon nanotubes/chitosan (GR/CNTs/CS) hybrid for voltammetric detection of methyl parathion (Liu, Yang, & Niu, 2013). composite materials based on metals, noble metals and their derivatives such as Cu (Luo et al., 2012), MnO_2 (Chen, Zhang, & Ye,

2008), Ag (Bai et al., 2014) and Au (Li et al., 2013) have been broadly investigated to prepare non-enzymatic sensors. Among those noble metal composites materials, Ag-based composites display high electrochemical properties as a sensor for H₂O₂ (Moradi Golsheikh et al., 2013b; Sawangphruk et al., 2014).

1.6 SENSOR TECHNIQUES FOR HYDROGEN PEROXIDE DETECTION

Laboratory methods for the determination of H₂O₂ concentrations may be classified into five categories as follows: Titrimetry; Spectrophotometry; Fluorescence; Chemiluminescence and Electrochemical methods. All the techniques will be reviewed, with special attention given to electrochemical methods.

1.6.1 Titration methods

Several titration schemes have been used for the determination of H₂O₂. In the permanganate method, a peroxide solution is titrated with permanganate (VII), which is reduced to manganese (II) in the presence of H₂O₂ (Yamada et al., 2010). This method is subject to interferences caused by both organic and inorganic substances that react with permanganate. Hurdis et al. reported the determination of H₂O₂ by creating oximetry. This method consists of the reduction of cerium (IV) in the form of ceric sulfate [Ce(SO₄)₂] to cerium (III) by H₂O₂ under acidic conditions in the presence of a ferroin indicator (Hurdis et.al 1954).

1.6.2 Spectrophotometric methods

Matsubara et al. used a water-soluble titanium (IV)-porphyrin complex, [TiO(tpypH₄)⁴⁺], to determine trace amounts of H₂O₂ (Matsubara, Kawamoto, & Takamura, 1992). It was observed that the absorbance of TiO(tpypH₄)⁴⁺ at 432 nm

decreased significantly in proportion to the concentration of H_2O_2 added which can be justified due to the consumption of $\text{TiO}(\text{tpypH}_4)^{4+}$ accompanied by the formation of $\text{TiO}_2(\text{tpypH}_4)^{4+}$. This reagent was used for the determination of H_2O_2 in water samples such as tap water and rainwater and absorbance was found to be proportional to H_2O_2 concentration in the range 1.0×10^{-8} to 2.8×10^{-6} M. Seller reported the use of potassium titanium (IV) oxalate for the spectrophotometric determination of H_2O_2 concentrations down to $10 \mu\text{M}$ (Sellers, 1980). The method is found particularly suitable for the determination of H_2O_2 in the presence of complexing and reducing agents, although fluoride interference was observed. The iodometric method is similar to the iodometric titration in that iodide is oxidized to iodine in the presence of molybdate catalyst.

1.6.3 Fluorescence methods

The spectrofluorimetric determination of H_2O_2 is generally based on an enzyme catalytic oxidation reaction of a fluorogenic substrate by H_2O_2 . Horseradish peroxidase (HRP) is a heme-containing enzyme and the most commonly used enzyme in H_2O_2 determination due to its high selectivity (Liu et al., 1999). Chang et al developed a sensing probe for H_2O_2 based on the HRP immobilization on $\text{Fe}_3\text{O}_4/\text{SiO}_2$ magnetic nanoparticles (Chang et al., 2009). H_2O_2 was activated in the presence of HRP and oxidized non-fluorescent (3-4-hydroxyphenyl) propionic acid (HPPA) to a fluorescent product with an emission maximum at 409 nm. Liu et al. used β -cyclodextrin (CD)-hemin instead of HRP as the catalyst in the spectrofluorometric determination of H_2O_2 (Liu et al., 1999). 4-methylphenol (p-cresol) was used as a substrate because it presented low fluorescence whereas the oxidation product showed high fluorescence intensity with a maximum at 410 nm. The use of β -cyclodextrin solved some of the drawbacks shown by HRP such as its cost and instability in solution.

1.6.4 Chemiluminescence methods

Several chemiluminescence methods for H₂O₂ determination involve the use of 5-amino-2,3-dihydro-1,4-phthalazinedione (luminol). When H₂O₂ is mixed with luminol in the presence of a catalyst, the decomposition of H₂O₂ leads to a sequence of reactions resulting in the release of photons from a luminol by-product. Either Co(II) or Cu(II) can be used as a catalysts for H₂O₂ decomposition (Hanaoka, Lin, & Yamada, 2000). Hanaoka et al. reported the determination of H₂O₂ by chemiluminescence (CL), using a heterogeneous catalyst, Co(II)-monoethanolamine complex immobilized on Dowex-50W resin (Hanaoka, et.al 2001). They developed a H₂O₂ flow sensor, which showed a linear ratio of CL versus the concentration of H₂O₂ in the range $2 \times 10^{-7} \rightarrow 2 \times 10^{-5}$ M and a detection limit of 1×10^{-7} M (S/N = 3). The application of the device to determine H₂O₂ in rainwater samples yielded satisfactory results. The use of luminol is subject to interferences in natural water.

Chemiluminescence provided a LOD lower than the titration and spectrophotometric methods. Titration methods seemed to be suitable for H₂O₂ detection at high concentrations, being inaccurate for the determination of H₂O₂ below 10^{-3} M. However, spectrophotometry allowed H₂O₂ detection down to 10^{-6} M, whereas 10^{-8} M H₂O₂ was achievable by fluorescence and chemiluminescence (Hanaoka et al., 2000). However, most of these techniques employed a partial or total human operation, making the automated quantification of H₂O₂ difficult. Moreover, the above-mentioned methods have been proved time-consuming and highly prone to interferences. All these drawbacks have led the search for alternative methods for H₂O₂ detection.

1.6.5 Electrochemical methods

Previous studies on electrodeposition of rGO on GCE surface have been conducted, for example, Mahmoudian et.al (Mahmoudian, 2012) reported the electrical properties of a sandwich of electrodeposited polypyrrole nanofibers between two layers of reduced graphene oxide nanosheets which, electrodeposition of rGO on GCE have been carried out in an aqueous solution of 7.0 mg l^{-1} GO and a 0.1 M phosphate buffer solution at a scan rate of 1.0 mV s^{-1} . The challenge associated with H_2O_2 detection was its accurate quantification at low concentration in samples containing possible interferences. Thus, one of the main drawbacks of the traditional techniques was their inability to give precise results in the presence of interferences such as chlorine, which is very common in water samples. Recently, electrochemical methods have exhibited inexpensive, sensitive and effective way to examine the reactions of many substances (Ballarin et al., 2004; Liu et al., 2014). Moreover, they are quite selective techniques, which allow the determination of a particular analyte by choosing the appropriate applied potential, eliminating possible interferences. The chemical sensor is a device that transforms real-time chemical information of its surrounding environment (from the concentration of a specific sample component to the total composition analysis), into an analytically useful signal (Crouch et al., 2005; J. Wang, 2008).

Generally, chemical sensors contain two basic components connected in series: a chemical recognition system (receptor) and a physico-chemical transducer. In the case of electrochemical sensors, the analytical information is obtained from the electrical signal that results from the interaction of the target analyte and the receptor. According to the nature of the electrical signal, the electrochemical sensors can be classified into the

following categories: Amperometric sensors; Potentiometric sensors; Conductometric sensors;

1.6.5.1 Amperometric sensors

Amperometric sensors are based on the measurement of the current obtained from the electrochemical oxidation or reduction of electroactive species. The signal transduction process is accomplished by controlling the potential of the working electrode at a fixed value (relative to a reference electrode) and monitoring the current as a function of time. The applied potential provides the driving force for the electron transfer reaction of the electroactive species (Chen et al., 2012). The resulting current is directly proportional to the rate of the electron transfer reaction and, therefore, to the bulk concentration of the electroactive species. The relationship between the moles, N , of electroactive species reacted (either oxidized or reduced) and the charge passed through the sensor, Q , is known as Faraday's Law (2-6):

$$N = Q/nF \quad (2-6)$$

Where n is the number of electrons transferred per mole and F is the Faraday constant ($F= 96487 \text{ C/mol}$) (Romer, 1982).

Many of the current devices for the determination of H_2O_2 are based on amperometric sensors. Li et al. reported the development of a disposable amperometric biosensor based on the screen printing technique for the commercial detection of H_2O_2 at -0.30 V (vs. a screen-printed Ag/AgCl pseudo-reference electrode) (Ricci et al., 2003). Horseradish peroxidase (HRP) was entrapped in a polypyrrole (PPy) film electropolymerized on the surface of the carbon screen-printed electrode. Potassium ferrocyanide was used as a mediator to improve the electron transfer between the enzyme and the electrode. The

sensor showed a sensitivity of $3.3 \times 10^{-2} \text{ AM}^{-1} \text{ cm}^{-2}$ and a relative standard deviation (RSD) of 10.24% ($n = 5$). Zhang et al. developed a sensitive amperometric H_2O_2 sensor based on a glassy carbon electrode modified with a composite made from thionin, EDTA, multiwalled carbon nanotubes (MWCNTs) and chitosan (CHIT) (Keying Zhang et al., 2010). Thionin was used as a mediator and was covalently immobilized onto the MWCNTs-CHIT film by means of EDTA activated by carbodiimide (EDC). The amperometric detection of H_2O_2 was carried out at approx. -0.40 V (vs. Ag/AgCl). The sensor showed high sensitivity with a LOD of $6.5 \times 10^{-8} \text{ M}$ ($S/N=3$) and a reproducibility of 5.6% (RSD) for $n = 3$. Lately, an increasing amount of research is being carried out and focusing on amperometric probes due to their high sensitivity and rapid performance. These amperometric sensors have been widely used for the determination of H_2O_2 as compared to other electrochemical techniques, as the H_2O_2 in the solution can be reduced via the following mechanism:

H_2O_2 can be directly reduced to yield H_2O (2-7).



1.6.5.2 Potentiometric sensors

Potentiometric measurements rely on the determination of the potential difference at zero current between either an indicator and a reference electrode or two reference electrodes separated by a permselective membrane (de la Escosura-Muñiz, 2008). The analytical information is obtained by observing the concentration changes of species generated or consumed in order to measure the generated potential (in a logarithmic function). The most important feature in a potentiometric measurement is that equilibrium conditions are established between electroactive species in solution and at the electrode.

This is in contrast to the diffusion-limited condition and characteristic of amperometric measurements leading to logarithmic relations between voltage and concentration rather than a linear relation. The relationship between the potential and the ionic concentration in solution in a potentiometric chemical sensor is given by the Nernst equation (2-8):

$$E = E^{\circ} - \frac{0.05916V}{Z} \log_{10} \frac{a_{Red}}{a_{Ox}} \quad (2-8)$$

Where E is the cell potential, E° is the standard cell potential, z is the number of moles of electrons transferred in the cell reaction, and a_{Red} and a_{Ox} are the chemical activities for the reductant and oxidant species, respectively.

1.6.5.3 Conductometric sensors

Conductometric (or resistive) sensors rely on the electrical resistance change that accompanies the interaction of a target analyte with a conductive layer (typically a polymer or ceramic) held between two electrodes (Janata, 2010). In the case of conductometric biosensors, changes in substrate and product concentrations resulting from the catalytic action of enzymes may bring about a net change in solution electrical conductivity. This conductivity change may result from a number of mechanisms:

- (i) Generation of ionic groups.
- (ii) Separation of unlike charges
- (iii) Proton generation and buffering
- (iv) Changes in the size of charge-carrying groups
- (v) Changes in the degree of association of ionic species.

In order to thoroughly define the selectivity of the sensors and improve their commercial utility, meticulous calibration with a variety of potential interferons is required. Conductometric sensors are generally inexpensive and quite simple to construct since they do not need a reference electrode. The conductometric transducers can be manufactured using simple thin film technology, and the voltage can be rather small which substantially decreases the power consumption and to reduce the safety risks when used in living organisms. Only few conductometric sensors for H₂O₂ determination have been reported in the literature because the relatively low impedance of aqueous media hinders the proper operation of the sensor.

University of Malaya

CHAPTER 3: EXPERIMENTAL PROCEDURES

1.7 INTRODUCTION

In this chapter, the synthesis and characterization of six novel solid-phase nanocomposites are described. They are AgNPs-PANINTs(A) and AgNPs-PANINTs(B), AgNPs-PANINRs, AgNPs-MWCNT-rGO(H), AgNPs-MWCNT-rGO(E) and AgNPs-PANINFs-rGO. Their experimental procedure for activity towards hydrogen peroxide detection is included in this chapter. Figure 3.1 shows the Methodology chart of this dissertation.

Table 3.1 Preparation methods of novel solid-phase nanocomposites

Novel solid-phase nanocomposites	Preparation methods
AgNPs-PANINTs (A)	One-step Chemical method using AgNO ₃ at RT
AgNPs-PANINRs	One-step Chemical method using AgNO ₃ at - 5° C
AgNPs-PANINTs (B)	One-step Chemical method using Ag(NH ₃) ₂ OH at RT
AgNPs-PANINFs -rGO	Sonochemical and hydrothermal methods using Ag(NH ₃) ₂ OH
AgNPs-MWCNT-rGO hydrothermal (H)	One-step hydrothermal method using Ag(NH ₃) ₂ OH
AgNPs-MWCNT-rGO electrodeposite (E)	One-step electrodeposition using Ag(NH ₃) ₂ OH

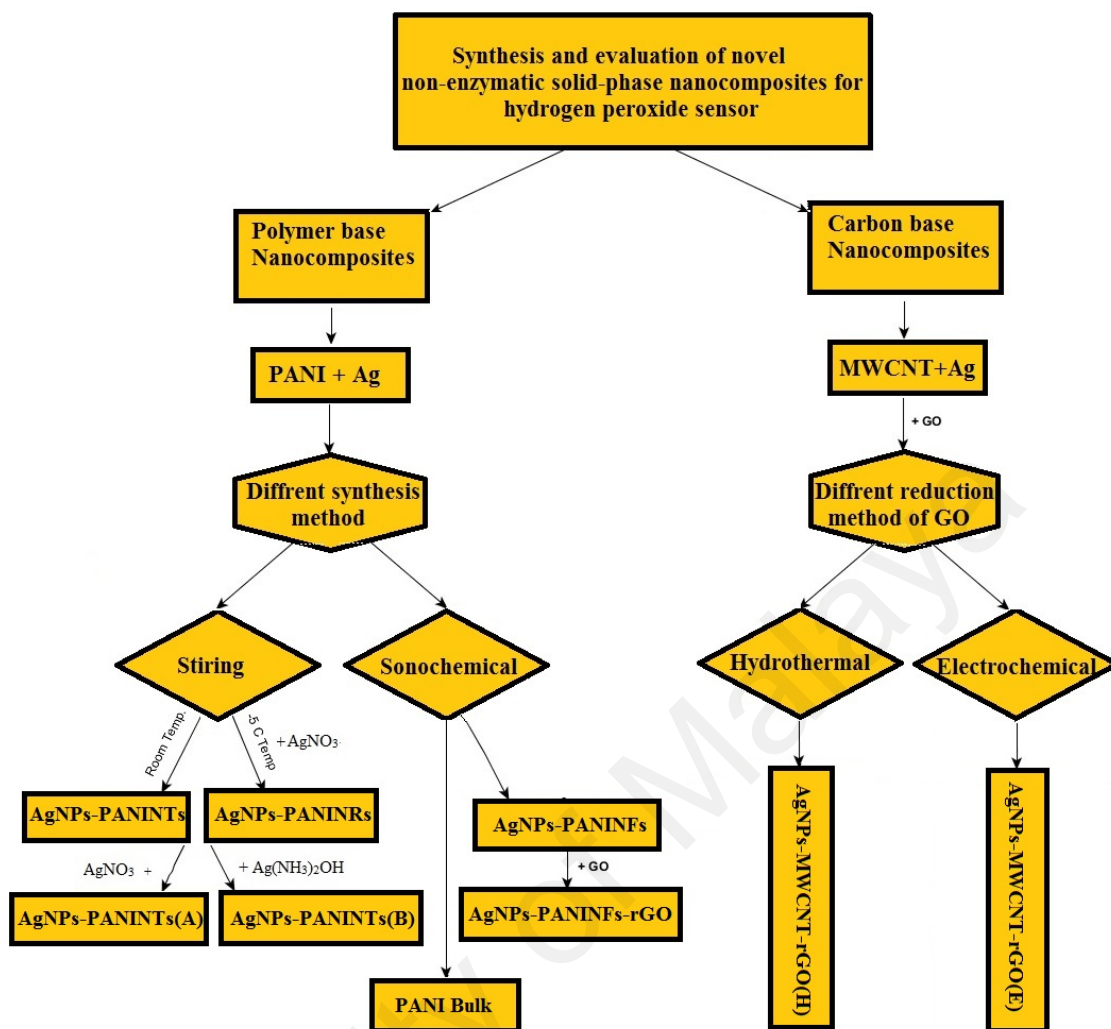


Figure 3.1 Methodology chart of this dissertation

1.8 CHEMICALS

Aniline, ammonium persulfate (APS), sodium phosphate dibasic dihydrate ($\text{HNa}_2\text{O}_4\text{P}\cdot 2\text{H}_2\text{O}$), and sodium phosphate monobasic ($\text{H}_2\text{NaO}_4\text{P}$) were purchased from Sigma-Aldrich. APS was used as an oxidant and the pure aniline was consistently stored in dark prior to the synthesis. Graphite flakes were purchased from Ashbury Inc. (NJ, USA). Sulfuric acid (H_2SO_4 , 98%), nitric acid (HNO_3 , 98%), potassium permanganate (KMnO_4 , 99.9%), hydrogen peroxide (H_2O_2 , 30%), Ammonia solution (NH_3 , 25%), and Silver nitrate (AgNO_3 , 99.7%) were purchased from Sigma-Aldrich. Multi-wall carbon

nanotubes (30–50 nm diameter and 15 μ m length), with >95% purity were obtained from DropSens (Spain). Moreover, all aqueous solutions were prepared with ultrapure water obtained from a Millipore system.

1.9 SYNTHESIS AND CHARACTERIZATIONS

1.9.1 Preparation of PANI

APS (0.22 g) was dissolved in 8 ml of the doubled-distilled water to fabricate an oxidant solution. Then the oxidant solution was added dropwise to the aniline monomer (0.03 ml) solution. The reaction mixture was stirred at 800 rpm at room temperature (25 °C) for 6 h. All the processes up to this point have been done at room temperature. Then, the system was immobilized for 48 h at 0-5 °C. The obtained precipitate was filtered and repeatedly washed out with doubled double-distilled water and ethanol, followed by drying under vacuum for 12 h at 50 °C.

1.9.1.1 Synthesis of polyaniline by bath sonochemical method

10 mL of aniline solution (0.1 M) was prepared and the pH was adjusted to 2.5 by addition of H₂SO₄. In the next step, 10 mL of freshly prepared ammonium persulfate (APS) solution (0.1 M) was added into the aniline solution en masse. The solution was placed in a vessel and then was put into ultrasound bath sonication for 2, 3, 4 and 5 min. The dark blue solution was centrifuged and washed exhaustively with distilled deionized water until the pH reaches 7.0. The obtained product was dried in a vacuum oven at 50 °C for 24 h.

1.9.2 Preparation of PANI nanofibers (PANINFs) via vertical sonication method

10 mL of aniline solution (0.1 M) was prepared and the pH was adjusted to 2.5 by addition of H₂SO₄. In the next step, 10 mL of freshly prepared ammonium persulfate (APS) solution (0.1 M) was added into the aniline solution en masse. The solution was placed in the sonochemical vessel and exposed to ultrasound irradiation using a vertical ultrasonic liquid processor (Misonix Sonicator S-4000, USA, 20 kHz) for 2, 3, 4 and 5 min which were later nominated into PANINFs-1, PANINFs-2, PANINFs-3 and PANINFs-4 respectively. The reaction mixture turned to blue color after about 100 s. The dark blue solution was centrifuged and washed exhaustively with distilled deionized water until the pH reaches 7.0. The obtained product was dried in a vacuum oven at 50 °C for 24 h.

1.9.3 Preparation of silver nanoparticles

The spherical silver nanoparticles is synthesized via citric reduction of a silver salt, where a citrate molecule acts as a reducing and capping agent at high temperatures (Campbell et al., 2009).

1.9.4 Preparation of silver ammonia solution

Silver-ammonia [Ag(NH₃)₂OH] solution was obtained by adding ammonia (1.0 wt.%) to silver nitrate solution (50 mM) until the precipitates were visually invisible to the naked eye (completely dissolved). The concentration of the synthesized Ag(NH₃)₂OH was approximately 40.0 mM (Van Dong, Ha, & Kasbohm, 2012).

1.9.5 Preparation of graphene oxide (GO)

The preparation of GO was done, through a modified Hummers method (Ming, 2010). Graphite flakes (Aldrich) was used for preparation of graphene oxide. 3.0 g of graphite flakes was first oxidized by reacting with concentrated phosphoric acid (H_3PO_4) and sulphuric acid (H_2SO_4) in 1:9 volume. The reaction vessel was immersed in an ice bath, and 18.0 g potassium chlorate was gradually added. The reaction was allowed to carry on for 3 days during stirring in order to fully oxidize graphite into graphite oxide (GO), then 30.0 % H_2O_2 (200 ml) was added and left it for 10 min to complete the oxidization. Later the GO was centrifuged and washed with 1.0 M HCl for 3 times (4000 rpm, 10 min). The GO was further centrifuged and filtered by deionized water to remove metal ions and until the GO reached to pH 7.0. If the gel form appears, it should be centrifuged with 96000 rpm to remove the gel. If it does not appear in the gel form, 4000 rpm can be used. The graphene oxide is exfoliated by applying mild sonication for 5 min to obtain yellow brown suspension (Figure 3.2).



Figure 3.2 Graphene oxide suspension

The exfoliated GO could be reduced to graphene by refluxing the GO solution with hydroquinone for 20 h. The final products were then centrifuged, washed, and finally vacuum-dried (D.C. Marcano et al., 2010) (Figure 3.3).

To remove any extra acid and salt from the prepared GO, the 0.05 wt.% of GO suspension in water was sonicated for 3 h before being dialyzed for another 6 h in doubled-distilled water. The obtained dialyzed GO was then centrifuged for 20 min at 3000 rpm for removing un-exfoliated GO, and it was then dried for 24 h at 50°C.



Figure 3.3 Graphene oxide

1.9.6 Functionalization of MWCNT by carboxylic groups (MWCNT-COOH)

Functionalized MWCNT (fMWCNT) by carboxylic group (MWCNT-COOH) was prepared by mild acid oxidation treatment method (Avilés et al., 2009). The MWCNT has been dispersed by ultrasonic bath in the mixture of concentrated H_2SO_4 and HNO_3 (3:1, v/v) for about 4 h at room temperature. Then resulted MWCNTs were washed and centrifuged with distilled water by (10,000 rpm) until the pH of the resulted MWCNTs solution became neutral and then it was left to be dried overnight at room temperature.

1.9.7 Synthesis of nanocomposites and electrode preparation

1.9.7.1 Preparation of Silver-Polyaniline nanotubes composites [AgNPs-PANINT(A)]

AgNPs-PANINTs(A) was prepared through a one-step method without adding any extra acid, template or surface modifier. The chemical polymerization performed by APS (0.22 g, 0.965 mmol) was dissolved in 8.0 mL of deionized water as an oxidant solution and aniline monomers. The oxidant solution was then added dropwise to the aniline monomer (0.03 mL, 0.322 mmol) solution. Then, AgNO₃ (0.02 g, 0.117 mmol) was added to the above mixture. The reaction mixture was stirred for 6 h at room temperature. Finally, the polymerization system was immobilized for 48 h at 0-5 °C. In this process, the remaining precipitate was washed several times with deionized water and then dried under vacuum for 24 h at 50 °C (Gao et al., 2009).

AgNPs-PANINTs (B) has been prepared to achieve better dispersion and smaller silver size, it was synthesized using the same earlier-described method but Ag(NH₃)₂OH solution (as prepared in 3.3.4.) was used as the source of AgNPs instead of AgNO₃. Their different volume ratio of Ag(NH₃)₂OH:PANI was observed to be 12:1, 6:1 and 3:1 respectively. Each mixture was stirred at 800 rpm at ambient temperature for 6 h and consecutively, immobilized for 48 h at 0-5 °C. The precipitation was filtered and washed out with DI and ethanol, followed by drying under vacuum for 12 h at 50 °C.

1.9.7.2 Preparation of H₂O₂ modified electrode of (AgNPs-PANINTs/GCE)

AgNPs-PANINTs (1.0 mg) was prepared into double-distilled water (1.0 mL) by 30 min of mild ultrasonication to achieve homogeneous suspension. Then 10.0 µl of the

prepared suspension was dropped onto the well-polished glassy carbon electrode, GCE (d=3 mm) and was left to be dried at room temperature for 24 h.

1.9.7.3 Preparation of silver nanoparticles-polyaniline nanorods composite (AgNPs-PANINRs);

The process of AgNPs-PANINRs preparation is exactly the same as preparation of AgNPs-PANINTs(A), except, the oxidant solution was added dropwise to the aniline monomer (0.03 mL, 0.322 mmol) solution in an ice bath instead of room temperature. Three different amounts of AgNO₃ loading i.e. 0.01, 0.03 and 0.05 g was used respectively to study the optimum amount of AgNPs distribution in the composite.

1.9.7.4 Preparation of H₂O₂ modified glassy carbon electrodes of AgNPs-PANINRs composite (AgNPs-PANINRs/GCE)

AgNPs-PANINRs (1.0 mg) were dispersed into double-distilled water (1.0 mL) by mild ultrasonication for 30 min to achieve a homogeneous suspension. Then, 10.0 µl of the prepared suspension was dropped onto a well-polished GCE (GCE Metrohm d=3 mm), and subsequently, the electrode was dried at room temperature for 24 h.

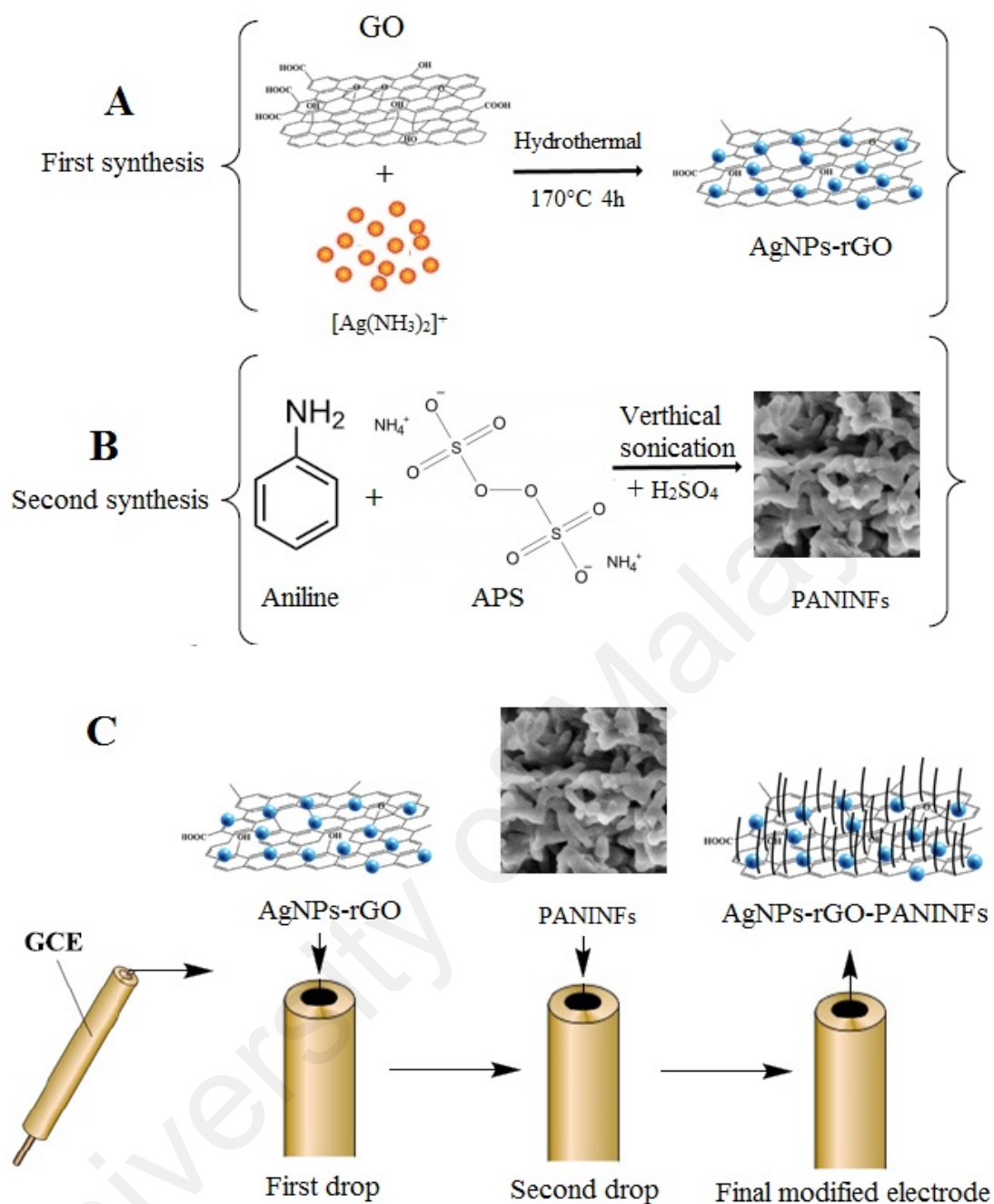
1.9.7.5 Preparation of Silver nanoparticle-reduce graphene oxide (AgNPs-rGO) composite

AgNPs-rGO was prepared by mixing the as-prepared solution of Ag(NH₃)₂OH with GO solution at three different volume ratios i.e. (3:1), (6:1) and (12:1) under stirring for 30 h. Then, the mixtures were placed in an autoclave and heated at 170 °C for 4 h, which were then called AgNPs-rGO-1 and AgNPs-rGO-2, and AgNPs-rGO-3, respectively. The obtained precipitate was then filtered and dried overnight at 50° C.

Previously, AgNO_3 has used as the source of AgNPs for most nanocomposites. To check the effect of using $\text{Ag}(\text{NH}_3)_2\text{OH}$ instead of AgNO_3 , the composite AgNPs-rGO has been prepared by adding GO to 0.04 M AgNO_3 with the volume ratio of 6:1 by applying the same synthesis method, which was then labeled as AgNPs-rGO-4.

1.9.7.6 Preparation of H_2O_2 Modified glassy carbon electrode of Silver nanoparticles-reduced graphene oxide-polyaniline nanofiber composite (AgNPs- PANINFs-rGO/GCE)

Glassy carbon electrode was chosen to act as the base electrode. By using alumina (under 1.00, 0.10 and 0.05 mm diameter) slurries, in the pre-experiment preparations, the clean GCE was polished to a mirror and subsequently washed by water which was previously distilled twice and ultrasonicated in distilled water and ethanol for 10 min respectively and then dried under high purity of N_2 gas flow. The formerly prepared AgNPs-rGO-1, AgNPs-rGO-2, AgNPs-rGO-3 and AgNPs-rGO-4 were carefully dropped on the surface of GCE in order to find the best ratio to detect hydrogen peroxide. Then different volumes (5.00, 10.00, 15.0, 20.0, 25.0 μL) of the optimized AgNPs-rGO dropped on the surface of GCE to optimize the volume amount of dropped composite on the modified electrode. To check the effect of polyaniline nanofibers (that was separately prepared; 3.2.2) on the surface modified electrode, 10.0 μL of PANINFs-1, PANINFs-2, PANINFs-3 and PANINFs-4 were dropped on the optimized AgNPs-rGO electrode (AgNPs-rGO/GCE). N_2 was purged before each process for 10 min in order to eliminate O_2 from electrolyte (Scheme. 3.1).



Scheme. 3.1 A: Preparation of AgNPs-rGO composite. B: Preparation of PANINFs by vertical sonication method. C: Fabrication of modified glassy carbon electrode with Silver nanoparticles-reduced graphene oxide-polyaniline nanofiber composite (AgNPs-PANINFs-rGO /GCE

1.9.8 Synthesis of silver nanoparticle- multi walled carbon nanotube-reduced-graphene nanocomposite (AgNPs-MWCNT-rGO) by hydrothermal method [AgNPs-MWCNT-rGO(H)]

The solution of MWCNT and GO was mixed with the ratio of 3:1 v/v. The AgNPs-MWCNT-rGO composite was prepared by mixing the freshly prepared $\text{Ag}(\text{NH}_3)_2\text{OH}$ solution with MWCNT-GO solution in three different volume ratios, which were (12: 1 v/v), (6:1 v/v), and (3:1, v/v) (Moradi Golsheikh et al., 2013b). All the solutions were stirred for 30 min. Then, the mixture was placed in an autoclave and heated at 170 °C for 4 h, which were later labeled as AgNPs-MWCNT-rGO-1, AgNPs-MWCNT-rGO-2, and AgNPs-MWCNT-rGO-3, respectively. After being cooled to room temperature, the product was isolated by centrifugation, washed several times with pure water and then dried overnight at 50 °C. As reported in the previous studies, AgNO_3 was used as AgNPs source for most of nanocomposites (Campbell & Compton, 2010; Gao et al., 2013). The AgNPs-MWCNT-rGO composite was prepared to check the effect of using $\text{Ag}(\text{NH}_3)_2\text{OH}$ instead of AgNO_3 , using the same volume ratio of MWCNT-GO to 0.04 M AgNO_3 with the volume ratio of 12:1, which was then called AgNPs-MWCNT-rGO-4.

1.9.8.1 Synthesis of silver nanoparticle-multi walled carbon nanotube (AgNPs-MWCNT) by stirring method

AgNPs-MWCNT was synthesized by adding the freshly prepared 40 mM $\text{Ag}(\text{NH}_3)_2\text{OH}$ to an aqueous solution (1.0 mg/mL) of MWCNT at (6:1, v/v) volume ratios under stirring for 4 h.

1.9.8.2 Synthesis of silver nanoparticle-multi walled carbon nanotube- graphene nanocomposite (AgNPs-MWCNT-GO) by stirring method

The solutions of MWCNT and GO were prepared in an aqueous solution (1.0 mg/mL) in a separate container. The mixture of MWCNT and GO was prepared with the ratio of 3:1 v/v. AgNPs-MWCNT-GO was made by mixing the freshly prepared $\text{Ag}(\text{NH}_3)_2\text{OH}$ solution with MWCNT/GO at three different volume ratios i.e. (12:1 v/v), (6:1 v/v), and (3:1 v/v) under stirring for 4 h, which were then nominated to AgNPs-MWCNT-GO-1 and AgNPs-MWCNT-GO-2, and AgNPs-MWCNT-GO-3, respectively (Moradi Golsheikh et al., 2013a). The obtained precipitate was then filtered and dried overnight at 50°C. Previously, AgNO_3 was used as the source of AgNPs for most nanocomposites (Campbell & Compton, 2010; R. Gao et al., 2013). The composite AgNPs-MWCNT-GO has been prepared to check the effect of using $\text{Ag}(\text{NH}_3)_2\text{OH}$ instead of AgNO_3 , by using the same volume ratio of MWCNT-GO to 0.04 M AgNO_3 with the volume ratio of 12:1, which was then called AgNPs-MWCNT-GO-4.

1.9.8.3 Preparation of H_2O_2 modified of AgNPs-MWCNT-GO/ GCE

AgNPs-MWCNT-GO nanocomposite (1.0 mg) was dispersed into double-distilled water (1.0 mL) for 30 min via mild ultrasonication to achieve homogeneous suspension. Then, 10 μL of the prepared suspension was dropped onto the well-polished GCE (GCE Metrohm d=3 mm), and left to dry at room temperature for 24 h to get AgNPs-MWCNT-GO nanocomposite modified glassy carbon electrodes (AgNPs-MWCNT-GO/GCE).

1.9.8.4 Preparation of H₂O₂ modified electrode of AgNPs-MWCNT-rGO/GCE electrode

The AgNPs-MWCNT-GO nanocomposite (1.0 mg) were dispersed into doubled distilled water (1.0 mL) by 30 min mild ultrasonication to achieve homogeneous suspension, then 10 μ L of prepared suspension was dropped onto the well polished GCEs (GCE Metrohm d=3.0 mm) and let it dry at room temperature for 24 h to get the AgNPs-MWCNT-rGO nanocomposite modified glassy carbon electrodes (AgNPs-MWCNT-GO/GCE).

1.9.8.5 Silver nanoparticle-multi walled carbon nanotube-reduced-graphene oxide- composite (AgNPs-MWCNT-rGO) by electrodeposition synthesis method [AgNPs-MWCNT-rGO(E)]

The electrodeposition of AgNPs-MWCNT-rGO(E) was conducted in three-electrode electrochemical cell. The water mixture of MWCNT-COOH (3.2.6) and GO (1.0 mg/mL) has been prepared with the ratio of 1:1 v/v and then the freshly prepared Ag(NH₃)₂OH solution was added to the obtained mixture in four different volume ratios of (3:1, v/v), (6:1 v/v), (12: 1 v/v) and (24: 1 v/v) and sonicated for 2 min to achieve homogeneity (Moradi Golsheikh et al., 2013a). The samples were labeled as AgNPs-MWCNT-rGO-1, AgNPs-MWCNT-rGO-2, AgNPs-MWCNT-rGO-3 and AgNPs-MWCNT-rGO-4, respectively. Cyclic voltammetry was carried out in the solutions on a potentiostat/galvanostat using a three-electrode system: GCE as the working electrode, a platinum coil as the counter electrode and a saturated calomel electrode (SCE) as the reference electrode. Five potential cycles were conducted between -1.50 and 0.00 V at scan rate of 25.0 mV/s to control the loading of deposition mass on the GCE electrode. The obtained modified working electrodes were washed with double-distilled water

before being used as a sensor. For comparison, AgNPs-MWCNT-rGO-5 and AgNPs-MWCNT-rGO-6 were prepared in the same conditions as AgNPs-MWCNT-rGO-3 using AgNO₃ solution (0.04 M) instead of Ag(NH₃)₂OH solution and unfunctional MWCNT instead of MWCNT-COOH, respectively.

1.9.9 Characterization

CHAPTER1: The morphologies of the composites were investigated by field emission scanning electron microscopy (FESEM, Quanta 200F) and the weight percentage of the composites were verified using energy dispersive X-ray (EDX) spectroscopy. The structures were analyzed by X-ray diffraction (XRD Siemens D5000). Transmission electron microscopy (TEM Philips CM200) was performed to obtain greater morphological details about the composites. A Fourier transform infrared spectroscopy Spectrum (400 FT-IR spectrometer) was used to obtain FT-IR spectra of the sample. The electrochemical measurements were performed using a three-electrode cell with a platinum wire as the counter electrode (CE), Silver chloride electrode (Ag/AgCl) (3.0 M KCl) as the reference electrode (RE) and a GCE (GCE Metrohm d=3 mm) as the working electrode (WE) in a 0.1 M phosphate buffer solution with pH 6.5, using a potentiostat/galvanostat (Model PGSTAT-302N from Autolab). All of the measurements were carried out at room temperature and all the electrochemical test were conducted three times. The GCE was polished with 1.00, 0.30 and 0.05 μm alumina slurries, before each use.

1.10 INSTRUMENTATION

1.10.1 Electrodeposition and electrochemical study of modified electrodes

Autolab PGSTAT-302N Potentiostat/Galvanostat has been used for investigation of and determination of electrochemical activity of the modified electrodes to detect H_2O_2 . The FRA software is included in Autolab PGSTAT-302N. This software can run some useful DC techniques such as cyclic voltammetry, chronoamperometry, chronopotentiometry and etc. The cyclic voltammetry technique was used for the detection of H_2O_2 and electropolymerization of nanocomposites and chronoamperometry was used for determination of linear range, limit of detection (LOD), limit of qualification (LOQ), selectivity and sensitivity of modified H_2O_2 sensors. The experiments were carried out at various scan rates in wide range of potential window through the Autolab PGSTAT-302N.

In addition, surface passivation was studied by electrochemical impedance spectroscopy (EIS) through the FRA software. Figure 3.4 shows the set-up of Autolab PGSTAT-302N including three electrodes, i.e. the working electrode, reference electrode and counter electrode.

The Electrochemical impedance spectroscopy (EIS) is an efficient technique to explore the characteristics of interfaces of modified electrodes. After several surface modifications, the conductivity characteristics were characterized by EIS. Meaningful discrepancy in the impedance spectra was detected.

One of the main factors in EIS is R_s or cell resistance, which consists of the solution and the electrolyte resistance.

CPE or the constant phase element was modelled as a non-ideal capacitor

$$CPE = \frac{-1}{(c_i\omega)^\alpha} \quad (4-4)$$

The charge present at a double layer interface is characterized by capacitance, C and used when the surface is heterogeneous. R_{ct} represents the resistance of charge transfer. The definition of the Warburg element is

$$Z_w = \frac{R_{dif}ctnh([i\tau\omega]^\alpha)}{(i\tau\omega)^\alpha} \quad (4-5)$$

R_{dif} is a diffusion resistance of electroactive species, τ a time constant that depends on the diffusion rate ($\tau = l^2/D$), where l is the effective diffusion thickness, and D is the effective diffusion coefficient of the species. At high frequencies, the impedance shows infinite diffusion behavior (phase angle 45°) and at low frequencies, it tends to show the capacitor behavior (phase angle 90°). α value of less than 0.50 implies the non-uniformity of the interface (as it happens with CPE non-ideal capacitance when $\alpha < 1$) (Pauliukaite et al., 2010).

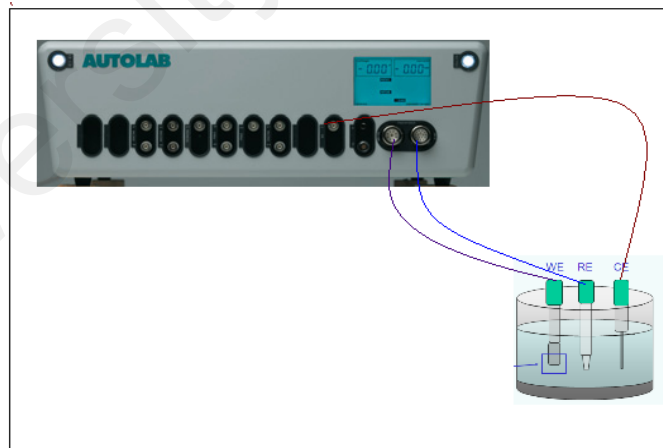


Figure 3.4 Set up of Autolab PGSTAT-302N

1.10.2 Field Emission Scanning Electron Microscope (FESEM) and Energy Dispersive X-Ray (EDX)

Scanning Electron Microscopy (SEM) is one of the most versatile and well-known analytical techniques. Compared to a customary optical microscope, the advantages of electron microscope are high magnification, large depth of focus, and high resolution, as well as easy sample preparation and observation. In this technique, electrons generated from an electron gun enter the surface of a sample and generate many low energy secondary electrons. The intensity of these secondary electrons is governed by the surface topography of the sample. An image of the sample surface is therefore constructed by measuring secondary electron intensity as a function of the position of the scanning primary electron beam. In addition to secondary electrons imaging, backscattered electron imaging, and Energy Dispersive X-Ray (EDX) analysis are widely used for chemical analysis and characterizations. The intensity of backscattered electrons generated by electron bombardment can be correlated to the atomic number of the element within the sampling volume. Hence, qualitative elemental information can be determined. The characteristic X-rays emitted from the sample serve as fingerprints and give elemental information for the samples, including semi-quantitative and quantitative information, as well as the line profiling and spatial distribution of elements (elemental/chemical mapping). SEM with X-ray analysis is an efficient, inexpensive, and non-destructive method for carrying out surface analyses. In department research spot, a state-of-the-art and high resolution FEI Quanta 200F field emission scanning electron microscope (FESEM) with an EDX system (INCA Energy 400) from OXFORD is available. Figure 3.5 shows a photograph of this microscope in department research spot.



Figure 3.5 A photograph of FESEM with EDX set-up.

1.10.3 X-Ray Diffraction (XRD)

The X-ray diffractometer is one of the non-destructive tools for the analysis of crystalline materials. The fingerprint characterization of these materials and the determination of their structure can be gained by using X-ray of the device patterns. The XRD analyses are based on Bragg's law. When the X-rays of wavelength λ are incident at an angle θ on a crystal lattice, a portion of these beams will be scattered in all directions. The necessary and sufficient condition for constructive interference is known as Bragg's law. According to the law, scattered waves originated from each atom will be in phase with each other. Figure 3.6 shows the geometric requirements for this condition. Bragg's law is follows:

$$n\lambda = 2 d_{hkl} \sin\theta \quad (3-1)$$

Where,

λ = the wavelength of the x-ray

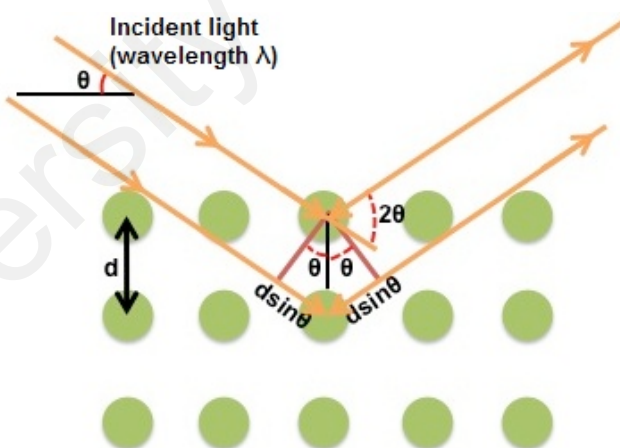
d = the spacing of the crystal layers (path difference)

θ = the incident angle (the angle between incident ray and the scatter plane)

n = an integer

The principle of Bragg's law is applied in the construction of instruments such as Bragg spectrometer, which is often used to study the structure of crystals and molecules.

All aspects of this formula are introduced in **Scheme 3.2** including $dhkl$, which is the interplanar spacing as a function of the Miller indices (h , k , and l) as well as the lattice parameters.



Scheme 3.1 Schematic of the diffraction of an X-rays beam by parallel atomic crystalline material.

The basic features of a classic XRD experiment, as well as our XRD set-up, are shown in Figure 3.6 In the research spot a Siemens D5000 XRD unit was used, with an X-ray source having wavelengths of $K\alpha = 1.5406 \text{ \AA}$. Usually, diffraction experiments

were applied at a fixed wavelength. Therefore, the measurement of the diffraction angles enables the calculation of the associated d_{hkl} and then the lattice constants.

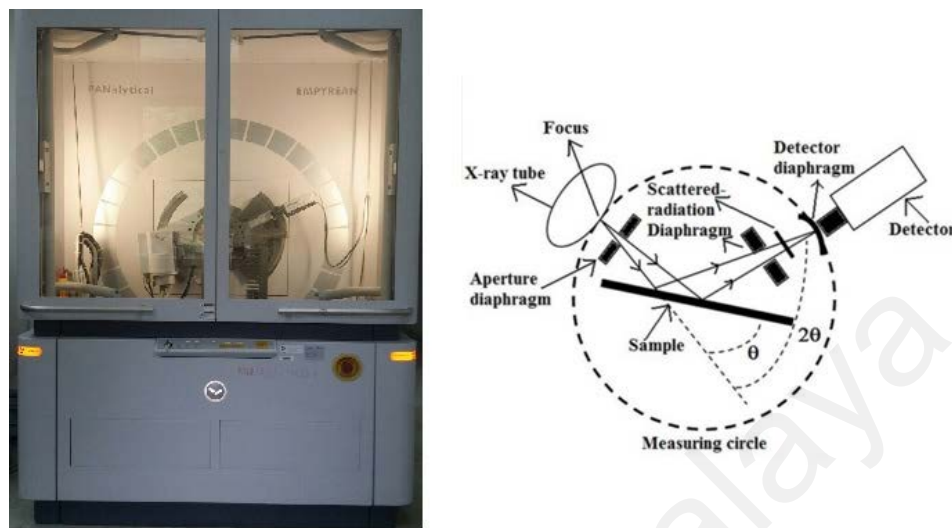


Figure 3.6 Basic features of a typical XRD experiment as well as the Siemens D5000 set-up.

1.10.4 Transmission Electron Microscopy (TEM)

Transmission electron microscopy (TEM) is a microscopy technique by a beam of electrons is based on an ultra-thin specimen and transmitted through it, interacting with the specimen as it passes through (Figure 3.7). Because of this interaction, an image is formed. The image is magnified and focused onto an imaging device, such as a layer of photographic film or a fluorescent screen, or is detected using a sensor (for example, CCD camera). The magnified transmitted signal can be observed through direct electron imaging or electron diffraction. Electron diffraction patterns are applied to determine the crystallographic structure of the materials. The cantilever is usually made up of silicon or silicon nitride with a tip radius of curvature about nanometers. When the tip is reached into the proximity of a sample surface, forces between the tip and the sample cause a deflection of the cantilever according to Hooke's law (Cappella & Dietler, 1999). The most applied method for cantilever deflection measurements is the beam deflection

method. In this method, laser light from a solid-state diode is reflected off the back of the cantilever and collected by a position-sensitive detector (PSD) consisting of two closely spaced photodiodes whose output signal is collected by a differential amplifier. Angular displacement of the cantilever results in one photodiode collecting more light than the other photodiode, producing an output signal (the difference between the photodiode signals normalized by their sum), which is proportional to the deflection of the cantilever. It detects cantilever deflections <10 nm (thermal noise limited). A long beam path (several centimeters) amplifies changes in beam angle (Scheme 3.2). Atomic force microscopy (AFM, PSIA XE-100) measurements were utilized to analyze the structures and surface morphologies.

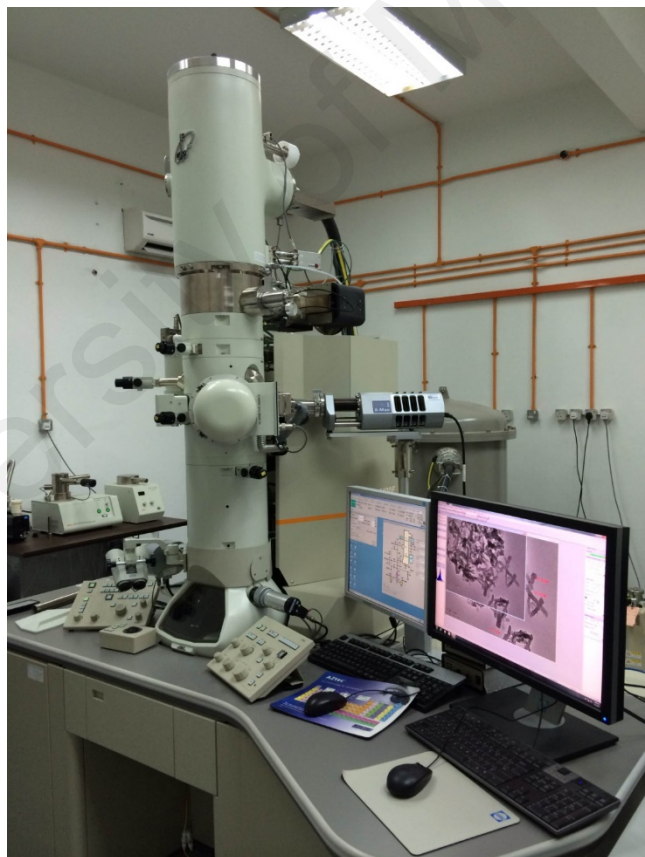
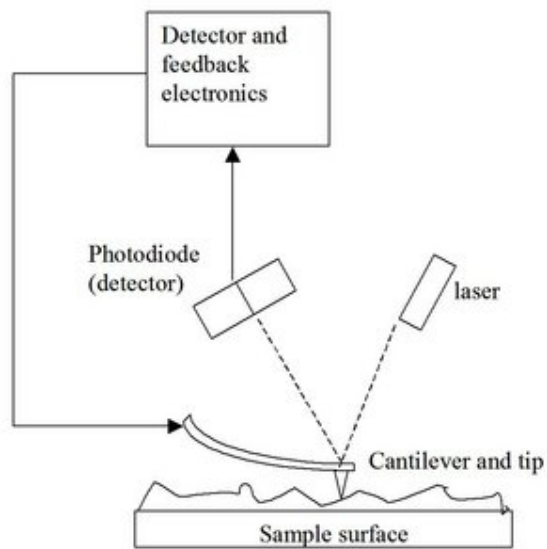


Figure 3.7 photograph of the TEM microscope unit



Scheme 3.3 Schematic of the AFM beam deflection method

University of Malaya

CHAPTER 4: RESULTS AND DISCUSSION

In this chapter, the results of six novel solid-phase nanocomposites and their electrochemical performance as hydrogen peroxide sensor are discussed and explained.

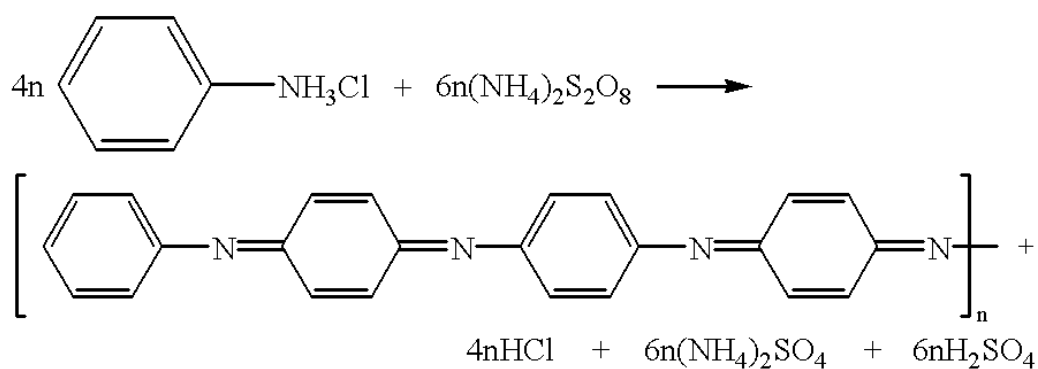
1.11 Silver-polyaniline nanotube composite [AgNPs-PANINTs(A)]

Our first composite is the polyaniline nanotube-silver nanoparticles composite [AgNPs-PANINTs(A)] which was examined as a sensor material for detection of H_2O_2 and the result showed that the composite exhibited a good catalytic activity toward the reduction of H_2O_2 . The prepared modified non-enzymatic H_2O_2 sensor displayed fast amperometric response time and low amount of limit of detection.

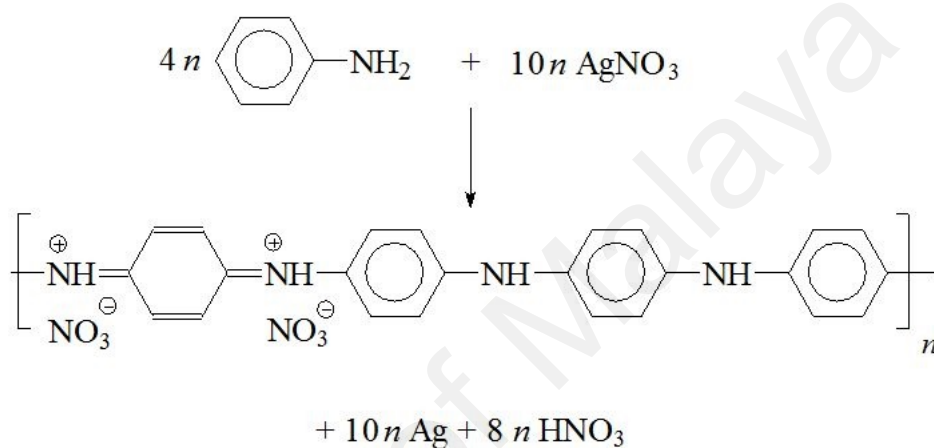
1.11.1 Morphology analysis of AgNPs-PANINTs(A) composite

As described in detail in chapter 3, ammonium persulfate (APS) was used as the oxidant agent to synthesize this nanocomposite. APS is a famous oxidant and PANI morphology can be changed by adjusting the APS amount (Cho et al., 2013). The scheme 4.1 shows the mechanism of aniline oxidation in the presence of APS while the sulfuric acid is a by-product.

The schemes 4.2 indicate that silver nitrite can act as an oxidant agent to produce PANI while the silver appears as a by-product. It shows that the PANI in emeraldine form can be used as a reductant for noble metal salts (Bouazza, Alonzo, & Hauchard, 2009; Stejskal, Prokeš, & Sapurina, 2009; Stejskal, Trchová, et al., 2009).



Scheme 4.1 The oxidation of aniline with ammonium peroxydisulfate



Scheme 4.2 Aniline is oxidized with silver nitrate to PANI nitrate and metallic silver.

Figure 4.1 shows the high-magnification FESEM image of resulted AgNPs-PANINTs(A) nanotubes composite. It can be seen that the PANINTs are cross-linked by each other to form a porous surface area in this composite. The nanomaterial properties depend on their shape, size and dimension. In particular, these kind of nanosize and high surface area materials, one dimensional (1D) nanomaterials like nanotubes have attracted intense in chemistry because of their particular sizes and morphologies (Ramana, 2014; Park, 2015). Gao et al. reported the one-step synthesized silver-polyaniline composite with a diameter of about 100 nm (Gao, 2009) while the AgNPs-PANINTs(A) composite obtained with diameter less than 100 nm size.

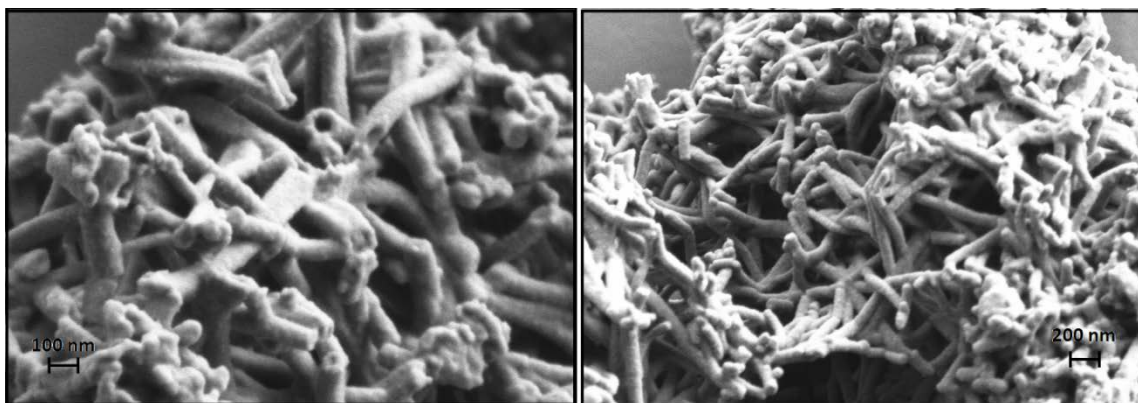


Figure 4.1. FESEM images of AgNPs-PANINTs(A) composite

1.11.2 XRD analysis, EDX and FT-IR spectroscopy characterization of AgNPs-PANINTs(A) composite

The chemical composition of AgNPs-PANINTs(A) composite elements was further determined by the Energy-dispersive X-ray spectroscopy (EDX), as shown in Figure 4.2. The observed peaks of C and N, Si and Ag are corresponding to PANI, silicon substrate and AgNPs in the composite, respectively. The weight percentage of each element of the composite is shown in Table 4.1. This result also confirms the Ag existence in the AgNPs-PANINTs(A) composite with adequate percentage.

Table 4.1 EDX data of AgNPs-PANINTs(A) composite

Elements (Wt%)	C	O	N	Si	Ag
	56.55	4.41	7.71	17.64	13.69

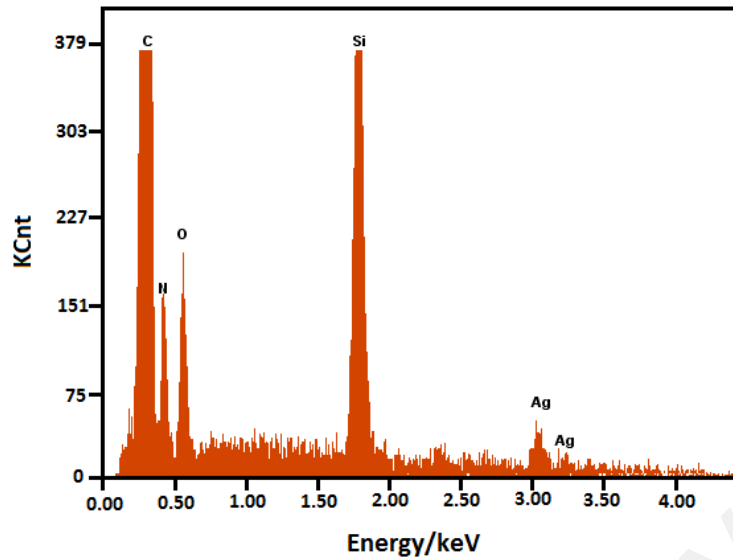


Figure 4.2 EDX result of AgNPs-PANINTs(A) composite

The XRD pattern of the AgNPs-PANINTs(A) is indicated in Figure 4.3 which the Ag intensity could be seen in 111, 200, 220 and 311 (Ref. code: 003-0921) confirming that the Ag particles in the AgNPs-PANINTs(A) composite are not in the Ag^+ form.

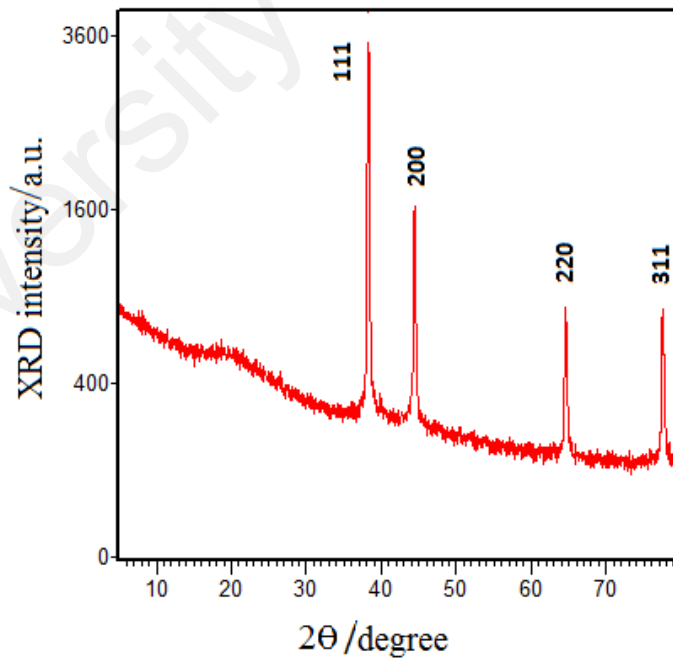


Figure 4.3 XRD pattern of AgNPs-PANINTs(A) composite

FT-IR spectra of PANI and AgNPs-PANINTs(A) composite are shown in Figure 4.4 (a) and Figure 4.4 (b) respectively. The large absorption peak in region of 1700-2800 cm^{-1} indicates free electron conduction in conductive polymers (Sazou & Georgolios, 1997). The characterization band at 3220 and 3310 cm^{-1} , represent N-H bond of PANI and AgNPs-PANINTs(A) composite respectively. The absorption peaks at 1610 and 1620 cm^{-1} can account for the C=N stretching of the quinoid of the PANI and AgNPs-PANINTs(A).

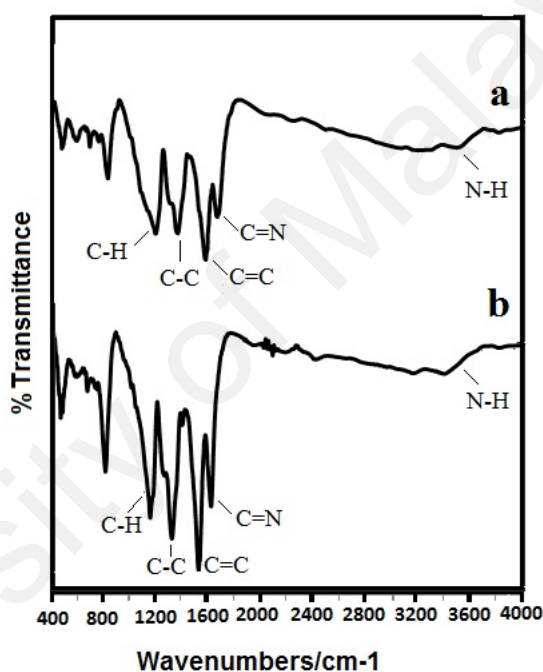


Figure 4.4. FT-IR of (a) PANINTs (b) AgNPs-PANINTs(A) composite

The absorption peaks at 1550 and 1583 cm^{-1} can be considered to C=C stretching of the benzenoid rings in PANI and AgNPs-PANINTs(A) (Tarachiwin et al., 2002). The observed peak at 1297 cm^{-1} is attributed to the C-C stretching of benzenoid structure of the PANI and at 1299 cm^{-1} for the same structure stretching of the AgNPs-PANINTs(A). The in-plane C-H bonding of quinoid structure of the observed peaks of the PANI and

AgNPs-PANINTs(A) can be found at 1181 and 1197 cm^{-1} respectively (Sazou & Georgiolos, 1997). The peaks at 799 and 805 cm^{-1} can be attributed to the out-of-plane bonding of C–H bond in aromatic ring. The sharpness and intensity of the peaks obviously increased in Ag-PANINTs as compared to PANI that could be due to the interaction between Ag and non-bonding electrons of PANI chains (Khanna et al., 2005; Patil et al., 2012).

1.11.3 Electrochemical characterization of AgNPs-PANINTs(A) composite

1.11.3.1 Cyclic voltammogram (CV) of the modified AgNPs-PANINTs(A)/GCE to hydrogen peroxide

The cyclic voltammetry studies were carried out to explore the bioelectrocatalytic activity of the AgNPs-PANINTs(A)/GCE toward H_2O_2 reduction. Figure 4.5 shows the cyclic voltammetric (CV) behavior of the bare GCE, the PANI, the AgNPs and the AgNPs-PANINTs(A) in a 0.2 M phosphate buffer solution (Na_2HPO_4 and NaH_2PO_4) pH 6.5 in the presence of 1.0 mM H_2O_2 . It was found that the response of GCE as compared to PANI and AgNPs is not noticeable. Comparatively by using AgNPs-PANINTs(A), one reduction peak at -0.60 V can be clearly seen with the remarkable increment in reducing current of H_2O_2 (Figure 4.5).

The high surface area of PANINTs (as shown in Figure 4.1) can increase its ability to H_2O_2 direct reduction. The presence of AgNPs in the composite made the H_2O_2 reduction irreversible thus, the Ag-PANINTs composite shows more sensitivity to H_2O_2 as compared to PANI and AgNPs exclusively. Scheme 4.3 shows the possible mechanisms of H_2O_2 reduction by the modified PANINT/GCE electrodes.

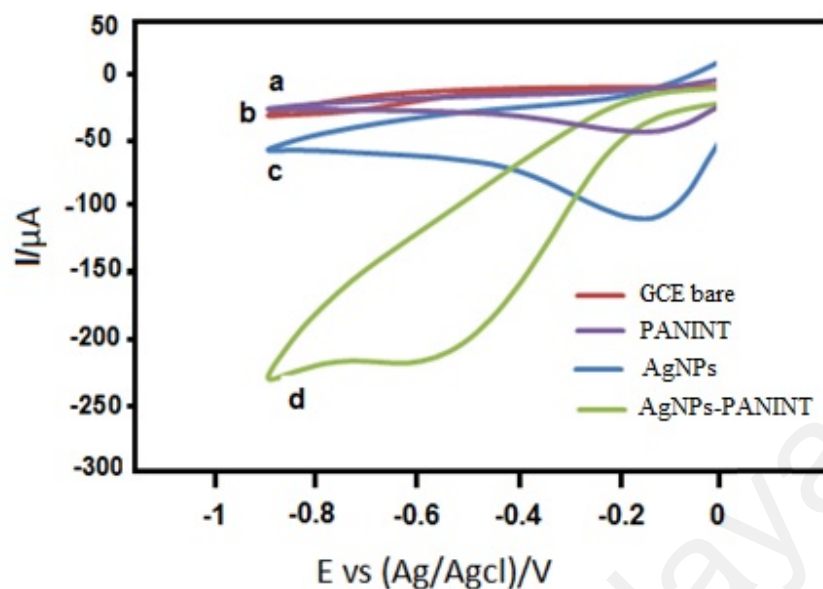


Figure 4.5 CVs of (a) bare GCE, (b) PANINTs/GCE, (c) AgNPs/GCE, (d) AgNPs-PANINTs(A)/GCE in 0.2 M phosphate buffer solution (Na_2HPO_4 and NaH_2PO_4) pH 6.5 in the presence of 1.0 mM H_2O_2 using 20 mVs^{-1} scan rate

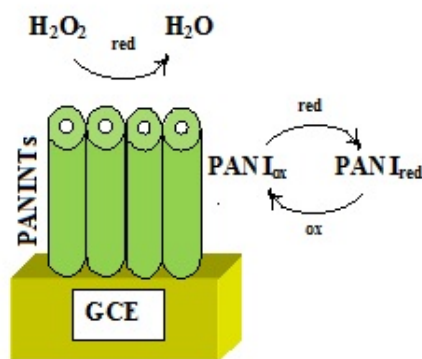
The H_2O_2 in the solution was reduced via the following mechanism:

H_2O_2 can be directly reduced to yield H_2O .



The process of reduction on the surface of the PANINRs under acidic conditions involves two electron transfer steps ((2) and (3)), and the final product of the reduction is H_2O (4) (Flätgen et al., 1999):





Scheme 4.3 The possible mechanisms of H_2O_2 reduction by the modified PANINT/GCE electrode.

1.11.3.2 Amperometric response of the modified electrode (AgNPs-PANINTs(A)/GCE) to hydrogen peroxide

The amperometric study was carried out to check the possible concentration range of the H_2O_2 detection. The outcome of amperometric response of the AgNPs-PANINTs(A) composite with a constant potential at -0.35 V by adding different concentration of H_2O_2 in 0.2 M phosphate buffer solution (Na_2HPO_4 and NaH_2PO_4) pH 6.5 is presented in Figure 4.6. The current of working electrode dramatically increased up to 95% of steady-state current within 3 s which is manifestly a fast amperometric response behavior. The steady-state calibration plot over the concentration range of (12 point) has been prepared from the amperometric response, as shown in Figure 4.6. The plot of H_2O_2 concentration range from 100 μM up to 50 mM shows linear behavior towards peak currents however, the R^2 value is unsatisfactory. The performance of AgNPs-PANINTs(A) was not impressive, therefore further improvement is needed.

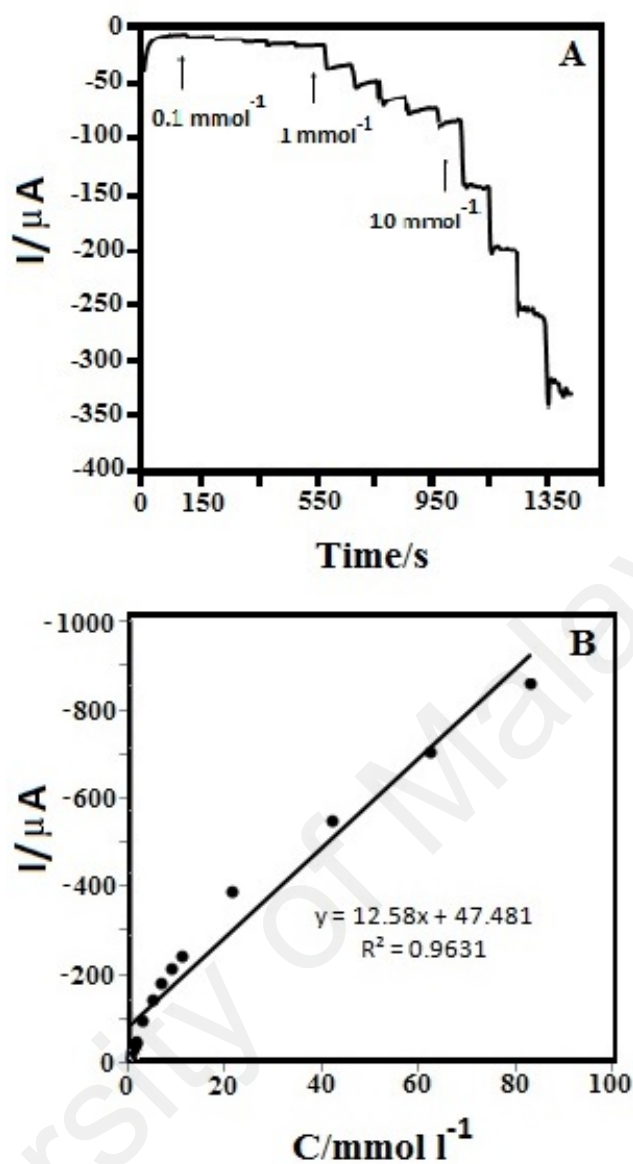


Figure 4.6 A: Steady-state response of AgNPs-PANINRs/GCE to successive injections of H₂O₂ in 0.2 M phosphate buffer solution (Na₂HPO₄ and NaH₂PO₄) pH 6.5 with an applied potential -0.35 V **B:** the steady-state current vs. H₂O₂ concentration.

1.12 Silver-polyaniline nanorods composite [AgNPs-PANINRs]

Different morphologies of AgNPs-PANI composites were prepared in order to develop electrochemical sensors, which can be obtained using simple and effective synthesis methods. By changing the synthesis temperature of the previous composite, the

morphology of composite changed to rod shape (AgNPs-PANINRs) instead of tube form (AgNPs-PANINTs(A)). In addition, by using the same amount of AgNO₃ loading, the silver nanoparticle amount was increased and optimized in the obtained composite.

1.12.1 Morphology analysis of AgNPs-PANINRs composite

Three different amounts of AgNO₃ (i.e. 0.01g, 0.03g and 0.05g) was used to study the optimum amount of AgNO₃ loading in the composite, respectively. The morphology of the prepared AgNPs-PANINRs composite was examined by field emission scanning electron microscopy (FESEM).

A high-magnification FESEM image of the AgNPs-PANINRs composite was prepared with 0.01, 0.03 and 0.05 g of silver as shown in Figure 4.7 a, b and c, respectively. Whereas, Figure 4.7 d indicates the AgNPs-PANINTs(A) with 0.01 g AgNO₃ loading (Gao et al., 2009) as the reference. By increasing the AgNO₃ amount from 0.01 to 0.03, PANINRs with higher decorated AgNPs amount were obtained. However, increasing the amount of AgNO₃ to 0.05 g resulted in agglomeration of AgNPs and it caused more secondary overgrowth in polymer structure.

The polymerization temperature of aniline with APS has a significant impact on the molecular structure, morphology and conductivity of the formed PANI (Stejskal et al., 1998). The increasing content of the structure defects in PANI chains as the polymerization temperature increased and these defects do not consist in a partial self-doping of PANI chains by sulfuric or other acidic groups (Bláha et al., 2013). Therefore, the rod shape is believed to be corresponded the preparation of the composite at a low temperature and the optimized amount of AgNO₃. Consequently, in this work, 0.03 g of AgNO₃ was found as the optimum amount Ag loading. Figure 4.7 (e, f and g) shows

normal, high and low magnifications backscatter FESEM images of the AgNPs-PANINRs composite with 0.03 g amount of AgNO₃ respectively. The images formed from the backscatter electrons clarify the existence of silver nanoparticles with homogenous dispersion in polymer matrix. Figure 4.7 (h) indicates the size distribution diagram of the polyaniline nanorods of AgNPs-PANINRs composite by using 0.03 g AgNO₃ in which the mean diameter size of obtained polyaniline nanorods is around 61 nm.

The morphology of the AgNPs-PANINRs was further confirmed by TEM. The tube morphology of PANI in AgNPs-PANINRs(A) composite can be clearly seen by synthesizing 0.03 g AgNO₃ at room temperature (Figure 4.8 a). However, a rod shape with a significant amount of the AgNPs was observed in the AgNPs-PANINRs composite that was polymerized by using 0.03 g AgNO₃ at low temperature (Figure 4.8 b).

The image of AgNPs-PANINRs also shows that the AgNPs were well dispersed in the polymer matrix. Figure 4.8 c shows the silver nanoparticles size distribution diagram of the AgNPs-PANINRs composite by using 0.03 g AgNO₃ and the mean size of the obtained silver nanoparticles are around 6.85 nm. The nanosize of the silver particles provides a large available surface area of silver on the surface of the composite. It has been reported that a large surface area of metal provides greater sensitivity for detecting H₂O₂ (Song et al., 2009).

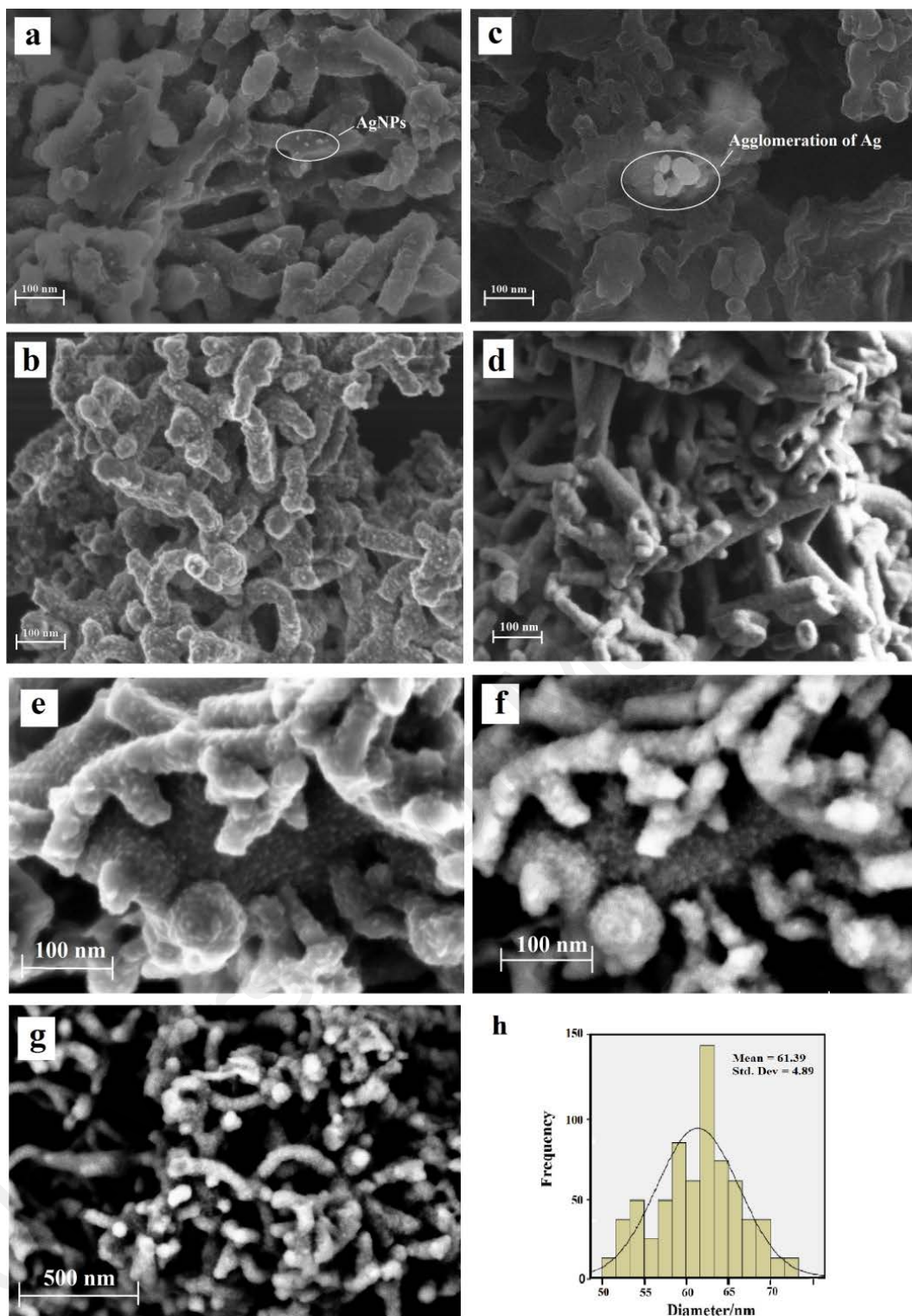


Figure 4.7. FESEM images of AgNPs-PANINRs composite by using 0.01 g AgNO₃ (a), AgNPs-PANINRs composite by using 0.03 g AgNO₃ (b), AgNPs-PANINRs composite by using 0.05 g AgNO₃(c), AgNPs-PANINRs(A) composite by using 0.01 g AgNO₃ and PANINRs (e) ,(f) and (g) Normal and backscatter FESEM images of AgNPs-PANINRs composite by using 0.03 g AgNO₃ respectively,(h) size distribution diagram of the polyaniline nanorods of AgNPs-PANINRs composite by using 0.03 g AgNO₃ .

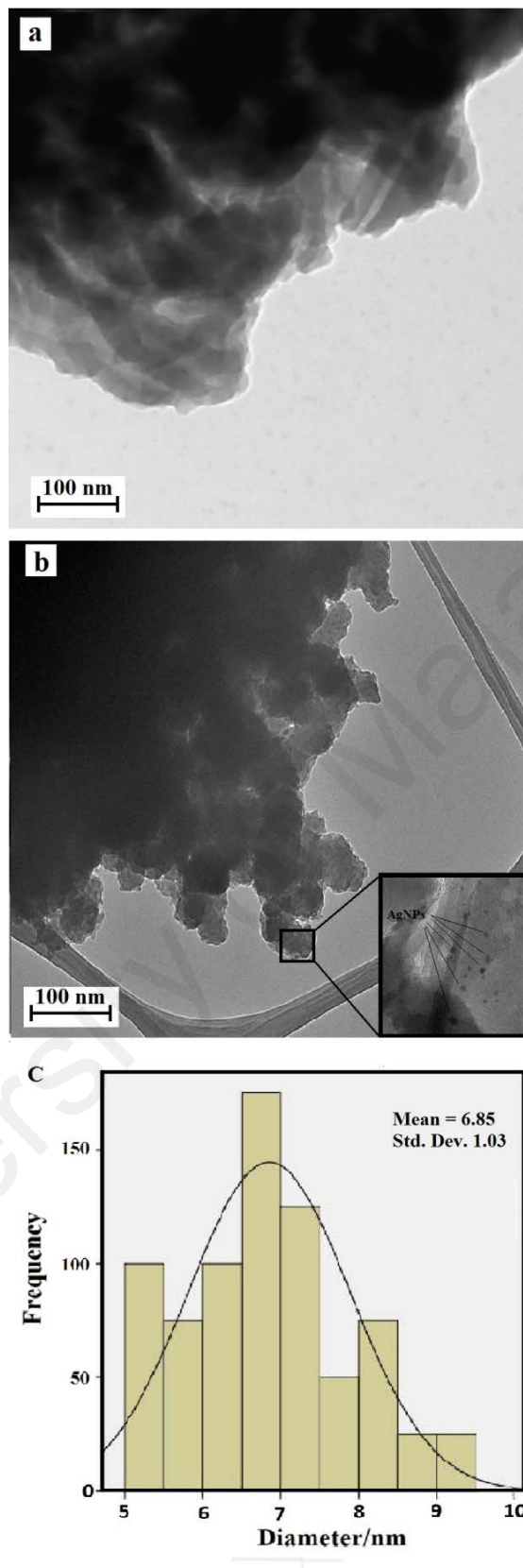


Figure 4.8. TEM image of (a) AgNPs-PANINTs(A) composite (b), AgNPs-PANINRs composite by using 0.03 g AgNO₃ and (c) size distribution diagrams of AgNPs-PANINRs.

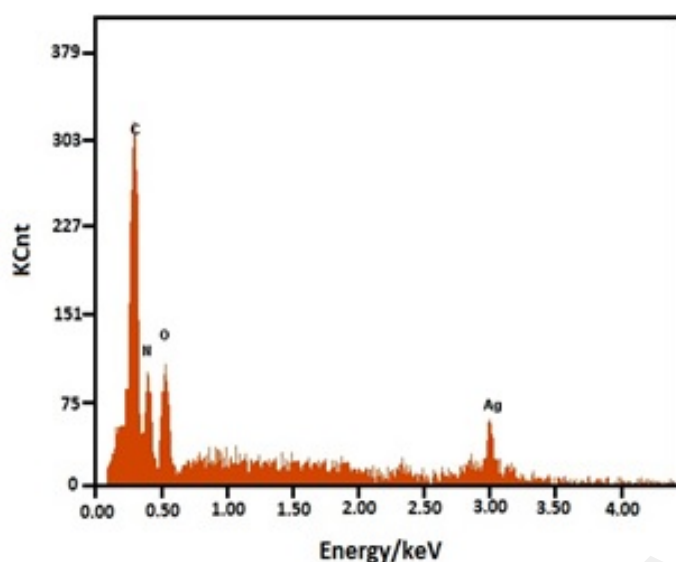


Figure 4.9 EDX result of AgNPs-PANIRs composite

Table 4.2. EDX data of AgNPs-PANIRs composite

Elements	C	O	N	Ag
(Wt.%)	71.05	5.39	9.49	14.07

Figure 4.10 shows the XRD patterns of the pure PANI (a) and AgNPs-PANIRs (b). In pattern (b), the peaks corresponding to the 111, 200, 220 and 311 planes of Ag (Ref. code: 003-0921) were observed. This result confirms the FESEM and TEM results indicating the presence of silver in the AgNPs-PANIRs composite. In addition, these peaks proved the presence of reduced Ag particles in the AgNPs-PANIRs composite, and no sign of the Ag⁺ form was observed (Golsheikh et al., 2013).

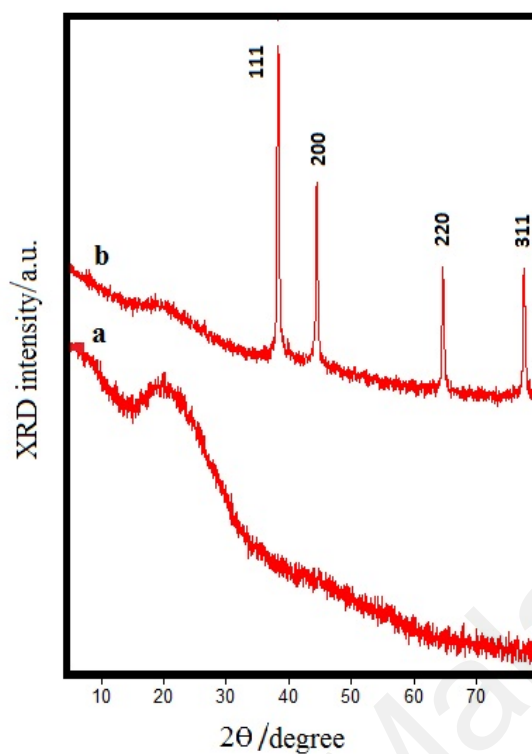


Figure 4.10. XRD pattern of (a) pure PANI (b) AgNPs-PANIRs composite

Figure 4.11 a and Figure 4.11 b show the FT-IR spectra where the bands at 3220 and 3150 cm^{-1} represent the N–H bonds in the PANI and AgNPs-PANIRs composite, respectively. A free electron conduction in conducting polymer resulted in a large absorption peak in the region of 1700–2800 cm^{-1} (Sazou & Georgolios, 1997). The absorption peaks at 1568 cm^{-1} can be attributed to the C=C stretching of the quinoid moieties of the PANI and 1567 cm^{-1} for AgNPs-PANIRs composite. In addition, the bands at 1483 and 1481 cm^{-1} were assigned to the C=C stretching of the benzenoid rings in the PANI and AgNPs-PANIRs composite, respectively (Tarachiwin et al., 2002). The observed peak at 1292 cm^{-1} , 1167 and 1181 cm^{-1} were attributed to the in-plane C–H stretching of the quinoid structure in the PANI and AgNPs-PANIRs composite, respectively (Sazou & Georgolios, 1997). The peaks at 795 and 798 cm^{-1} were assigned

to the out-of-plane stretching of the C–H bonds in the aromatic ring. The sharpness and intensity of the absorption peaks were remarkably greater for the AgNPs-PANINRs composite than for the PANI. These effects can be attributed to the interaction between Ag and non-bonding electrons in the PANI chains (Khanna et al., 2005; Patil et al., 2012).

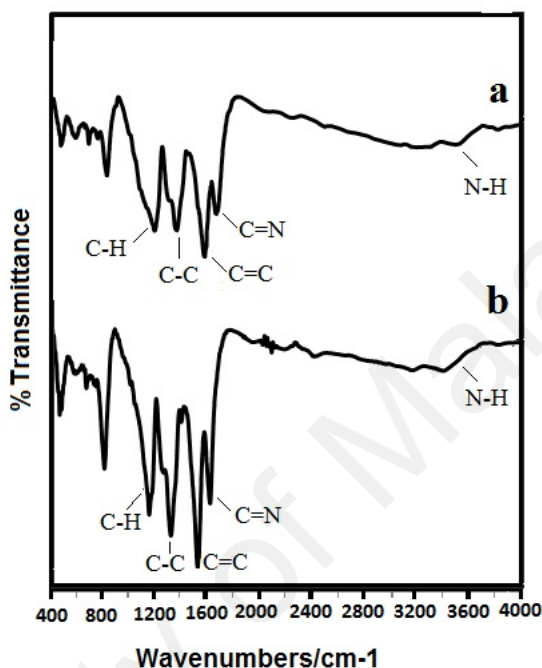


Figure 4.11. FT-IR of (a) pure PANI (b) AgNPs-PANINRs composite.

1.12.2 Electrochemical characterization of AgNPs-PANINRs composite

All the samples modeled by an electrical equivalent circuit depicted in Figure 4.12 consisting of electrolyte resistance (R_s), charge transfer resistance (R_{ct}), and double layer capacitance (C_{dl}). A constant phase element (CPE) was introduced into the circuit instead of a pure capacitor to give a more accurate fit. Figure 4.12 shows the Nyquist impedance plots of the Bare (a), PANI (b), AgNPs-PANINTs(A) (c) and AgNPs-PANINRs (d) electrodes recorded in $[\text{Fe}(\text{CN})_6]^{3-/4-}$ containing 0.1 M KCl solution in the frequency

range of 0.1 Hz to 100 kHz. The EIS of the bare GCE shows a larger semicircle than other modified electrodes, indicating low conductive property of GCE (66098Ω). Figure 4.12 b shows that by modifying GCE with PANI (4637Ω), the conductivity totally increases (almost 14 times) which is mainly due to rapid electron transfer attributed to the excellent conductivity of PANI. The R_{ct} dramatically decreases to 287 and 149Ω for AgNPs-PANINTs(A) and AgNPs-PANINRs respectively. Indicating that the conductivity of PANI has been improved by incorporating Ag nanoparticles into the polymer matrix. Moreover, the R_{ct} of AgNPs-PANINRs is two times smaller than AgNPs-PANINTs(A) implying that Ag nanoparticles with nanorods PANI structure are more conductive than Ag with nanotubes PANI structure.

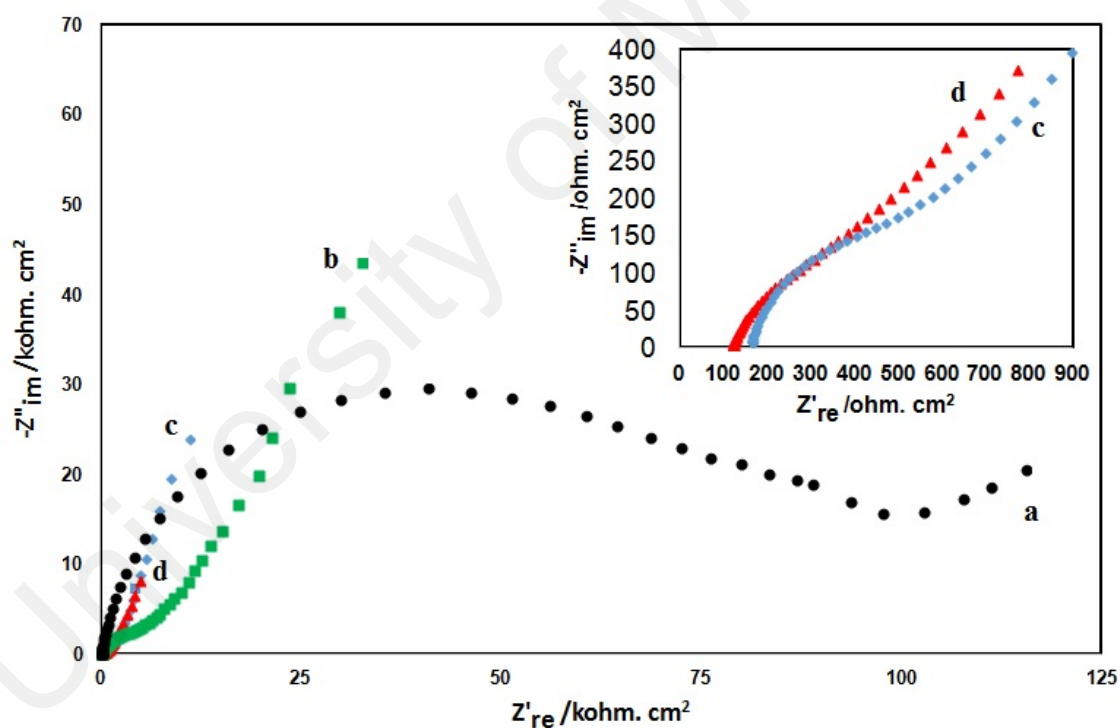


Figure 4.12. Nyquist plots of (a) bare electrode, (b) PANI, (c) AgNPs-PANINTs(A) and (d) AgNPs-PANINRs

Figure 4.13 A and B shows the Bode and Phase plots and the excellent agreement between the experimental results and the parameters obtained from equivalent circuit model where the chi-squared (χ^2) is minimized at 10^{-4} . The Randles circuit depicted in the inset of Figure 4.13 A. was used to model the impedance of the modified electrode. It consists of R_s , R_{ct} , CPE, and diffusion impedance (Z_w). In the Randles circuit, it is assumed that R_{ct} and Z_w are parallel to the interfacial double layer capacitance.

Figure 4.14 shows the effect of the applied potential on the reduction current of the AgNPs-PANINRs composite over the range of -0.15 to -0.50 V when using the modified AgNPs-PANINRs/GCE in a 0.20 M phosphate buffer solution (Na_2HPO_4 and NaH_2PO_4) at pH 6.5 in the presence of 1.0 mM H_2O_2 . The steady-state current increased significantly when using a potential greater than -0.30 V. A high analyte-dependent value could be obtained by selecting the appropriate working potential. The lowest feasible negative potential (-0.35 V) to achieve good selectivity should be chosen as the applied working potential.

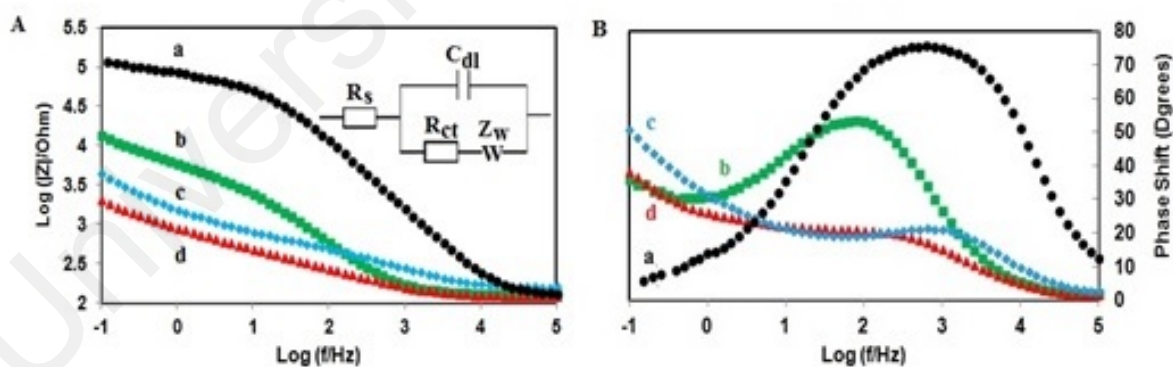


Figure 4.13 A: Bode plots of (a) bare electrode, (b) PANI, (c) AgNPs-PANINTs(A) and (d) AgNPs-PANINRs. B: EIS Bode $\log f$ vs. θ plots at Nyquist plots of (a) bare electrode, (b) PANI, (c) AgNPs-PANINTs(A) and (d) AgNPs-PANINRs.

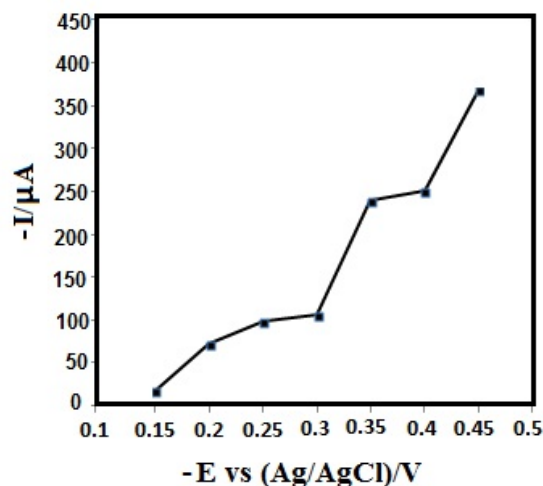


Figure 4.14. Effect of the applied potential on the current response of AgNPs-PANINRs/GCE to 1.0 mM H₂O₂ in 0.2 M phosphate buffer solution (Na₂HPO₄ and NaH₂PO₄) pH 6.5

1.12.2.1 Cyclic voltammogram (CV) of the modified electrode (AgNPs-PANINRs/GCE) to hydrogen peroxide

Figure 4.15 A (a-e) shows the cyclic voltammetric (CV) behavior of the bare GCE PANI/GCE, AgNPs/GCE and the modified electrodes in a 0.2 M phosphate buffer solution (Na₂HPO₄ and NaH₂PO₄, pH 6.5) in the presence of 1.0 mM H₂O₂ respectively. The bare GCE shows a weak response to H₂O₂, as shown in Figure 4.15 A(a). The comparison of the responses of the AgNPs/GCE (Figure 4.15 A(c)), with the PANINRs/GCE (Figure 4.15 A(e)) indicates that there was an increase in the current density for PANINRs/GCE (Figure 4.15 A(e)), which corresponds to better sensitivity for the detection of H₂O₂ and confirmed the electroactivity of this polymer for sensing H₂O₂ (Y. Yang & Mu, 2005). The presence of silver in the AgNPs-PANINTs(A) (Figure 4.15 A(d)) and AgNPs-PANINRs (Figure 4.15 A(e)) composites resulted in a remarkable reduction peak current density of -0.28 mA.cm⁻² in response to H₂O₂. AgNPs-PANINRs (Figure 4.15 A(e)) composite shows reduction peak current density (-0.28 mA) that is higher than AgNPs-PANINTs(A) ((Figure 4.15 A(d)) composite

reduction peak current density due to its higher silver nanoparticle amount in polymer matrix of AgNPs-PANINRs.

Since the AgNPs-PANINRs shows better reduction peak towards H_2O_2 , further investigations have been focused will only be focusing on this composite. Figure 4.15 B(a) and Figure 4.15 B(b) present the comparative results of AgNPs-PANINRs composite in the presence and absence of H_2O_2 respectively. According to the previous studies with the same concentration of H_2O_2 , the modified electrode shows the greatest reduction peak current as compared to other modified electrode surfaces. For example, the AgNPs-UTPNS/GCE (UTPNS: ultrathin polypyrrole nanosheets) and AgNPs-polypyrrole/GCE only had reduction peaks of approximately 0.25 and -0.049 $\text{mA}\cdot\text{cm}^{-2}$ in response to H_2O_2 , respectively (Mahmoudian, et al., 2012; Qin et al., 2011). The increment in the current of reduction peak current for the AgNPs-PANINRs composite (around 0.27 $\text{mA}\cdot\text{cm}^{-2}$) is expected to happen because of two important factors which lead to the improvement in performance of the metal-polymer composite as compared to other materials. The first factor is the nanosize of the silver particles in the AgNPs-PANINRs composite, and the second factor is the rod shape of the PANINRs, which resulted in a high surface area for AgNPs deposition and, consequently, a large amount of AgNPs on the surface can be obtained. With gradual addition of H_2O_2 a reduction peak at around -0.85 V on the bare GCE with the increasing peak current as a function of H_2O_2 concentration is observed. The same procedure was followed by using PANI/GCE as working electrode and the responses of PANI/GCE electrode was recorded to the gradual addition of H_2O_2 (Figure 4.15 a). During the gradual addition of H_2O_2 , PANI based redox peaks remained as unchanged, indicating that PANI does not interact with H_2O_2 and the presence of H_2O_2 does not affect the redox processes of PANI (Çeken, Kandaz, & Koca, 2012).

The standard redox potential of Silver is 0.80 V. Therefore, due the presence of silver nanoparticle in the PANI composite the redox potential of H_2O_2 was slightly has been shifted a bit to positive potential and have appeared around 0.72 V.

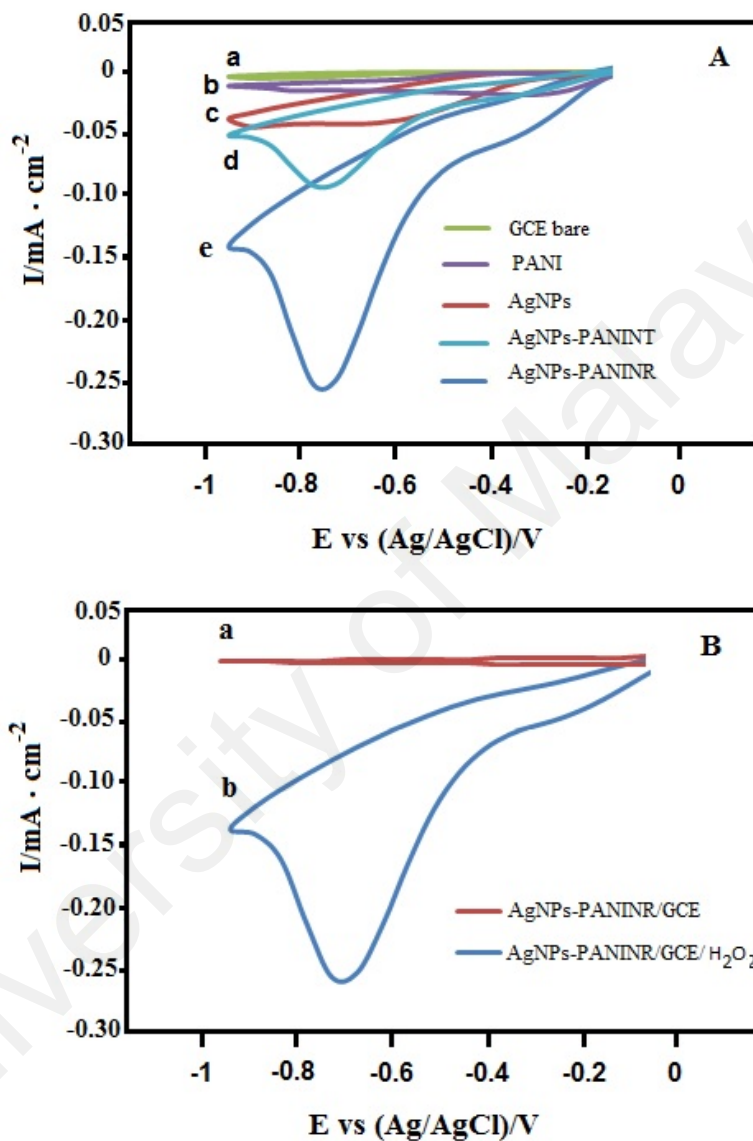


Figure 4.15. A CVs of (a) bare GCE, (b) PANINRs/GCE, (c) AgNPs/GCE, (d) AgNPs-PANINRs/GCE in 0.2 M phosphate buffer solution (Na_2HPO_4 and NaH_2PO_4) pH 6.5 in the presence of 1.0 mM H_2O_2 using 20 mVs^{-1} scan rate and Fig. 8.B CVs of AgNPs-PANINRs/GCE in 0.2 M phosphate buffer solution (Na_2HPO_4 and NaH_2PO_4) pH 6.5 in the presence of 1.0 mM H_2O_2 using 20 mVs^{-1} scan rate without H_2O_2 (a) and with H_2O_2 (b).

1.12.2.2 Amperometric response of the modified AgNPs-PANINRs/GCE electrode to hydrogen peroxide

As shown in Figure 4.16, the potential of -0.35 V is the best candidate for the applied working potential. The current-time plot for the AgNPs-PANINRs/GCE with different H₂O₂ concentrations in 0.2 M phosphate buffer solution (Na₂HPO₄ and NaH₂PO₄) at pH 6.5 is presented in Figure 4.16.a for an applied potential of -0.35 V. The current of the working electrode dramatically increased up to 95% of the steady-state current within 5 s, indicating of a fast amperometric response. A steady-state calibration curve for the AgNPs-PANINRs-modified electrode was observed from the amperometric response, as shown is Figure 4.16. The calibration curve of the low concentration and high concentration is shown in Figure 4.16 b and Figure 4.16 c respectively. Two linear steady-state amperometric detection ranges were estimated to be from 0.1 mM up to 10 mM for low concentration of H₂O₂ and the other one is linear with different slops from 10-70 mM. The limit of detection (LOD) and the limit of qualification (LOQ) were determined by using the following equations:

$$\text{LOD} = 3S_B / b \quad (4-5)$$

$$\text{LOQ} = 10 S_B / b \quad (4-6)$$

Where b is the slope of the calibration curve and S_B is the standard deviation of the blank solution (Moldoveanu, 2004).

The limit of detection (LOD) and the limit of qualification (LOQ) for low concentration area were estimated to be 0.13 μM and 0.45 μM respectively, and for high concentration area, the limit of detection (LOD) and the limit of qualification (LOQ) were obtained as 0.33 μM and 1.12 μM respectively, at a signal-to-noise ratio of 3.

Additionally, the stability of the sensor was assessed by measuring the response current of the modified electrode. After 7 days, only 5.3% of the current signal was lost. This result indicates that the AgNPs-PANIRs-modified electrode has good stability for detecting H_2O_2 . The electrode-to-electrode reproducibility is approximated to be in the presence of 1.0 mM H_2O_2 in 0.2 M (pH 6.5) at three electrodes (AgNPs-PANIR/GCE) prepared in the same condition, which yielded a relative standard deviation of 4.1%.

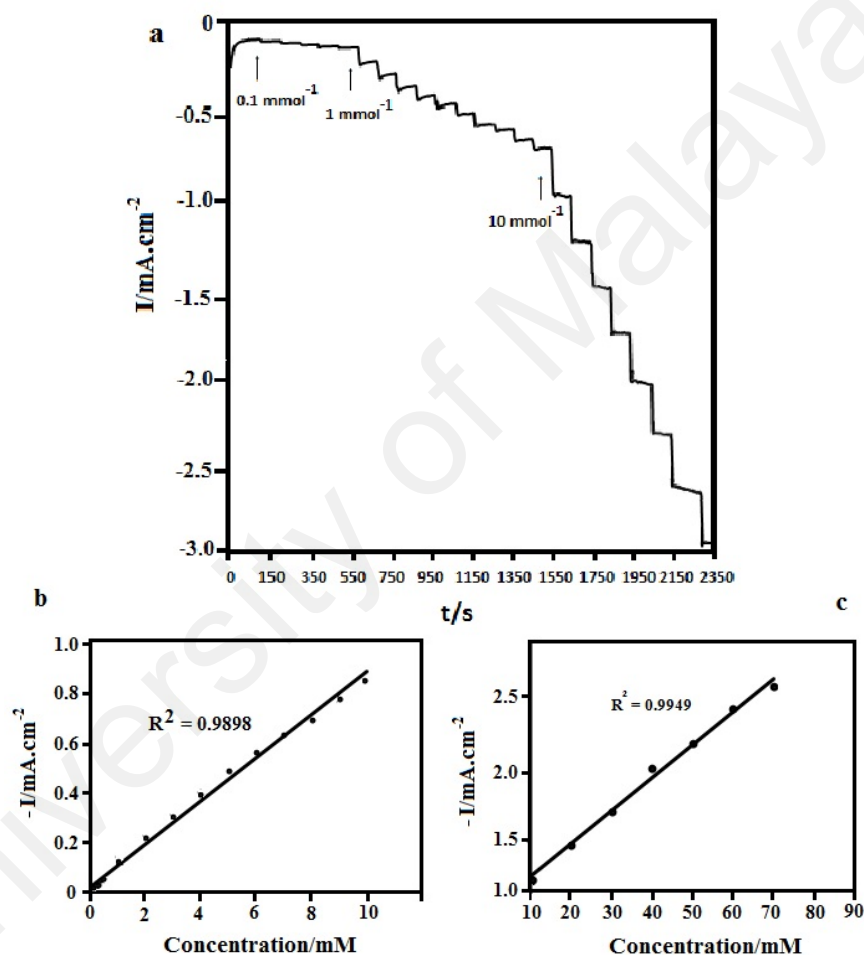


Figure 4.16. Steady-state response of AgNPs-PANIRs/GCE to successive injections of H_2O_2 in 0.2 M phosphate buffer solution (Na_2HPO_4 and NaH_2PO_4) pH 6.5 with an applied potential -0.35 V (b) calibration curves of low and (c) high concentrations of H_2O_2 steady-state response of AgNPs-PANIRs/GCE.

In real samples, some co-existing electroactive species such as ascorbic acid and glucose might affect the sensor response. The effects of the interference compounds on

the H_2O_2 sensor were studied by comparing the amperometric responses of the electroactive species (0.1 mM) with H_2O_2 (1.0 mM) at the potential of -0.35 V under a stirring condition. The effect of common interfering kinds on AgNPs-PANINRs/GCE modified electrode was studied. Figure 4.17 shows the amperometric response of the modified electrode towards addition of 1.0 mM H_2O_2 that is followed by 1.0 mM H_2O_2 , glucose, glycine, ethanol, ascorbic acid and again 1.0 mM H_2O_2 into 0.20 M phosphate buffer solution (pH 6.5). As can be seen, very weak signals responded with the interfering substances that indicates good selectivity towards H_2O_2 by using AgNPs-PANINRs/GCE modified electrode.

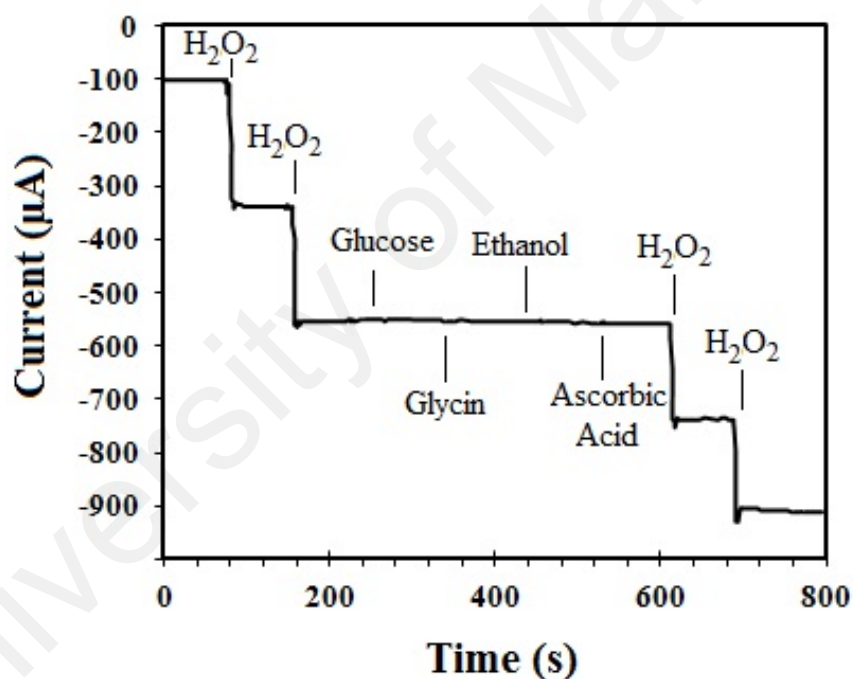


Figure 4.17 Amperometric response of AgNPs-PANINRs/GCE electrode upon the successive addition of 1.0 mM H_2O_2 , 1.0 mM H_2O_2 , glucose, glycine, ethanol, ascorbic acid, 1.0 mM H_2O_2 and again 1.0 mM H_2O_2 into 0.2 M phosphate buffer solution (pH 6.5) with an applied potential - 0.35 V under a stirring condition.

Table 4.3 compares the LOD and the liner range of the AgNPs-PANINRs-modified electrodes with those of other electrodes investigated in pervious voltammetric H_2O_2 studies. The LOD obtained in this work is lower than the LODs obtained in most

previous studies, and the results are comparable to those for ultra-thin polypyrrole nanosheets decorated with silver nanoparticles (AgNPs/UTPNSs), which showed good performance as non-enzymatic amperometric sensors.

Table 4.3 Comparison the LOD value from previous reports and this work with different methods

Modified Electrode	LOD (μM)	Liner range (mM)	References
AgNPs-PPYCs	0.90	0.1-70	(Qin et al., 2011)
AgCl-PANI	0.28	1.3-10	(Porchelvi et al., 2013)
AgNPs-MWCNT-rGO	0.90	0.1-100	(Lorestani et al., 2014)
Ag NSBs-PPy	0.68	0.1-50	(Mahmoudian et al., 2014)
AgNPs-Collagen	0.70	0.005-40.6	(Song et al., 2009)
AgNPs-UTPNSs	0.57	0.1-90	(Mahmoudian, et al., 2012)
AgNPs-PANINFs	0.25	0.1-60	(Zhong et al., 2013b)
AgNPs-CNT	1.60	0.05-8	(Shi et al., 2011)
AgNPs-rGO-PANI	7.10	0.1-80	(Liu, Wang, et al., 2011)
PdNP-AuNAE	5.00	1-6	(Jamal et al., 2012)
AgNPs-PANINRs	0.13	0.1-10	This work
	0.33	10-70	

1.13 Silver-polyaniline nanotube composite [AgNPs-PANINTs(B)] using silver ammonia complex $\text{Ag}(\text{NH}_3)_2\text{OH}$

The homogenous distribution of nanosize silver nanoparticles in PANINTs matrix could be achieved using $\text{Ag}(\text{NH}_3)_2\text{OH}$ as the precursor, instead of silver nitrate which was used in our first compound (Moradi Golsheikh et al., 2013b). In this work, small diameter silver particles were nicely distributed in the composite in order to achieve desirable sensor application toward H_2O_2 detection using optimized amount of silver ammonia complex and the composite showed an excellent sensitivity, wide linear range and high selectivity.

1.13.1 Morphology analysis of AgNPs-PANINTs(B) composite

FESEM images and silver particle size distribution diagrams of AgNPs-PANINTs(B) nanocomposites prepared using different volume ratios of PANI/ $\text{Ag}(\text{NH}_3)_2\text{OH}$ 12, 6 and 3 (as explained before at 3.3.6.1) are shown in Figure 4.18 (a-f). As seen in Figure 4.18 (a-c), by increasing the concentration of $\text{Ag}(\text{NH}_3)_2\text{OH}$, the size of reduced silver particles increased from 13.32 to 25.76 nm, suggesting that the particle diameter and the quantity of reduced silver particle in the nanocomposite matrix also increased, and therefore, some silver agglomeration was seen in AgNPs-PANINTs(B) nanocomposite structure. By changing the AgNO_3 , instead of $\text{Ag}(\text{NH}_3)_2\text{OH}$ in the mixture, the Ag particle size dramatically increased from 13.32 (Figure 4.18 b) to 78.82 nm (Figure 4.18 h) mean particle diameter. The high surface area by using $\text{Ag}(\text{NH}_3)_2\text{OH}$ instead of AgNO_3 provides more sensitivity to detect H_2O_2 (Y. Song et al., 2009). The FESEM image of AgNPs-PANINTs(B) nanocomposite, which was prepared using PANI/ AgNO_3 volume ratio of 12, is shown in Figure 4.18 g and its silver nanoparticle size distribution diagram is shown in Figure 4.18 h as reference.

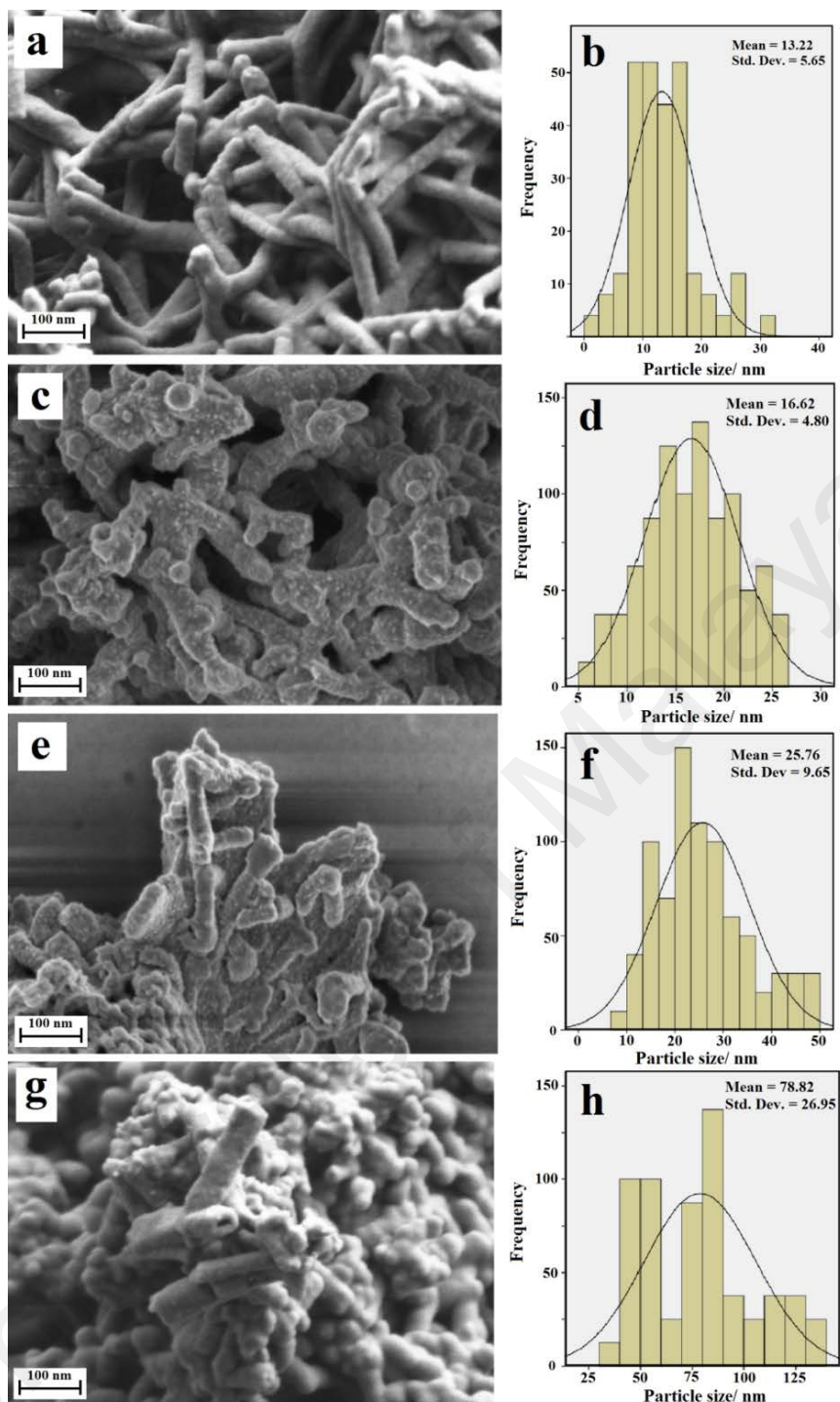


Figure 4.18. FESEM images and size distribution diagram of AgNPs-PANINTs(B) composite prepared by using the solution with PANI to $\text{Ag}(\text{NH}_3)_2\text{OH}$ (0.04 M) volume ratios of 12 (a and b), 6 (c and d), and 3 (e and f) and using the solution with PANINTs to AgNO_3 (0.04 M) volume ratio of 12 (g and h).

1.13.2 XRD analysis, EDX and FT-IR spectroscopy characterization of AgNPs-PANINTs(B) composite

The chemical composition of AgNPs-PANINTs(B) composite was further examined by the Energy-dispersive X-ray spectroscopy (EDX), as shown in Figure 4.19 A. The C and N peaks came from PANI; the Si and Ag peaks came from silicon substrate and the AgNPs of the composite respectively.

The weight percentage of each composite's elements was shown in Table 4.4. This result also confirms the existence of Ag in the AgNPs-PANINTs(B) composite with adequate percentage. The XRD pattern of the AgNPs-PANINTs(B) exhibits a relatively marginal peak at 111, 200, 220 and 311 (Ref. code: 003-0921) (Figure 4.19 B) that could confirm that the Ag particles in the AgNPs-PANINTs(B) composite are not in the Ag⁺ form.

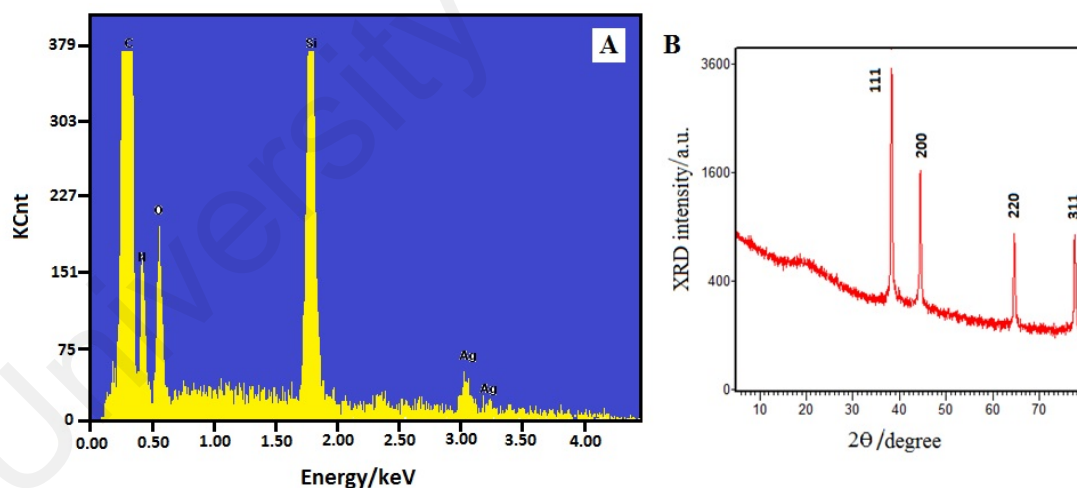


Figure 4.19 A: EDX results of AgNPs-PANINTs(B) composite. B: XRD pattern of AgNPs-PANINTs(B) composite.

Table 4.4 EDX data of AgNPs-PANINTs(B) composite

Elements	C	O	N	Ag
(Wt.%)	60.96	12.12	8.91	18.01

The FT-IR spectra of PANI and AgNPs-PANINTs(B) composite are displayed in Figure 4.20 a and Figure 4.20 b respectively. The large absorption peak in region of 1700-2800 cm^{-1} indicates free electron conduction in the conductive polymers (Sazou & Georgolios, 1997). The characterization band at 3220 and 3310 cm^{-1} , represents N-H bond of PANI and AgNPs-PANINTs(B) composite respectively. The absorption peaks at 1610 and 1620 cm^{-1} could be accounted for the C=N stretching of the quinoid of the PANI and AgNPs-PANINTs(B). The absorption peaks at 1550 and 1583 cm^{-1} could be considered as C=C stretching of the benzenoid rings in PANI and AgNPs-PANINTs(B) (Tarachiwin et al., 2002). The observed peak at 1297 cm^{-1} is attributed to the C-C stretching of benzenoid of the PANI and the 1299 cm^{-1} peak of the same structure stretching of the AgNPs-PANINTs(B). The in-plane C-H bonding of quinoid structure of the observed peaks of the PANI and AgNPs-PANINTs(B) could be found at 1181 and 1197 cm^{-1} respectively (Sazou & Georgolios, 1997). The peaks at 799 and 805 cm^{-1} could be considered with the out-of-plane bonding of C-H bond in aromatic ring. The sharpness, shifts and intensity of the peaks obviously increased in AgNPs-PANINTs(B) as compared to PANI that could be due to the interaction between Ag and non-bonding electrons of PANI chains (Khanna et al., 2005; Patil et al., 2012).

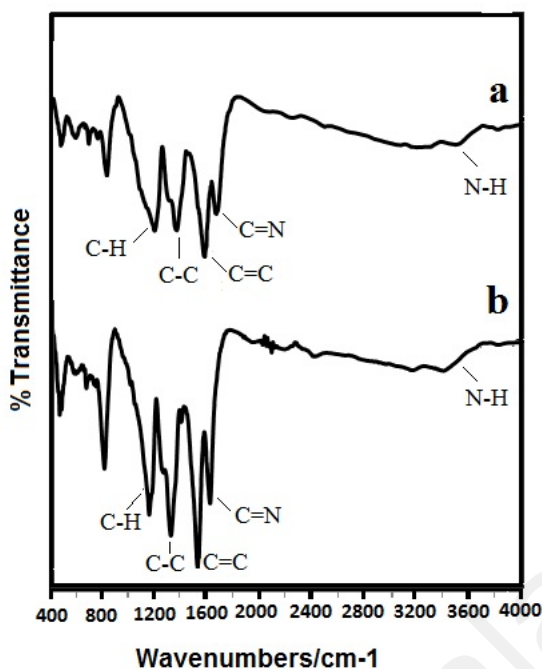


Figure 4.20. FT-IR of (a) PANINTs (b) AgNPs-PANINTs(B) composite

1.13.3 Electrochemical characterization of modified AgNPs-PANINTs(B)/GCE

Figure 4.21 shows the relationship between the applied potential in chronoamperometry and the reduction current of H_2O_2 . The affiliation of the amperometric response on the applied potential of the AgNPs-PANINTs(B)/GCE electrode was evaluated over the range of -0.10 to -0.50 V. The current response was gradually increased when the applied potential were increased from -0.10 to -0.50 V, although, the response current decreased, when it goes toward more negative potential than -0.35 V. The least negative potential that shows the highest current was a suitable working potential to achieve good selectivity. So, -0.35 V was the best potential for reduction of H_2O_2 by AgNPs-PANINTs(B)/GCE modified electrode.

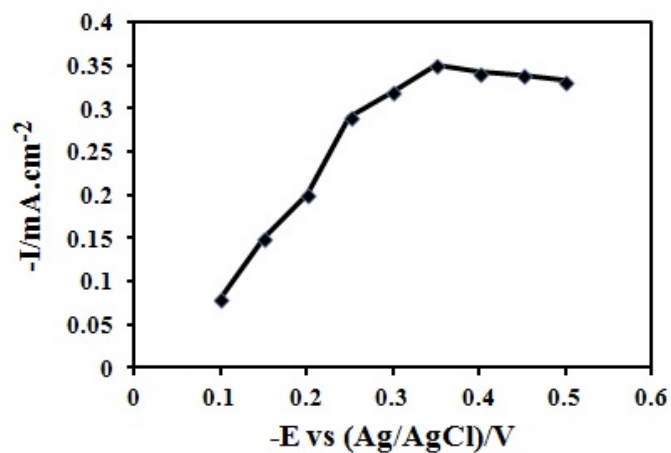


Figure 4.21 Effect of the applied potential on the current response of 1.0 mM H₂O₂ on the AgNPs-PANINTs(B)/GCE electrode in 0.2 M PBS (pH 6.5).

Figure 4.22 indicates the effect of the pH value of the phosphate buffer solution on the reduction current of H₂O₂ on AgNPs-PANINTs(B)/GCE electrode. The current response dramatically increased with increase of the pH from 4.5 to 6.5 and gradually decreased at pH higher than 6.5. The result suggested that pH 6.5 was the optimized pH for the electrochemical reduction of H₂O₂.

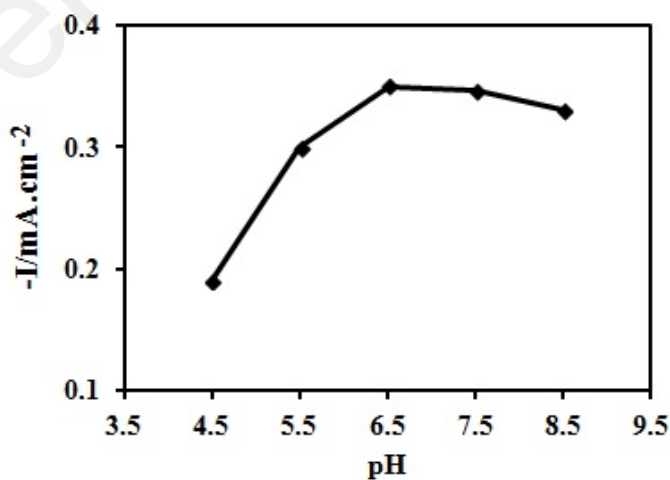


Figure 4.22 Effect of the pH of PBS on the current response of 1.0 mM H₂O₂ on the AgNPs-PANINTs(B)/GCE electrode.

1.13.3.1 Cyclic voltammogram (CV) of the modified electrode (AgNPs-PANINTs(B)/GCE) to hydrogen peroxide

The cyclic voltammetry studies were carried out to find out the bioelectrocatalytic activity of the AgNPs-PANINT/GCE towards H_2O_2 reduction (Y. Yang & Mu, 2005). Figure 4.23 A. shows the cyclic voltammetric (CV) behavior of the bare GCE, the PANI, the AgNPs and the AgNPs-PANINT-2 in a 0.2 M phosphate buffer solution (Na_2HPO_4 and NaH_2PO_4) at pH 6.5 in the presence of 1.0 mM H_2O_2 . It was found that the response of GCE as compared to PANI and AgNPs is not noticeable. In comparison, the large increase of AgNPs-PANINRs to reduced H_2O_2 is completely remarkable. By increasing the silver ratios from 12:1 to 3:1 AgNPs-PANINTs(B)-1 (Figure 4.23 B.a), AgNPs-PANINT-2 (Figure 4.23 B.b) and AgNPs-PANINTs(B)-3 (Figure 4.23 B.c) respectively, the cathodic peaks for the reduction of H_2O_2 alternatively increase, because of big particle size and agglomeration of silver particles in the nanocomposite. Among AgNPs-PANINTs(B)/GCE electrodes, AgNPs-PANINTs(B)-2 (Figure 4.23 B.b) exhibited better reduction activity towards H_2O_2 due to their small particle size and high density of AgNPs. Using AgNO_3 (Figure 4.23 B.d) instead of $\text{Ag}(\text{NH}_3)_2\text{OH}$ (Figure 4.23 B.b) it was observed that reduction activity towards H_2O_2 decreased, because of the dramatic increase of particle size and high density of AgNPs. The reduction activity of the AgNPs-PANINTs(B)-2/GCE electrode is significantly better than the AgNPs-PANINTs(B)-4/GCE electrode.

The PANI modified electrode shows increases in the reduction peak current as compare to bare GCE indicating that H_2O_2 can directly reduce in the presence of PANI. The high surface area of PANINTs can increase its ability to H_2O_2 direct reduction. The presence of AgNPs in the composite made the H_2O_2 reduction irreversible thus, the

AgNPs-PANINTs(B) composite shows more sensitivity to H₂O₂ as compared to PANI and AgNPs exclusively.

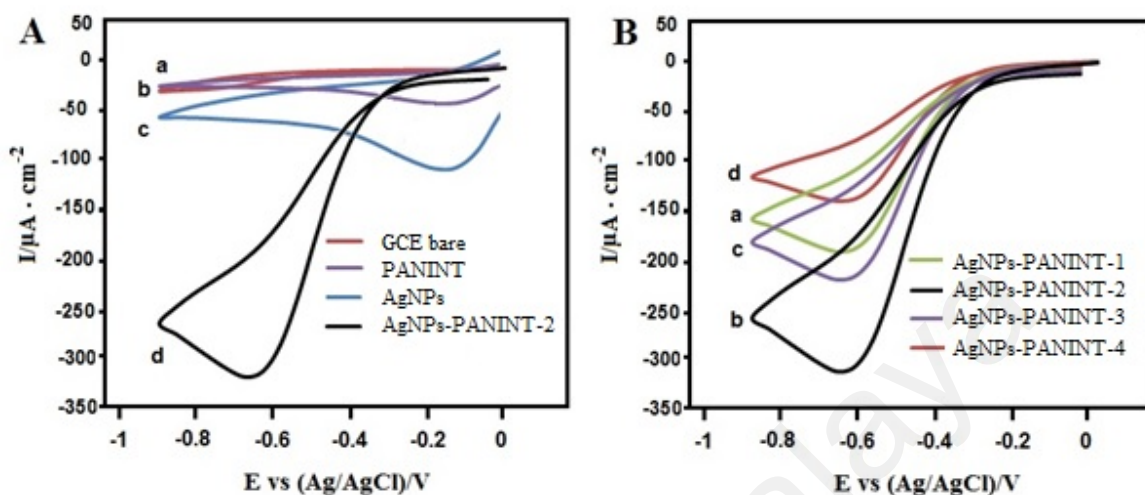
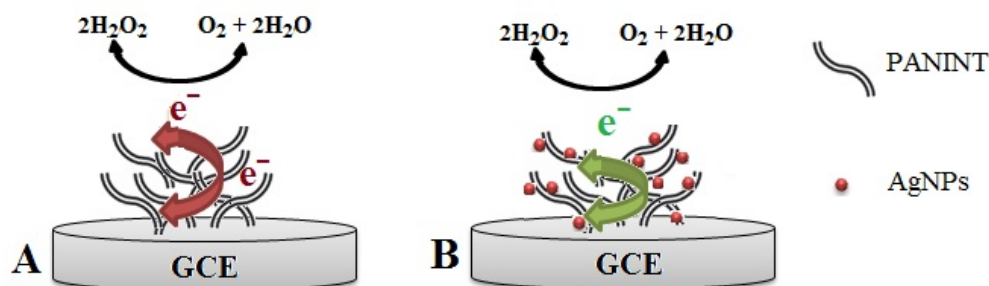


Figure 4.23 A: CVs of (a) bare GCE, (b) PANINT/GCE, (c) Ag/GCE, (d) AgNPs-PANINTs(B)-2/GCE and B: CVs of Modified AgNPs-PANINTs(B) nanocomposite using different volume ratios of Ag(NH₃)₂OH (0.04 M) of 12, 6, and 3 respectively (b–c), and AgNPs-PANINTs(B)/GCE prepared by using AgNO₃ (0.04 M) volume ratio of 12 (d) in 0.2 M phosphate buffer solution (Na₂HPO₄ and NaH₂PO₄) pH 6.5 in the presence of 1.0 mM H₂O₂ using 20.0 mVs⁻¹ scan rate.

The transfer of the required electrons to reduction of H₂O₂ could be facilitated by modifying GCE with conductive PANINT (PANINT/GCE) (Scheme.4.4. A). AgNPs could extremely intensify the electron-transfer reactivity of the AgNPs-PANINTs(B) composite. Therefore the reduction of H₂O₂ is increased by the catalyst effect of AgNPs (Gan et al., 2004) (Scheme.4.4. B).

At lower frequencies, the linear part corresponds to the diffusion process. All the electrodes fitted by an electrical equivalent circuit as shown in Figure 4.24, which consists of resistance of electrolyte (R_s), charge transfer resistance (R_{ct}), and double layer capacitance (C_{dl}) of the electrode.



Scheme 4.4 Possible mechanism of H_2O_2 reduction by (a) PANINT/GCE electrode and (b) AgNPs-PANINTs(B)/GCE electrode.

To give a more accurate fit, a constant phase element (CPE) is proposed into the equivalent circuit instead of a pure capacitor. For simulating the impedance behavior of modified electrodes, Randles circuit model was used. Figure 4.24 shows the Nyquist impedance plots of (a) bare electrode, (b) PANINT and (c) AgNPs-PANINTs(B)-2 electrodes. The impedance data recorded in $[\text{Fe}(\text{CN})_6]^{3-/4-}$ solution in the frequency range of 0.1 Hz to 100 KHz followed by applying a signal amplitude of 5 mV (around the open circuit potential). The validity of fitting to the corresponding circuit was evaluated by minimizing the chi-squared (χ^2) to 10^{-4} .

The EIS data of the bare GCE showed a larger semicircle than other modified electrodes which indicates low conductive property of GCE (30181 Ω). Figure 4.24 presents that by modifying GCE with PANINT (11341 Ω), the semicircle diameter totally decreases (almost 2.6 times) principally due to rapid electron transfer corresponded to the good conductivity of PANINT. The R_{ct} dramatically decreased to 287 Ω for AgNPs-PANINTs(B)-2, which indicates that incorporating of Ag nanoparticles into the matrix of polymer, improves the conductivity.

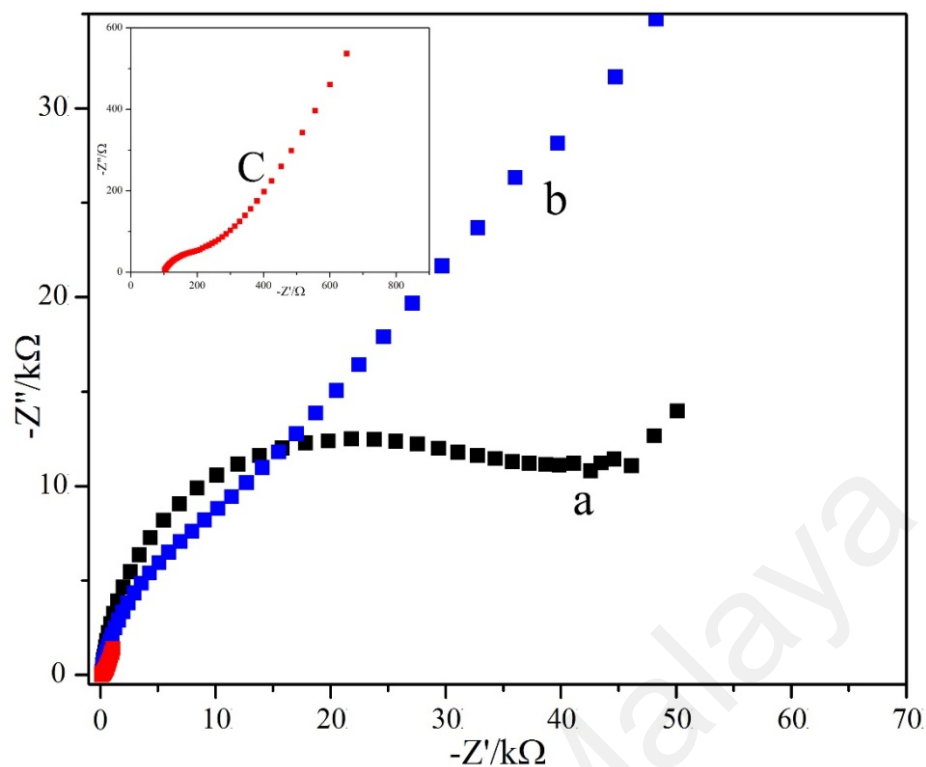


Figure 4.24 Nyquist diagrams of (a) GCE, (b) PANINT/GCE and (c) AgNPs-PANINTs(B)-2/GCE in 0.1 M KCl solution containing 1.0 mM $\text{Fe}(\text{CN})_6^{3-/4-}$ (1:1).

1.13.3.2 Amperometric response of the modified electrode (AgNPs-PANINTs(B)/GCE) to hydrogen peroxide

Figure 4.25 shows the amperometric response of the AgNPs-PANINTs(B) composite with a constant potential at -0.35 V by adding different concentrations of H_2O_2 in 0.2 M phosphate buffer solution (Na_2HPO_4 and NaH_2PO_4) at pH 6.5. The current of the working electrode dramatically increased up to 95% of the steady-state current within 3 s which shows a fast amperometric response behavior.

Table 4.5 Shows the EIS parameters achieved by equivalent circuits of bare electrode and modified electrodes in 0.1 M KCl solution containing 1.0 mM $\text{Fe}(\text{CN})_6^{3-/4-}$ (1:1).

Table 4.5 EIS parameters achieved by equivalent circuits of bare electrode, PANINT and AgNPs-PANINTs(B)-2/GCE in 0.1 M KCl solution containing 1.0 mM Fe(CN)₆^{3-/4-} (1:1).

Electrode	R _s (Ω)	R _{ct1} (Ω)	Q ₁ (nMho)	W (μMho)	n
Bare	149	30181	332	33	0.87
PANINT	138	11341	871	-	0.85
AgNPs-PANINTs(B)-2	110	114	44	857	0.71

The steady-state calibration plot over the concentration range of (12 point) was prepared from the amperometric response. The plot of H₂O₂ concentration range from 100 μM up to 90 mM shows linear behavior towards peak currents. Based on the linear section, the linear regression equation of $I = 0.0316 (\mu\text{A}\cdot\text{mM}^{-1}) + 0.2006$ ($R^2 = 0.9986$) is determined, increasing from 0.1 mM to 90 mM (Figure 4.25 B).

The limit of detection (LOD) and the limit of qualification (LOQ) are estimated to be 0.2 μM, 0.8 μM respectively at the signal to noise ratio of 3 (Moldoveanu, 2004). The response current of the modified AgNPs-PANINTs(B) was checked again after 7 days to know the stability of the sensor. The result still shows good stability and just the 5.6 % of the current signal was disappeared.

The effect of common interfering species on AgNPs-PANINTs(B) modified electrode was studied. Figure 4.26 shows the amperometric response of the modified electrode towards addition of 1.0 mM H₂O₂ which is followed by glucose, glycine and ascorbic acid into 0.2 M phosphate buffer solution (pH 6.5). As can be seen, these interfering substances responded with very weak signals demonstrating that this modified electrode has a good selectivity towards H₂O₂.

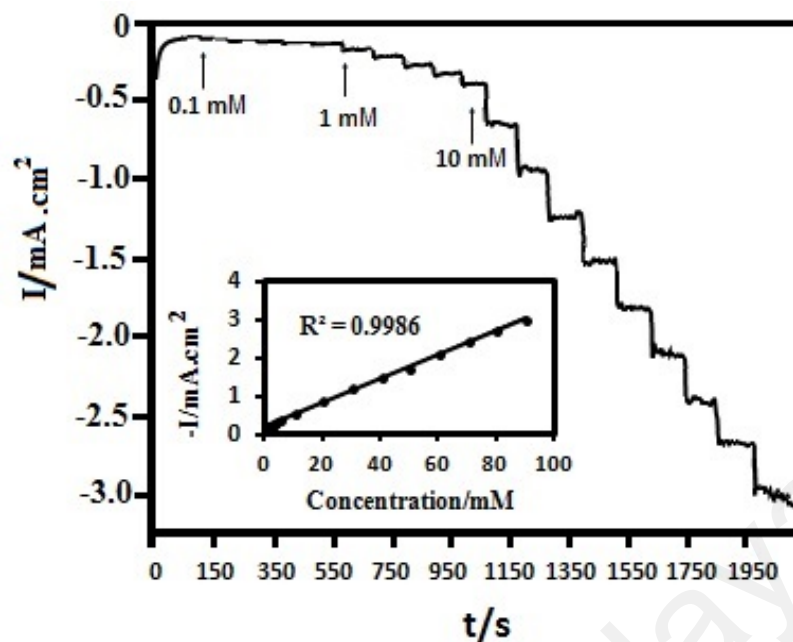


Figure 4.25. Steady-state response of AgNPs-PANINTs(B)/GCE to successive injections of H_2O_2 in 0.2 M phosphate buffer solution (Na_2HPO_4 and NaH_2PO_4) pH 6.5 with an applied potential -0.35 V. The inset is the corresponding calibration curve.

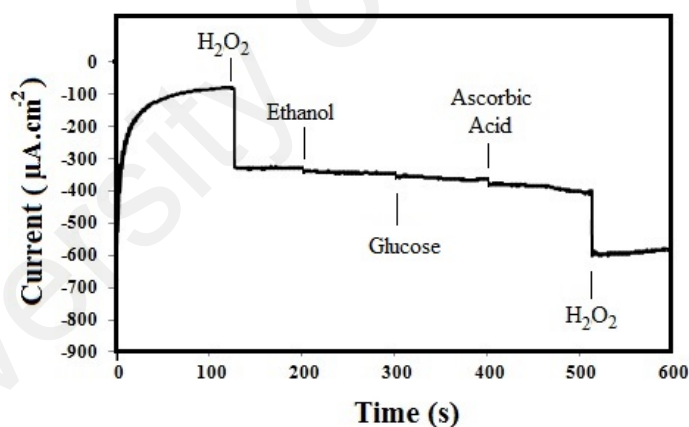


Figure 4.26 Amperometric response of AgNPs-PANINTs(B)/GCE electrode upon the successive addition of 1.0 mM H_2O_2 , glucose, ethanol and ascorbic acid into 0.2 mM H_2O_2 in phosphate buffer solution (pH 6.5) with an applied potential -0.35 V under a stirring condition.

The liner range and LOD of the proposed AgNPs-PANINTs(B) modified electrode was compared with some of the best previous voltammetric non-enzymatic hydrogen peroxide sensors and has been summarized in Table 4.6. The characterization response of the proposed amperometric sensor shows better results as compared to most

of the articles, but quite similar to some of these amperometric sensors (Liu, Wang, et al., 2011; Qin et al., 2011; Shi et al., 2011; Song et al., 2009). This result is comparable to ultra-thin polypyrrole nanosheets decorated with silver nanoparticles (AgNPs/UTPNSs) which have shown desired performance as a non-enzymatic amperometric sensor (Mahmoudian, et al., 2012).

The Ag-PANINTs modified electrode offered a direct electrochemical response as a non-enzymatic sensor for determination of H₂O₂. The observed long stability, high sensitivity and low LOD of the obtained nano sensor have demonstrated that the Ag-PANINTs nanocomposite is an effective non-enzymatic H₂O₂ sensor. Therefore, it demonstrates a new pattern of direct H₂O₂ detection by non-enzymatic amperometric sensor.

Table 4.6. Comparison of the LOD value of the previous reports and this work from different methods

Modify Electrode	Performance	Liner range	References
	LOD (μ M)	(mM)	
AgNPs/PPYCs	0.9	0.1-70	(Qin et al., 2011)
AgNPs/UTPNSs	0.57	0.1-90	(Mahmoudian et al., 2012)
AgNPs/PANINFs	0.25	0.1-60	(Zhong et al., 2012)
AgNPs/CNT	1.6	0.05-8	(Shi et al., 2011)
AgNPs/rGO/PANI	7.1	0.1-80	(Liu,Wang, et al., 2011)
AgNPs-PANINRs	0.13	0.1-10	This work
	0.33	10-70	
AgNPs-PANINTs(B)	0.6	0.1-100	This work

1.14 Polyaniline nanofibers-silver nanoparticles decorated reduced graphene oxide nanocomposites [AgNPs-PANINFs-rGO]

In AgNPs-PANINFs-rGO composite, the rGO combining with PANI was introduced. Three methods of AgNPs-PANINTs(A), AgNPs-PANINTs(B) and AgNPs-PANINRs which have been previously elaborated in chapter 3 were used. Reduced graphene oxide (rGO) decorated with silver nanoparticles (AgNPs) was reduced by a hydrothermal method as named AgNPs-rGO. $\text{Ag}(\text{NH}_3)_2\text{OH}$ was used as the source of AgNPs. Polyaniline with nanofibers morphology (PANINFs) was then synthesized by vertical sonochemical method in the presence of sulfuric acid. The modified electrode was prepared by dropping obtained AgNPs-rGO and PANINFs on the glassy carbon electrode (GCE). In this composite, silver ammonia complex is used as the source of AgNPs. The silver nanoparticles were homogeneously distributed on the rGO surface with a narrow nanosize distribution.

1.14.1 Morphology analysis of bulk PANI by bath sonication

The FESEM results of synthesized PANI in the presence of H_2SO_4 at different exposure times by bath sonication methods are given in Figure 4.27 (a-d) which clearly show the agglomeration phenomena can be observed with the increase of exposure time from 2 min to 5 min.

1.14.2 Morphology analysis of PANINFs

The FESEM results of synthesized PANI in the presence of H_2SO_4 at different exposure times (as previous explained at 3.3.2) are given in Figure 4.28 (a) which obviously shows the PANINFs synthesized after 2 min exposure time to ultrasonic irradiation. The agglomeration phenomena can be observed with the increase of exposure time from 2 min to 5 min.

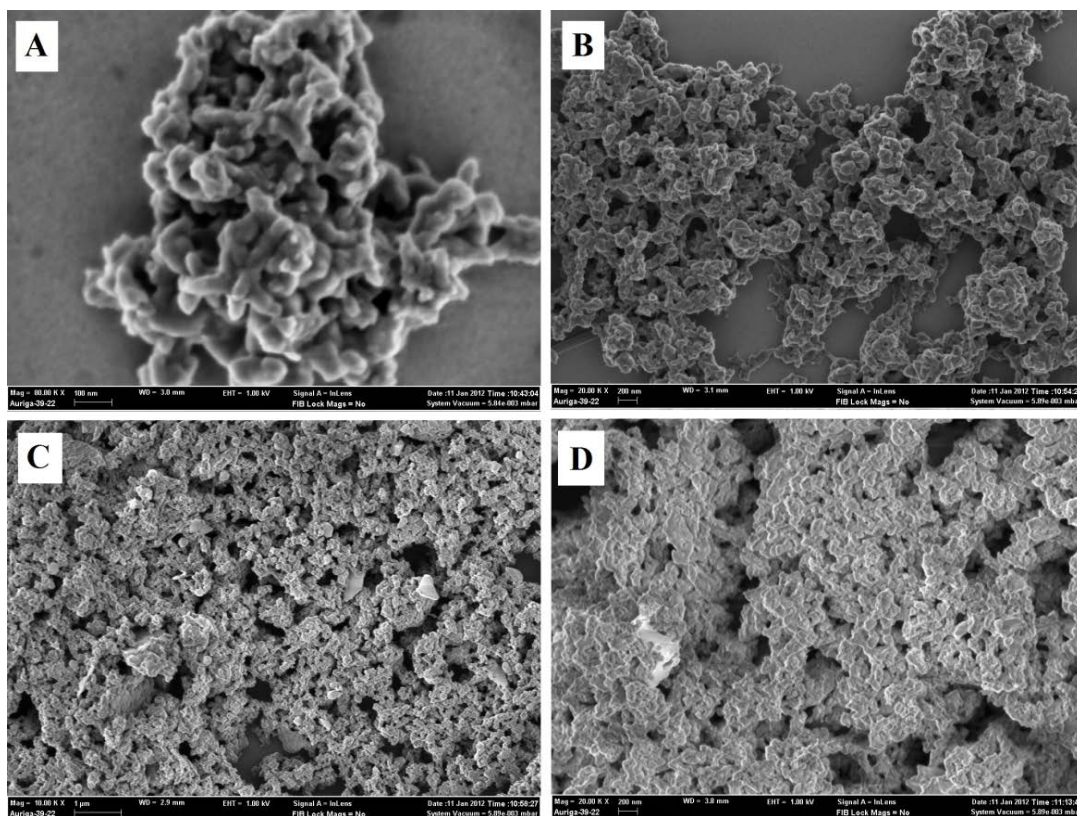


Figure 4.27 FESEM images of PANI synthesized with different ultrasonic irradiation time; (a) 2 min, (b) 3 min, (c) 4 min, (d) 5 min.

It is reported that PANINFs tend to agglomerate like interconnected network instead of bundles with the increase of reaction time (Wang et al., 2008). The increase of PANINFs agglomeration is due to the increase in the surface area and Van der Waals forces of the PANINFs. The formation of PANINFs in chemical interfacial polymerization method consists of three steps: chemical reaction, nucleation and growth. The homogeneous nucleation step occurs during the nanofiber synthesis process (Li & Kaner, 2006). Homogeneous nucleation in aqueous solution can occur due to sufficient super-saturation of the reaction mixture (Tran et al., 2008). It is observed that the change in color of the reaction mixture can be considered as an indicator of the reaction rate. The reaction mixture is observed to have changes in color from light to dark blue just after 100 s upon exposure to ultrasonic irradiation which indicates the PANI formation

(Royappa et al., 2001). Comparing the present work with previous reports show a decrease in the preparation time of the PANINFs (Huang et al., 2003). The observation of the reaction mixture with time shows that the blue color intensity increases with the increase of the exposure time towards ultrasonic irradiation. The reason of this phenomenon is due to the over-oxidation and agglomeration process. The previous studies have shown that the PANINFs size depends on the dopant size and monomer concentration. The nanofiber diameter length also increases with the increase in the acid strength (Su et al., 2007). PANINFs was synthesized in H_2SO_4 solution because of the uniformly narrow diameters and dense network structure (Ge et al., 2012). The FESEM results confirm that the optimum exposure time for the synthesis of large surface area of PANINFs is 2 min. The TEM image at 2 min reaction time was recorded and the size of PANINFs is estimated around 39 ± 8 nm (Figure 4.29).

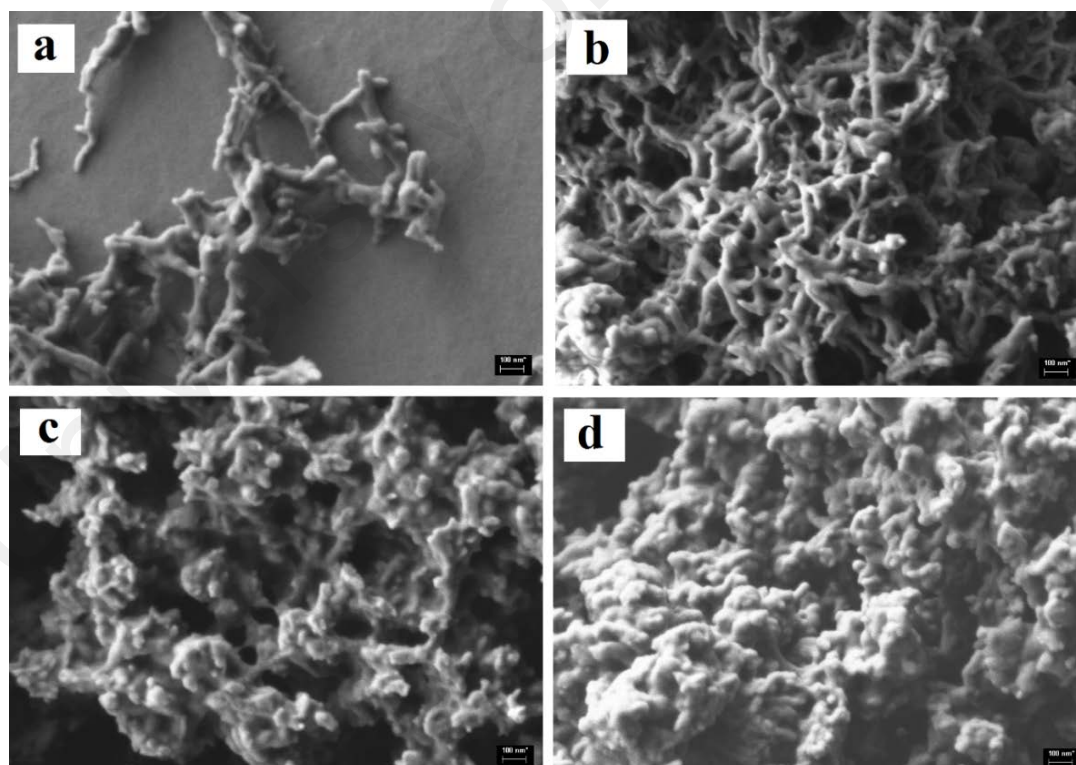


Figure 4.28 FESEM images of PANINFs synthesized with different ultrasonic irradiation time; (a) 2 min, (b) 3 min, (c) 4 min, (d) 5 min.

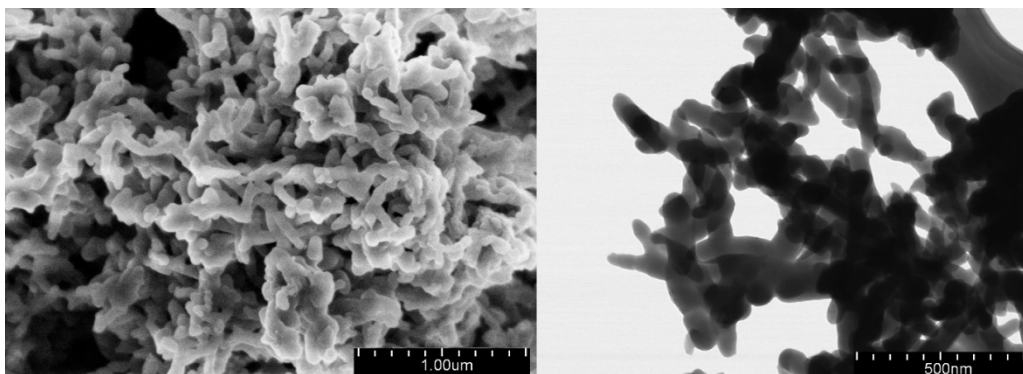


Figure 4.29 From left to right FESEM and TEM images of PANINFs-2

Figure 4.30A shows the UV-vis spectra of 0.1 mg synthesized PANINFs by sonochemical method in the presence of H₂SO₄ at different exposure times, dissolved in 40 mL dimethyl sulfoxide (DMSO). The existence of the broad peak from 800 nm confirmed the presence of doped PANINFs. The doped PANINFs showed two absorption peaks in the UV-Vis region of 400 to 800 nm.

These peaks corresponded to the electronic transition from the valence band to the polaron band of the doped emeraldine oxidation state ($\pi \rightarrow \pi^*$) of PANI (Mendes et al., 2011). The UV-Vis results showed that the increase of exposure time not only increased the absorbance intensity but also shifted the absorbance peaks to the lower wavelength. Gradually longer irradiation times, from 2 to 5 min caused a blue shift from 349 to 341 nm. This phenomenon was due to the creation of an inter-band charge transfer from the benzenoid to quinoid moieties in the PANINFs. The blue shift in UV-Vis the spectra of the PANINFs was due to the increase of the selective sites for the interaction between the dopants and quinoid ring in the PANINFs (Ameen et al., 2010; Su et al., 2007). Therefore, it can be concluded that van der Waals forces increased and subsequently the nanofiber size increased with agglomeration, due to the longer exposure time. The increase of van der Waals forces could explain the increase of the agglomeration process with the increase

in exposure time. Figure 4.30 B shows the photo images of PANINFs after different sonication times.

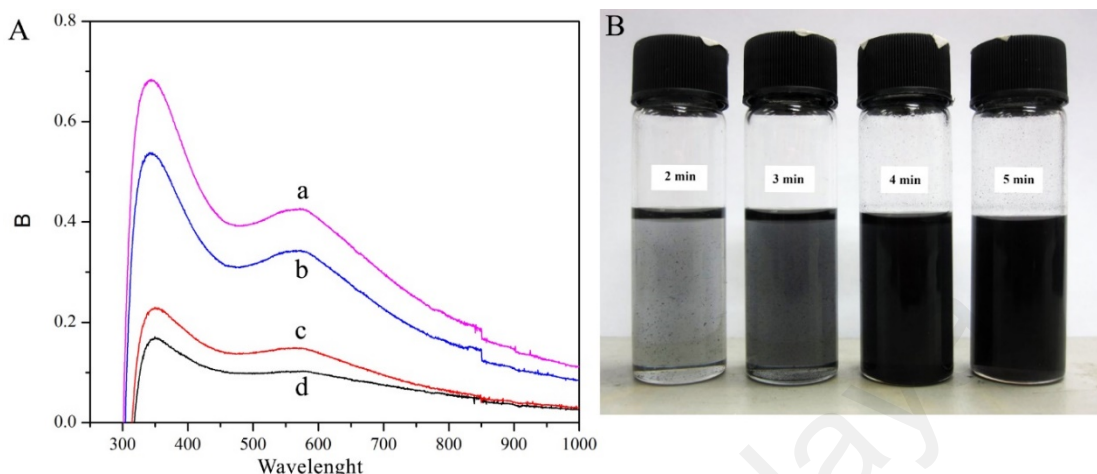


Figure 4.30 (A) UV Vis spectra of (a) PANINFs-4, (b) PANINFs-3, (c) PANINFs-2 (d) PANINFs-1. (B) Photo image of PANINFs after different sonication times

1.14.3 Morphology analysis of rGO

rGO was prepared separately via hydrothermal method. The FESEM and TEM images of rGO produced via hydrothermal method are shown in Figure 4.31 A and B respectively. The transparency of rGO is due to its reduction by hydrothermal way.

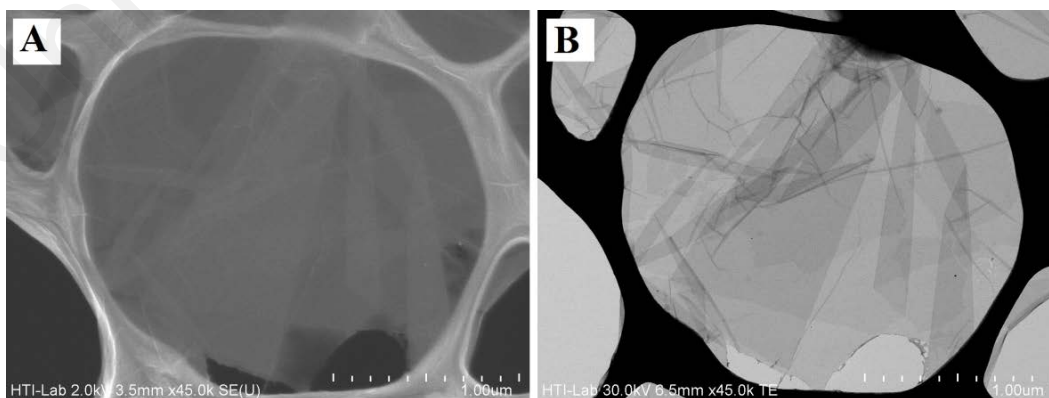


Figure 4.31 FESEM and TEM images of rGO

Figure 4.32 shows the 3D AFM images of rGO that is indicating that the thickness of rGO wrinkles is around 80 nm.

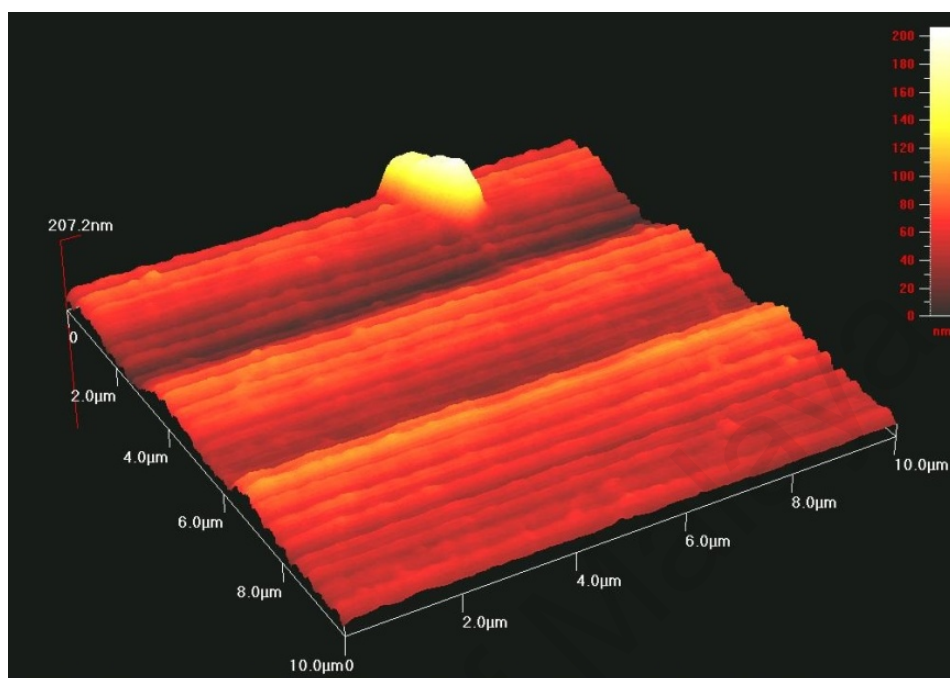


Figure 4.32 the 3D AFM images of rGO

1.14.4 Morphology analysis of AgNPs-rGO

The formation of AgNPs-rGO composites was characterized by TEM analysis as shown in Figure 4.33. It is clearly seen that the rGO has been decorated with small AgNPs about several nanometers in diameter, and almost all the AgNPs were uniformly distributed on the rGO substrate. TEM images along with the size distribution diagram for different AgNPs-rGO ratios prepared by volume ratio of 3:1 (a, b), 6:1 (c, d), and 12:1 (e, f) are displayed in Figure 4.33. In addition, Figure 4.33 (g, h) shows the TEM image and size distribution diagram of 6:1 AgNPs-rGO (AgNO₃ as the source of AgNPs) as reference. As can be seen in Figure 4.33 a number of small black dots are observed on the rGO. These images further revealed that density of Ag nanoparticles blend with rGO.

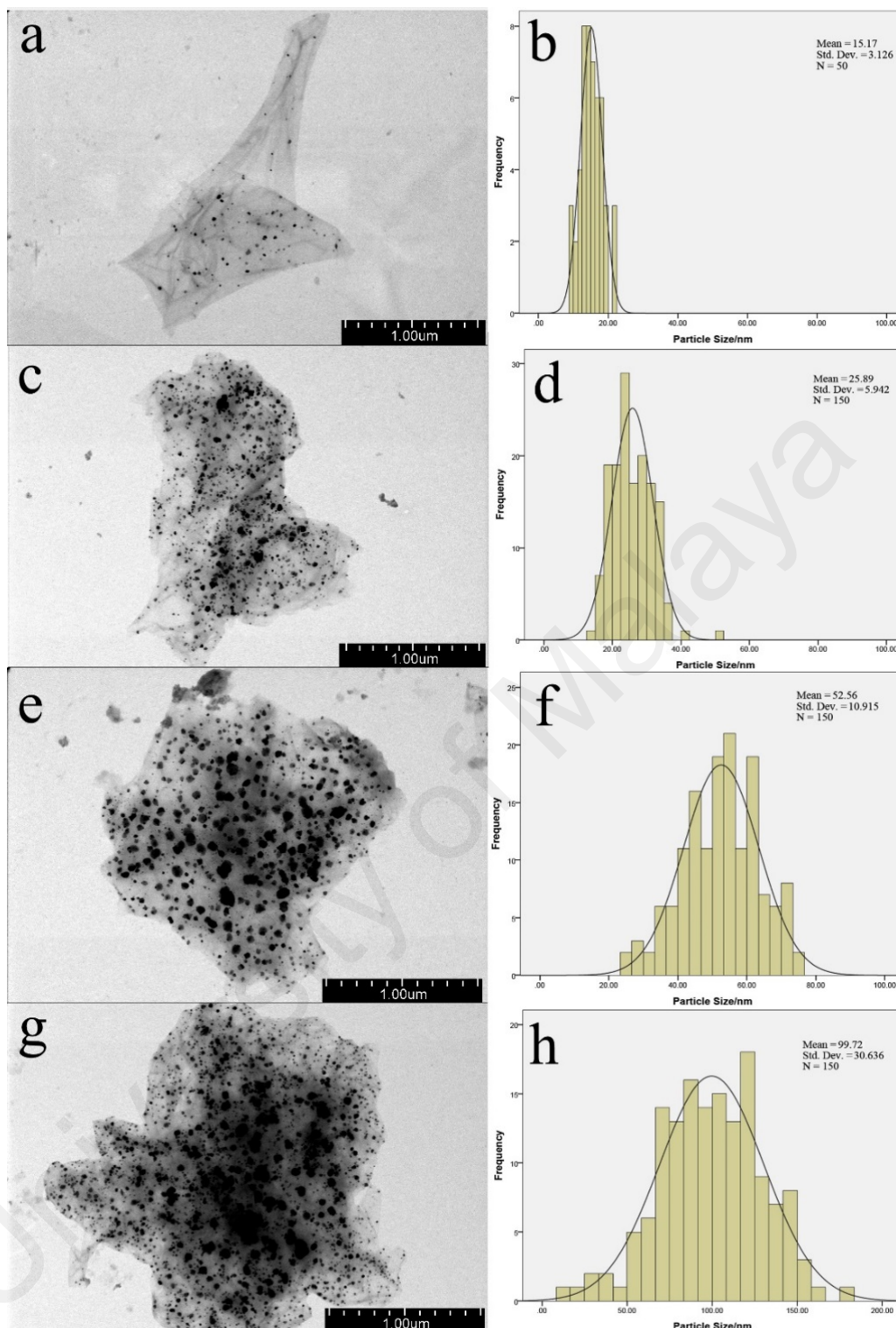


Figure 4.33 TEM images and size distribution diagram of AgNPs-rGO composite prepared by using the solution with GO to $\text{Ag}(\text{NH}_3)_2\text{OH}$ (0.04 M) volume ratios of 12 (a and b), 6 (c and d), and 3 (e and f) and using the solution with a GO to AgNO_3 (0.04 M) volume ratio of 12 (g and h).

By increasing the $\text{Ag}(\text{NH}_3)_2\text{OH}$ concentration (Figure 4.33 (a-f)), the average of particle size and total particle numbers also raised, and the size distribution was widened. In Figure 4.33 (c, d), the nanosize silver particles with an average size of 25.89 nm and a narrow particle size distribution have been well distributed on the surface of graphene nanosheet. In (12:1) ratio of AgNPs-rGO Figure 4.33 (e, f), the agglomeration of silver particles was observed. Figure 4.33 (g, h) shows the effect of silver precursor types on the coverage density and particle size on surface of graphene. With using AgNO_3 solution, the average particle size raised up to 99.72 nm and size distribution broadened which is mainly due to the fact that as compared with AgNO_3 , $\text{Ag}(\text{NH}_3)_2\text{OH}$ has a higher stability and reduction resistance, preventing the growth of large Ag particles. All the above observations suggest the formation of AgNPs decorated rGO. Three different ratios of AgNPs-rGO were labelled as AgNPs-rGO-1 (3:1) and AgNPs-rGO-2 (6:1) and AgNPs-rGO-3 (12:1) while AgNPs-rGO-4 is the 6:1 ratio of AgNPs-rGO (AgNO_3 as the source of AgNPs).

1.14.5 XRD analysis, EDX and FT-IR spectroscopy characterization of AgNPs-PANINFs-rGO composite

Figure 4.34 (a, b and c) displays the FT-IR spectrum of GO, AgNPs-rGO-2/GCE and AgNPs-PANINFs-rGO/GCE composites, respectively. For graphene oxide, the peaks at 1740, 1620 and 1379 are related to stretching $\text{C}=\text{O}$, sp^2 -hybridized $\text{C}=\text{C}$ group and O-H bending, C-OH stretching and C-O-C stretching, respectively while the broad peak centered at 3253 cm^{-1} is corresponded to the stretching vibrations of O-H groups (Makharza et al., 2013). In addition, the peaks at 1155 and 1043 cm^{-1} can be assigned to C-O vibration of alkoxy or epoxy (Pham et al., 2011). For AgNPs-rGO-2, the peaks located at 1690, 1440, 2836 and 2932 cm^{-1} are attributed to the sp^2 hybridized $\text{C}=\text{C}$ group

and O-H bending, O-H deformation and stretching vibration of CH₂ (symmetric and asymmetric) groups, respectively (Golsheikh et al., 2013).

For GO, the peak located at 1740 cm⁻¹ cannot be seen for AgNPs-rGO, showing that the group of carbonyl was eliminated by the electrochemical reduction (Guo et al., 2009). The broad peak at 3341 cm⁻¹ for AgNPs-rGO is likely to be assigned to the O-H stretching vibration of absorbed water molecules.

Figure 4.34 c shows the FT-IR spectrum of PANINFs synthesized in the presence of H₂SO₄ after 3 min of exposure time to ultrasonic radiation. The absorption band at 1590 and 1500 cm⁻¹ are assigned to the stretching vibration peak of C=C from the quinone and benzene ring (Hong-Xing et al., 2010), respectively.

The absorption peak at around 1300 cm⁻¹ is attributed to the stretching vibration of C-N in the benzene ring. The characteristic peaks at around 1140 and 820 cm⁻¹ are related to plane bending vibration of C-H and benzene ring, respectively. The FT-IR result confirms that PANI was successfully synthesized after 3 min exposure time and shows that this method is a facile way for the preparation of nanoscale PANI. In addition, the FT-IR result indicates shifts to the lower wavenumber for all characteristic PANINFs bands which is due to the existence of strong interaction between PANINFs and doped acid as well as the adsorption of silver nanoparticles.

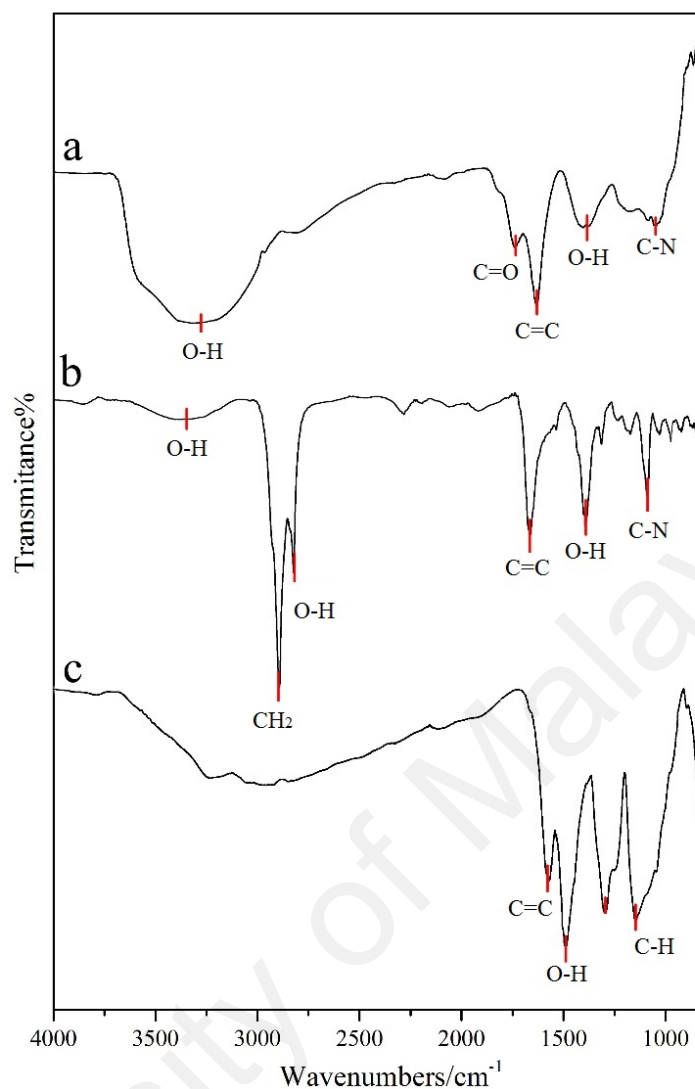


Figure 4.34 FT-IR spectra for (a) GO, (b) AgNPs-rGO, (c) AgNPs-PANINFs-2-rGO-2

Figure 4.35A shows that the X-ray diffraction (XRD) patterns confirm the formation of GO and AgNPs-rGO. In Figure 4.35 b, peak at 10.5° is related to GO characteristic peak, while the small peak appeared at $\sim 23^\circ$ is assigned to the elimination of surface oxygen-containing groups (Mayavan, Sim, & Choi, 2012). The small hump in AgNPs-rGO-2 nanocomposite at $\sim 11^\circ$ shows that the GO has been successfully reduced to rGO via electrochemical reduction. Meanwhile, the prominent peaks at 38.1° , 44.3° , 64.5° , and 77.5° for AgNPs-rGO-2 nanocomposites in Figure 4.35 c are related to the (111), (200), (220), and (311) crystallographic planes of face-centered cubic nanoparticles of silver, respectively [ref. code: 003-0921] (Zainy et al., 2012). The sharp peak located

at 38.5° is related to crystalline silver nanoparticles, affirmed the formation of high purity as synthesized crystalline silver (Liu, Tian, et al., 2011b; Teo et al., 2012; Xie et al., 2012).

The chemical composition and weight percentage of each element in the composite were further characterized by EDX (Figure 4.35B). The observed peak for N are believed to originate from the PANINFs, the observed peaks for C are belong to PANINFs and rGO also the O peak is originate from rGO and the Ag peaks from the AgNPs in the composites. These results also confirmed the appropriate percentage of Ag in the composite.

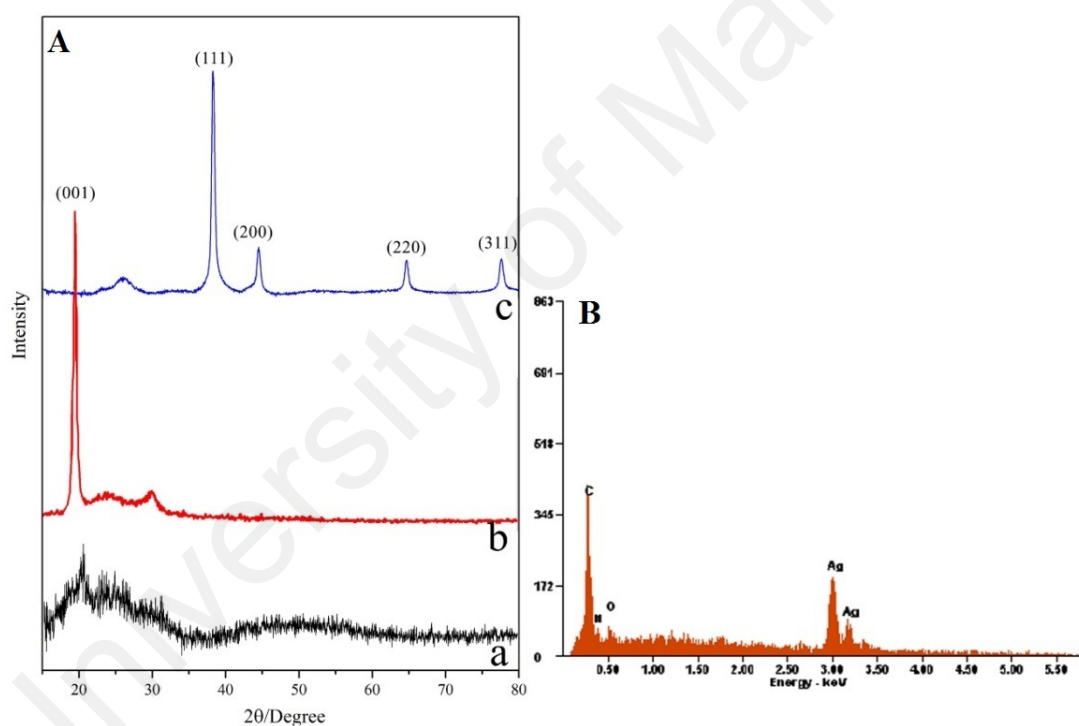


Figure 4.35 (A) XRD pattern of (a) AgNPs-PANINFs-rGO-2, (b) GO and (c) AgNPs-rGO-2 and (B) EDX spectra of AgNPs-PANINFs-rGO-2.

1.14.6 Electrochemical characterization of AgNPs-PANINFs-rGO composite

Electrocatalytic reduction of AgNPs-rGO-1, 2, 3/GCE and AgNPs-rGO-4/GCE in N_2 saturated 0.1 M PBS at pH 6.5 in the presence of 1.0 mM H_2O_2 (scan rate: 0.05 V/s) are shown in Figure 4.36 b. It is obviously seen that the response of the bare GCE toward the reduction of H_2O_2 is weak. In contrast, the AgNPs-rGO/GCE exhibits a remarkable catalytic current peak about $500 \text{ mA}\cdot\text{cm}^{-2}$ in intensity at -0.38 V vs. SCE. These observations indicated that the AgNPs/rGO nanocomposites exhibit notable catalytic ability for H_2O_2 reduction. Five different volumes of AgNPs-rGO were investigated to study the optimum volume of drop cast. Figure 4.36 a shows that $20 \mu\text{L}$ is the optimum volume amount of AgNPs-rGO to detect.

1.14.6.1 Cyclic voltammogram (CV) of the modified electrode (AgNPs-PANINFs-rGO /GCE) to hydrogen peroxide

Electrocatalytic reduction of AgNPs-rGO-1, 2, 3/GCE and AgNPs-rGO-4/GCE in N_2 saturated 0.1 M PBS in the presence of 1.0 mM H_2O_2 at the scan rate of 50 mVs^{-1} (pH 6.5) is shown in Figure 4.36 b. As can be seen, the bare GCE response toward the reduction of H_2O_2 is highly weak. On the other hand, the AgNPs-rGO/GCE shows a significant catalytic current peak around $500 \text{ mA}\cdot\text{cm}^{-2}$ at -0.38 V vs. SCE. These observations confirmed that the AgNPs-rGO nanocomposites show remarkable catalytic activity for H_2O_2 reduction.

The catalytic activities of almost all AgNPs-rGO/GCE electrodes are significantly better than AgNPs-rGO-4/GCE. The comparison between AgNPs-rGO-1/GCE, AgNPs-rGO-2/GCE and AgNPs-rGO-3/GCE which were synthesized in the $\text{Ag}(\text{NH}_3)_2\text{OH}$ solution, shows that the AgNPs-rGO-2/GCE has the highest electrocatalytic activity mainly because of higher available surface area. As compared with AgNPs-rGO-1/GCE,

the particle density of AgNPs-rGO-2/GCE is higher and although particle density for AgNPs-rGO-2/GCE, is lower than AgNPs-rGO-3/GCE, particle size of AgNPs increased due to agglomeration, which led to lower surface area. FESEM images approved the results of CVs.

In order to investigate drop cast volume, four different volumes of AgNPs-PANINFs-rGO-2 were prepared and as can be seen in Figure 4.36 c, the optimum volume was selected. 10 μL of PANINFs-1 (2 min), PANINFs-2 (3 min), PANINFs-3 (4 min) and PANINFs-4 (5 min) were dropped on the optimized AgNPs-rGO electrode (AgNPs-rGO-2/GCE) to study the effect of sonication time of polyaniline on the hydrogen peroxide detection. Figure 4.36 d presents the CVs of different PANINFs (PANINFs-1, PANINFs-2, PANINFs-3 and PANINFs-4) in 0.1 M PBS in the presence of 1.0 mM of H_2O_2 (pH 6.5). It is indicated that the responses of the modified electrodes with the PANINFs are not highly significant toward the reduction of H_2O_2 . In contrast, the PANINFs-2 shows a typical catalytic current peak about $2.1 \text{ mA}\cdot\text{cm}^{-2}$ centered at -0.60 V vs SCE in the presence of 1.0 mM H_2O_2 . However, the AgNPs-rGO/GCE exhibits better electrochemical response in the presence of H_2O_2 as compared to modified electrodes with the PANINFs individually. All these observations demonstrate that the AgNPs- PANINFs/rGO nanocomposites exhibit excellent catalytic performance toward H_2O_2 reduction.

The polyaniline in the nanofiber form provides remarkable high surface area similar to PANINTs and PANINRs forms for reduction of H_2O_2 . During the reduction of H_2O_2 , the polyaniline can undergo the overoxidation, and as previously shown, H_2O_2 directly is reduced in the vicinity of PANINFs (1 and 2) (Mahmoudian, et al., 2012; Mahmoudian et al., 2013) With increasing the surface area of the PANINFs, the reduction of H_2O_2 could increase as well:

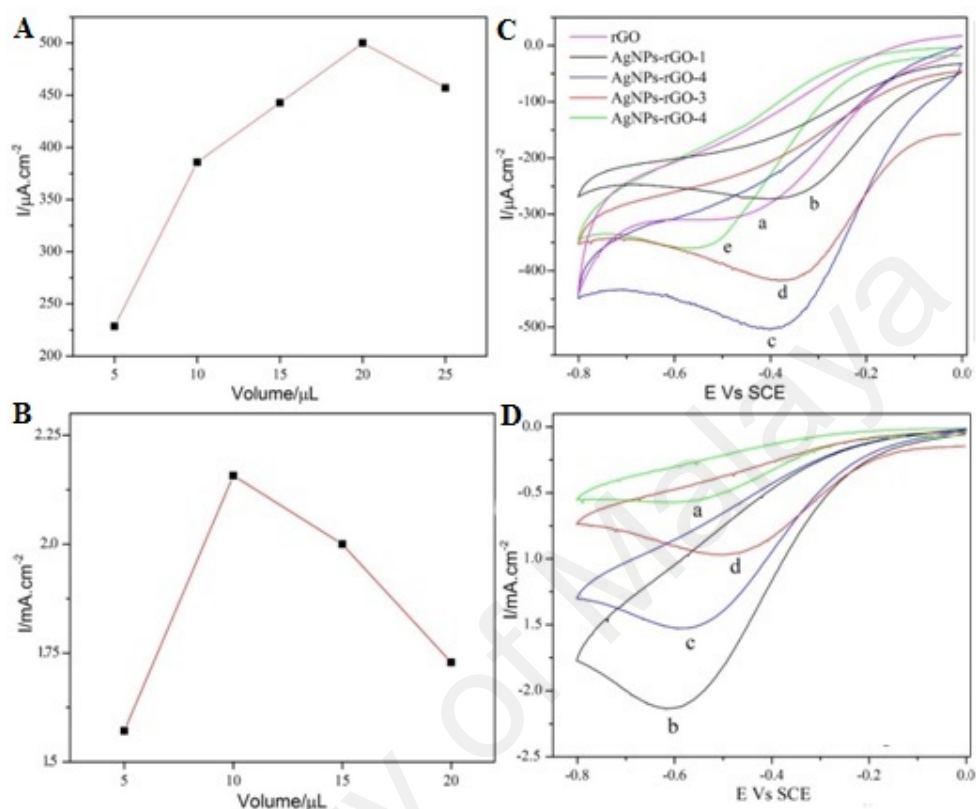


Figure 4.36 (A) optimized the AgNPs-rGO volume ratio to detect H₂O₂; (B) optimized the PANINFs volume ratio to detect H₂O₂; (C) CVs of different modified electrodes: (a) AgNPs-rGO-1/GCE, (b) AgNPs-rGO-2/GCE, (c) AgNPs-rGO-3/GCE and (d) AgNPs-rGO-4/GCE in 0.1 M PBS (pH 6.5) with adding 1.0 mM H₂O₂. (c) CVs of AgNPs-rGO-2/GCE in 0.1 M PBS (pH 6.5) in the presence of 1.0 mM H₂O₂ at scan rate of 50 mVs⁻¹; (D) the CVs of different PANINFs (PANINFs-1, PANINFs-2, PANINFs-3 and PANINFs-4) in 0.1 M PBS in the presence of 1.0 mM of H₂O₂ (pH 6.5).

1.14.6.2 Amperometric response of the modified electrode (AgNPs-PANINFs-rGO /GCE) to hydrogen peroxide

Amperometric $i-t$ curve is the regularly utilized technique to assess the electrocatalytic activities of electrochemical sensors. Figure 4.37 (A) shows The current response affected by applied potential in the presence of 1.0 mM H₂O₂ on the AgNPs-rGO coated GCE in 0.1 M phosphate buffer solution (pH 6.5). Figure 4.37 (B) displays the current response of AgNPs- PANINFs-rGO-2/GCE with successive addition of H₂O₂

into PBS at pH 6.5 under the applied potential of -0.60 V in the stirring condition (2000 rpm). Figure 4.37 (C) displays the current response of AgNPs- PANINFs-rGO-2/GCE with successive addition of H₂O₂ into PBS at pH 6.5 under the applied potential of -0.60 V in the stirring condition (2000 rpm) in low concentrations. The response time was fast (less than 3 s) and with increasing the concentration of H₂O₂ from 0.1 mM to 110 mM, the current increased linearly. In calibration curve, the sensor shows two linear sections for the response to H₂O₂ (Figure 4.37 D and E). Based on the first linear section, the linear regression ($R^2=0.991$) is determined, increasing from 0.1 mM to 5.0 mM while, in a higher concentration of H₂O₂, the second linear section raised up to 110 mM ($R^2= 0.999$). For two linear parts shown in Figure 4.37 (D, E), the LOD and LOQ (S/N=3) are calculated to be 0.682 μ M, 2.274 μ M and 0.117 μ M, 0.389 μ M, respectively.

1.14.7 Repeatability, reproducibility and stability

The repeatability, reproducibility and stability of the prepared sensor were studied. Five modified electrodes were prepared under the same condition and relative standard deviation (RSD) of the current response toward 1.0 mM H₂O₂ was found to be 2.14%, confirming that the results can be reproducible. The repeatability of one sensor to determine 1.0 mM H₂O₂ was good. The RSD was 1.22% for 10 successive assays. In order to investigate the stability of AgNPs-PANINFs-2-rGO-2 electrode, the modified electrode was stored at ambient condition and the current was periodically monitored for 14 days (Figure 4.38). The sensor retains around 90.03% of its initial response after 2 weeks (I_0 and I are the response current in the first and following days, respectively). Regarding the overall performance, it can be concluded that AgNPs-PANINFs-2-rGO-2 shows a good repeatability, reproducibility and stability. The effect of electroactive interfering species on modified electrode was evaluated. Figure 4.38 (inset) shows the amperometric response of PANINFs-2-AgNPs-rGO-2 towards the successive addition of

1 mM H₂O₂. This was followed by the addition of glucose, ascorbic acid, ethanol and uric acid into 0.1 M PBS at pH 6.5. The current response of the mentioned electroactive interfering species was quite negligible which confirmed that PANINFs-2-AgNPs-rGO-2 had a superior selectivity towards H₂O₂.

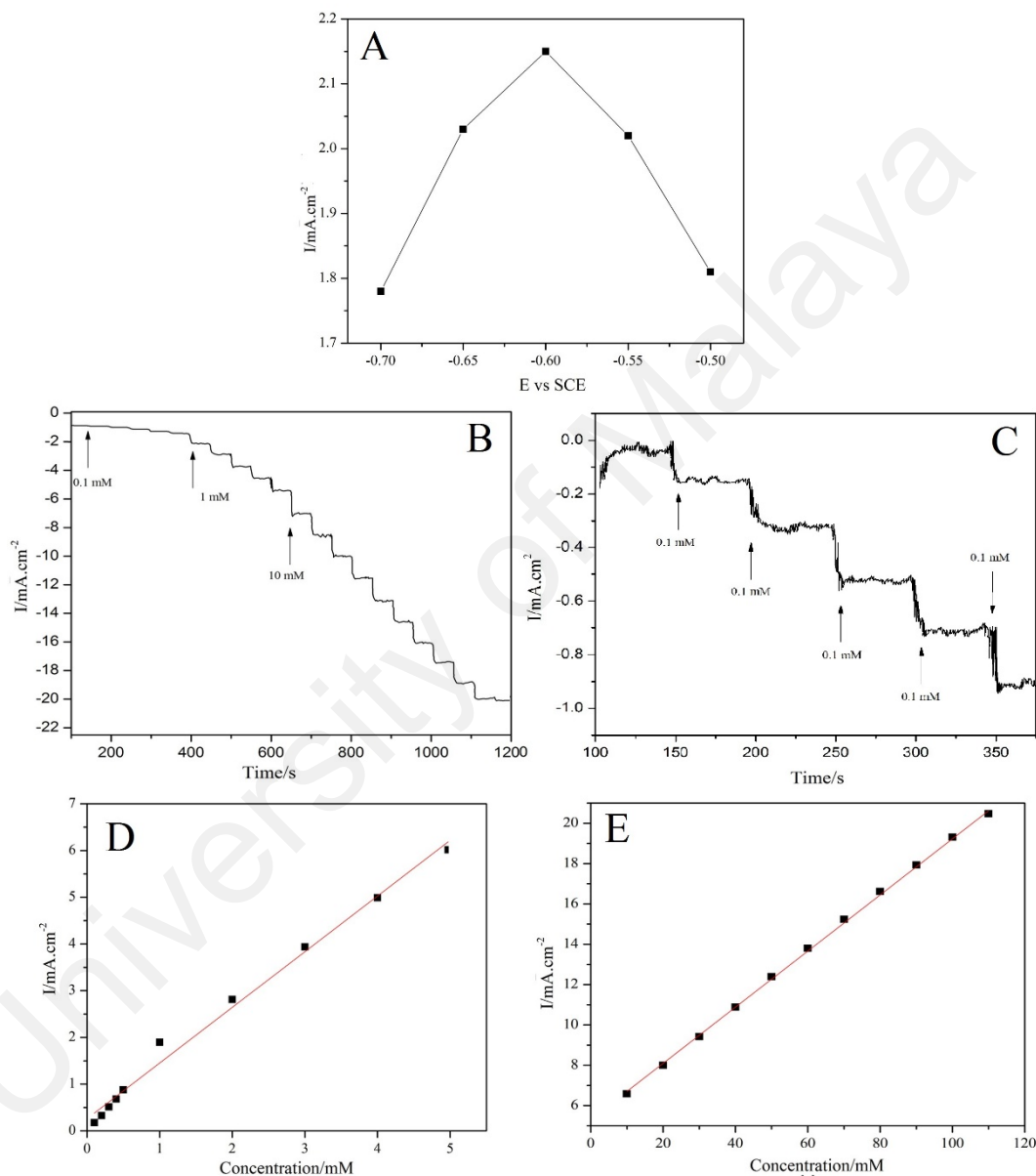


Figure 4.37 A: The current response affected by applied potential in the presence of 1.0 mM H₂O₂ on the AgNPs-rGO coated GCE in 0.1 M phosphate buffer solution (pH 6.5); B: the current response of AgNPs- PANINFs-rGO-2/GCE with successive addition of H₂O₂ into PBS at pH 6.5 under the applied potential of -0.60 V; C: the current response of AgNPs- PANINFs-rGO-2/GCE with successive addition of H₂O₂ into PBS at pH 6.5 under the applied potential of -0.60 V at low concentrations; D: the corresponding calibration curve of low concentration H₂O₂; E: the corresponding calibration curve of high concentration H₂O₂.

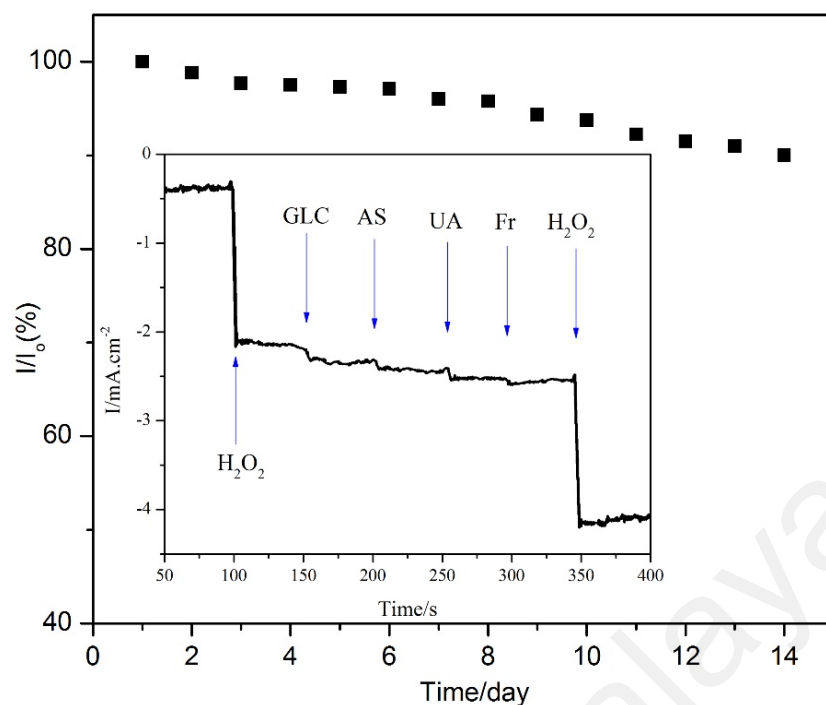


Figure 4.38 Long-term stability of the AgNPs-PANINFs-2-rGO-2 studied in 2 weeks

As listed in Table 4.7 the detection limit and the linear range of AgNPs-PANINFs-rGO/GCE are better and wider than other modified electrodes based on polyaniline, silver and reduced graphene oxide.

In summary, by an effective and simple method and through adding PANI and silver nanostructure to the rGO matrix, we successfully improved the ability of the present composite was successfully improved to detect H_2O_2 as compared to the first, second and third composites. AgNPs-PANINFs-rGO/GCE exhibited lower limit of detection and wider linear range as H_2O_2 sensor. The modified AgNPs-PANINFs-rGO-2 electrode exhibits a wide linear range up to 110 mM towards H_2O_2 and shows two linear range with a high sensitivity and a low detection limit for each section, which can be interpreted due to the high available surface area of as-synthesized AgNPs-PANINFs-rGO-2 sensor. Fabrication easiness, high sensitivity and selectivity, wide linear range and low detection limit make AgNPs-PANINFs-2-rGO-2/GCE an excellent amperometric sensor for H_2O_2 .

Table 4.7. Comparison between LOD and linear range of different nonenzymatic H₂O₂ sensors

Modify Electrode	Performance		References
	LOD (μ M)	Liner range (mM)	
Ag NPs-NFs/GCE	62	0.1–80	(Tian, Liu, & Sun, 2010)
PANI-Pd NPs	2.6	10–700	(Ivanov et al., 2013)
AgNP-rGO- benzylamine	31.3	0.1–100	(Liu, Tian, et al., 2011a)
ERGO-Ag/GCE	1.6	0.1–100	(Golsheikh et al., 2013)
PDA-RGO-Ag-based	2.7	0.0005-8	(Fu et al., 2015)
AgNPs- PANINFs/GCE	250	1–12	(Abdulrahman, 2012)
Ag-AgCl nanoboxe/GCE	1.7	0.005–15.0	(Li et al., 2015)
Pt-MWCNTs- PANI/GCE	2.0	0.007–2.5	(hong et al., 2012)
PDDA-rGO- AgNPs/GCE	35	0.1–41	(Liu et al., 2013a)
PANI-SWCNTs/Pt	1.2	0.001–1.0	(Wang, Yun, & Zheng, 2009)
AgNPs-PANINRs	0.13	0.1-10	This work
	0.33	10-70	
AgNPs-PANINTs(B)	0.6	0.1-100	This work
AgNPs-PANINFs- rGO/GCE	0.682	0.1-5	This work
	0.117	10-110	

1.15 Carbon base composites for hydrogen peroxide sensing

In this part, the focus of this study is on using carbon-based materials as the main material replacing PANI and evaluating them as H₂O₂ sensor. This idea is based on remarkable performance of these materials as nanocomposites for H₂O₂ sensing reported in the literature (Shao et al., 2010; Wang, 2005).

1.15.1 Silver nanoparticle- carbon nanotube reduced-graphene oxide composite by hydrothermal method [AgNPs-MWCNT-rGO(H)]

1.15.1.1 Morphology analysis of AgNPs-MWCNT-rGO(H)

The first carbon base nanocomposite in the present study is combination of hydrothermal reduced graphene oxide, MWCNT and AgNPs. As mentioned in literature review, rGO and MWCNT can provide high conductive surface area for AgNPs deposition. Therefore, herein the first time the combination of rGO and MWCNT is reported. Since the Ag(NH₃)₂OH provides smaller size of decorated AgNPs in the obtained nanocomposites, therefore Ag(NH₃)₂OH was focused as source of AgNPs in the present study. However, the performance of AgNO₃ as AgNPs source was still investigated in AgNPs-MWCNT-rGO(H) composite has been prepared via hydrothermal method as mentioned in 3.3.6.12.

The TEM micrograph in Figure 4.39 shows the AgNPs-MWCNT-rGO(H) nanocomposite prepared by aqueous solution of volume ratios of MWCNT-GO (1.0 mg.mL⁻¹), (3:1, v/v) to Ag(NH₃)₂OH volume in a 6:1 ratio.

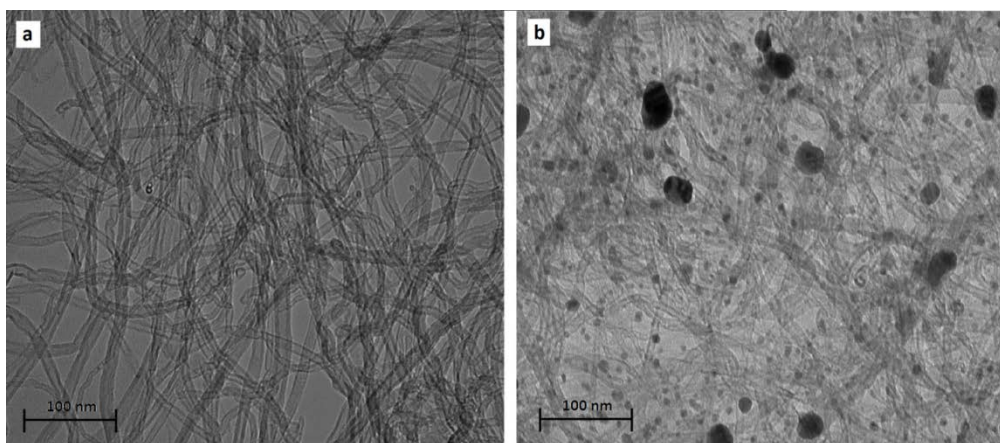


Figure 4.39 TEM images of MWCNT-rGO without Ag (a) and the AgNPs-MWCNT-rGO(H) with volume ratios of MWCNT-GO ($1.0 \text{ mg}\cdot\text{mL}^{-1}$), (3:1, v/v) to $\text{Ag}(\text{NH}_3)_2\text{OH}$ (0.04 M) volume ratios of 6 (b)

FESEM images and silver nanoparticle size distribution diagrams of AgNPs-MWCNT-rGO(H) nanocomposites prepared using different volume ratios of MWCNT-GO ($1.0 \text{ mg}\cdot\text{mL}^{-1}$), (3:1, v/v) to $\text{Ag}(\text{NH}_3)_2\text{OH}$ and (0.04 M) 12, 6 and 3 are shown in Figure 4.40 (a and b), (c and d) and (e and f), respectively. The FESEM image of AgNPs-MWCNT-rGO(H) nanocomposite, which was prepared using MWCNT-GO ($1.0 \text{ mg}\cdot\text{mL}^{-1}$), (3:1, v/v) to AgNO_3 (0.04 M) volume ratio of 12 is shown in Figure 4.40 g and its silver nanoparticle size distribution diagram is shown in Figure 4.40 h. As seen in Figure 4.40 (a-e), by increasing the concentration of $\text{Ag}(\text{NH}_3)_2\text{OH}$, the size of reduced silver particles increased from 12.73 to 22.00 nm, suggesting that the particle diameter and the quantity of reduced silver particle in the nanocomposite matrix also increased, and therefore, some silver agglomeration was seen on the surface of MWCNT and GO. By changing the AgNO_3 , instead of $\text{Ag}(\text{NH}_3)_2\text{OH}$ in the mixture, the Ag particle size dramatically increased from 12.73 (Figure 4.40 b) to 45.59 (Figure 4.40 h) mean particle diameter. GO with negative charge increased in number through neutralization by the alkaline $\text{Ag}(\text{NH}_3)_2\text{OH}$ in order to absorb more $[\text{Ag}(\text{NH}_3)_2]^+$ ions than AgNO_3 , leading to the creation of more initial nucleation sites (Y. Zhang et al., 2012) and greater stability

and resistance to reduction of $\text{Ag}(\text{NH}_3)_2\text{OH}$ over AgNO_3 , as well as prevention of growing of Ag into large particles (Kaniyankandy et al., 2007).

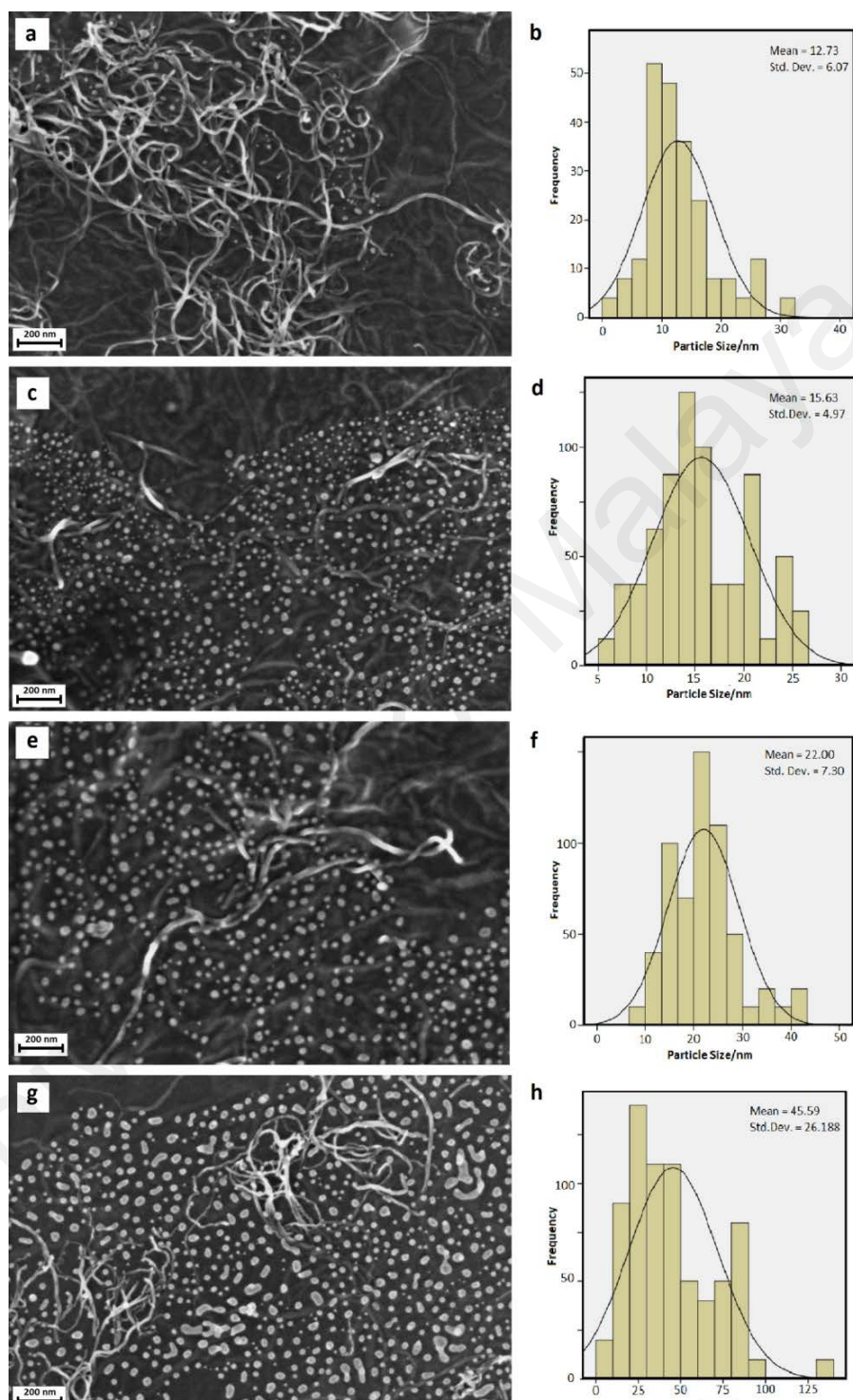


Figure 4.40 FESEM images and size distribution diagram of AgNPs-MWCNT-rGO(H) composite prepared by using the solution with MWCNT/GO (3:1, v/v) to $\text{Ag}(\text{NH}_3)_2\text{OH}$ (0.04 M) volume ratios of 12 (a and b), 6 (c and d), and 3 (e and f) and using the solution with a MWCNT-GO (3:1, v/v) to AgNO_3 (0.04 M) volume ratio of 12 (g and h).

1.15.2 XRD analysis, EDX and FT-IR spectroscopy characterization of AgNPs-MWCNT-rGO(H) composite

Figure 4.41 shows that the XRD patterns of MWCNT (a), GO (b), rGO (c) and AgNPs-MWCNT-rGO(H) nanocomposite (d). GO (b) has a sharp peak at 10.8° , which proved inter-planer spacing (0.82 nm) of the typical feature of GO (d_{002}) (Xie et al., 2012). The XRD pattern of MWCNT (a) indicates the presence of two peaks at 25.8° and 42.8° which corresponded to the inter-layer spacing (0.34 nm) of the nanotube (d_{002}) and the d_{100} reflecting of the carbon atoms, respectively (Endo et al., 1997).

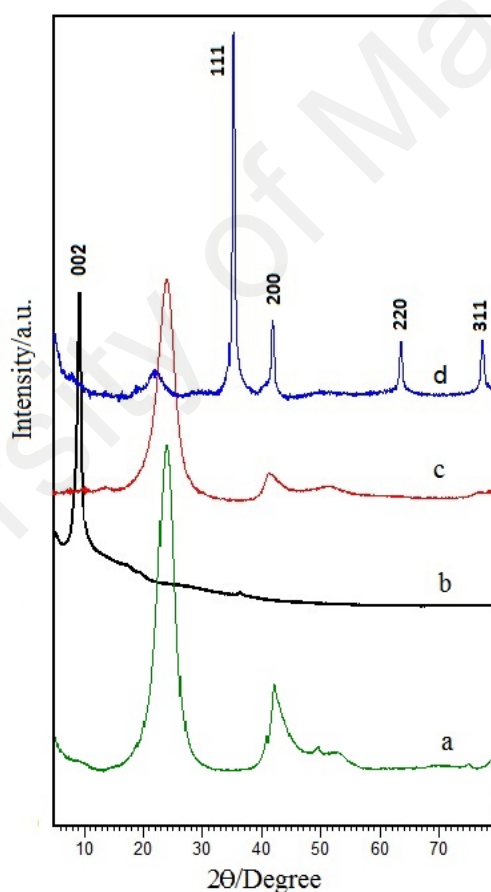


Figure 4.41 XRD patterns of MWCNT (a), GO (b) rGO (c) and AgNPs-MWCNT-rGO(H) composite (d)

After hydrothermal reduction, all of the intensities of the related oxygen peaks were sharply decreased in the rGO sample (c), as compared to GO (b), indicating that the delocalized p conjugation is restored in our rGO sample (Cui et al., 2011). At the AgNPs-MWCNT-rGO(H) nanocomposite XRD pattern (d) the intensity for the 111, 200, 220 and 311 of Ag (Ref. code: 003-0921) can be obviously seen. High intensity of Ag peaks decreased GO and MWCNT peaks, but they still could be seen. This result demonstrates that AgNPs-MWCNT-rGO(H) nanocomposite were successfully fabricated (Zhang et al., 2001).

FT-IR spectra for GO, rGO, MWCNT and AgNPs-MWCNT-rGO(H) nanocomposites are shown in Figure 4.42 a, b, c and d respectively. For GO (Figure 4.42 a), the broad stretching vibrations for O–H peak centered at 3265 cm^{-1} were recorded. The peaks at 1727 , 1623 , 1367 , and 1056 cm^{-1} were assigned to C=O stretching, C=C stretching bands for aromatic rings and O–H bending, C–OH stretching and C–O–C stretching, respectively. Furthermore, the peaks at 1041 and 1161 cm^{-1} were related to C–O vibration of alkoxy or epoxy groups (Pham et al., 2011). The peak at 32670 cm^{-1} in the rGO spectrum is attributed to O–H groups that obviously shows the reduction of O–H groups as compared to GO by using hydrothermal way and the bands at 1610 and 1358 cm^{-1} are related to C–O and C–OH, respectively (Figure 4.42 b). The peak 1025 cm^{-1} in the rGO spectrum are recognized as the C–O stretching vibration of the epoxy and alkoxy groups (M. Li et al., 2014). The existence of MWCNT in the composite could also be confirmed using FT-IR spectroscopy (Figure 4.42 c). A band centered at 1599 cm^{-1} and a shoulder at 1350 cm^{-1} were related to C=C stretching vibrations, while the band at 1117 cm^{-1} was associated with C–O stretching vibrations (Dubey et al., 2005).

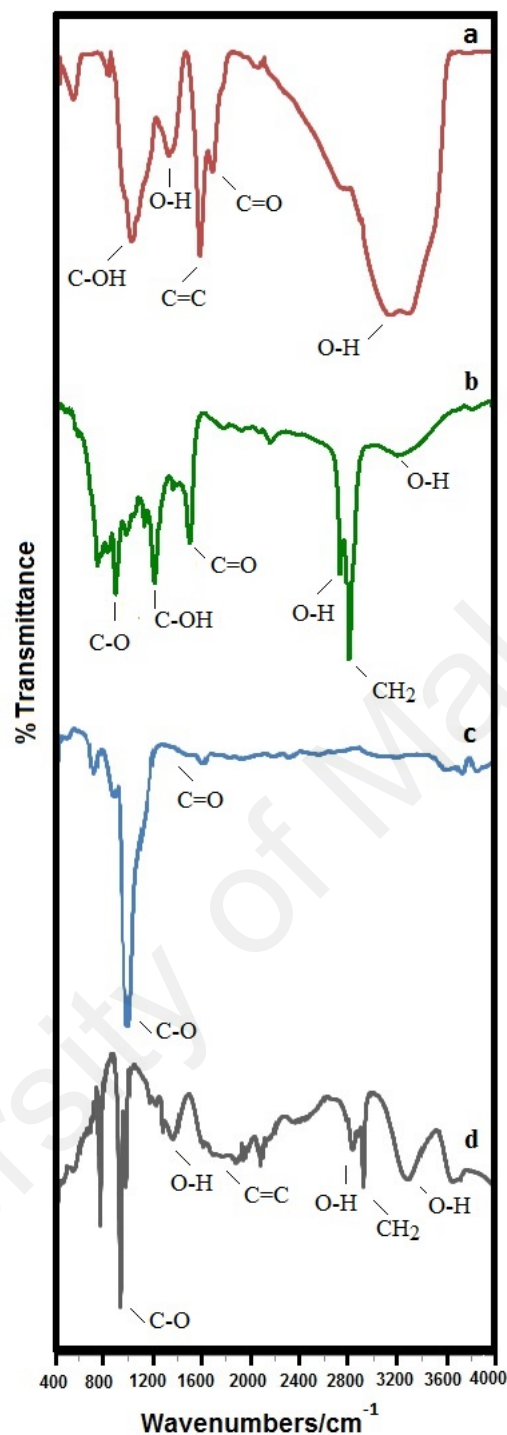


Figure 4.42 FT-IR spectra of GO (a), rGO (b) MWCNT (c) and AgNPs-MWCNT-rGO(H) composite (d)

For the AgNPs-MWCNT-rGO(H) nanocomposite (Figure 4.42 d), the peaks at 1066, 1642, 1418, 2853, and 2925 cm^{-1} were assigned to C–O stretching vibrations, C=C stretching bands for aromatic rings and O–H bending, O–H deformation, as well as symmetric and asymmetric stretching vibrations of CH₂ groups, respectively (Cheng et

al., 2013). The broad peak of 3300 cm^{-1} for AgNPs-MWCNT-rGO(H) nanocomposite could be attributed to O–H stretching vibrations of the absorbed water molecules (Pham et al., 2011). The O–H peak of rGO dramatically reduced as compared to the broad stretching vibrations O–H peak of GO centered at 3265 cm^{-1} (Figure 4.42 a) caused by hydrothermal reduction.

1.15.2.1 Electrochemical characterization of AgNPs-MWCNT-rGO(H) composite

Figure 4.43 presents the Nyquist plot of impedance spectra for bare and modified GCE electrodes with GO, MWCNT, AgNPs-MWCNT-GO and AgNPs-MWCNT-rGO(H) in 0.1 M KCl solution which contained 1.0 mM $\text{Fe}(\text{CN})_6^{3-/4-}$ (1:1). For each of these electrodes, the experiments were carried out three times to minimize error.

The obtained EIS spectra of AgNPs-MWCNT-GO and AgNPs-MWCNT-rGO(H) modified GCE electrodes show two areas: a semicircular part related to electron transfer process at high frequencies, and a linear part related to diffusion control at lower frequencies. R_{ct} or electron transfer resistance at the surface of the electrode can be assessed by exploiting the semicircle diameter.

The EIS data as well fitted well with the corresponding circuit shown in Figure 4.43 in which the chi-squared (χ^2) was minimized at 10^{-4} . The equivalent circuits contain the EIS characteristics of modified electrodes which are symbolized by C (capacitance) and R_{ct} (Resistance) attached subsequently with the double layer capacitance and W (Warburg impedance). The observed Warburg impedance was a 45° straight line, which was recognized in the mid- and low-frequency areas suggesting that the diffusion controlled process occurred.

As shown in Figure 4.43 as compared to bare GCE, modified GO on a GCE surface caused the semicircle to drastically rise, implying that GO performed as an

insulating layer that caused the interfacial charge transfer to be challenging. MWCNT showed behavior akin to GO, but with some differences, in which MWCNT showed a semicircle with smaller diameter suggesting better conductivity compared to GO. As AgNPs-MWCNT-GO possessed noble metal, it had smaller diameter as compared to CNT and GO. Since GO hydrothermally reduced to rGO (AgNPs-MWCNT-rGO(H)), the semicircle diameter was smaller and displayed higher conductivity as compared to other modified electrodes. This can be explained by the existence of smaller band gap in rGO, which is ideal for electron conduction and leads to lower R_{ct} (Mahmoudian, et al. 2012).

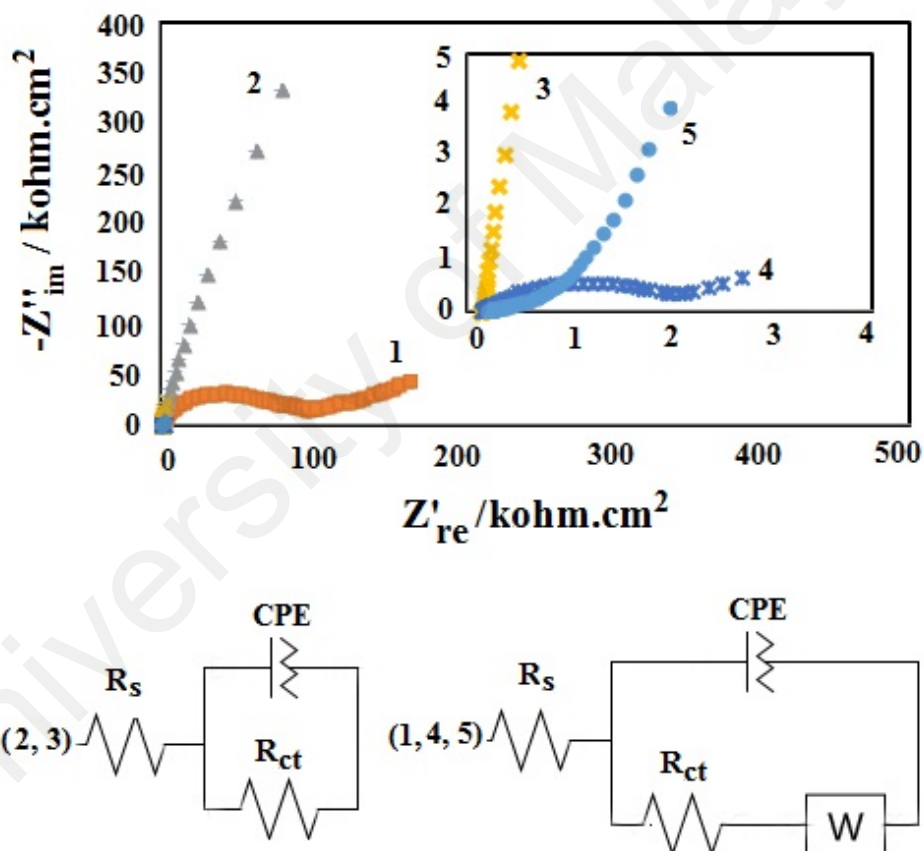


Figure 4.43 Nyquist Plots of: (1) bare GCE, (2) GO, (3) CNT, (4) AgNPs-MWCNT-GO and (5) AgNPs-MWCNT-rGO(H) and their equivalents circuits in 1.0 mM $\text{Fe}(\text{CN})_6^{3-/4-}$ (1:1) solution with 0.1 M KCL supporting electrolyte.

1.15.2.2 Cyclic voltammogram (CV) of the modified electrode (AgNPs-MWCNT-rGO(H)/GCE) to hydrogen peroxide

All of these composite parts were known to exhibit catalytic activity to reduce hydrogen peroxide individually. The cyclic voltammetric (CVs) of modified GCE with all silver volume ratios of AgNPs-MWCNT-rGO(H) nanocomposites (AgNPs-MWCNT-rGO(H)/GCE) was carried out in 0.2 M phosphate buffer solution (PBS) at pH 6.5 in the presence of 1.0 mM H₂O₂. As shown in Figure 4.44, compared to bare GCE (Figure 4.44 a), all modified AgNPs-MWCNT/GCE (Figure 4.44 e), AgNPs-MWCNT-GO/GCE (Figure 4.44 f) and AgNPs-MWCNT-rGO(H)/GCE (Figure 4.44 g) electrodes exhibited considerable cathodic peaks for the reduction of H₂O₂, through AgNPs-MWCNT-rGO(H)/GCE electrodes showed higher reduction towards H₂O₂. Electrodes that were individually modified with MWCNT (Figure 4.44 b), GO (Figure 4.44 c) and AgNPs (Figure 4.44 d) did not show significant reduction effect toward H₂O₂.

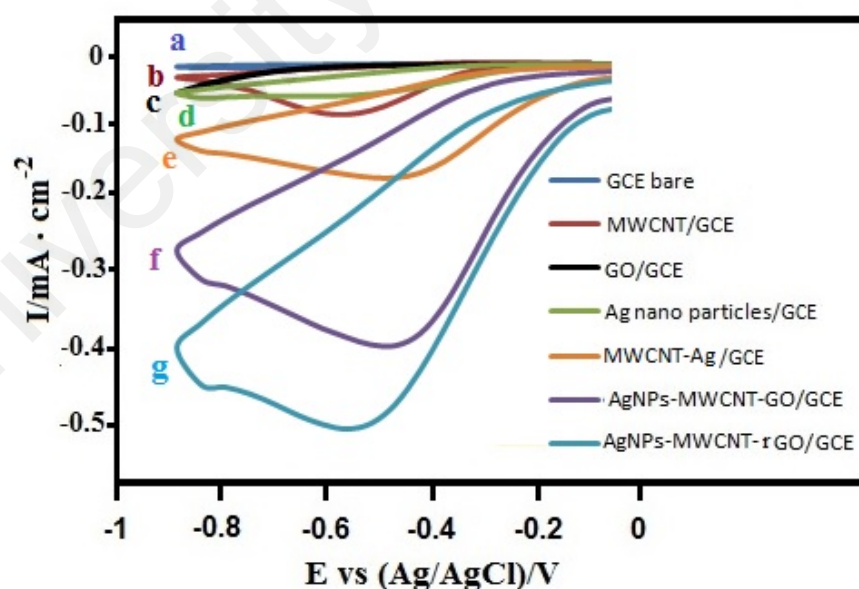
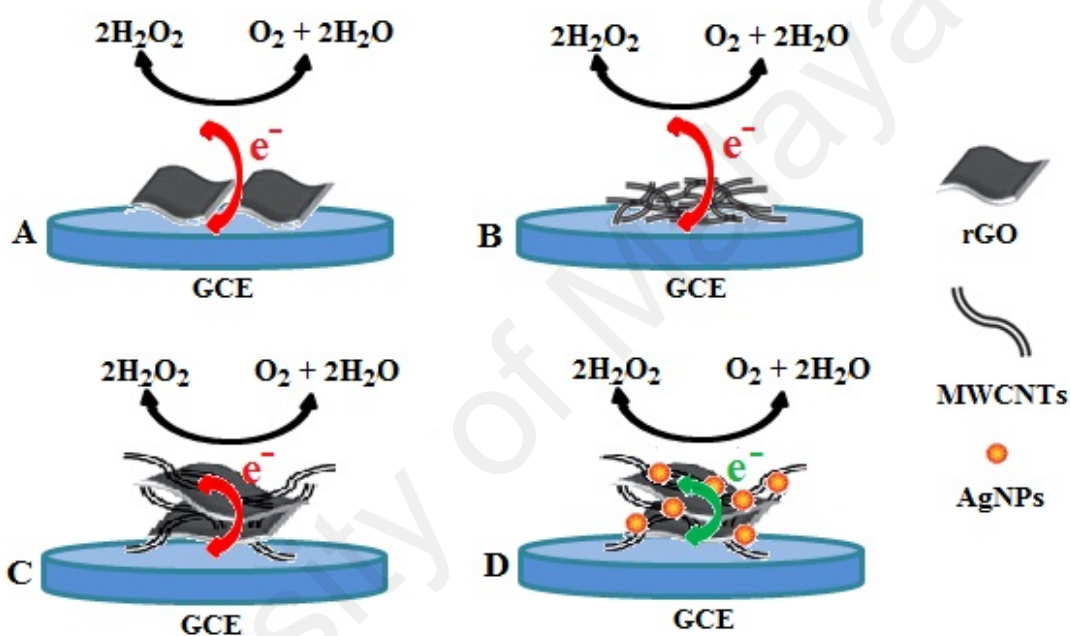


Figure 4.44 CVs of various electrodes in 0.2 M PBS (pH 6.5) in the presence of 1.0 mM H₂O₂: bare GCE (a), MWCNT/GCE (b), GO/GCE (c), Ag nanoparticles/GCE (d), AgNPs-MWCNT/GCE (e) and AgNPs-MWCNT-GO/GCE(f) and AgNPs-MWCNT-rGO(H)/GCE (d).

Possible mechanisms of H_2O_2 reduction by this modified GCE electrodes are shown in Scheme. 4.5 The conductivity of rGO and MWCNT facilitates the electron transfer of rGO/GCE (Scheme. 4.5 A) and MWCNT/GCE (Scheme. 4.5 B) electrodes to reduction of H_2O_2 . AgNPs could greatly enhance the electron-transfer reactivity of the AgNPs-MWCNT-rGO(H) composite thus the reduction of H_2O_2 is mediated by the catalyst effect of AgNPs (Gan et al., 2004) (Scheme. 4.5 D).



Scheme 4.5 Possible mechanisms of H_2O_2 reduction by the modified GCE electrodes

The above experimental results show that the electrochemical reduction of H_2O_2 could be achieved by using AgNPs-MWCNT-rGO(H) composite modified sensor. The factors that may affect the response of the sensor were studied to improve the performance of the sensor. Figure 4.45 shows the relationship between the applied potential in chronoamperometry and the reduction current of H_2O_2 . The affiliation of the amperometric response on the applied potential of the AgNPs-MWCNT-rGO(H)/GCE electrode was evaluated over the range of -0.10 to -0.50 V. The current response gradually increased when the applied potential increased from -0.10 to -0.50 V although, when the

potential was more negative than -0.35 V, the response current decreased. The least negative potential that shows a high analyte-dependent current was a suitable working potential to achieve good selectivity. So, -0.35 V was the best potential for reduction of H_2O_2 by AgNPs-MWCNT-rGO(H)/GCE modified electrode.

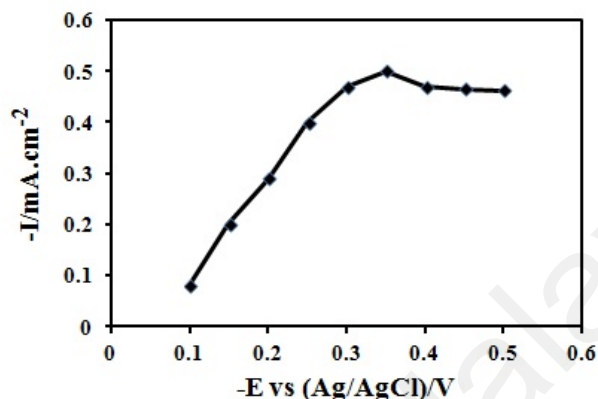


Figure 4.45 Effect of the applied potential on the current response of 1.0 mM H_2O_2 on the AgNPs-MWCNT-rGO(H)/GCE electrode in 0.2 M PBS (pH 6.5).

Figure 4.46 indicates the effect of the pH value of the phosphate buffer solution on the reduction current of H_2O_2 on AgNPs-MWCNT-rGO(H)/GCE electrode. The current response was dramatically increased with the increase of the pH from 4.5 to 6.5 and gradually decreased at higher than pH 6.5 . It is recommended that pH= 6.5 was the optimized pH for the electrochemical reduction of H_2O_2 .

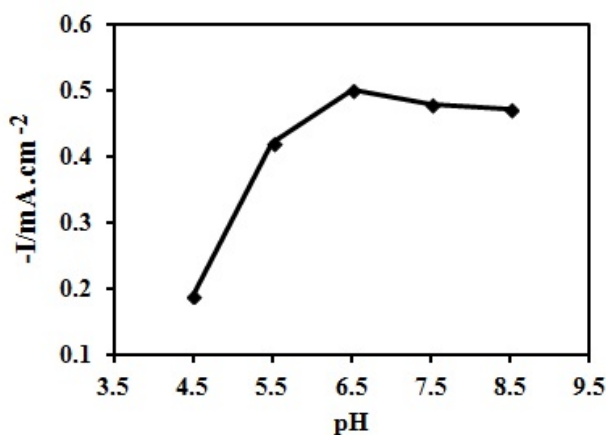


Figure 4.46 Effect of the pH of PBS on the current response of 1.0 mM H_2O_2 on the AgNPs-MWCNT-rGO(H)/GCE electrode.

Figure 4.47 shows the comparison between the catalytic activities of modified AgNPs-MWCNT-rGO(H)/GCE electrodes prepared under similar conditions using different precursors, i.e. $\text{Ag}(\text{NH}_3)_2\text{OH}$ and AgNO_3 .

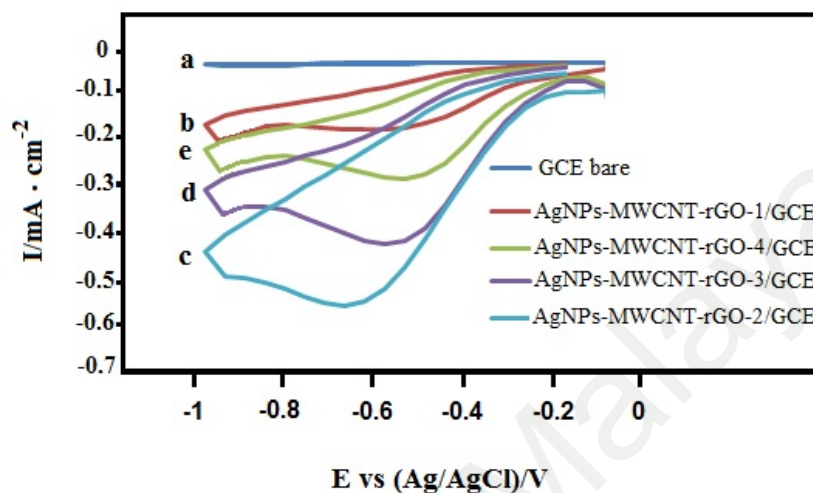


Figure 4.47 CVs of various electrodes in 0.2 M PBS (pH 6.5) in the presence of 1.0 mM H_2O_2 : bare GCE (a), AgNPs-MWCNT-rGO(H)/GCE prepared by using different volume ratios of MWCNT-GO (3:1, v/v) to $\text{Ag}(\text{NH}_3)_2\text{OH}$ (0.04 M) of 12, 6, and 3, respectively (b–d), and AgNPs-MWCNT-rGO(H)/GCE prepared by using the solution with MWCNT-GO (3:1, v/v) to AgNO_3 (0.04 M) volume ratio of 12 (e).

The H_2O_2 reduction ability of modified AgNPs-MWCNT-rGO(H)/GCE electrodes of the (Figure 4.47 c) AgNPs-MWCNT-rGO(H)-2 and AgNPs-MWCNT-rGO(H)-3 (Figure 4.47 d) composites were dramatically higher than AgNPs-MWCNT-rGO(H)-1 (Figure 4.47 b) and AgNPs-MWCNT-rGO(H)-4 (Figure 4.47 e), which used AgNO_3 instead of $\text{Ag}(\text{NH}_3)_2\text{OH}$. The larger available surface area of smaller AgNPs on the composite could cause better catalytic activity toward sensing H_2O_2 . Comparatively, among the modified AgNPs-MWCNT-rGO(H)/GCE electrodes prepared using $\text{Ag}(\text{NH}_3)_2\text{OH}$, the (Figure 4.47 c) AgNPs-MWCNT-rGO(H)-2 composite showed better reduction activity than the two other volume ratios. One plausible explanation for this phenomenon was that the AgNPs-MWCNT-rGO(H)-2 composite possesses higher silver

particle density and lower silver particle size than the other one, which agreed with a previous studies reporting which observed that electrocatalytic activity of silver nanoparticles increases with increasing particle density and decreases with increasing particle size (Aimin Yu et al., 2012b). The peak reduction for all AgNPs-MWCNT-rGO(H) electrodes increased in current and shifted to positive potential as the size and density of AgNPs were increased. Therefore, the CV profiles corroborated the observations from the FESEM images.

1.15.2.3 Amperometric detection of hydrogen peroxide at modified AgNPs-MWCNT-rGO(H)/GCE

The typical current-time plot of the AgNPs-MWCNT-rGO(H) with different H₂O₂ concentrations in 0.2 M phosphate buffer solution of Na₂HPO₄ and NaH₂PO₄ at pH 6.5 was studied as shown in Figure 4.48 at an applied potential of -0.35 V.

The current of the working electrode dramatically increased up to 95% steady-state current within 3 s, and demonstrated a fast amperometric response behavior. The steady-state calibration curve of AgNPs-MWCNT-rGO(H) modified electrode could be prepared from the amperometric response, as shown in Figure 4.48 in which, the inset indicates the calibration curve of the sensor. The linear steady-state amperometric detection range was estimated to be from 100 μ M to 100 mM with a linear regression equation of $I = 0.833 \text{ (mA mM}^{-1}) + 2.24 \text{ (R}^2 = 0.9985)$ of H₂O₂. The limit of detection (LOD) and the limit of quantification (LOQ) were estimated to be 0.90 and 3.2 respectively at a signal-to-noise ratio of 3. Moreover, the sensor stability was checked by measuring the current response of the modified electrode. After 7 days, only 5.2 % of the current signal was lost. This illustrates an excellent stability of AgNPs-MWCNT-rGO(H) modified electrode for the purpose of detecting H₂O₂. The electrode-to-electrode reproducibility was approximated to be in the presence of 1.0 mM H₂O₂ in phosphate

buffer solution of Na_2HPO_4 and NaH_2PO_4 0.2 M (pH 6.5) at three electrodes (AgNPs-MWCNT-rGO(H)) that have been prepared in the same conditions, which yielded a relative standard deviation of 4.5%.

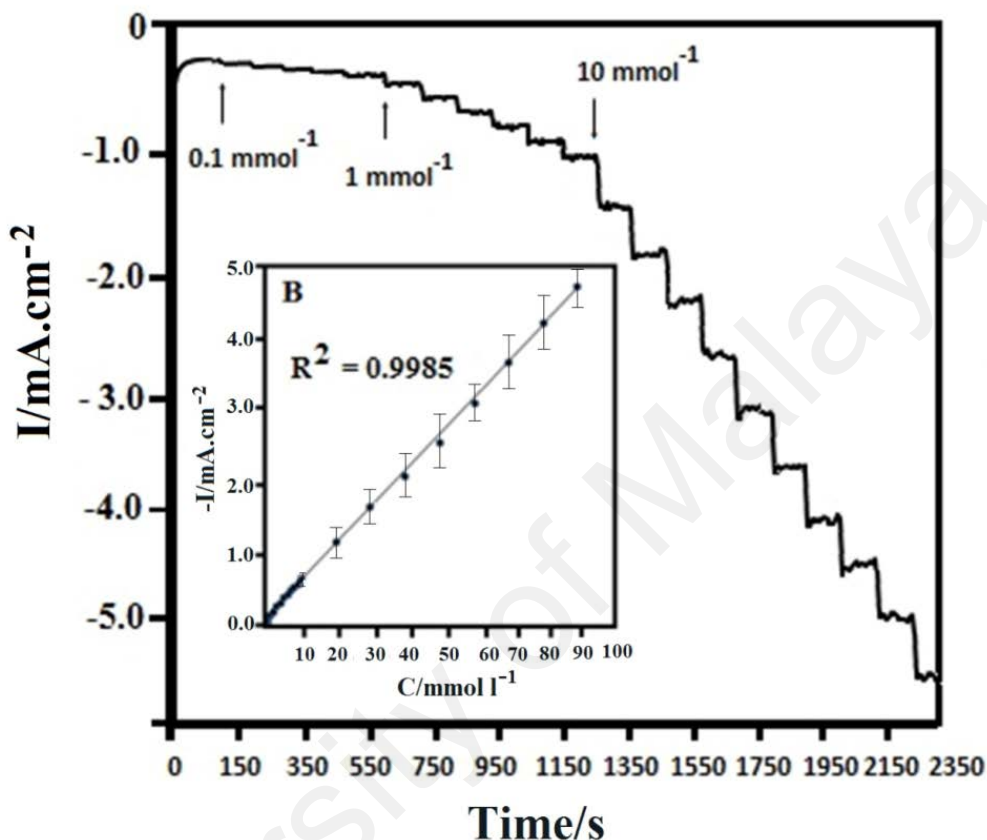


Figure 4.48 Steady-state response of the AgNPs-MWCNT-rGO(H)/GCE electrode to consecutive injection of H_2O_2 into the stirred 0.2 M PBS (pH 6.5) with an applied potential of - 0.35 V (a) and the corresponding calibration curve (b).

The effect of common interfering species on AgNPs-MWCNT-rGO(H) modified electrode was studied. Figure 4.49 shows the amperometric response of the modified electrode towards the addition of 1.0 mM H_2O_2 which has followed by glucose, glycine, ethanol and ascorbic acid into 0.2 M phosphate buffer solution (pH 6.5). As can be seen, these interfering substances responded with quite very weak signals, demonstrating that this modified electrode has a good selectivity towards H_2O_2 .

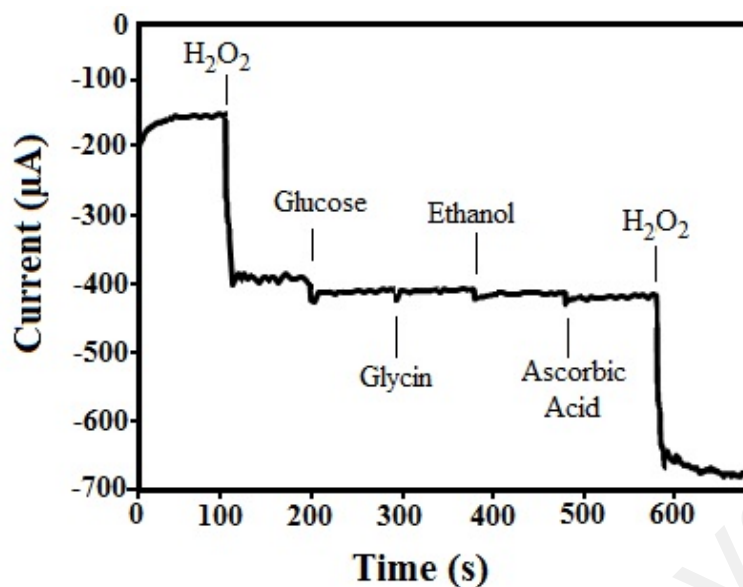


Figure 4.49 Amperometric response of AgNPs-MWCNT-rGO(H)/GCE electrode upon the successive addition of 1.0 mM H₂O₂, glucose, glycine, ethanol and ascorbic acid into 0.2 M phosphate buffer solution (pH 6.5) with an applied potential -0.35 V under a stirring condition.

Table 4.8 compares the limit of detection and the linear range of obtained AgNPs-MWCNT-rGO(H) modified electrode with some of the previous voltammetric H₂O₂ reports. Based on this comparative analysis, it has found that the AgNPs-MWCNT-rGO(H) modified electrode is capable of achieving a favorable detection limit and linear range to sense H₂O₂.

Table 4.8 compares the limit of detection and the linear range of obtained AgNPs-MWCNT-rGO(H) modified electrode with some of the previous voltammetric H₂O₂ reports (Fang et al., 2012; Guo et al., 2012; Liu, Tian, et al., 2011a; Lu, Chang, et al., 2011; Moradi Golsheikh et al., 2013a; Song et al., 2009; Zhao et al., 2009). Based on this comparative analysis, it is found that the AgNPs-MWCNT-rGO(H) modified electrode is capable of achieving a favorable detection limit and linear range to sense H₂O₂.

Table 4.8 Comparison the LOD value of the previous reports and this work from different methods

Modify Electrode	Performance		References
	LOD (μM)	Liner range (mM)	
Ag NPs-GN-R/GCE	28	0.1-40	(M. Fang et al., 2012)
AgNPs/collagen/GCE	0.7	0.005-40.6	(Song et al., 2009)
Ag NPs-MWCNT/Au	0.5	0.05-17	(Lu, Chang, et al., 2011)
AgNP/GO/ssDNA/Au	1.9	0.1-20	(Guo et al., 2012)
AgNP/rGO/benzylamine/GCE	31.3	0.1-100	(Liu, Tian, et al., 2011a)
ERGO-Ag/GCE	1.6	0.1-100	(Golsheikh et al., 2013)
AgNPs-MWCNT-rGO(H)/GCE	0.9	0.1-100	This work

Silver nanoparticle- carbon nanotube-reduced-graphene-oxide nanocomposite (AgNPs-MWCNT-rGO(H)) was successfully synthesized by a simple and environmentally friendly one-step hydrothermal method. The advantage of this method is that it did not require any toxic solvent or chemical to reduce the graphite oxide. Most Ag nanoparticles that existed on the composite using silver ammonia complex instead of silver nitrate were well dispersed with small and narrow-sized distributions. The AgNPs-MWCNT-rGO(H) composite exhibited excellent sensitivity for electrochemical detection of hydrogen peroxide in a cyclic voltammetry curve. The present work provides us with a low cost, simple preparation, one-step, environmentally benign and green synthetic method of preparing AgNPs-MWCNT-rGO(H)/GCE nanocomposites, which ultimately works as an effective non-enzymatic electrochemical H_2O_2 sensor.

1.15.3 Electrodeposited silver nanoparticle-reduced-graphene oxide-carbon nanotube nanocomposites [AgNPs-MWCNT-rGO(E)]

A silver nanoparticle – reduced graphene oxide – multiwall carbon nanotube composite [AgNPs-MWCNT-rGO(E)] was successfully electrodeposited on glassy carbon electrode using one-step cyclic voltammetric method. By carboxylic functionalization of multiwall carbon nanotube (3.2.6.8), it could be electrodeposited simultaneously with graphene oxide and silver nanoparticles. $\text{Ag}(\text{NH}_3)_2\text{OH}$ has used as the source of AgNPs to get uniform distribution of AgNPs in the composite.

Figure 4.50 indicates that the CV profiles of AgNPs-MWCNT-rGO(E) show three cathodic peaks in the negative scan of the first cycle irrespective of the volume ratio. Four cycles were done for composite electrodeposition. The reduction of electrochemically active oxygen-containing groups on graphene sheets and MWCNT-COOH was identified with the first peak (I) (Chen et al., 2011). The second peak (II) is ascribed with the reduction of Ag^+ to Ag (Kaniyankandy et al., 2007; Sharma et al., 2011), These two peaks seem to merge in some silver ratios for example AgNPs-MWCNT-rGO(E)-3 (Figure 4.50 A.b). The irreversible electrochemical reduction of GO and MWCNT-COOH caused a cathodic peak (III) (Chen et al., 2011; Guo et al., 2009). Furthermore, the increases of reduction current caused by the increase of $[\text{Ag}(\text{NH}_3)_2]^+$ ions demonstrate the increasing amount of loading material on the GCE surface. Figure 4.50 B compares the CV profile of the solutions containing AgNPs-MWCNT-rGO(E)-5 (Figure 4.50 B.a), AgNPs-MWCNT-rGO(E)-6 (Figure 4.50 B.b) and AgNPs-MWCNT-rGO(E)-3 (Figure 4.50 B.c). The stability of $[\text{Ag}(\text{NH}_3)_2]^+$ is higher than Ag^+ , therefore, the reduction peak of Ag^+ Therefore, ions shifted to positive potentials (Kaniyankandy et al., 2007).

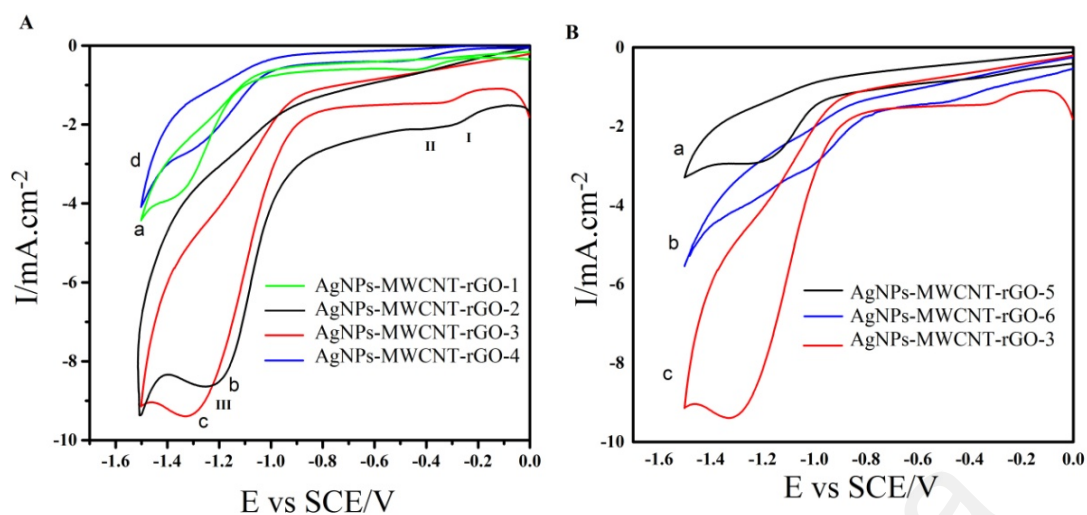
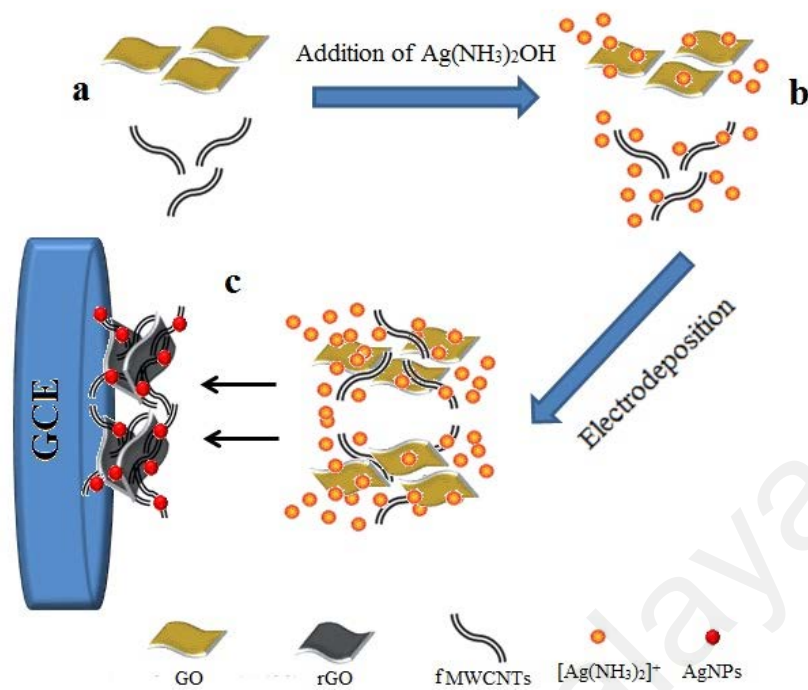


Figure 4.50 A: Cyclic Voltammogram of AgNPs-MWCNT-rGO(E)-1(a), AgNPs-MWCNT-rGO(E)-2 (b), AgNPs-MWCNT-rGO(E)-3 (c), AgNPs-MWCNT-rGO(E)-4 (d) B: Cyclic voltammogram of AgNPs-MWCNT-rGO(E)-5 (a), AgNPs-MWCNT-rGO(E)-6 (b), AgNPs-MWCNT-rGO(E)-3 (c)

Scheme. 4.6 shows the formation mechanism of the AgNPs-MWCNT-rGO(E) nanocomposite via the one-step electrodeposition method. Due to the hydroxyl and carboxyl groups on the surface of MWCNT-COOH and GO, their Deionized water (DI water) base suspension is negatively-charged (Hua et al., 2011; Li et al., 2008) (Scheme. 4.6 a). Therefore, by electrostatic attraction, the positively-charged $[\text{Ag}(\text{NH}_3)_2]^+$ ions are adsorbed on negatively-charged GO sheets and MWCNT-COOH (Scheme. 4.6 b).

By applying a negative potential on the GO nanosheets and MWCNT-COOH, the adsorbed $[\text{Ag}(\text{NH}_3)_2]^+$ ions are deposited on the surface of GCE and reduced in the AgNPs-MWCNT-rGO(E) nanocomposite (Scheme. 4.6c) while the remaining $[\text{Ag}(\text{NH}_3)_2]^+$ ions in the aqueous solution are deposited and reduced on the formed AgNPs on the surface of the nanocomposite, that had initially caused the formation of AgNPs or the growth of nucleation of new AgNPs. Therefore, when the concentration of $[\text{Ag}(\text{NH}_3)_2]^+$ ions increases, AgNPs density also increases.



Scheme 4.6 Schematic mechanism of the formation of AgNPs-MWCNT-rGO(E) nanocomposite via electrodeposition method

1.15.4 XRD analysis, EDX and FT-IR spectroscopy characterization of AgNPs-MWCNT-rGO(E) composite

Figure 4.51 illustrates the XRD patterns of MWCNT (Figure 4.51 a), MWCNT-COOH (Figure 4.51 b), GO (Figure 4.51 c), rGO (Figure 4.51 d) and AgNPs-MWCNT-rGO(E) nanocomposite (Figure 4.51 e). The XRD pattern of MWCNT (a) shows two peaks at 25.8° and 42.8° corresponding to the inter-layer spacing (0.34 nm) of the nanotube (d_{002}) and the d_{100} reflecting of the carbon atoms, respectively (Endo et al., 1997).

After an acid treatment of MWCNTs, the functional carboxylic groups appeared on the surface of MWCNTs and the diffraction peaks are estimated to belong to the graphite structure (002) and (100) planes of the MWCNTs (Figure 4.51 b) (Safari &

Gandomi-Ravandi, 2014). GO (c) has a sharp peak at 10.8° which demonstrating interplaner spacing (0.82 nm) which is a typical feature of GO (d_{002}) (Xie et al., 2012). After electrodeposition, all intensities of related oxygen peaks sharply decreased in the rGO sample (d) when compared to GO (c), indicating that the delocalized p conjugation is restored in our rGO sample (Cui et al., 2011). In the AgNPs-MWCNT-rGO(E) nanocomposite XRD pattern (e), the intensity for the 111, 200, 220 and 311 of Ag (Ref. code: 003-0921) can be obviously seen. The high intensity of Ag peaks decreased GO and MWCNT peaks, but could still be observed. This result demonstrates that a AgNPs-MWCNT-rGO(E) nanocomposite was successfully fabricated (Zhang et al., 2001).

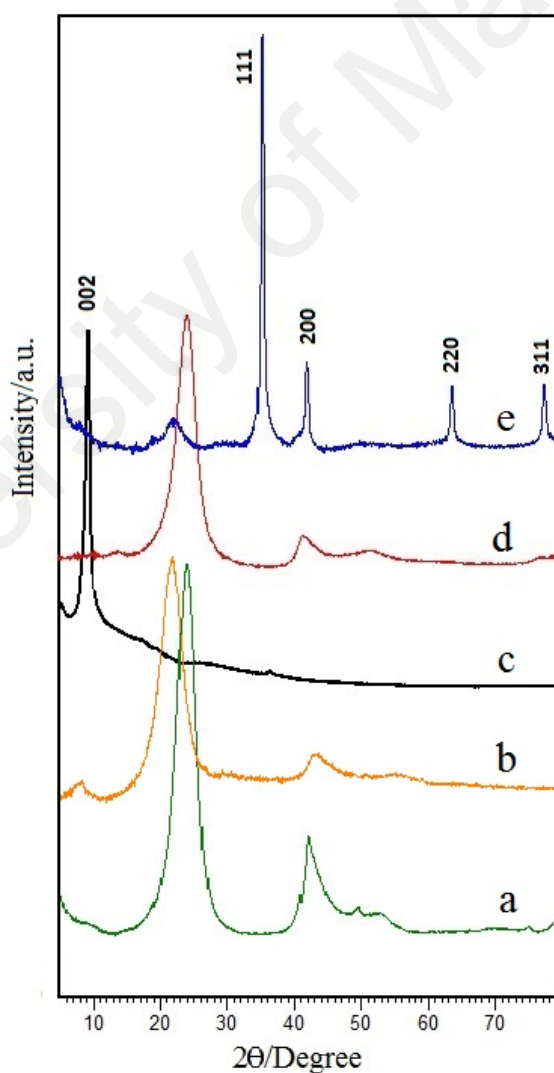


Figure 4.51 XRD patterns of MWCNT (a), MWCNT-COOH (b), GO (c), rGO (d) and AgNPs-MWCNT-rGO(E) nanocomposite (e).

FT-IR spectra for MWCNT, MWCNT-COOH, GO, rGO and AgNPs-MWCNT-rGO(E) nanocomposites are shown in Figure 4.52 a, b, c, d and e respectively. The MWCNT FT-IR spectrum is shown in a. A band centered at 1664 cm^{-1} was due to C=C stretching vibrations, while the band at 1141 cm^{-1} was associated with C-O stretching vibrations (Dubey et al., 2005). Functional MWCNT-COOH FT-IR (Figure 4.52 b) indicated bands at 3871 cm^{-1} and 3335 cm^{-1} which can be explained due to O-H vibrations. A sharp spectrum at 1637 cm^{-1} was associated with C=O stretching vibrations. A FT-IR spectrum comparison of MWCNT (Figure 4.52 a) with MWCNT-COOH (Figure 4.52 b) confirms that acid treatment has been successfully done on MWCNTs. For GO (Figure 4.52 c), the broad stretching vibrations for a O-H peak centered at 3265 cm^{-1} was recorded. Peaks at 1727, 1623, 1367, and 1056 were attributed to C=O stretching, C=C stretching bands for aromatic rings and O-H bending, C-OH stretching and C-O-C stretching, respectively. Furthermore, the peaks at 1041 and 1161 cm^{-1} were related to C-O vibration of alkoxy or epoxy groups. (Pham et al., 2011). The peak at 3267 cm^{-1} in the rGO spectrum is attributed to O-H groups which shows the reduction of O-H groups as compared to GO by using electrochemical way and the bands at 1610 and 1358 cm^{-1} are related to C=O and C-OH, respectively (Figure 4.52 d). The peak at 1025 cm^{-1} in the rGO spectrum is recognized as the C-O stretching vibration of the epoxy and alkoxy groups (Li et al., 2014). The rGO O-H peak is dramatically lower as compared to the broad stretching vibrations where the O-H peak of GO is centered at 3265 cm^{-1} (Figure 4.52 c) caused by electrodeposition. For the AgNPs-MWCNT-rGO(E) nanocomposite (Figure 4.52 d), the peaks at 1672, 1288 and 2865 cm^{-1} were assigned to C=O stretching vibrations, C=C stretching bands for aromatic rings and O-H bending, O-H deformation, as well as symmetric and asymmetric stretching vibrations of CH_2 groups, respectively (Cheng et al., 2013). The broad peaks of 3318 and 3844 cm^{-1} for

AgNPs-MWCNT-rGO(E) nanocomposite could be attributed to O–H stretching vibrations of the absorbed water molecules (Pham et al., 2011).

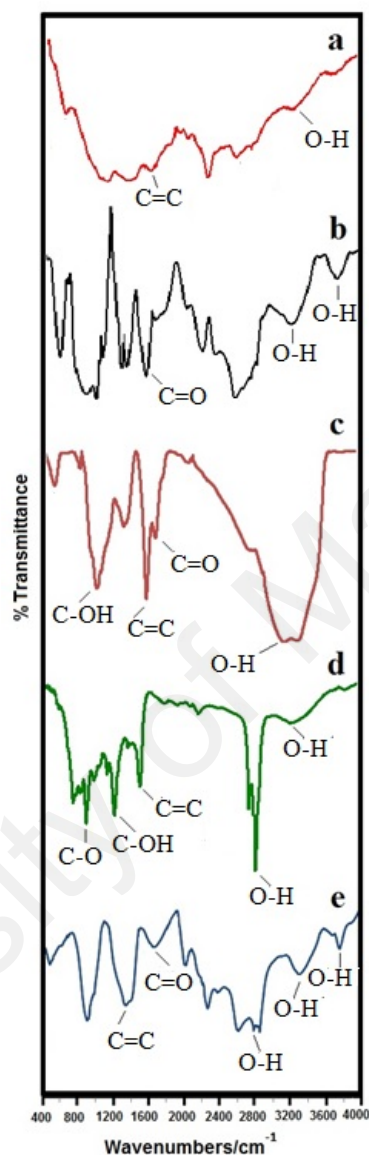


Figure 4.52 FT-IR spectra for MWCNT(a), MWCNT-COOH(b), GO(c), rGO(d) and AgNPs-MWCNT-rGO(E) nanocomposites(e).

1.15.4.1 Morphology analysis of AgNPs-MWCNT-rGO(E)

FESEM images and silver particle size distribution diagrams of AgNPs-MWCNT-rGO(E) nanocomposites prepared using different volume ratios are shown in Figure 4.53 (a and b),(c and d), (e and f) and (g and h), respectively.

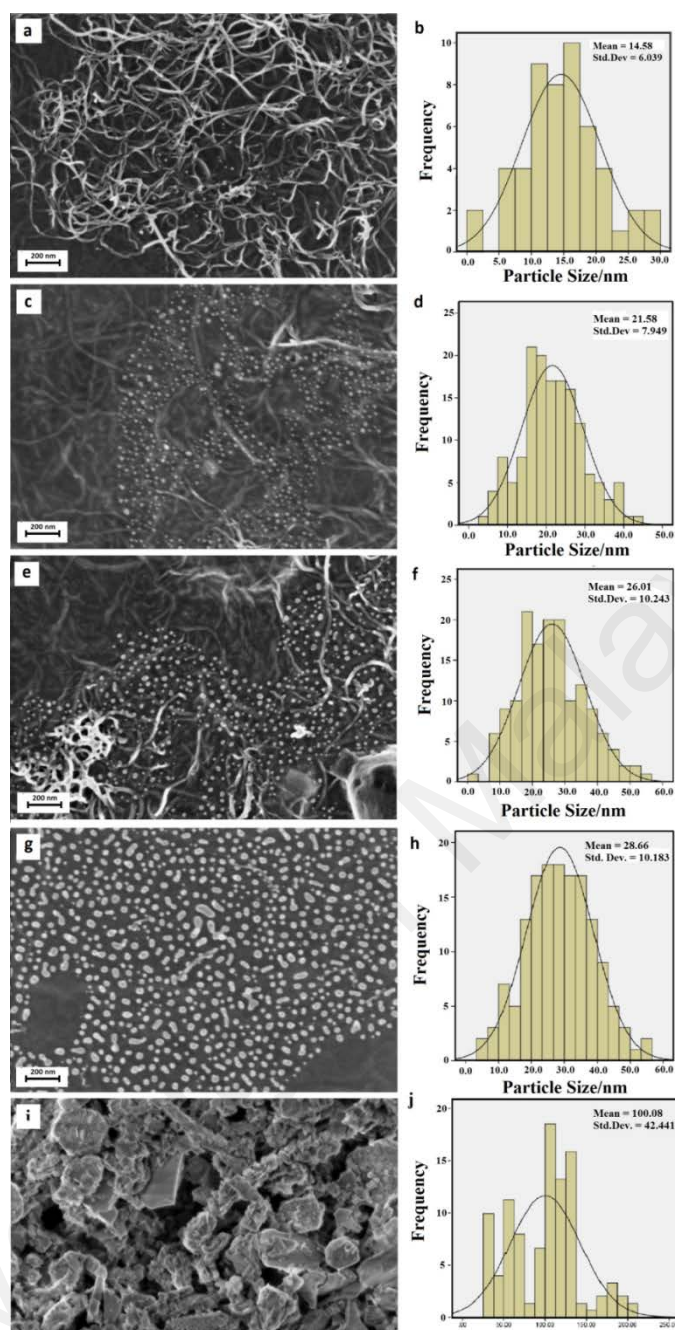


Figure 4.53 FESEM images and size distribution diagram of AgNPs-MWCNT-rGO(E) composite prepared by using the solution with MWCNT-COOH and GO (1.0 mg/mL) ratio of 1:1 v/v to $\text{Ag}(\text{NH}_3)_2\text{OH}$ (0.04 M) volume ratios of 3 (a and b), 6 (c and d), and 12 (e and f), 24 (g and h) and using the solution with MWCNT-COOH and GO (1.0 mg/mL) ratio of 1:1 v/v to AgNO_3 (0.04 M) volume ratio of 12 (i and j)

The FESEM image of the AgNPs-MWCNT-rGO(E)-3 nanocomposite is shown in 4.53 i and its silver nanoparticle size distribution diagram is shown in 4.53 j. As seen in 4.53 (a-g), when the $\text{Ag}(\text{NH}_3)_2\text{OH}$ concentration increased, the silver particles size also increased from 14.58 to 28.66 nm suggesting that increasing the amount of silver in the nanocomposite caused an agglomeration of reduced silver particles. Therefore, the silver

particles diameter and quantity dramatically increased. By using AgNO_3 , instead of $\text{Ag}(\text{NH}_3)_2\text{OH}$ in the mixture, the mean Ag particle diameter size dramatically increased from 26.01 (4.53 e and f) to 100.08 (4.53 i and j). GO with a negative charge increased through the neutralization of the alkaline $\text{Ag}(\text{NH}_3)_2\text{OH}$ in order to absorb more $[\text{Ag}(\text{NH}_3)_2]^+$ ions than AgNO_3 . This led to the creation of more initial nucleation sites (Zhang et al., 2012), greater stability and resistance to the reduction of $\text{Ag}(\text{NH}_3)_2\text{OH}$ over AgNO_3 , preventing the growth of Ag into large particles (Kaniyankandy et al., 2007).

1.15.4.2 Cyclic voltammogram (CV) of the modified AgNPs-MWCNT-rGO(E)/GCE to hydrogen peroxide

AgNPs are commonly used for the reduction of hydrogen peroxide due to their high catalytic activity. Cyclic voltammetric (CVs) of modified GCE using all silver volume ratios of AgNPs-MWCNT-rGO(E) nanocomposites (AgNPs-MWCNT-rGO(E)/GCE) were carried out in a 0.2 M phosphate buffer solution (PBS) at pH 6.5 in the presence of 1.0 mM H_2O_2 . As shown in Figure 4.54 A, all silver ratios of modified AgNPs-MWCNT-rGO(E)/GCE electrodes possess considerable cathodic peaks for the reduction of H_2O_2 as compared to bare GCE. By increasing the silver ratio from 3:1 to 12:1 (AgNPs-MWCNT-rGO(E)-1 (Figure 4.54 b), AgNPs-MWCNT-rGO-2 (Figure 4.54 A.c) and AgNPs-MWCNT-rGO-3 (Figure 4.54 A.d) AgNPs-MWCNT-rGO(E) respectively), the cathodic peaks for the reduction of H_2O_2 alternatively increases. Meanwhile, increasing the silver ratio to 24:1 (AgNPs-MWCNT-rGO(E)-4 (Figure 4.54 A.e)) shows decreasing cathodic peaks toward H_2O_2 that is obviously due to big particle size and agglomeration of silver particles in the nanocomposite. Among AgNPs-MWCNT-rGO(E)/GCE electrodes, the AgNPs-MWCNT-rGO(E)-3 (Figure 4.54 A.d) exhibited better reduction activity towards H_2O_2 due to its small particle size and high density of AgNPs. Figure 4.54 B shows the effect of AgNO_3 (AgNPs-MWCNT-rGO(E)-

5 (Figure 4.54 B.a)) usage instead of $\text{Ag}(\text{NH}_3)_2\text{OH}$ (AgNPs-MWCNT-rGO(E)-3 (Figure 4.54 B.c)) and MWCNT (AgNPs-MWCNT-rGO(E)-6 (Figure 4.54 B.b)) instead of MWCNT-COOH (AgNPs-MWCNT-rGO(E)-3 (Figure 4.54 B.c)). The reduced activity of the AgNPs-MWCNT-rGO(E)-3/GCE electrode is significantly better than the AgNPs-MWCNT-rGO(E)-5/GCE electrode. A plausible reason is that AgNPs-MWCNT-rGO(E)-3 consists of smaller AgNPs formed on the nanocomposite, which results in higher surface area and increased catalytic activity. The functionalization of MWCNT to MWCNT-COOH provided a negative charge on the surface to adsorb more $[\text{Ag}(\text{NH}_3)_2]^+$ ions therefore the AgNPs-MWCNT-rGO(E)-3/GCE electrode obviously exhibits better catalyst activity towards H_2O_2 as compared to the AgNPs-MWCNT-rGO(E)-6/GCE electrode due to its higher surface area. These results are consistent with a previous study which implies that electrocatalytic activity of silver nanoparticles decreases with increased particle size and increases with increased particle density (Aimin Yu et al., 2012a). Therefore, the CV profiles results support FESEM images data.

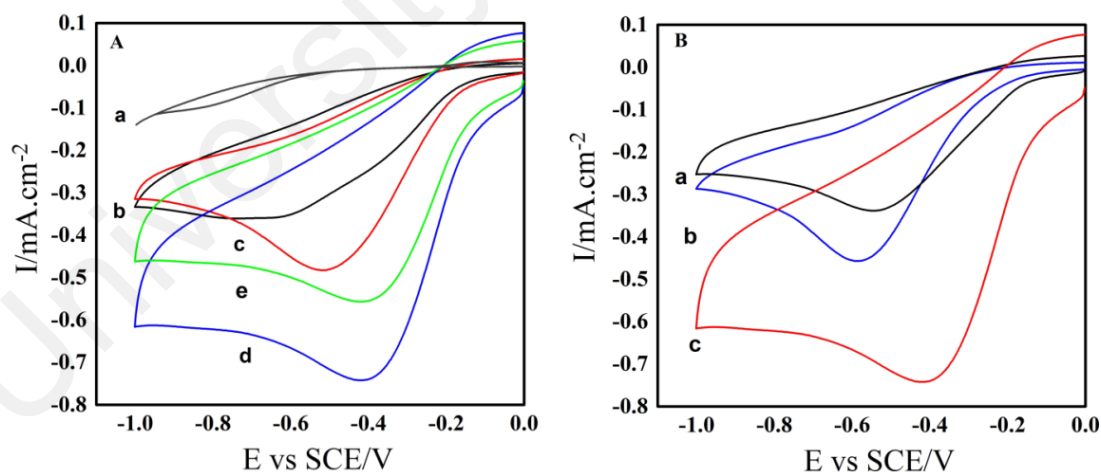


Figure 4.54 CVs of various electrodes in 0.2M PBS (pH 6.5) while there is 1.0 mM H_2O_2 : bare GCE(a), AgNPs-MWCNT-rGO(E)/GCE obtained by MWCNT-COOH and GO (1.0 mg/mL) ratio of 1:1 v/v and $\text{Ag}(\text{NH}_3)_2\text{OH}$ (0.04 M) with different volume ratios of 3, 6, 12 and 24 (b–e), respectively, and B: CVs of various electrodes in 0.2M PBS (pH 6.5) while there is 1.0 mM H_2O_2 of MWCNT-COOH and GO (1.0 mg/mL) ratio of 1:1 v/v and AgNO_3 (0.04 M) with a volume ratio of 12, MWCNT and GO (1.0 mg/mL) ratio of 1:1 v/v and $\text{Ag}(\text{NH}_3)_2\text{OH}$ (0.04 M) with a volume ratio of 12 and MWCNT-COOH and GO (1.0 mg/mL) ratio of 1:1 v/v and $\text{Ag}(\text{NH}_3)_2\text{OH}$ (0.04 M) volume ratios 12 (a–c) respectively.

Figure 4.55 presents the Nyquist plot of impedance spectra for bare and modified GCE electrodes with GO, MWCNT, AgNPs-MWCNT-GO, AgNPs-MWCNT-rGO(E) hydrothermal and electrodeposited AgNPs-MWCNT-rGO(E) composite in 0.1 M KCl solution which contained 1.0 mM $\text{Fe}(\text{CN})_6^{3-/4-}$ (1:1). For each of these electrodes, the experiments were carried out three times to minimize error.

The obtained EIS spectra of AgNPs-MWCNT-GO, hydrothermal AgNPs-MWCNT-rGO(E) and electrodeposited AgNPs-MWCNT-rGO(E) modified GCE electrodes show two areas: a semicircular part related to electron transfer process at high frequencies, and a linear part related to diffusion control at lower frequencies. R_{ct} or electron transfer resistance at the surface of the electrode can be assessed by exploiting the semicircle diameter.

The EIS is well fitted well with the corresponding circuit shown in Figure 4.55 in which chi-squared (χ^2) was minimized at 10^{-4} . The equivalent circuits possess the EIS characteristics of modified electrodes which are symbolized by C (capacitance) and Rct (Resistance) subsequently attached with the double layer capacitance and W (Warburg impedance). The observed Warburg impedance was a 45° straight line, which was recognized in the mid- and low-frequency areas suggesting that the diffusion controlled process occurred.

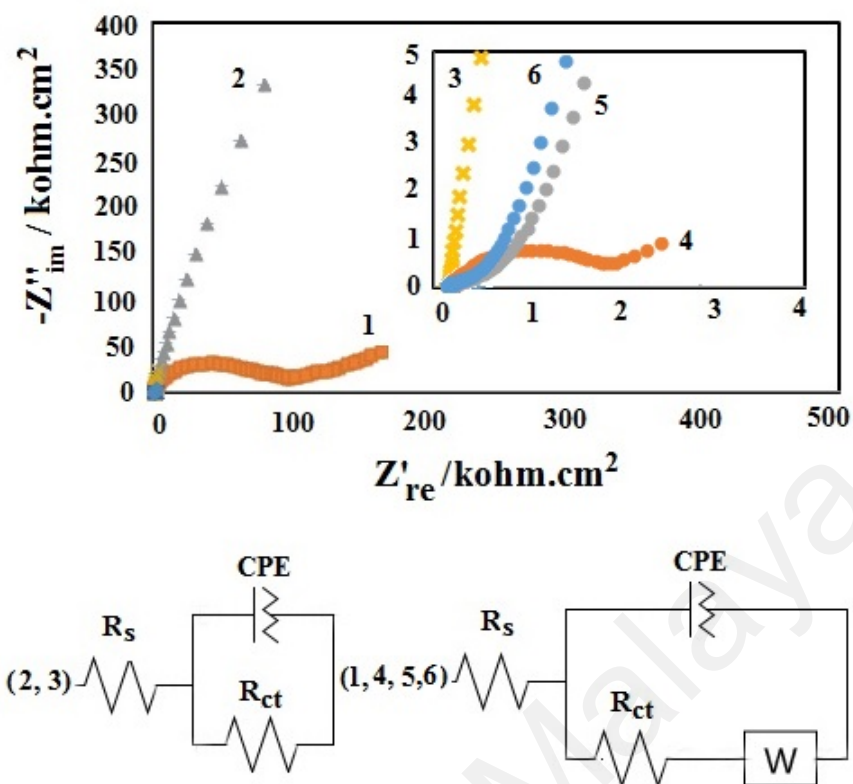


Figure 4.55 Nyquist Plots of: (1) bare GCE, (2) GO, (3) CNT, (4) AgNPs-MWCNT-GO and (5) AgNPs-MWCNT-rGO(H) hydrothermal (6) electrodeposited AgNPs-MWCNT-rGO(E) and their equivalents circuits in 1 mM $\text{Fe}(\text{CN})_6^{3-/4-}$ (1:1) solution with 0.1 M KCL supporting electrolyte.

As shown in Figure 4.55, when compared to bare GCE, modified GO on a GCE surface caused the semicircle to drastically rise, implying that GO performed as an insulating layer that caused the interfacial charge transfer to be challenging. MWCNT showed behavior akin to GO, but with a difference that MWCNT showed a semicircle with smaller diameter suggesting better conductivity as compared to GO. As AgNPs-MWCNT-rGO(E) possess noble metal, it had smaller diameter as compared to CNT and GO. As GO electrochemically reduced to rGO (AgNPs-MWCNT-rGO(E)), the semicircle diameter was smaller and displayed higher conductivity as compared to reduce GO hydrothermally to rGO (AgNPs-MWCNT-rGO(E)) modified electrode. This can be explained by the existence of smaller band gap in rGO, which is ideal for electron conduction and leads to lower Rct (Mahmoudian, et al, 2012).

1.15.4.3 Amperometric detection of H₂O₂ at modified AgNPs-MWCNT-rGO(E)/GCE electrode

Figure 4.56 A indicates the amperometric response of the AgNPs-MWCNT-rGO(E)-3/GCE electrode at -0.35 V in a 0.2 M PBS buffer (pH: 6.5) against consecutive H₂O₂ concentration step changes. The reduction current changes rapidly with a fractional added of H₂O₂, achieving a 95% steady-state current within 3 s which displays fast amperometric response behavior.

The Figure 4.56 inset shows the corresponding calibration curve of the AgNPs-MWCNT-rGO(E)-3/GCE electrode. The current response of the AgNPs-MWCNT-rGO(E)-3/GCE electrode was shown to be linear within the range of low and high concentrations of H₂O₂. Two linear steady-state amperometric detection ranges were estimated to fall within the range of 0.1 mM up to 10.0 mM for a low concentration of H₂O₂ (Figure 4.56 B) while high concentration is linear with different slopes from 10 to 100 mM (Figure 4.56 C). The limit of detection (LOD) for low concentration areas is estimated to be 0.4 μ M ($R^2 = 0.9976$) while for high concentration areas, it is estimated to be 1.4 μ M ($R^2 = 0.9977$) based on a signal-to-noise ratio of 3. The stability of the sensor is estimated by measuring the response current of the modified electrode. After 7 days, only 4.7% of the current signal has been lost. The electrode-to-electrode reproducibility is approximated to be at 1.0 mM H₂O₂ in 0.2 M PBS (pH 6.5) for four electrodes AgNPs-MWCNT-rGO(E)-3/GCE prepared in the same conditions, yielding a relative standard deviation (RSD) of 4.3%.

The effect of common interfering species on the AgNPs-MWCNT-rGO(E)-3/GCE electrode was studied. Figure 4.56 D shows the amperometric response of the modified electrode towards the addition of 1.0 mM H₂O₂ and this is followed by the addition of glucose, glycine, ethanol and ascorbic acid into the 0.2 M phosphate buffer

solution (pH 6.5). As can be seen, these interfering substances responded with very weak signals which demonstrates that this modified electrode has good selectivity towards H_2O_2 .

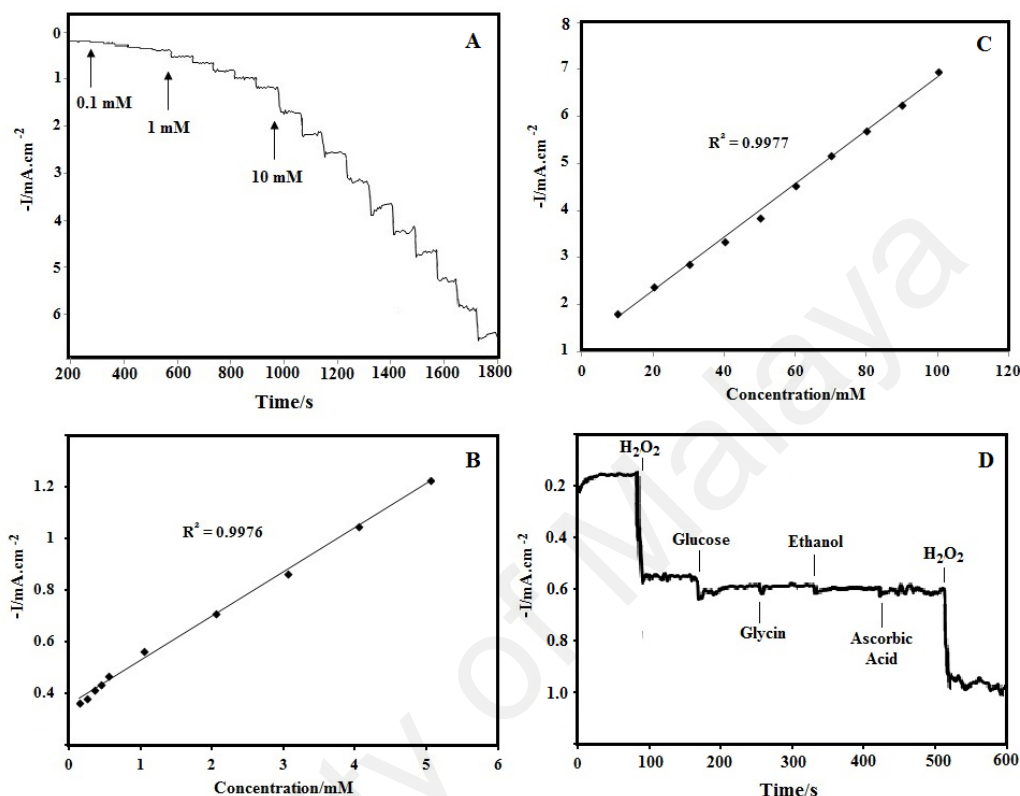


Figure 4.56 A: Steady-state response of the AgNPs-MWCNT-rGO(E)-3/GCE electrode to consecutive H_2O_2 injection into the stirred 0.2 M PBS (pH 6.5) with an applied potential of -0.35 V. B: Low concentration corresponding calibration curve. C: high concentration corresponding calibration curve. D: Amperometric response of AgNPs-MWCNT-rGO(E)-3/GCE electrode upon the successive addition of 1.0 mM H_2O_2 , glucose, glycine, ethanol and ascorbic acid into 0.2M phosphate buffer solution (pH 6.5) with an applied potential -0.35 V under a stirring condition.

Based on the comparative analysis between different types of electrodes shown in Table 4.9, the present AgNPs-MWCNT-rGO(E)-3/GCE electrode is able to offer an excellent detection limit and linear range to detect H_2O_2 . Based on the comparative analysis between different types of electrodes shown, the AgNPs-MWCNT-rGO(E) was successfully electrodeposited using a simple and environmentally friendly CV method. It

was demonstrated that the AgNPs that existed on the composite were well dispersed with small and narrow-sized distributions using silver ammonia complex instead of silver nitrate. Furthermore, the MWCNT-COOH was the key component to the one-step electrodeposition of MWCNT in the AgNPs-MWCNT-rGO(E) composite.

The obtained modified electrodeposited AgNPs-MWCNT-rGO(E) composite electrode showed better sensitivity for electrochemical detection of hydrogen peroxide in a cyclic voltammetry curve as compared to the modified hydrothermal AgNPs-MWCNT-rGO(E) composite electrode due to more reduction of oxygenated groups by electrodeposition presses. The present method provides us with a low cost, simple preparation, one-step method to fabricate electrodes as an effective non-enzymatic electrochemical H₂O₂ sensor.

Table 4.9 A comparison of this work with the other works in the literature regarding the performance of the H₂O₂ measure.

Modify Electrode	LOD (μ M)	Linear range (mM)	References
Ag NPs-GN-R/GCE	28	0.1-40	(Qin et al., 2011)
Ag NPs-MWCNT/Au	0.5	0.05-17	(Lu, Chang, et al., 2011)
AgNP-GO-ssDNA/Au	1.9	0.1-20	(Guo et al., 2012)
AgNP-rGO-benzylamine/GCE	31.3	0.1-100	(Liu, Tian, et al., 2011a)
ERGO-Ag/GCE	1.6	0.1-100	(Moradi Golsheikh et al., 2013b)
N-graphene-Agnanodendrities	0.26	0.1-80	(Tajabadi et al., 2014)
AgNPs-MWCNT-rGO(H)/GCE	0.9	0.1-100	This work
AgNPs-MWCNT-rGO(E)/GCE	0.4	0.1-10	This work
	1.4	10-100	

CHAPTER 5: CONCLUSION

Six novel solid-phase nanocomposites with different morphologies and materials combination were successfully synthesized using a simple and effective method for non-enzymatic H_2O_2 sensor. The first four composites were based on PANI as the polymer matrix. The AgNPs-PANINTs(A) and AgNPs-PANINRs describe two different morphologies of PANI, which are nanotubes and nanorods, respectively, by only changing the temperature of reaction. In AgNPs-PANINTs(A) and AgNPs-PANINRs, AgNO_3 was used as a source of Ag nanoparticles (AgNPs). The sensing performance of AgNPs-PANINRs/GCE towards H_2O_2 is better than AgNPs-PANINTs(A)/GCE with the LOD of 0.13 (μM) for linear range of 0.1-10 mM and LOD of 0.33 (μM) for linear range of 10-70 mM, because the amount of AgNPs loading and distribution are higher in rod shape. AgNPs-PANINTs(B)/GCE displayed the nanotube morphology of nanocomposite but by using $\text{Ag}(\text{NH}_3)_2\text{OH}$ as the source of AgNPs. Better distribution of AgNPs were achieved in the AgNPs-PANINTs(B) and the performance of obtained composite is significantly greater than AgNPs-PANINTs(A) which is prepared with AgNO_3 as a source of silver in the composite. AgNPs-PANINTs(B)/GCE shows 0.1-100 mM linear range with LOD amount of 0.6 (μM), while we could not get a linear range for H_2O_2 detection via AgNPs-PANINTs(B)/GCE modified electrode. Combination of two different methods in synthesizing AgNPs-PANINFs -rGO was conducted to obtain a better performance of materials for sensing H_2O_2 . Graphene oxide (GO) decorated with silver nanoparticles (AgNPs), was reduced by a hydrothermal method (AgNPs-rGO). Then, polyaniline nanofibers (PANINFs) were synthesized by vertical sonochemical method in the presence of sulfuric acid. The modified electrode prepared by dropping obtained AgNPs-rGO and PANINFs on the glassy carbon electrode (GCE). The results

obtained from Fourier-transform infrared transmission spectroscopy and X-ray diffraction approved that the GO and polyaniline nanofibers were successfully reduced and polymerized, respectively and the silver nanoparticles were formed. Field emission scanning electron microscope images indicated that the silver nanoparticles were homogeneously distributed on the rGO surface with a narrow nanosize distribution and the polyaniline nanofiber structure shows a diameter range of approximately 30-50 nm. The first linear section was in the range of 0.1 mM to 5 mM with a limit of detection of 0.682 μM and the second linear section raised to 110 mM with a correlation factor of 0.117 μM (S/N of 3).

AgNPs-MWCNT-rGO(H) was successfully synthesized by a simple and environmentally friendly one-step hydrothermal method. The advantage of this method is that it did not require any toxic solvent or chemical to reduce the graphite oxide. Most Ag nanoparticles that exist on the composite using silver ammonia complex instead of silver nitrate were well dispersed with small and narrow-sized distributions. The AgNPs-MWCNT-rGO(H)/GCE composite exhibited excellent sensitivity for electrochemical detection of hydrogen peroxide in a cyclic voltammetry curve. The composite showed considerable electrocatalytic activity towards the reduction of hydrogen peroxide, leading to a non-enzymatic electrochemical sensor with a fast amperometric response time of less than 3 s. The first linear section ranges from 0.1 mM to 10 mM with a 0.4 μM detection limit and the second linear section range goes up to 100 mM with a 1.4 μM detection limit at a signal-to-noise ratio of 3.

AgNPs-MWCNT-rGO(E)/GCE was successfully electrodeposited using a simple and environmentally friendly CV method. It was demonstrated that the Ag nanoparticles that exist on the composite were well dispersed with small and narrow-sized distributions using silver ammonia complex instead of silver nitrate. Furthermore, the MWCNT-

COOH was the key component to the one-step electrodeposition of MWCNT in the AgNPs-MWCNT-rGO(E) composite. The obtained AgNPs-MWCNT-rGO(E)/GCE modified electrode showed higher sensitivity for electrochemical detection of hydrogen peroxide in a cyclic voltammetry curve as compared to the AgNPs-MWCNT-rGO(H) composite. Table 5.1 shows the performance of obtained composites as modified electrodes to detect H₂O₂. As the lower limit of detection is the smallest amount of H₂O₂ measured in terms of moles, therefore the lowest LOD indicated the best action of prepared H₂O₂ sensor.

Table 5.1 Comparison of result on modified electrode with solid phase nanocomposite based as non-enzymatic H₂O₂ sensor

Modify Electrode	Performance	
	LOD (μM)	Linear range (mM)
AgNPs-PANINTs(A)/GCE	-	Not linear
AgNPs-PANINRs/GCE	0.13	0.1-10
	0.33	10-70
AgNPs-PANINTs(B)/GCE	0.6	0.1-100
AgNPs-PANINFs-rGO/GCE	0.682	0.1-5
	0.117	10-110
AgNPs-MWCNT-rGO(E)/GCE	0.4	0.1-10
	1.4	10-100
AgNPs-MWCNT-rGO(H)/GCE	0.9	0.1-100

High sensitivity, stability, reproducibility, and lower detection limits are among the advantages of these modified electrodes. The modified electrodes in this work could be used as sensors for highly sensitive electrode, for catalytic reduction and simultaneous

determination of hydrogen peroxide. The AgNPs-PANINFs-rGO/GCE shows the lowest LOD among the prepared nanocomposites due to homogeneously distribution of AgNPs on the rGO surface with a narrow nanosize distribution and the polyaniline nanofiber structure that provided high surface area and low detection limit as hydrogen peroxide sensor.

1.16 Recommendation for Future Work

Although the results presented here have demonstrated the effectiveness of the H₂O₂ sensor approach, it could be further developed in a number of ways:

1. Real Sample

The developed sensor can be used to check the amount of hydrogen peroxide content in real samples; for example; tooth paste.

2. Alloy nanocomposites

By using two different noble metals at the same time with any mentioned nanocomposites matrix, it would be a hope to prepare more effective H₂O₂ sensor.

3. Functionalization of rGO

In AgNPs-MWCNT-rGO(E) the effect of carboxylic functionalization on MWCNT has been checked. The rGO also could be functionalized with any other functional groups to achieve better dispersion and less agglomeration of composite components.

REFERENCES

- Abdulrahman, O. (2012). Ag nanoparticles decorated polyaniline nanofibers: synthesis, characterization, and applications toward catalytic reduction of 4-nitrophenol and electrochemical detection of H₂O₂ and glucose. *Catalysis Science & Technology*, 2(4), 800-806.
- Ameen, S., Akhtar, M. S., Kim, Y. S., Yang, O.-B., & Shin, H.-S. (2010). Sulfamic acid-doped polyaniline nanofibers thin film-based counter electrode: application in dye-sensitized solar cells. *The Journal of Physical Chemistry C*, 114(10), 4760-4764.
- Anilkumar, P., & Jayakannan, M. (2009). Large-scale synthesis of polyaniline nanofibers based on renewable resource molecular template. *Journal of Applied Polymer Science*, 114(6), 3531-3541.
- Arya, S. K., Datta, M., & Malhotra, B. D. (2008). Recent advances in cholesterol biosensor. *Biosensors and Bioelectronics*, 23(7), 1083-1100.
- Aussawasathien, D., Dong, J. H., & Dai, L. (2005a). Electrospun polymer nanofiber sensors. *Synthetic Metals*, 154(1), 37-40.
- Aussawasathien, D., Dong, J. H., & Dai, L. (2005b). Electrospun polymer nanofiber sensors. *Synthetic Metals*, 154(1-3), 37-40.
- Avilés, F., Cauich-Rodríguez, J. V., Moo-Tah, L., May-Pat, A., & Vargas-Coronado, R. (2009). Evaluation of mild acid oxidation treatments for MWCNT functionalization. *Carbon*, 47(13), 2970-2975.
- Bai, W., Nie, F., Zheng, J., & Sheng, Q. (2014). Novel Silver Nanoparticle–Manganese Oxyhydroxide–Graphene Oxide Nanocomposite Prepared by Modified Silver Mirror Reaction and Its Application for Electrochemical Sensing. *ACS Applied Materials & Interfaces*, 6(8), 5439-5449.
- Bale, S. S., Asuri, P., Karajanagi, S. S., Dordick, J. S., & Kane, R. S. (2007). Protein-Directed Formation of Silver Nanoparticles on Carbon Nanotubes. *Advanced Materials*, 19(20), 3167-3170.
- Ballarin, B., Fraleoni-Morgera, A., Frascaro, D., Marazzita, S., Piana, C., & Setti, L. (2004). Thermal inkjet microdeposition of PEDOT: PSS on ITO-coated glass and characterization of the obtained film. *Synthetic Metals*, 146(2), 201-205.
- Baranchikov, A. Y., Ivanov, V. K., & Tretyakov, Y. D. (2007). Sonochemical synthesis of inorganic materials. *Russian Chemical Reviews*, 76(2), 133.
- Bein, T., & Stucky, G. D. (1996). *Nanostructured Materials*: ACS Publications.
- Bláha, M., Varga, M., Prokeš, J., Zhigunov, A., & Vohlídál, J. (2013). Effects of the polymerization temperature on the structure, morphology and conductivity of

polyaniline prepared with ammonium peroxodisulfate. *European Polymer Journal*, 49(12), 3904-3911.

- Bouazza, S., Alonzo, V., & Hauchard, D. (2009). Synthesis and characterization of Ag nanoparticles–polyaniline composite powder material. *Synthetic Metals*, 159(15), 1612-1619.
- Brodie, B. C. (1859). On the atomic weight of graphite. *Philosophical Transactions of the Royal Society of London*, 149, 249-259.
- Camargo, P. H. C., Satyanarayana, K. G., & Wypych, F. (2009). Nanocomposites: synthesis, structure, properties and new application opportunities. *Materials Research*, 12(1), 1-39.
- Campbell, F. W., Belding, S. R., Baron, R., Xiao, L., & Compton, R. G. (2009). Hydrogen peroxide electroreduction at a silver-nanoparticle array: investigating nanoparticle size and coverage effects. *The Journal of Physical Chemistry C*, 113(21), 9053-9062.
- Campbell, F. W., & Compton, R. G. (2010). The use of nanoparticles in electroanalysis: an updated review. *Analytical and Bioanalytical Chemistry*, 396(1), 241-259.
- Cappella, B., & Dietler, G. (1999). Force-distance curves by atomic force microscopy. *Surface Science Reports*, 34(1), 1-104.
- Çeken, B., Kandaz, M., & Koca, A. (2012). Electrochemical hydrogen peroxide sensor based on cobalt phthalocyanine captured in polyaniline film on a glassy carbon electrode. *Journal of Porphyrins and Phthalocyanines*, 16(04), 380-389.
- Chang, G., Luo, Y., Lu, W., Liao, F., & Sun, X. (2011). Hydrothermal synthesis of ultra-highly concentrated, well-stable Ag nanoparticles and their application for enzymeless hydrogen peroxide detection. *Journal of Nanoparticle Research*, 13(7), 2689-2695.
- Chang, Q., Deng, K., Zhu, L., Jiang, G., Yu, C., & Tang, H. (2009). Determination of hydrogen peroxide with the aid of peroxidase-like Fe₃O₄ magnetic nanoparticles as the catalyst. *Microchimica Acta*, 165(3-4), 299-305.
- Chen, H., Zhang, Z., Cai, D., Zhang, S., Zhang, B., Tang, J., & Wu, Z. (2011). A hydrogen peroxide sensor based on Ag nanoparticles electrodeposited on natural nano-structure attapulgite modified glassy carbon electrode. *Talanta*, 86, 266-270.
- Chen, J., Zhang, W.-D., & Ye, J.-S. (2008). Nonenzymatic electrochemical glucose sensor based on MnO₂/MWNTs nanocomposite. *Electrochemistry Communications*, 10(9), 1268-1271.
- Chen, L., Tang, Y., Wang, K., Liu, C., & Luo, S. (2011). Direct electrodeposition of reduced graphene oxide on glassy carbon electrode and its electrochemical application. *Electrochemistry Communications*, 13(2), 133-137.
- Chen, W., Cai, S., Ren, Q.-Q., Wen, W., & Zhao, Y.-D. (2012). Recent advances in electrochemical sensing for hydrogen peroxide: a review. *Analyst*, 137(1), 49-58.

- Cheng, C., Nie, S., Li, S., Peng, H., Yang, H., Ma, L., Zhao, C. (2013). Biopolymer functionalized reduced graphene oxide with enhanced biocompatibility via mussel inspired coatings/anchors. *Journal of Materials Chemistry B*, 1(3), 265-275.
- Chiang, J.-C., & MacDiarmid, A. G. (1986). 'Polyaniline': protonic acid doping of the emeraldine form to the metallic regime. *Synthetic Metals*, 13(1), 193-205.
- Chiou, N. R., & Epstein, A. J. (2005). Polyaniline nanofibers prepared by dilute polymerization. *Advanced Materials*, 17(13), 1679-1683.
- Cho, S., Kwon, O. S., You, S. A., & Jang, J. (2013). Shape-controlled polyaniline chemiresistors for high-performance DMMP sensors: effect of morphologies and charge-transport properties. *Journal of Materials Chemistry A*, 1(18), 5679-5688.
- Crouch, E., Cowell, D. C., Hoskins, S., Pittson, R. W., & Hart, J. P. (2005). A novel, disposable, screen-printed amperometric biosensor for glucose in serum fabricated using a water-based carbon ink. *Biosensors and Bioelectronics*, 21(5), 712-718.
- Cui, P., Lee, J., Hwang, E., & Lee, H. (2011). One-pot reduction of graphene oxide at subzero temperatures. *Chemical Communications*, 47(45), 12370-12372.
- Dinesh, B., Mani, V., Saraswathi, R., & Chen, S.-M. (2014). Direct electrochemistry of cytochrome c immobilized on a graphene oxide-carbon nanotube composite for picomolar detection of hydrogen peroxide. *RSC Advances*, 4(54), 28229-28237.
- Ding, H., Shen, J., Wan, M., & Chen, Z. (2008). Formation Mechanism of Polyaniline Nanotubes by a Simplified Template-Free Method. *Macromolecular Chemistry and Physics*, 209(8), 864-871.
- Dreyer, D. R., Park, S., Bielawski, C. W., & Ruoff, R. S. (2010). The chemistry of graphene oxide. *Chemical Society Reviews*, 39(1), 228-240.
- Dubey, P., Muthukumar, D., Dash, S., Mukhopadhyay, R., & Sarkar, S. (2005). Synthesis and characterization of water-soluble carbon nanotubes from mustard soot. *Pramana*, 65(4), 681-697.
- Endo, M., Takeuchi, K., Hiraoka, T., Furuta, T., Kasai, T., Sun, X., Dresselhaus, M. (1997). Stacking nature of graphene layers in carbon nanotubes and nanofibres. *Journal of Physics and Chemistry of Solids*, 58(11), 1707-1712.
- Falcon, H., & Carbonio, R. (1992). Study of the heterogeneous decomposition of hydrogen peroxide: its application to the development of catalysts for carbon-based oxygen cathodes. *Journal of Electroanalytical Chemistry*, 339(1), 69-83.
- Fan, J. P., Bian, X. F., Niu, Y. C., Bai, Y. W., Xiao, X. X., Yang, C. C., Yang, J. Y. (2013). Formation of three-dimensional nano-porous silver films and application toward electrochemical detection of hydrogen peroxide. *Applied Surface Science*, 285, 185-189.

- Fang, M., Chen, Z., Wang, S., & Lu, H. (2012). The deposition of iron and silver nanoparticles in graphene–polyelectrolyte brushes. *Nanotechnology*, 23(8), 085704.
- Fang, Y., Zhang, D., Qin, X., Miao, Z., Takahashi, S., Anzai, J.-i., & Chen, Q. (2012). A non-enzymatic hydrogen peroxide sensor based on poly (vinyl alcohol)–multiwalled carbon nanotubes–platinum nanoparticles hybrids modified glassy carbon electrode. *Electrochimica Acta*, 70, 266-271.
- Feng, L., Gao, G., Huang, P., Wang, X., Zhang, C., Zhang, J., Cui, D. (2011). Preparation of Pt Ag alloy nanoisland/graphene hybrid composites and its high stability and catalytic activity in methanol electro-oxidation. *Nanoscale research letters*, 6(1), 1-10.
- Flätgen, G., Wasle, S., Lübke, M., Eickes, C., Radhakrishnan, G., Doblhofer, K., & Ertl, G. (1999). Autocatalytic mechanism of H₂O₂ reduction on Ag electrodes in acidic electrolyte: experiments and simulations. *Electrochimica Acta*, 44(25), 4499-4506.
- Fu, L., Lai, G., Jia, B., & Yu, A. (2015). Preparation and Electrocatalytic Properties of Polydopamine Functionalized Reduced Graphene Oxide-Silver Nanocomposites. *Electrocatalysis*, 6(1), 72-76.
- Gan, X., Liu, T., Zhong, J., Liu, X., & Li, G. (2004). Effect of silver nanoparticles on the electron transfer reactivity and the catalytic activity of myoglobin. *ChemBioChem*, 5(12), 1686-1691.
- Gao, F., Qi, X., Cai, X., Wang, Q., Gao, F., & Sun, W. (2012). Electrochemically reduced graphene modified carbon ionic liquid electrode for the sensitive sensing of rutin. *Thin Solid Films*, 520(15), 5064-5069.
- Gao, R., Hu, N., Yang, Z., Zhu, Q., Chai, J., Su, Y., Zhang, Y. (2013). Paper-like graphene-Ag composite films with enhanced mechanical and electrical properties. *Nanoscale research letters*, 8(1), 1-8.
- Gao, W., Tjiu, W. W., Wei, J., & Liu, T. (2014). Highly sensitive nonenzymatic glucose and H₂O₂ sensor based on Ni(OH)₂/electroreduced graphene oxide-Multiwalled carbon nanotube film modified glass carbon electrode. *Talanta*, 120, 484-490.
- Gao, Y., Shan, D., Cao, F., Gong, J., Li, X., Ma, H.-y., Qu, L.-y. (2009). Silver/polyaniline composite nanotubes: one-step synthesis and electrocatalytic activity for neurotransmitter dopamine. *The Journal of Physical Chemistry C*, 113(34), 15175-15181.
- Ge, C., Yang, X., Li, C., & Hou, B. (2012). Synthesis of polyaniline nanofiber and copolymerization with acrylate through in situ emulsion polymerization. *Journal of Applied Polymer Science*, 123(1), 627-635.
- Ghadimi, H., MA Tehrani, R., Ali, A. S. M., Mohamed, N., & Ab Ghani, S. (2013). Sensitive voltammetric determination of paracetamol by poly (4-vinylpyridine)/multiwalled carbon nanotubes modified glassy carbon electrode. *Analytica Chimica Acta*, 765, 70-76.

- Golsheikh, A. M., Huang, N. M., Lim, H. N., Zakaria, R., & Yin, C.-Y. (2013). One-step electrodeposition synthesis of silver-nanoparticle-decorated graphene on indium-tin-oxide for enzymeless hydrogen peroxide detection. *Carbon*, 62, 405-412.
- Gooding, J. J. (2005). Nanostructuring electrodes with carbon nanotubes: A review on electrochemistry and applications for sensing. *Electrochimica Acta*, 50(15), 3049-3060.
- Grayfer, E. D., Makotchenko, V. G., Nazarov, A. S., Kim, S. J., & Fedorov, V. E. (2011). Graphene: Chemical approaches to the synthesis and modification. *Russian Chemical Reviews*, 80(8), 751-770.
- Gu, Z., Wang, J., Li, L., Chen, L., & Shen, Q. (2014). Formation of polyaniline nanotubes with different pore shapes using α -, β - and γ -cyclodextrins as templates. *Materials Letters*, 117, 66-68.
- Guermoune, A., Chari, T., Popescu, F., Sabri, S. S., Guillemette, J., Skulason, H. S., Siaj, M. (2011). Chemical vapor deposition synthesis of graphene on copper with methanol, ethanol, and propanol precursors. *Carbon*, 49(13), 4204-4210.
- Guo, H.-L., Wang, X.-F., Qian, Q.-Y., Wang, F.-B., & Xia, X.-H. (2009). A green approach to the synthesis of graphene nanosheets. *ACS nano*, 3(9), 2653-2659.
- Guo, Y., Sun, X., Liu, Y., Wang, W., Qiu, H., & Gao, J. (2012). One pot preparation of reduced graphene oxide (RGO) or Au (Ag) nanoparticle-RGO hybrids using chitosan as a reducing and stabilizing agent and their use in methanol electrooxidation. *Carbon*, 50(7), 2513-2523.
- Han, L., Wang, Q., Tricard, S., Liu, J., Fang, J., Zhao, J., & Shen, W. (2013). Amperometric detection of hydrogen peroxide utilizing synergistic action of cobalt hexacyanoferrate and carbon nanotubes chemically modified with platinum nanoparticles. *RSC Advances*, 3(1), 281-287.
- Han, Z., Dong, W., & Xu, D. (2011). *Preparation of graphene nanosheets by in-situ oxidation-exfoliation method*, 5(7), 140-142
- Hanaoka, S., Lin, J.-M., & Yamada, M. (2000). Chemiluminescence behavior of the decomposition of hydrogen peroxide catalyzed by copper (II)-amino acid complexes and its application to the determination of tryptophan and phenylalanine. *Analytica Chimica Acta*, 409(1), 65-73.
- Hanaoka, S., Lin, J.-M., & Yamada, M. (2001). Chemiluminescent flow sensor for H₂O₂ based on the decomposition of H₂O₂ catalyzed by cobalt (II)-ethanolamine complex immobilized on resin. *Analytica Chimica Acta*, 426(1), 57-64.
- Honda, M., Kodera, T., & Kita, H. (1986). Electrochemical behavior of H₂O₂ at Ag in HClO₄ aqueous solution. *Electrochimica Acta*, 31(3), 377-383.
- Hong-Xing, Y., Meng-Meng, L., Yang, H., Yun-Ze, L., & Xin, S. (2010). Electrical resistance response of polyaniline films to water, ethanol, and nitric acid solution. *Chinese Physics B*, 19(8), 088105.

- Hua, M.-Y., Lin, Y.-C., Tsai, R.-Y., Chen, H.-C., & Liu, Y.-C. (2011). A hydrogen peroxide sensor based on a horseradish peroxidase/polyaniline/carboxy-functionalized multiwalled carbon nanotube modified gold electrode. *Electrochimica Acta*, 56(25), 9488-9495.
- Hua, M. Y., Lin, Y. C., Tsai, R. Y., Chen, H. C., & Liu, Y. C. (2011). A hydrogen peroxide sensor based on a horseradish peroxidase/polyaniline/carboxy-functionalized multiwalled carbon nanotube modified gold electrode. *Electrochimica Acta*, 56(25), 9488-9495.
- Huang, J., & Kaner, R. B. (2004a). A general chemical route to polyaniline nanofibers. *Journal of the American Chemical Society*, 126(3), 851-855.
- Huang, J., & Kaner, R. B. (2004b). Nanofiber formation in the chemical polymerization of aniline: a mechanistic study. *Angewandte Chemie*, 116(43), 5941-5945.
- Huang, J., Virji, S., Weiller, B. H., & Kaner, R. B. (2003). Polyaniline nanofibers: facile synthesis and chemical sensors. *Journal of the American Chemical Society*, 125(2), 314-315.
- Huang, X., Qi, X., Boey, F., & Zhang, H. (2012). Graphene-based composites. *Chemical Society Reviews*, 41(2), 666-686.
- Huang, Y., & Lin, C. (2009). Exploration of the formation mechanisms of polyaniline nanotubes and nanofibers through a template-free method. *Synthetic Metals*, 159(17), 1824-1830.
- Huang, Z. M., Zhang, Y. Z., Kotaki, M., & Ramakrishna, S. (2003). A review on polymer nanofibers by electrospinning and their applications in nanocomposites. *Composites Science and Technology*, 63(15), 2223-2253.
- Hummers Jr, W. S., & Offeman, R. E. (1958). Preparation of graphitic oxide. *Journal of the American Chemical Society*, 80(6), 1339-1339.
- Hurdis, E., & Romeyn Jr, H. (1954). Accuracy of determination of hydrogen peroxide by cerate oxidimetry. *Analytical Chemistry*, 26(2), 320-325.
- Ivanov, S., Tsakova, V., & Bund, A. (2013). Formation and electroanalytical performance of polyaniline-palladium nanocomposites obtained via Layer-by-Layer adsorption and electroless metal deposition. *Electrochimica Acta*, 90, 157-165.
- Jamal, M., Hasan, M., Mathewson, A., & Razeeb, K. M. (2012). Non-enzymatic and highly sensitive H₂O₂ sensor based on Pd nanoparticle modified gold nanowire array electrode. *Journal of the Electrochemical Society*, 159(11), B825-B829.
- Jin, E., Bian, X., Lu, X., & Wang, C. (2012). Fabrication of multiwalled carbon nanotubes/polypyrrole/Prussian blue ternary composite nanofibers and their application for enzymeless hydrogen peroxide detection. *Journal of Materials Science*, 47(10), 4326-4331.
- Jing, X., Wang, Y., Wu, D., & Qiang, J. (2007). Sonochemical synthesis of polyaniline nanofibers. *Ultrasonics Sonochemistry*, 14(1), 75-80.

- Kan, X., Zhou, H., Li, C., Zhu, A., Xing, Z., & Zhao, Z. (2012). Imprinted electrochemical sensor for dopamine recognition and determination based on a carbon nanotube/polypyrrole film. *Electrochimica Acta*, 63(2), 69-75.
- Kaniyankandy, S., Nuwad, J., Thinaharan, C., Dey, G., & Pillai, C. (2007). Electrodeposition of silver nanodendrites. *Nanotechnology*, 18(12), 125610.
- Khan, U., O'Neill, A., Porwal, H., May, P., Nawaz, K., & Coleman, J. N. (2011). Size selection of dispersed, exfoliated graphene flakes by controlled centrifugation. *Carbon*, 50(2):470-475
- Khanna, P., Singh, N., Charan, S., & Viswanath, A. K. (2005). Synthesis of Ag/polyaniline nanocomposite via an in situ photo-redox mechanism. *Materials Chemistry and Physics*, 92(1), 214-219.
- Kim, M., Hwang, Y., & Kim, J. (2014). Fabrication of graphene-carbon nanotube papers decorated with manganese oxide nanoneedles on the graphene sheets for supercapacitors. *Physical Chemistry Chemical Physics*, 16(1), 351-361.
- Kirchner, P., Reiser, S., Pütz, P., Keusgen, M., & Schöning, M. J. (2012). Characterisation of polymeric materials as passivation layer for calorimetric H₂O₂ gas sensors. *Physica Status Solidi (A) Applications and Materials Science*, 209(5), 859-863.
- Kleiner, L., & Matthiesen, M. (1989). Electrical devices containing conductive polymers: Google Patents.
- Konwer, S., Guha, A. K., & Dolui, S. K. (2013). Graphene oxide-filled conducting polyaniline composites as methanol-sensing materials. *Journal of Materials Science*, 48(4), 1729-1739.
- Kosynkin, D. V., Higginbotham, A. L., Sinitskii, A., Lomeda, J. R., Dimiev, A., Price, B. K., & Tour, J. M. (2009). Longitudinal unzipping of carbon nanotubes to form graphene nanoribbons. *Nature*, 458(7240), 872-876.
- Li, D., & Kaner, R. B. (2006). Shape and aggregation control of nanoparticles: not shaken, not stirred. *Journal of the American Chemical Society*, 128(3), 968-975.
- Li, D., Müller, M. B., Gilje, S., Kaner, R. B., & Wallace, G. G. (2008). Processable aqueous dispersions of graphene nanosheets. *Nature nanotechnology*, 3(2), 101-105.
- Li, D., Wang, Y., & Xia, Y. (2003). Electrospinning of polymeric and ceramic nanofibers as uniaxially aligned arrays. *Nano Letters*, 3(8), 1167-1171.
- Li, J., Li, H., Hu, H., Zhao, Y., & Wang, Q. (2015). Preparation and application of polymer nano-fiber doped with nano-particles. *Optical Materials*, 40, 49-56.
- Li, J. P., & Gu, H. N. (2006). A selective cholesterol biosensor based on composite film modified electrode for amperometric detection. *Journal of the Chinese Chemical Society*, 53(3), 575-582.

- Li, M., Bo, X., Mu, Z., Zhang, Y., & Guo, L. (2014). Electrodeposition of nickel oxide and platinum nanoparticles on electrochemically reduced graphene oxide film as a nonenzymatic glucose sensor. *Sensors and Actuators B: Chemical*, *192*, 261-268.
- Li, W., Kuai, L., Qin, Q., & Geng, B. (2013). Ag–Au bimetallic nanostructures: co-reduction synthesis and their component-dependent performance for enzyme-free H₂O₂ sensing. *Journal of Materials Chemistry A*, *1*(24), 7111-7117.
- Li, X., Liu, Y., Zheng, L., Dong, M., Xue, Z., Lu, X., & Liu, X. (2013). A novel nonenzymatic hydrogen peroxide sensor based on silver nanoparticles and ionic liquid functionalized multiwalled carbon nanotube composite modified electrode. *Electrochimica Acta*.
- Li, Y.-F., Liu, Y.-Z., Yang, Y.-G., Wang, M.-Z., & Wen, Y.-F. (2012). Reduced graphene oxide/MWCNT hybrid sandwiched film by self-assembly for high performance supercapacitor electrodes. *Applied Physics A*, *108*(3), 701-707.
- Li, Y., Zheng, J., Sheng, Q., & Wang, B. (2015). Synthesis of Ag@AgCl nanoboxes, and their application to electrochemical sensing of hydrogen peroxide at very low potential. *Microchimica Acta*, *182*(1-2), 61-68.
- Lian, W., Wang, L., Song, Y., Yuan, H., Zhao, S., Li, P., & Chen, L. (2009). A hydrogen peroxide sensor based on electrochemically roughened silver electrodes. *Electrochimica Acta*, *54*(18), 4334-4339.
- Liang, M., Jin, F., Liu, R., Su, R., Qi, W., Yu, Y., He, Z. (2013). Enhanced electrochemical detection performance of multiwall carbon nanotubes functionalized by aspartame. *Journal of Materials Science*, *48*(16), 5624-5632.
- Lin, J., He, C., Zhao, Y., & Zhang, S. (2009). One-step synthesis of silver nanoparticles/carbon nanotubes/chitosan film and its application in glucose biosensor. *Sensors and Actuators B: Chemical*, *137*(2), 768-773.
- Liu, C., Teng, Y., Liu, R., Luo, S., Tang, Y., Chen, L., & Cai, Q. (2011). Fabrication of graphene films on TiO₂ nanotube arrays for photocatalytic application. *Carbon*, *49*(15), 5312-5320.
- Liu, C., Yu, Z., Neff, D., Zhamu, A., & Jang, B. Z. (2010). Graphene-based supercapacitor with an ultrahigh energy density. *Nano Letters*, *10*(12), 4863-4868.
- Liu, L., Shi, L., Chu, Z., Peng, J., & Jin, W. (2014). Prussian blue nanocubes modified graphite electrodes for the electrochemical detection of various analytes with high performance. *Sensors and Actuators B: Chemical*, *202*, 820-826.
- Liu, S., Tian, J., Wang, L., & Sun, X. (2011a). A method for the production of reduced graphene oxide using benzylamine as a reducing and stabilizing agent and its subsequent decoration with Ag nanoparticles for enzymeless hydrogen peroxide detection. *Carbon*, *49*(10), 3158-3164.

- Liu, S., Tian, J., Wang, L., & Sun, X. (2011b). Microwave-assisted rapid synthesis of Ag nanoparticles/graphene nanosheet composites and their application for hydrogen peroxide detection. *Journal of Nanoparticle Research*, 13(10), 4539-4548.
- Liu, S., Wang, L., Tian, J., Luo, Y., Zhang, X., & Sun, X. (2011). Aniline as a dispersing and stabilizing agent for reduced graphene oxide and its subsequent decoration with Ag nanoparticles for enzymeless hydrogen peroxide detection. *Journal of Colloid and Interface Science*, 363(2), 615-619.
- Liu, X., Xu, X., Zhu, H., & Yang, X. (2013a). Synthesis of graphene nanosheets with incorporated silver nanoparticles for enzymeless hydrogen peroxide detection. *Analytical Methods*, 5(9), 2298-2304.
- Liu, X., Xu, X., Zhu, H., & Yang, X. (2013b). Synthesis of graphene nanosheets with incorporated silver nanoparticles for enzymeless hydrogen peroxide detection. *Anal. Methods*, 5(9), 2298-2304.
- Liu, Y., Yang, S., & Niu, W. (2013). Simple, rapid and green one-step strategy to synthesis of graphene/carbon nanotubes/chitosan hybrid as solid-phase extraction for square-wave voltammetric detection of methyl parathion. *Colloids and Surfaces B: Biointerfaces*, 108, 266-270.
- Liu, Z., Cai, R., Mao, L., Huang, H., & Ma, W. (1999). Highly sensitive spectrofluorimetric determination of hydrogen peroxide with β -cyclodextrin-hemin as catalyst. *Analyst*, 124(2), 173-176.
- Lorestani, F., Shahnava, Z., Mn, P., Alias, Y., & Manan, N. S. (2014). One-step hydrothermal green synthesis of silver nanoparticle-carbon nanotube reduced-graphene oxide composite and its application as hydrogen peroxide sensor. *Sensors and Actuators B: Chemical*, 347, 816-823.
- Lu, W., Chang, G., Luo, Y., Liao, F., & Sun, X. (2011). Method for effective immobilization of Ag nanoparticles/graphene oxide composites on single-stranded DNA modified gold electrode for enzymeless H₂O₂ detection. *Journal of Materials Science*, 46(15), 5260-5266.
- Lu, W., Liao, F., Luo, Y., Chang, G., & Sun, X. (2011). Hydrothermal synthesis of well-stable silver nanoparticles and their application for enzymeless hydrogen peroxide detection. *Electrochimica Acta*, 56(5), 2295-2298.
- Lu, X., Dou, H., Gao, B., Yuan, C., Yang, S., Hao, L., Zhang, X. (2011). A flexible graphene/multiwalled carbon nanotube film as a high performance electrode material for supercapacitors. *Electrochimica Acta*, 56(14), 5115-5121.
- Luo, J., Jiang, S., Zhang, H., Jiang, J., & Liu, X. (2012). A novel non-enzymatic glucose sensor based on Cu nanoparticle modified graphene sheets electrode. *Analytica Chimica Acta*, 709, 47-53.
- Luo, Y., Lu, W., Chang, G., Liao, F., & Sun, X. (2011). One-step preparation of Ag nanoparticle-decorated coordination polymer nanobelts and their application for enzymeless H₂O₂ detection. *Electrochimica Acta*, 56(24), 8371-8374.

- Ma, X., Gao, M., He, X., & Li, G. (2010). Morphology tailoring of nano/micro-structured conductive polymers, composites and their applications in chemical sensors. *Recent patents on nanotechnology*, 4(3), 150-163.
- MacDiarmid, A., Chiang, J., Richter, A., & Epstein, A. (1987). Polyaniline: a new concept in conducting polymers. *Synthetic Metals*, 18(1), 285-290.
- Mahmoudian, M., Alias, Y., & Basirun, W. (2012). The electrical properties of a sandwich of electrodeposited polypyrrole nanofibers between two layers of reduced graphene oxide nanosheets. *Electrochimica Acta*, 72, 53-60.
- Mahmoudian, M., Alias, Y., Basirun, W., & Ebadi, M. (2012). Preparation of ultra-thin polypyrrole nanosheets decorated with Ag nanoparticles and their application in hydrogen peroxide detection. *Electrochimica Acta*, 72, 46-52.
- Mahmoudian, M., Alias, Y., Basirun, W., Golsheikh, A. M., & Jamali-Sheini, F. (2013). Synthesis of polypyrrole coated manganese nanowires and their application in hydrogen peroxide detection. *Materials Chemistry and Physics*, 141(1), 298-303.
- Mahmoudian, M., Alias, Y., Basirun, W., Woi, P. M., & Yousefi, R. (2014). Synthesis of Polypyrrole Coated Silver Nanostrip Bundles and Their Application for Detection of Hydrogen Peroxide. *Journal of the Electrochemical Society*, 161(9), H487-H492.
- Mahmoudian, M. R., Alias, Y., Basirun, W. J., & Ebadi, M. (2012). Preparation of ultra-thin polypyrrole nanosheets decorated with Ag nanoparticles and their application in hydrogen peroxide detection. *Electrochimica Acta*, 72, 46-52.
- Makharza, S., Cirillo, G., Bachmatiuk, A., Ibrahim, I., Ioannides, N., Trzebicka, B., Rummeli, M. H. (2013). Graphene oxide-based drug delivery vehicles: functionalization, characterization, and cytotoxicity evaluation. *Journal of Nanoparticle Research*, 15(12), 1-26.
- Malinauskas, A., Malinauskiene, J., & Ramanavičius, A. (2005). Conducting polymer-based nanostructured materials: electrochemical aspects. *Nanotechnology*, 16(10), R51.
- Marcano, D. C., Kosynkin, D. V., Berlin, J. M., Sinitskii, A., Sun, Z., Slesarev, A., Tour, J. M. (2010). Improved synthesis of graphene oxide. *ACS nano*, 4(8), 4806-4814.
- Marcano, D. C., Kosynkin, D. V., Berlin, J. M., Sinitskii, A., Sun, Z., Slesarev, A., Tour, J. M. (2010). Improved synthesis of graphene oxide. *ACS nano*, 4(8), 4806-4814.
- Matsubara, C., Kawamoto, N., & Takamura, K. (1992). Oxo [5, 10, 15, 20-tetra (4-pyridyl) porphyrinato] titanium (IV): an ultra-high sensitivity spectrophotometric reagent for hydrogen peroxide. *Analyst*, 117(11), 1781-1784.
- Mayavan, S., Sim, J.-B., & Choi, S.-M. (2012). Simultaneous reduction, exfoliation and functionalization of graphite oxide into a graphene-platinum nanoparticle hybrid for methanol oxidation. *Journal of Materials Chemistry*, 22(14), 6953-6958.

- Mendes, L. C., Falco, A. P. S., Pinho, M. S., & Marques, P. O. (2011). Sulfonated polyaniline: influence of sulfonation routes on its thermal and structural characteristics. *Materials Research*, 14(4), 466-471.
- Merkoçi, A., Pumera, M., Llopis, X., Pérez, B., del Valle, M., & Alegret, S. (2005). New materials for electrochemical sensing VI: carbon nanotubes. *TRAC Trends in Analytical Chemistry*, 24(9), 826-838.
- Miao, Y., Chia, L., Goh, N., & Tan, S. (2001). Amperometric glucose biosensor based on immobilization of glucose oxidase in chitosan matrix cross-linked with glutaraldehyde. *Electroanalysis*, 13(4), 347-349.
- Ming, H. N. (2010). Simple room-temperature preparation of high-yield large-area graphene oxide. *International journal of nanomedicine*, 6.
- Moldoveanu, S. (2004). Solutions and challenges in sample preparation for chromatography. *Journal of Chromatographic Science*, 42(1), 1-14.
- Moradi Golsheikh, A., Huang, N., Lim, H., Zakaria, R., & Yin, C.-Y. (2013a). One-step electrodeposition synthesis of silver-nanoparticle-decorated graphene on indium-tin-oxide for enzymeless hydrogen peroxide detection. *Carbon*, 62, 405-412
- Moradi Golsheikh, A., Huang, N., Lim, H., Zakaria, R., & Yin, C.-Y. (2013b). One-step electrodeposition synthesis of silver-nanoparticle-decorated graphene on indium-tin-oxide for enzymeless hydrogen peroxide detection. *Carbon*, 62, 405-412.
- Nakamura, M., Nakanishi, M., & Yamamoto, K. (1996). Influence of physical properties of activated carbons on characteristics of electric double-layer capacitors. *Journal of Power Sources*, 60(2), 225-231.
- Nasab, S. E. H., Nasab, A. H., Ataei, S. A., & Amiri, N. (2013). Fabrication an Modified Electrode via Ionic-liquid/Bamboo-like Carbon Nanotube/Prussian Blue Nano Particles as a Highly Sensitive Nano-Composite for Detection of H₂O₂. *Int. J. Electrochem. Sci*, 8, 8800-8811.
- Ndangili, P. M., Waryo, T. T., Muchindu, M., Baker, P. G. L., Ngila, C. J., & Iwuoha, E. I. (2010). Ferrocenium hexafluorophosphate-induced nanofibrillarity of polyaniline-polyvinyl sulfonate electropolymer and application in an amperometric enzyme biosensor. *Electrochimica Acta*, 55(14), 4267-4273.
- Newman, J. D., & Turner, A. P. (2005). Home blood glucose biosensors: a commercial perspective. *Biosensors and Bioelectronics*, 20(12), 2435-2453.
- Nie, H., Yao, Z., Zhou, X., Yang, Z., & Huang, S. (2011). Nonenzymatic electrochemical detection of glucose using well-distributed nickel nanoparticles on straight multi-walled carbon nanotubes. *Biosensors and Bioelectronics*, 30(1), 28-34.
- Norouzi, P., Faridbod, F., Larijani, B., & Ganjali, M. R. (2010). Glucose biosensor based on MWCNTs-Gold nanoparticles in a Nafion film on the glassy carbon electrode using flow injection FFT continuous cyclic voltammetry. *Int. J. Electrochem. Sci*, 5, 1213-1224.

- Novoselov, K. S., Geim, A. K., Morozov, S., Jiang, D., Zhang, Y., Dubonos, S., Firsov, A. (2004). Electric field effect in atomically thin carbon films. *Science*, 306(5696), 666-669.
- Pan, L., Pu, L., Shi, Y., Song, S., Xu, Z., Zhang, R., & Zheng, Y. (2007). Synthesis of polyaniline nanotubes with a reactive template of manganese oxide. *Advanced Materials*, 19(3), 461-464.
- Pan, L., Qiu, H., Dou, C., Li, Y., Pu, L., Xu, J., & Shi, Y. (2010). Conducting polymer nanostructures: template synthesis and applications in energy storage. *International journal of molecular sciences*, 11(7), 2636-2657.
- Park, S., An, J., Piner, R. D., Jung, I., Yang, D., Velamakanni, A., Ruoff, R. S. (2008). Aqueous suspension and characterization of chemically modified graphene sheets. *Chemistry of Materials*, 20(21), 6592-6594.
- Patil, D. S., Pawar, S. A., Devan, R. S., Ma, Y.-R., Moholkar, A., Kim, J. H., Patil, P. (2012). Investigations on silver/polyaniline electrodes for electrochemical supercapacitor. *Physical Chemistry Chemical Physics*, 14(34):11886-11895
- Pauliukaite, R., Ghica, M. E., Fatibello-Filho, O., & Brett, C. (2010). Electrochemical impedance studies of chitosan-modified electrodes for application in electrochemical sensors and biosensors. *Electrochimica Acta*, 55(21), 6239-6247.
- Pei, S., & Cheng, H.-M. (2012). The reduction of graphene oxide. *Carbon*, 50(9), 3210-3228.
- Pham, V. H., Cuong, T. V., Hur, S. H., Oh, E., Kim, E. J., Shin, E. W., & Chung, J. S. (2011). Chemical functionalization of graphene sheets by solvothermal reduction of a graphene oxide suspension in N-methyl-2-pyrrolidone. *Journal of Materials Chemistry*, 21(10), 3371-3377.
- Poorahong, S., Thammakhet, C., Thavarungkul, P., & Kanatharana, P. (2012). Cauliflower polyaniline/multiwalled carbon nanotube electrode and its applications to hydrogen peroxide and glucose detection. *Pure and Applied Chemistry*, 84(10), 2055-2063.
- Porchelvi, K., Sudarvizhi, A., & Pandian, K. (2013). Single Pot Synthesis of Spherical Polyaniline Stabilized AgCl Nanoparticles by Interfacial Polymerization Method and Study Its Application on Electrochemical Detection of Hydrazine and Hydrogen peroxide. *Int. J. Electrochem. Sci*, 8, 4160-4173.
- Pumera, M., Ambrosi, A., Bonanni, A., Chng, E. L. K., & Poh, H. L. (2010). Graphene for electrochemical sensing and biosensing. *TRAC Trends in Analytical Chemistry*, 29(9), 954-965.
- Qin, X., Lu, W., Luo, Y., Chang, G., & Sun, X. (2011). Preparation of Ag nanoparticle-decorated polypyrrole colloids and their application for H₂O₂ detection. *Electrochemistry Communications*, 13(8), 785-787.

- Raghavendra, S., Khasim, S., Revanasiddappa, M., Prasad, M. A., & Kulkarni, A. (2003). Synthesis, characterization and low frequency ac conduction of polyaniline/fly ash composites. *Bulletin of Materials Science*, 26(7), 733-739.
- Rajabzade, H., Daneshgar, P., Tazikeh, E., & Mehrabian, R. Z. (2012). Functionalized Carbon Nanotubes with Gold Nanoparticles to Fabricate a Sensor for Hydrogen Peroxide Determination. *Journal of Chemistry*, 9(4), 2540-2549.
- Raof, J. B., Ojani, R., Hasheminejad, E., & Rashid-Nadimi, S. (2012). Electrochemical synthesis of Ag nanoparticles supported on glassy carbon electrode by means of p-isopropyl calix arene matrix and its application for electrocatalytic reduction of H₂O₂. *Applied Surface Science*, 258(7), 2788-2795.
- Ricci, F., Amine, A., Palleschi, G., & Moscone, D. (2003). Prussian Blue based screen printed biosensors with improved characteristics of long-term lifetime and pH stability. *Biosensors and Bioelectronics*, 18(2), 165-174.
- Ricci, F., Moscone, D., Tuta, C., Palleschi, G., Amine, A., Poscia, A., Messeri, D. (2005). Novel planar glucose biosensors for continuous monitoring use. *Biosensors and Bioelectronics*, 20(10), 1993-2000.
- Rivas, G. A., Rubianes, M. D., Rodríguez, M. C., Ferreyra, N. F., Luque, G. L., Pedano, M. L., Parrado, C. (2007). Carbon nanotubes for electrochemical biosensing. *Talanta*, 74(3), 291-307.
- Romer, R. H. (1982). What do “voltmeters” measure?: Faraday’s law in a multiply connected region. *American Journal of Physics*, 50(12), 1089-1093.
- Royappa, A. T., Steadman, D. D., Tran, T. L., Nguyen, P. T., Prayaga, C. S., Cage, B., & Dalal, N. (2001). Synthesis of sulfonated polyaniline by polymerization of the aniline heterodimer 4-aminodiphenylamine-2-sulfonic acid. *Synthetic Metals*, 123(2), 273-277.
- Safari, J., & Gandomi-Ravandi, S. (2014). Fe₃O₄-CNTs nanocomposites: a novel and excellent catalyst in the synthesis of diarylpyrimidinones using grindstone chemistry. *RSC Advances*, 4(22), 11486-11492.
- Salabat, A., Mirhoseini, F., Mahdieh, M., & Saydi, H. (2015). Novel nanotube-shaped polypyrrole-Pd composite prepared using reverse microemulsion polymerization and its evaluation as an antibacterial agent. *New Journal of Chemistry*, 39(5):4109-4114
- Sawangphruk, M., Sanguansak, Y., Krittayavathananon, A., Luanwuthi, S., Srimuk, P., Nilmoung, S., Limtrakul, J. (2014). Silver nanodendrite modified graphene rotating disk electrode for nonenzymatic hydrogen peroxide detection. *Carbon*, 70, 287-294.
- Sazou, D., & Georgolios, C. (1997). Formation of conducting polyaniline coatings on iron surfaces by electropolymerization of aniline in aqueous solutions. *Journal of Electroanalytical Chemistry*, 429(1), 81-93.

- Schniepp, H. C., Li, J.-L., McAllister, M. J., Sai, H., Herrera-Alonso, M., Adamson, D. H., Aksay, I. A. (2006). Functionalized single graphene sheets derived from splitting graphite oxide. *The Journal of Physical Chemistry B*, 110(17), 8535-8539.
- Sellers, R. M. (1980). Spectrophotometric determination of hydrogen peroxide using potassium titanium (IV) oxalate. *Analyst*, 105(1255), 950-954.
- Shahnavaz, Z., Lorestani, F., Alias, Y., & Woi, P. M. (2014). Polypyrrole-ZnFe₂O₄ Magnetic Nano-composite with core-shell structure for glucose sensing. *Applied Surface Science*.
- Shao, Y., Wang, J., Wu, H., Liu, J., Aksay, I. A., & Lin, Y. (2010). Graphene based electrochemical sensors and biosensors: a review. *Electroanalysis*, 22(10), 1027-1036.
- Sharma, D. K., Ott, A., O'Mullane, A. P., & Bhargava, S. K. (2011). The facile formation of silver dendritic structures in the absence of surfactants and their electrochemical and SERS properties. *Colloids and Surfaces A: Physicochemical and Engineering Aspects*, 386(1), 98-106.
- Shi, Y., Liu, Z., Zhao, B., Sun, Y., Xu, F., Zhang, Y., Li, Z. (2011). Carbon nanotube decorated with silver nanoparticles via noncovalent interaction for a novel nonenzymatic sensor towards hydrogen peroxide reduction. *Journal of Electroanalytical Chemistry*, 656(1), 29-33.
- Soliman, M. G. M., Pelaz, B., Parak, W. J., & del Pino, P. (2015). Phase Transfer and Polymer Coating Methods towards Improving Stability of Metallic Nanoparticles for Biological Applications. *Chemistry of Materials*, 27(3):990-997.
- Song, E., & Choi, J.-W. (2013). Conducting polyaniline nanowire and its applications in chemiresistive sensing. *Nanomaterials*, 3(3), 498-523.
- Song, X. C., Wang, X., Zheng, Y. F., Ma, R., & Yin, H. Y. (2011). A hydrogen peroxide electrochemical sensor based on Ag nanoparticles grown on ITO substrate. *Journal of Nanoparticle Research*, 13(10), 5449-5455.
- Song, Y., Cui, K., Wang, L., & Chen, S. (2009). The electrodeposition of Ag nanoparticles on a type I collagen-modified glassy carbon electrode and their applications as a hydrogen peroxide sensor. *Nanotechnology*, 20(10), 105501.
- Stankovich, S., Dikin, D. A., Piner, R. D., Kohlhaas, K. A., Kleinhammes, A., Jia, Y., Ruoff, R. S. (2007). Synthesis of graphene-based nanosheets via chemical reduction of exfoliated graphite oxide. *Carbon*, 45(7), 1558-1565.
- Stejskal, J., Prokeš, J., & Sapurina, I. (2009). The reduction of silver ions with polyaniline: The effect of the type of polyaniline and the mole ratio of the reagents. *Materials Letters*, 63(8), 709-711.
- Stejskal, J., Riede, A., Hlavatá, D., Prokeš, J., Helmstedt, M., & Holler, P. (1998). The effect of polymerization temperature on molecular weight, crystallinity, and electrical conductivity of polyaniline. *Synthetic Metals*, 96(1), 55-61.

- Stejskal, J., Trchová, M., Kovářová, J., Brožová, L., & Prokeš, J. (2009). The reduction of silver nitrate with various polyaniline salts to polyaniline–silver composites. *Reactive and Functional Polymers*, 69(2), 86-90.
- Su, B., Tong, Y., Bai, J., Lei, Z., Wang, K., Mu, H., & Dong, N. (2007). Acid doped polyaniline nanofibers synthesized by interfacial polymerization. *INDIAN JOURNAL OF CHEMISTRY SECTION A*, 46(4), 595.
- Tajabadi, M., Basirun, W., Lorestani, F., Zakaria, R., Baradaran, S., Amin, Y., Sookhakian, M. (2014). Nitrogen-doped graphene-silver nanodendrites for the non-enzymatic detection of hydrogen peroxide. *Electrochimica Acta*, 151, 126-133.
- Tarachiwin, L., Kiattibutr, P., Ruangchuay, L., Sirivat, A., & Schwank, J. (2002). Electrical conductivity response of polyaniline films to ethanol–water mixtures. *Synthetic Metals*, 129(3), 303-308.
- Teo, P., Lim, H., Huang, N., Chia, C., & Harrison, I. (2012). Room temperature in situ chemical synthesis of Fe₃O₄/graphene. *Ceramics International*, 38(8), 6411-6416.
- Tian, J., Li, H., Lu, W., Luo, Y., Wang, L., & Sun, X. (2011). Preparation of Ag nanoparticle-decorated poly (m-phenylenediamine) microparticles and their application for hydrogen peroxide detection. *Analyst*, 136(9), 1806-1809.
- Tian, J., Liu, S., & Sun, X. (2010). Supramolecular microfibrils of o-phenylenediamine dimers: oxidation-induced morphology change and the spontaneous formation of Ag nanoparticle decorated nanofibers. *Langmuir*, 26(19), 15112-15116.
- Tran, H. D., Wang, Y., D'Arcy, J. M., & Kaner, R. B. (2008). Toward an understanding of the formation of conducting polymer nanofibers. *ACS nano*, 2(9), 1841-1848.
- Tsai, Y.-C., Hsu, P.-C., Lin, Y.-W., & Wu, T.-M. (2009). Electrochemical deposition of silver nanoparticles in multiwalled carbon nanotube-alumina-coated silica for surface-enhanced Raman scattering-active substrates. *Electrochemistry Communications*, 11(3), 542-545.
- Van Dong, P., Ha, C. H., & Kasbohm, J. (2012). Chemical synthesis and antibacterial activity of novel-shaped silver nanoparticles. *International Nano Letters*, 2(1), 1-9.
- Wan, M. (2008). A template-free method towards conducting polymer nanostructures. *Advanced Materials*, 20(15), 2926-2932.
- Wang, G., Yang, J., Park, J., Gou, X., Wang, B., Liu, H., & Yao, J. (2008). Facile synthesis and characterization of graphene nanosheets. *The Journal of Physical Chemistry C*, 112(22), 8192-8195.
- Wang, J. (2005). Carbon-nanotube based electrochemical biosensors: A review. *Electroanalysis*, 17(1), 7-14.
- Wang, J. (2008). Electrochemical glucose biosensors. *Chemical Reviews*, 108(2), 814-825.

- Wang, J., Musameh, M., & Lin, Y. (2003). Solubilization of carbon nanotubes by Nafion toward the preparation of amperometric biosensors. *Journal of the American Chemical Society*, 125(9), 2408-2409.
- Wang, L., Zeng, Y., Shen, A., Zhou, X., & Hu, J. (2015). Three dimensional nano-assemblies of noble metal nanoparticle–infinite coordination polymers as specific oxidase mimetics for degradation of methylene blue without adding any cosubstrate. *Chemical Communications*.
- Wang, Q., & Yun, Y. (2013). Nonenzymatic sensor for hydrogen peroxide based on the electrodeposition of silver nanoparticles on poly (ionic liquid)-stabilized graphene sheets. *Microchimica Acta*, 180(3-4), 261-268.
- Wang, Q., Yun, Y., & Zheng, J. (2009). Nonenzymatic hydrogen peroxide sensor based on a polyaniline-single walled carbon nanotubes composite in a room temperature ionic liquid. *Microchimica Acta*, 167(3-4), 153-157.
- Wang, Z.-l., Xu, D., Huang, Y., Wu, Z., Wang, L.-m., & Zhang, X.-b. (2012). Facile, mild and fast thermal-decomposition reduction of graphene oxide in air and its application in high-performance lithium batteries. *Chemical Communications*, 48(7), 976-978.
- Welch, C., Banks, C., Simm, A., & Compton, R. (2005). Silver nanoparticle assemblies supported on glassy-carbon electrodes for the electro-analytical detection of hydrogen peroxide. *Analytical and Bioanalytical Chemistry*, 382(1), 12-21.
- Wessling, B. (1998). Dispersion as the link between basic research and commercial applications of conductive polymers (polyaniline). *Synthetic Metals*, 93(2), 143-154.
- Wildgoose, G. G., Banks, C. E., & Compton, R. G. (2006). Metal nanoparticles and related materials supported on carbon nanotubes: methods and applications. *Small*, 2(2), 182-193.
- Woo, S., Kim, Y.-R., Chung, T. D., Piao, Y., & Kim, H. (2012). Synthesis of a graphene–carbon nanotube composite and its electrochemical sensing of hydrogen peroxide. *Electrochimica Acta*, 59, 509-514.
- Wu, B.-Y., Hou, S.-H., Yin, F., Li, J., Zhao, Z.-X., Huang, J.-D., & Chen, Q. (2007). Amperometric glucose biosensor based on layer-by-layer assembly of multilayer films composed of chitosan, gold nanoparticles and glucose oxidase modified Pt electrode. *Biosensors and Bioelectronics*, 22(6), 838-844.
- Wu, S., Lan, X., Cui, L., Zhang, L., Tao, S., Wang, H., Meng, C. (2011). Application of graphene for preconcentration and highly sensitive stripping voltammetric analysis of organophosphate pesticide. *Analytica Chimica Acta*, 699(2), 170-176.
- Xie, G., Cheng, J., Li, Y., Xi, P., Chen, F., Liu, H., Xu, Z. (2012). Fluorescent graphene oxide composites synthesis and its biocompatibility study. *Journal of Materials Chemistry*, 22(18), 9308-9314.

- Xu, Y., Sheng, K., Li, C., & Shi, G. (2010). Self-assembled graphene hydrogel via a one-step hydrothermal process. *ACS nano*, 4(7), 4324-4330.
- Yamada, Y., Fukunishi, Y., Yamazaki, S.-i., & Fukuzumi, S. (2010). Hydrogen peroxide as sustainable fuel: electrocatalysts for production with a solar cell and decomposition with a fuel cell. *Chemical Communications*, 46(39), 7334-7336.
- Yang, M., Ma, J., Zhang, C., Yang, Z., & Lu, Y. (2005). General Synthetic Route toward Functional Hollow Spheres with Double-Shelled Structures. *Angewandte Chemie International Edition*, 44(41), 6727-6730.
- Yang, P., Wei, W., Tao, C., Xie, B., & Chen, X. (2008). Nano-silver/multi-walled carbon nanotube composite films for hydrogen peroxide electroanalysis. *Microchimica Acta*, 162(1-2), 51-56.
- Yang, Y., & Mu, S. (2005). Determination of hydrogen peroxide using amperometric sensor of polyaniline doped with ferrocenesulfonic acid. *Biosensors and Bioelectronics*, 21(1), 74-78.
- Yin, P., Kim, T.-H., Choi, J.-W., & Lee, K. (2013). Prospects for graphene-nanoparticle-based hybrid sensors. *Physical Chemistry Chemical Physics*, 15(31):12785-12799
- Yu, A., Roes, I., Davies, A., & Chen, Z. (2010). Ultrathin, transparent, and flexible graphene films for supercapacitor application. *Applied Physics Letters*, 96(25), 253105
- Yu, A., Wang, Q., Yong, J., Mahon, P. J., Malherbe, F., Wang, F., Wang, J. (2012a). Silver nanoparticle-carbon nanotube hybrid films: Preparation and electrochemical sensing. *Electrochimica Acta*, 74(0), 111-116.
- Yu, A., Wang, Q., Yong, J., Mahon, P. J., Malherbe, F., Wang, F., Wang, J. (2012b). Silver nanoparticle-carbon nanotube hybrid films: Preparation and electrochemical sensing. *Electrochimica Acta*, 74, 111-116.
- Yu, B., Feng, J., Liu, S., & Zhang, T. (2013). Preparation of reduced graphene oxide decorated with high density Ag nanorods for non-enzymatic hydrogen peroxide detection. *RSC Advances*, 3(34), 14303-14307.
- Yu, J. H., Fridrikh, S. V., & Rutledge, G. C. (2004). Production of submicrometer diameter fibers by two-fluid electrospinning. *Advanced Materials*, 16(17), 1562-1566.
- Zainy, M., Huang, N., Kumar, S. V., Lim, H., Chia, C., & Harrison, I. (2012). Simple and scalable preparation of reduced graphene oxide-silver nanocomposites via rapid thermal treatment. *Materials Letters*, 89, 180-183.
- Zeng, F., Sun, Z., Sang, X., Diamond, D., Lau, K. T., Liu, X., & Su, D. S. (2011). In situ one-step electrochemical preparation of graphene oxide nanosheet-modified electrodes for biosensors. *ChemSusChem*, 4(11), 1587-1591.

- Zhang, K., Mao, L., & Cai, R. (2000). Stopped-flow spectrophotometric determination of hydrogen peroxide with hemoglobin as catalyst. *Talanta*, 51(1), 179-186.
- Zhang, K., Zhang, L., Xu, J., Wang, C., Geng, T., Wang, H., & Zhu, J. (2010). A sensitive amperometric hydrogen peroxide sensor based on thionin/EDTA/carbon nanotubes—chitosan composite film modified electrode. *Microchimica Acta*, 171(1-2), 139-144.
- Zhang, S., Ren, F., Wu, W., Zhou, J., Sun, L., Xiao, X., & Jiang, C. (2012). Modified in situ and self-catalytic growth method for fabrication of Ag-coated nanocomposites with tailorable optical properties. *Journal of Nanoparticle Research*, 14(9), 1-13.
- Zhang, X., Goux, W. J., & Manohar, S. K. (2004). Synthesis of polyaniline nanofibers by “nanofiber seeding”. *Journal of the American Chemical Society*, 126(14), 4502-4503.
- Zhang, Y., Yuan, X., Wang, Y., & Chen, Y. (2012). One-pot photochemical synthesis of graphene composites uniformly deposited with silver nanoparticles and their high catalytic activity towards the reduction of 2-nitroaniline. *Journal of Materials Chemistry*, 22(15), 7245-7251.
- Zhang, Z., Zhang, L., Wang, S., Chen, W., & Lei, Y. (2001). A convenient route to polyacrylonitrile/silver nanoparticle composite by simultaneous polymerization–reduction approach. *Polymer*, 42(19), 8315-8318.
- Zhao, B., Liu, Z., Liu, Z., Liu, G., Li, Z., Wang, J., & Dong, X. (2009). Silver microspheres for application as hydrogen peroxide sensor. *Electrochemistry Communications*, 11(8), 1707-1710.
- Zhao, W., Wang, H., Qin, X., Wang, X., Zhao, Z., Miao, Z., Chen, Q. (2009). A novel nonenzymatic hydrogen peroxide sensor based on multi-wall carbon nanotube/silver nanoparticle nanohybrids modified gold electrode. *Talanta*, 80(2), 1029-1033.
- Zhong, H., Yuan, R., Chai, Y., Zhang, Y., Wang, C., & Jia, F. (2012). Non-enzymatic hydrogen peroxide amperometric sensor based on a glassy carbon electrode modified with an MWCNT/polyaniline composite film and platinum nanoparticles. *Microchimica Acta*, 176(3-4), 389-395.
- Zhong, L., Gan, S., Fu, X., Li, F., Han, D., Guo, L., & Niu, L. (2012). Electrochemically controlled growth of silver nanocrystals on graphene thin film and applications for efficient nonenzymatic H₂O₂ biosensor. *Electrochimica Acta*, 89, 222-228
- Zhong, L., Gan, S., Fu, X., Li, F., Han, D., Guo, L., & Niu, L. (2013a). Electrochemically controlled growth of silver nanocrystals on graphene thin film and applications for efficient nonenzymatic H₂O₂ biosensor. *Electrochimica Acta*, 89(0), 222-228.
- Zhong, L., Gan, S., Fu, X., Li, F., Han, D., Guo, L., & Niu, L. (2013b). Electrochemically controlled growth of silver nanocrystals on graphene thin film and applications for efficient nonenzymatic H₂O₂ biosensor. *Electrochimica Acta*, 89, 222-228.

Zhou, M., Zhai, Y., & Dong, S. (2009). Electrochemical sensing and biosensing platform based on chemically reduced graphene oxide. *Analytical Chemistry*, 81(14), 5603-5613.

University of Malaya

Appendix

Honors and Awards

1. Bronze medal for 1 minute presentation of “One step synthesis of Ag nanoparticles-polyaniline nanorodseres and it application in hydrogen peroxide detection” (4th INTERNATIONAL CONFERENCE ON FUNCTIONAL MATERIALS AND DEVICES 2013 ICFMD-2013)
2. Silver medal for 1 minute presentation of “One step synthesis of Ag nanoparticles-polyaniline nanorodseres and it application in hydrogen peroxide detection” (4th INTERNATIONAL CONFERENCE ON FUNCTIONAL MATERIALS AND DEVICES 2013 ICFMD-2013)
3. **Lorestani, F., Shahnavaaz, Z., Mn, P., Alias, Y., & Manan, N. S. (2015). One-step hydrothermal green synthesis of silver nanoparticle-carbon nanotube reduced-graphene oxide composite and its application as hydrogen peroxide sensor. *Sensors and Actuators B: Chemical*, 208: 389-398. It is listed under the most downloaded articles in Science Direct in the last 90 days. (Most downloaded Sensor and Actuator B: Chemicals)**

International conferences

1. Application of silver decorated graphene nanosheets-polyaniline nanofibers composites as a hydrogen peroxide sensor (conference International Conference on Ionic Liquids (ICIL 13) - 2013)
2. One step synthesis of Ag nanoparticles- polyaniline nanorodseres and it application in hydrogen peroxide detection (4th INTERNATIONAL CONFERENCE ON FUNCTIONAL MATERIALS AND DEVICES 2013 ICFMD-2013)

3. One step synthesis of Ag nanoparticles- polyaniline nanorods and its application in hydrogen peroxide detection (4th INTERNATIONAL CONFERENCE ON FUNCTIONAL MATERIALS AND DEVICES 2013 ICFMD-2013)

Publications

Published papers based on this thesis

1. **LoRESTANI, F***, ShahnavaZ, Z., Mn, P., Alias, Y., & Manan, N. S.* (2015). One-step hydrothermal green synthesis of silver nanoparticle-carbon nanotube reduced-graphene oxide composite and its application as hydrogen peroxide sensor. **Sensors and Actuators B: Chemical**, 208: 389-398. Journal impact factor : **3.840**
2. **LoRESTANI, F***, Nia, P. M., Alias, Y., & Manan, N. S.* (2015). One-Step Synthesis of Different Silver-Polyaniline Composite Morphologies for Enzymless Hydrogen Peroxide Detection. **Journal of the Electrochemical Society**, 162: B193-B200. Journal impact factor : **2.859**.
3. **LoRESTANI, F***, ShahnavaZ, Z., Nia, P. M., Alias, Y., & Manan, N. S.* (2015). One-step preparation of silver-polyaniline nanotube composite for non-enzymatic hydrogen peroxide detection. **Applied Surface Science**. Journal impact factor : **2.538**

Submitted papers based on this thesis

1. **LoRESTANI, F***, Alias, Y., & Manan, N. S.* Simple, rapid and green one-step electrodeposition synthesis of silver nanoparticle-reduced graphene oxide-carbon nanotube composite for enzymeless hydrogen peroxide sensor. submitted to **Analytica chimica Acta**, Journal impact factor : **4.517**
2. **LoRESTANI, F***, Nia, P. M., Alias, Y., & Manan, N. S.* Sonochemical and hydrothermal approaches for modified electrode based on novel polyaniline nanofibers-silver

nanoparticles decorated graphene oxide composite for hydrogen peroxide detection.
submitted to **Electrochimica Acta**, Journal impact factor : **4.086**

Other published papers

1. Shahnavaaz, Z., **Lorestani, F.**, Meng, W. P., & Alias, Y. (2015). Core-shell–CuFe₂O₄/PPy nanocomposite enzyme-free sensor for detection of glucose. **Journal of Solid State Electrochemistry** 1-11. Journal impact factor : **2.234**
2. Nia, P. M., Meng, W. P., **Lorestani, F.**, Mahmoudian, M., & Alias, Y. (2015). Electrodeposition of copper oxide/polypyrrole/reduced graphene oxide as a nonenzymatic glucose biosensor. **Sensors and Actuators B: Chemical**, 209: 100-108. Journal impact factor : **3.840**
3. Tajabadi, M., Basirun, W., **Lorestani, F.**, Zakaria, R., Baradaran, S., Amin, Y., Sookhakian, M. (2015). Nitrogen-doped graphene-silver nanodendrites for the non-enzymatic detection of hydrogen peroxide. **Electrochimica Acta**, 151: 126-133. Journal impact factor : **4.086**
4. Shahnavaaz, Z., **Lorestani, F.**, Alias, Y., & Woi, P. M. (2014). Polypyrrole–ZnFe₂O₄ magnetic nano-composite with core–shell structure for glucose sensing. **Applied Surface Science**, 317: 622-629. Journal impact factor : **2.538**